INVESTIGATIONS OF ENZYME ACTIVE-SITE ARCHITECTURES AND CATALYSIS

by

Laura C. McGary

Submitted in partial fulfilment of the requirements
for the degree of Master of Science

at

Dalhousie University
Halifax, Nova Scotia
August, 2022

TABLE OF CONTENTS

LIST OF TABLES

LIST OF FIGURES

LIST OF SCHEMES

ABSTRACT

Sodium methyl hex-5-ynoyl phosphate (SMHP) was synthesized as an activity-based probe designed to target protein architectures with nucleophiles adjacent to a cationic binding site. Activity-based protein profiling revealed that SMHP modified 281 enzymes from the cell-lysate of *Pseudomonas lemognei*, including D-3-hydroxybutyrate dehydrogenase and CTP synthase. The sites of modification were investigated using fluorescence-based activity studies, LC-MS/MS, and kinetics. The inactivation of L-fuconate dehydratase by 3-hydroxypyruvate and the effects of Tris buffer were also explored. With increasing Tris concentrations, the k_{inact}^{app} and K_I^{app} values decreased, but the $k_{inact}^{app}/K_I^{app}$ remained unchanged (~0.018 ± 0.002 $M^{-1}s^{-1}$). Finally, the Cys→Ser variants (C76S and C186S) of glutamate racemase from *Fusobacterium nucleatum* were constructed. The C76S variant exhibited greater catalytic efficiency in the D→L reaction direction at higher pH values; however, this preferred 'unidirectional' behavior was not observed for the C186S variant in the L→D reaction direction.

LIST OF ABBREVIATIONS USED

ABP	activity-based probe
ABPP	activity-based protein profiling
ADP	adenosine-5′-diphosphate
ATCC	American Type Culture Collection
ATP	adenosine-5′-triphosphate
BPA	biotin picolyl azide
BSA	bovine serum albumin
CD	circular dichroism
CTP	cytidine-5′-triphosphate
CTPS	cytidine-5′-triphosphate synthase
CuAAC	copper (I)-catalyzed azide-alkyne cycloaddition
Da	Dalton
DON	6-diazo-5-oxo-L-norleucine
2,3-DPG	2,3-diphosphoglycerate
DTT	dithiothreitol
EC	enzyme commission
EDTA	ethylenediaminetetraacetic acid
EGTA	ethylene glycol tetraacetic acid
ENS	enolase superfamily of enzymes
ESI	electrospray ionization
*Fn*GR	glutamate racemase from *Fusobacterium nucleatum*
FPA	fluorescein picolyl azide
FPLC	fast protein liquid chromatohraphy
FucD	L-fuconate dehydratase
GLH	glycolaldehdye
GR	glutamate racemase
GTP	guanidine-5′-triphosphate
Hb	hemoglobin
3-HBDH	D-3-Hydroxybutyrate dehydrogenase

HEPES	4-(2-hydroxyethyl)-1-piperazineethanesulfonic acid
3-HP	3-hydroxypyruvate
HPLC	high-performance liquid chromatography
IAA	iodoacetamide
IPTG	isopropyl β-D-1-thiogalactopyranoside
LB	lysogeny broth
LC-MS	liquid chromatography-mass spectrometry
LC-MS/MS	liquid chromatography-tandem mass spectrometry
*Lf*GR	glutamate racemase from *Lactobacillus fermenti*
MAP	methyl acetyl phosphate
MR	mandelate racemase
MS	mass spectrometry
MW	molecular weight
m/*z*	mass-to-charge ratio
n	Hill number
NAD^+	nicotinamide adenine dinucleotide – oxidized form
NADH	nicotinamide adenine dinucleotide – reduced form
NMR	nuclear magnetic resonance
OD	optical density
PBS	phosphate-buffered saline
SDR	short-chain dehydrogenase/reductase superfamily of enzymes
SDS-PAGE	sodium dodecyl sulfate polyacrylamide gel electrophoresis
SMHP	sodium methyl hex-5-ynoyl phosphate
THPTA	tris(hydroxypropyltriazolyl)methylamine
THF	tetrahydrofuran
Tris	tris(hydroxymethyl)aminomethane
UTP	uridine-5′-triphosphate
UV	ultraviolet
WT	wild-type

ACKNOWLEDGEMENTS

I would first like to sincerely thank my supervisor, Dr. Stephen Bearne for kindly welcoming me into his lab, and for his continued guidance and support throughout my M.Sc. I feel extremely grateful to have learned from someone so dedicated and passionate about research, who has truly inspired and challenged me from start to finish, allowing me to become the scientist I am today.

I would like to thank my supervisory committee members Dr. Jan Rainey and Dr. David Jakeman for their time and guidance throughout my M.Sc. I would also like to thank Dr. Alejandro Cohen (Biological Mass Spectrometry Core Facility, Dalhousie University) for his assistance with the the LC-MS and LC-MS/MS experiments. A special thank you to Roisin McDevitt for immediately making me feel welcome in Halifax and for all your support throughout each step of the way. I am extremely grateful to past and present members of the Bearne lab for their guidance, encouragement, and scientific contributions: Oliver Kuehm, Tom Gillis, Dr. Krishna Desireddy, Josh Hayden, Amanda Black, Meghan Hamilton, Chris Fetter, and Gemma Regan.

Many thanks to the NSERC-CREATE BioActives program for funding my research along with the opportunities the program has afforded. I am also thankful for the teaching assistant positions that I held throughout my degree within the Biochemistry and Molecular Biology department, with a special thanks to Heidi Mackinnon, Paul Briggs, and Dr. Shawn Xiong for providing me with these opportunities.

I would also like to thank my two previous supervisors from my undergraduate research at the University of Guelph- Dr. Gale Bozzo (Guelph campus) and Dr. Laura Van Eerd (Ridgetown campus) who both inspired me to pursue graduate research. I

would like to extend my gratitude to PhD candidate, Nicole Unterlander, who mentored me throughout my time in Dr. Bozzo's lab and has continued to support me throughout my graduate journey at Dalhousie as well.

I am very grateful for my University of Guelph, B.Sc. friends, especially Sarah Kirsh, Amanda Bakke, James Arrey, and Harrison Young, who are all at different schools for their M.Sc./PhD programs from coast-to-coast across Canada, but who have continued to be an instrumental support system for one another from start to finish. Finally, for all their encouragement throughout my M.Sc., I would like to thank my parents, Paul and Diane McGary, and sister, Paige McGary — I am forever grateful for your endless support.

CHAPTER 1 INTRODUCTION

In this thesis, three major topics will be discussed: (i) investigations of protein architectures using an activity-based probe (Chapter 2), (ii) evaluation of the inactivation of L-fuconate dehydratase by 3-hydroxypyruvate and the effects of Tris buffer (Chapter 3), and (iii) the re-engineering of glutamate racemase to address the question of whether the enzyme can be made preferentially "unidirectional" (Chapter 4).

Investigating protein architectures using an activity-based probe (Chapter 2)

Activity-based protein profiling (ABPP) is a chemical proteomic technique used to identify proteins and their functional state (Cravatt *et al*., 2008; Kozarich, 2003; Peng & Hulleman, 2019; Willems *et al*., 2014), identify enzyme inhibitors (Galmozzi *et al*., 2014; Niphakis & Cravatt, 2014), and classify enzymes that share conserved structural features (Kozarich, 2003; Patricelli *et al*., 2007). In Chapter 2 of this thesis, I describe the synthesis of sodium methyl hex-5-ynoyl phosphate (SMHP), a small-molecule activity-based probe designed to target proteins architectures with a nucleophile adjacent to a cationic binding site. The anionic monomethyl acyl phosphate warhead of this probe structurally resembles methyl acetyl phosphate (MAP), a compound previously shown to irreversibly inactivate 3-hydroxybutyrate dehydrogenase (3-HBDH) (Kluger & Tsui, 1980, 1986) and modify hemoglobin (Hb) (Ueno *et al*., 1986, 1989; Xu *et al*., 1999). Given the structural similarity to MAP, and the hydrolytic stability of the acyl phosphate warhead (Di Sabato & Jencks, 1961a, 1961b), I show that SMHP also modifies these proteins. Consequently, I set out to use SMHP to identify proteins containing this architecture within a cell-lysate proteome from *Pseudomonas lemognei*, which was

employed for the proof-of-principle experiment since it natively expresses expresses 3-HBDH. Using a copper (I)-catalyzed azide-alkyne cycloaddition (CuAAC) reaction between the probe-modified proteins from the *P. lemognei* proteome and a biotin-azide tag to obtain proteins that had reacted with SMHP, I used LC-MS/MS to identify 281 enzymes, including 3-HBDH and CTP synthase (CTPS). I then characterized the interaction of SMHP and MAP with purified 3-HBDH from *P. lemognei* and CTP synthase (CTPS) from *E. coli* using fluorescent tagging, LC-MS/MS, and kinetic studies to determine the sites of modification.

Evaluating the inactivation of L-fuconate dehydratase by 3-hydroxypyruvate and the effects of Tris buffer (Chapter 3)

L-Fuconate dehydratase (FucD) is a member of the mandelate racemase (MR) subgroup within the enolase superfamily of enzymes (ENS), that catalyzes the conversion of L-fuconate to 2-keto-3-deoxy-L-fuconate in a β-elimination reaction. 3-Hydroxypyruvate (3-HP) was previously discovered to irreversibly inactivate MR, where the catalytic residues, Lys 166 and His 297, were identified as binding determinants for the inhibitor (Nagar *et al*., 2015). Given that members of the MR subgroup share conserved active-site residues, Chris Fetter, a previous M.Sc. student in the Bearne lab, sought to investigate whether 3-HP could also inactivate FucD (Fetter, 2019). Interestingly, Chris Fetter determined that the efficiency of inactivation (k_{inact}/K_I) of FucD by 3-HP was significantly lower (0.023 ± 0.001 $M^{-1}s^{-1}$) (Fetter, 2019) than that observed for the inactivation of MR 83 ± 8 $M^{-1}s^{-1}$ (Nagar *et al*., 2015). The inactivation of MR was previously shown to occur via a Schiff-base mechanism, yielding an 86-Da enol(ate)/aldehyde adduct with Lys 166 (Nagar *et al*., 2015). While Chris Fetter observed

86-Da adducts with Lys 220 (analogous to Lys 166 of MR) using LC-MS/MS analysis, surprisingly, 58-Da adducts were also observed with Lys 220 and with other nucleophilic residues outside of the active site. The combination of kinetics and LC-MS/MS findings suggested the possibility that despite the conserved catalytic machinery among MR subgroup members, FucD was being inactivated by 3-HP through a different mechanism than that reported for MR.

Building on the findings of Chris Fetter, my goal was to investigate whether the reduced rate of inactivation observed for FucD was potentially a consequence of the buffer used, tris(hydroxymethyl)aminomethane (Tris), given the known ability of primary amines to form Schiff-base products with carbonyl groups, such as aldehydes and ketones. In this work, time-dependent inactivation studies of FucD by 3-HP were conducted at varying concentrations of Tris. Interestingly, Tris was found to protect against the inactivation of FucD in a concentration-dependent manner, where the k_{inact}^{app} and K_I^{app} values decreased with respect to increasing Tris-Cl concentrations, but the $k_{inact}^{app}/K_I^{app}$ remained unchanged. Protection studies with L-fuconate revealed that 3-HP-dependent inactivation of FucD does not appear to occur at the active site. Finally, intact ESI-MS studies are described that assess size and number of adducts formed when 3-HP-dependent inactivation of FucD was conducted in 5 mM versus 50 mM Tris-Cl buffer.

Can the bidirectional activity of glutamate racemase be re-engineered to become preferentially 'unidirectional'? (Chapter 4)

Glutamate racemase (GR) is an amino acid racemase that catalyzes the interconversion of L-glutamate and D-glutamate via a two-base mechanism, specifically, by two catalytic Cys residues (Glavas & Tanner, 1999). Glutamate racemase plays a

critical role in the biosynthesis of bacterial cell walls, wherein D-glutamate, is an essential component of peptidoglycan, which protects bacteria from osmotic rupture (Fisher, 2008; Lundqvist *et al*., 2007; Van Heijenoort, 2001). Glaves and Tanner (1999) previously investigated the substitution of the two catalytic Cys residues of GR from *Lactobacillus fermenti* (*Lf*GR) to Ser residues (C73S and C184S) and found that the k_{cat}/K_m values for the C73S variant increased ~10-fold in the D→L reaction direction between pH 7.0 to 9.0, but the k_{cat}/K_m values for the C184S variant remained largely unchanged over this pH range. However, the authors only investigated the pH-dependencies of the variants in the D→L reaction direction.

With GR from oral pathogen *Fusobacterium nucleatum* (*Fn*GR), which was previously purified and characterized in the Bearne Lab (Potrykus *et al*., 2009), my objective was to construct *Fn*GR Cys to Ser variants, C76S and C186S, and determine whether these variants were active, and, if so, to explore whether the variants would exhibit preferential 'unidirectional' behavior at increased pH values, which was anticipated based on findings by Glaves and Tanner (1999). Indeed, the variants retained some residual enzymatic activity, and, while the C76S *Fn*GR variant exhibited greater efficiency in the D→L reaction direction at higher pH values, this preferred 'unidirectional' behavior was not observed for the C186S variant in the L→D reaction direction.

CHAPTER 2 INVESTIGATING PROTEIN ARCHITECTURES USING AN ACTIVITY-BASED PROBE

2.1 INTRODUCTION

2.1.1 ACTIVITY-BASED PROTEIN PROFILING

Activity-based protein profiling (ABPP) is a rapidly emerging chemical proteomic technique used to identify proteins and their functional state (Cravatt *et al*., 2008; Kozarich, 2003; Peng & Hulleman, 2019; Willems *et al*., 2014), identify enzyme inhibitors (Galmozzi *et al*., 2014; Niphakis & Cravatt, 2014), and classify enzymes that share conserved structural features (Kozarich, 2003; Patricelli *et al*., 2007). The ABPP approach uses small-molecule probes that are designed to covalently modify the active site(s) of an individual protein, or family of proteins, based on shared structural motifs (Cravatt *et al*., 2008; Willems *et al*., 2014). Protein activity can be assessed both *in vitro* and *in vivo* in various forms of biological systems, such as cell-lysates, tissues, and whole organisms (Deng *et al*., 2020). This technique has therefore become an important approach for drug discovery and development, wherein potential inhibitors can be screened against a plethora of enzymes in parallel to determine their selectivity and potency within complex systems (Wright *et al*., 2009; Wright & Cravatt, 2007).

2.1.2 STRUCTURE AND MECHANISM OF ACTIVITY-BASED PROBES

Activity-based probes (ABPs) typically consist of three functional groups: a binding group, a reactive group, and a reporter tag (Niphakis & Cravatt, 2014). The binding group is often designed to mimic structural and electronic characteristics of the substrate or an inhibitor of a given type of enzyme that directs the probe towards the active site of the target proteins based on conserved structural or mechanistic features

(Deng *et al*., 2020; Niphakis & Cravatt, 2014). The reactive group, also termed the "warhead", reacts to form a covalent bond with the protein and is often either an electrophilic or a photoreactive functional group (Cravatt *et al*., 2008; Liu *et al*., 2015). Warheads must be carefully designed to avoid nonspecific, off-target reactions (Shindo & Ojida, 2021). Ideally, the warhead should exhibit high stability under physiological conditions, yet be highly reactive towards proteins containing the targeted catalytic or structural motif (Kozarich, 2003; Shindo & Ojida, 2021). Electrophilic groups, such as epoxides, sulfonates, lactones, and fluorophosphates are more commonly employed in ABPP, as opposed to photoreactive groups, and typically react to form covalent bonds with conserved active-site nucleophiles (Deng *et al*., 2020; S. Wang *et al*., 2018). However, in the absence of such conserved active-site nucleophiles, photoreactive groups, such as benzophenones, diazirines, and aryl azides, are used to generate a highly reactive species, such as a nitrene or carbene upon UV irradiation, that then forms a covalent bond with the site of interest (McKenna *et al*., 2021). A caveat to using a photoactivated group as the reactive group is the increased likelihood of nonspecific labelling as a result of the highly reactive species that is generated upon UV irradiation (Shindo & Ojida, 2021). Moreover, in contrast to electrophilic groups that only modify catalytically active proteins, photoreactive warheads label both inactive and active proteins and are therefore less frequently used in ABPP studies (Shindo & Ojida, 2021). Lastly, the reporter tag is often either biotin, a fluorophore, or a group that may be modified in an orthogonal reaction (e.g., click chemistry), which permit the analysis of probe-labelling events (Niphakis & Cravatt, 2014).

Click chemistry has become an attractive strategy utilized in ABPP because it permits probes to be designed that do not suffer the limitations that arise as a consequence of the large, bulky structure of reporter tags, such as poor cell permeability and inaccessibility to protein active sites (Speers & Cravatt, 2009; S. Wang *et al*., 2018). Typically, proteins are first labelled with a small-molecule ABP that contains a terminal azide or alkyne. The alkyne or azide of the probe is then reacted with the azide or alkyne, respectively, of a reporter group via a copper (I)-catalyzed azide-alkyne cycloaddition (CuAAC) reaction to yield thermally and hydrolytically stable 1,4-disubstituted 1,2,3-triazole products (**Scheme 2.1**) (Deng *et al*., 2020; Kolb & Sharpless, 2003; Li & Zhang, 2016 Rostovtsev *et al*., 2002; Speers & Cravatt, 2004; S. Wang *et al*., 2018).

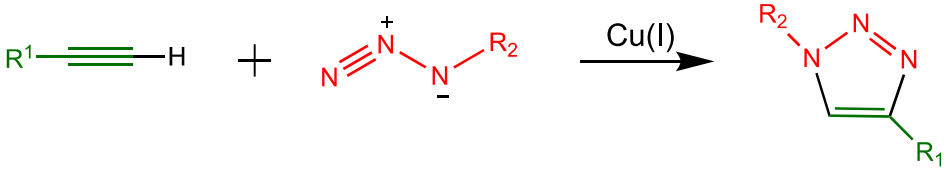

Scheme 2.1 General CuAAC reaction.

The CuAAC reaction (click chemistry) was first described by Sharpless and colleagues in 2002 as a Cu(I)-catalyzed, stepwise variant of Huisgen's 1,3-dipolar cycloaddition between azides and alkynes, that showed a 10^6-10^7-fold increase in the reaction rate relative to the uncatalyzed reaction (Kolb & Sharpless, 2003; Li & Zhang, 2016; Rostovtsev *et al*., 2002). Sodium ascorbate is the most commonly used reducing agent for copper(II) reduction in the CuAAC reaction, but hydroxylamine and tris(2-carboxyethyl)phosphine hydrochloride (TCEP) have also been employed (Presolski *et al*., 2011; Rodionov *et al*., 2007; Rostovtsev *et al*., 2002). Accelerating ligands such as

tris(hydroxypropyltriazolyl)methylamine (THPTA) and tris-[(1-benzyl-1H-1,2,3-triazol-4-yl)methyl]amine (TBTA) contain copper-chelating moieties, which are commonly employed to improve the kinetics of the CuAAC reaction (Hong *et al*., 2010; Presolski *et al*., 2011; Rodionov *et al*., 2007). Typically, five equivalents of ligand are used for every one equivalent of copper (Hong *et al*., 2010; Presolski *et al*., 2011). As sacrificial reducing agents, these ligands maintain the cuprous oxidation state to not only accelerate the reaction, but further to protect against reactive oxygen species-induced toxicity that arises from the CuAAC reaction, thus, improving the biocompatibility of the reaction when conducted *in vivo* (Hong *et al*., 2010; Presolski *et al*., 2011). While conditions for the CuAAC reaction can be optimized, in general, the reaction is described as highly robust and flexible, proceeding efficiently over a broad pH range (~ 4 – 12), over a broad temperature range, and in a variety of solvents (Presolski *et al*., 2011; Rodionov *et al*., 2007; Rostovtsev *et al*., 2002).

2.1.3 ANALYSIS OF ABPP EVENTS

Methods for the identification and quantification of probe-labelled proteins differ based on the type of reporter tag used. Proteins tagged with fluorophores, such as rhodamine, cyanine, and fluorescein, are typically resolved on an SDS-PAGE gel and most commonly visualized using in-gel fluorescence scanning (Wright *et al*., 2009). In contrast, biotinylated proteins are first enriched on streptavidin or avidin beads, since their affinity for biotin is extremely high with dissociation constants (K_d) of 4×10^{-14} M (Green, 1990) and ~10^{-15} M (Green, 1963b, 1963a), respectively (Galmozzi *et al*., 2014). The bead-bound biotinylated proteins are subsequently washed thoroughly to remove

non-biotinylated proteins and subjected to on-bead trypsin digestion (Galmozzi *et al*., 2014; Speers & Cravatt, 2009). The resulting peptides are then analyzed using LC-MS/MS. Fluorescent tagging is an attractive approach for the rapid analysis of samples and can be used for most activity-based applications (Wright *et al*., 2009). However, due to the lack of sensitivity, fluorescent tagging is a more limited approach as low abundance proteins in a proteome may not be detected (Deng *et al*., 2020). To overcome this limitation, biotin tagging can be employed to identify proteins from complex proteomes and identify enzyme inhibitors due to the high sensitivity and resolution of the MS-based approach (Cravatt *et al*., 2008; Deng *et al*., 2020; Niphakis & Cravatt, 2014).

2.1.4 TARGET DISCOVERY

The identification of proteins in various biological systems remains one of the primary applications of ABPP. Probes can be designed as either "broad-spectrum" or "tailor-made" (Niphakis & Cravatt, 2014). Broad-spectrum probes are typically used to target a large number of enzymes that share common structural or catalytic features, which can include entire enzyme families, such as serine hydrolases (Liu *et al*., 1999), oxidoreductases (Wright *et al*., 2009), phosphatases (Kumar *et al*., 2004), kinases (Patricelli *et al*., 2007), glycosidases (S. J. Williams *et al*., 2006), and metalloproteases (Saghatelian *et al*., 2004). The ability to profile families or classes of enzymes in parallel within a mechanistically similar enzyme group allows for the identification of individual members that are differentially active or expressed in a disease state for example (Cravatt *et al*., 2008; Nomura *et al*., 2010). Once identified, these enzymes can become therapeutic targets for the development of inhibitors (Niphakis & Cravatt, 2014). While

broad-spectrum probes are more commonly employed, tailor-made probes, which target a distinct set of enzymes, or an individual enzyme of interest, offer unique advantages in ABPP (Deng *et al*., 2020). Tailor-made probes are highly selective, allowing for the low-abundance proteins to be profiled that may otherwise be obscured by the presence of high-abundance proteins using a broad-spectrum probe (Niphakis & Cravatt, 2014). In addition, these selectively designed probes are commonly used to localize specific proteins(s) within cells, tissues, and organisms (Deng *et al*., 2020; Niphakis & Cravatt, 2014).

ABPP also provides a valuable means of assigning uncharacterized enzymes into a class, based on their ability to react with a given probe (Jessani *et al*., 2005; Niphakis & Cravatt, 2014). Further, determining the active-site architectures of these enzymes can facilitate the determination of specific substrates for the enzyme and further, the design of inhibitors (Jessani *et al*., 2005; Niphakis & Cravatt, 2014). Jessani and colleagues (2005) used ABPP to classify sialic acid 9-*O*-acetylesterase, a previously uncharacterized enzyme due to the lack of amino acid sequence similarity to any enzyme class, into the serine hydrolase superfamily. ABPP provides the ability to classify previously cryptic enzymes on the basis of probe reactivity and specific labelling sites, rather than by amino acid sequence comparisons (Jessani *et al*., 2005).

2.1.5 INHIBITOR DISCOVERY

The discovery and optimization of enzyme inhibitors is another primary application of ABPP technology in proteomics. From complex proteomes, potential inhibitors can be screened against a plethora of enzymes in parallel to determine their

selectivity and potency (Nomura *et al*., 2010; Patricelli *et al*., 2007; Wright & Cravatt, 2007). Thereafter, inhibitors can be refined to improve their potency towards selected enzyme(s) (Cravatt *et al*., 2008). This ABPP approach to inhibitor discovery greatly improves the throughput of inhibitor screening by alleviating the requirement for recombinant protein expression and purification (Niphakis & Cravatt, 2014).

In this method, proteins are preincubated with an irreversible or reversible competitive inhibitor for a defined period of time, then they are reacted with the ABP, followed by analysis using either in-gel fluorescence scanning (fluorescent tag) or LC-MS/MS (biotin tag) (**Figure 2.1**) (Galmozzi *et al*., 2014). A reduction or loss in signal intensity using either reporter tag is indictive of competitive inhibition and the reduction in the number of free sites that can be labelled by the ABP (Patricelli *et al*., 2007). While competitive irreversible inhibitors are more commonly employed in ABPP, competitive reversible inhibitors can also be studied under modified conditions (Adibekian *et al*., 2012; Leung *et al*., 2003). Analysis of competitive irreversible inhibitors is more straightforward, as once enzymes are covalently modified by an irreversible inhibitor, those sites cannot be later modified by the addition of the ABP probe (Galmozzi *et al*., 2014; Niphakis & Cravatt, 2014). In contrast, the inhibition by reversible inhibitors requires a kinetically controlled approach to determine how quickly inactivation by the ABP occurs relative to the reversible inhibitor (Adibekian *et al*., 2012; Galmozzi *et al*., 2014; Leung *et al*., 2003; Niphakis & Cravatt, 2014).

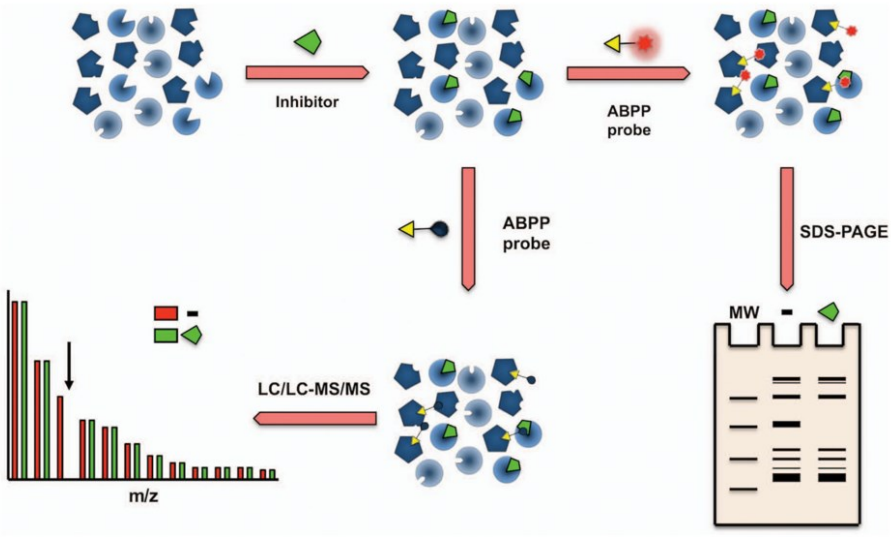

Figure 2.1 Competitive activity-based protein profiling. Proteins are pre-incubated with no inhibitor (control) or with inhibitor (sample) and are subsequently reacted with the activity-based probe, followed by analysis using in-gel fluorescence scanning or LC-MS/MS for fluorescent tagging or biotin tagging, respectively. Competitive inhibition is demonstrated by the reduction or complete loss in signal intensity in both methods (Galmozzi *et al*., 2014).

2.1.6 IDENTIFICATION OF PROTEINS WITH CONSERVED ARCHETECTURES

Another ABPP proteomic strategy involves targeting proteins that contain conserved architectures, rather than targeting a specific enzyme family with a given catalytic mechanism. For example, Patricelli and colleagues (2007) used nucleotide acyl phosphate probes with an initial goal of targeting protein kinases from human cancer cell lines and further profiling their inhibition using known kinase inhibitors. In their probe design, either ATP or ADP was used as the structural scaffold (binding group) to direct the probe to the ATP-binding pocket (Patricelli *et al*., 2007). Once bound, the acyl phosphate moiety (reactive group) was attacked by one of two conserved active-site lysine residues (Patricelli *et al*., 2007). Given that numerous enzymes can bind ATP/ADP, the resulting proteome coverage targeted by these probes was described as

broadly specific, which predominantly targeted not only protein kinases, metabolic kinases, and ATPases, but also GTPases, FAD/NAD-utilizing enzymes, adenine nucleotide synthetic enzymes, and DNA/RNA binding enzymes (Patricelli *et al*., 2007). Unlike most ABPP approaches reported in the literature that contain a more specific binding group and reactive warhead designed to solely target a specific family of enzymes, these findings by Patricelli and colleagues (2007) demonstrated a more broad-spectrum probe design that could modify a diverse array of ADP/ATP-binding proteins that share conserved structural motifs. For my research, the objective was to develop an activity-based probe that could covalently modify proteins containing a specific protein architecture; specifically, those with a nucleophile adjacent to a cationic binding site.

2.1.7 TWO PROTEINS WITH KNOWN ARCHITECTURES CONTAINING A NUCLEOPHILIE ADJACENT TO A CATIONIC BINDING SITE

2.1.7.1 D-3-Hydroxybutyrate dehydrogenase

2.1.7.1.1 Reaction and metabolic role

D-3-Hydroxybutyrate dehydrogenase (3-HBDH) (EC 1.1.1.30) is a homo-tetrameric enzyme that catalyzes the reversible reduction of acetoacetate to D-3-hydroxybutyrate using the coenzyme NADH (**Scheme 2.2**) (Hoque *et al*., 2008, 2009; Kanazawa *et al*., 2016). 3-HBDH belongs to the short-chain dehydrogenase/reductase (SDR) superfamily of enzymes, which is found in all three domains of life (Aneja *et al*., 2002; Cahill, 2006; Krishnakumar *et al*., 2008; Machado *et al*., 2020). The structure and active-site architecture will be discussed in full detail in Section 2.3.9. Briefly, SDR family members share highly conserved three-dimensional structures and conserved

active-site residues, including the catalytic tetrad: Asn-Ser-Tyr-Lys (Filling *et al*., 2002; Kavanagh *et al*., 2008; Machado *et al*., 2020; Nakashima *et al*., 2009). Catalysis by 3-HBDH from *Pseudomonas lemognei* occurs via an ordered Bi-Bi kinetic mechanism, whereby NADH/NAD^+ must bind before acetoacetate/D-3-hydroxybutyrate (Kluger *et al*., 1978).

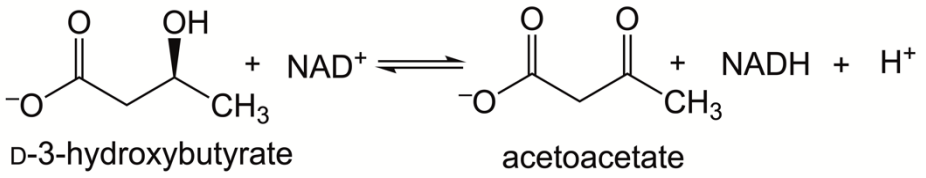

Scheme 2.2 Reversible, stereospecific reaction catalyzed by 3-HBDH

Acetoacetate, D-3-hydroxybutyrate, and acetone are water-soluble ketone bodies that serve as vital energy sources when glucose supplies are low (Hoque *et al*., 2009; Kanazawa *et al*., 2016; Newman & Verdin, 2014). In humans, ketone bodies are synthesized in the liver (Kanazawa *et al*., 2016). Acetoacetate and D-3-hydroxybutyrate are transported to organs such as the brain, heart, and kidney where they are converted into two molecules of acetyl-CoA during periods of strenuous exercise or prolonged starvation (Cahill, 2006; Kanazawa *et al*., 2016). The accumulation of ketone bodies to excess concentrations, however, can lead to ketoacidosis and is most commonly observed in cases of type I diabetes (Hoque *et al*., 2009). Under normal conditions, D-3-hydroxybutyrate is the most abundant ketone body in the blood, accounting for approximately 75% of ketone bodies present at normal levels, where acetoacetate is less stable and can undergo nonenzymatic decarboxylation to yield acetone, which is excreted

(Custer *et al*., 1983; Koch & Feldbruegge, 1987; Shimomura *et al*., 2013). However, during ketoacidosis, the level of D-3-hydroxybutyrate is much higher than normal to varying degrees and is therefore used as a means of diagnosing ketoacidosis (Koch & Feldbruegge, 1987; Kwan *et al*., 2006; Shimomura *et al*., 2013). Given the severe and life-threatening nature of ketoacidosis, 3-HBDH is of therapeutic interest as a both a probe for monitoring D-3-hydroxybutyrate levels in the blood and for inhibitor design to alleviate symptoms of ketoacidosis (Kanazawa *et al*., 2016; Kwan *et al*., 2006; Nakashima *et al*., 2009; Shimomura *et al*., 2013; Tan *et al*., 1975).

2.1.7.1.2 Inactivation of 3-HBDH by methyl acetyl phosphate

3-HBDH from *P. lemognei* exhibits high specificity for its substrates, acetoacetate and D-3-hydroxybutyrate, as only 3-ketocarboxylic acid homologues and acetone sulfonate have been shown to be suitable alternative substrates for the enzyme (Delafield *et al*., 1965; Kluger *et al*., 1978). Kluger and colleagues suggested that a cationic binding site at the active site of 3-HBDH serves as the recognition site for the anionic carboxylate group of the substrate (Kluger *et al*., 1978; Kluger & Tsui, 1981). They further suggested that a second group, a conjugate base of hydrogen bond donor, subsequently interacts with the carbonyl group of acetoacetate and the corresponding hydroxyl group of D-3-hydroxybutyrate (Kluger *et al*., 1978). Given this model, methyl acetyl phosphate (MAP) was designed and synthesized as a substrate analogue for acetoacetate with intent of irreversibly inactivating 3-HBDH (Kluger & Tsui, 1980). MAP was designed to be highly stable in the absence of nonenzymatic nucleophiles, such that the anionic

phosphate group of MAP must first interact with the cationic binding site of 3-HBDH prior to acetylation of the adjacent nucleophile (**Figure 2.2**) (Kluger & Tsui, 1980).

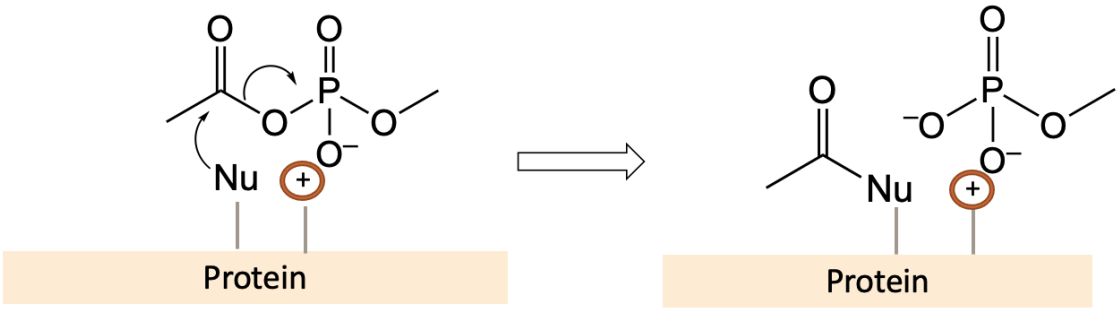

Figure 2.2 Covalent modification of proteins with active-site nucleophiles adjacent to a cationic binding site by MAP.

MAP was found to be both a competitive inhibitor and an irreversible inactivator of 3-HBDH (Kluger & Tsui, 1986). The observed pseudo first-order rate constant (k_{obs}) for the inactivation of 3-HBDH by MAP was found to be highly dependent on pH, where the rate of inactivation increased from pH 6.5-8.9 (Kluger & Tsui, 1986). Moreover, the pH-dependence of the rate of inactivation suggested to Kluger and co-workers that acetylation within the 3-HBDH active site occurs at a base with a pK_a of 8.2 (Kluger & Tsui, 1986). Due to the high reactivity of acetyl phosphates towards primary amines (Di Sabato & Jencks, 1961a, 1961b), these authors postulated that the reactive site was a lysine residue that resided adjacent to a cationic site, since such an architecture would be expected to perturb the pK_a downward, therefore, explaining the reduced pK_a of 8.2 and increased reactivity of the nucleophile (Kluger & Tsui, 1986). While the pH-dependence of the inactivation provided evidence suggesting that the attacking nucleophile is a lysine, no further studies were conducted to confirm this hypothesis nor to determine the specific active-site lysine residue(s) being modified.

Further, protection studies using methyl acetonylphosphonate, a substrate analogue and strong competitive inhibitor against acetoacetate, in the presence of coenzyme NADH, demonstrated clear protection against the inactivation of 3-HBDH by MAP (Kluger & Tsui, 1986). This observation further demonstrated that the acetylation by MAP occurs at the cationic active site of 3-HBDH (Kluger & Tsui, 1986).

2.1.7.2 Modification of Hb by MAP

Extending the use of MAP to other proteins, MAP was later shown to acetylate hemoglobin (Hb) (Ueno *et al*., 1986, 1989; Xu *et al*., 1999). The discovery of compounds that acetylate Hb is of therapeutic interest for the treatment of sickle cell disease (Xu *et al*., 1999). These compounds are designed to target the 2,3-diphosphoglycerate (2,3-DPG) binding site, resulting in the reduced binding of 2,3-DPG and thus increasing the affinity of Hb for oxygen (Klotz & Tam, 1973). Since 2,3-DPG is a trianionic compound that binds at the cationic region at the center of the Hb tetramer, MAP, bearing a single negative charge, was suggested to be a potent acetylating agent of nucleophiles within this cleft (Ueno *et al*., 1986, 1989; Xu *et al*., 1999). Ueno *et al.* (1986, 1989) first used high-performance liquid chromatography (HPLC) peptide mapping to identify three residues of human Hb modified by MAP within the 2,3-DPG binding cleft between the β-chains of the tetramer: βVal 1, βLys 82, and βLys 144 (**Figure 2.3**). Xu *et al*. (1999) later confirmed these findings using heteronuclear multi-quantum coherence spectroscopy and heteronuclear single-quantum coherence spectroscopy NMR studies and determined that there was a clear preference towards the MAP-dependent acetylation of βLys 82 relative to βVal 1 and βLys 144.

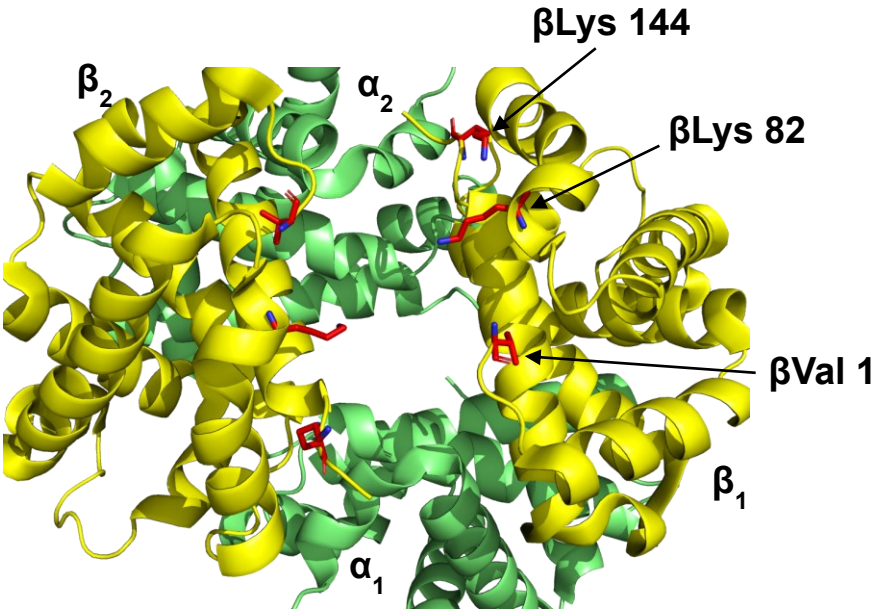

Figure 2.3 Acetylation of Hb by MAP. Three residues in the 2,3-DPG binding cleft between the β-chains of the tetramer were covalently modified by MAP: Val 1, Lys 82, and Lys 144 (PDB: 1DKE) (Ueno *et al*., 1986).

Similarly, aspirin (acetylsalicylate) is an anionic compound that has been found to acetylate Hb (Bridges *et al*., 1975; Klotz & Tam, 1973; Xu *et al*., 1999). In agreement with the pH-dependent inactivation study of 3-HBDH by MAP (Kluger & Tsui, 1986), the acetylation of Hb by aspirin was also found to be pH-dependent, with the rate of reaction increasing from pH 6.5-8.5, exhibiting a plateau from pH 8.5-9.0, and decreasing above pH 9.5 (Bridges *et al*., 1975). Bunn and colleagues (1975) therefore suggested that the acetylation of Hb is likely to occur primarily at lysine residues, which agrees with conclusions made by Kluger and Tsui (1986) with 3-HBDH as previously discussed. Xu *et al*. (1999) later confirmed these early findings by conducting protection studies with aspirin and MAP, determining that both compounds modify βLys 82 in the 2,3-DPG binding cleft.

2.1.8 OVERVIEW OF THIS WORK

ABPP is becoming an increasingly employed strategy in the field of proteomics due to its large diversity of applications and ability to profile proteins in highly complex proteomes. For this work, I synthesized sodium methyl hex-5-ynoyl phosphate (SMHP), a small-molecule probe, designed to target protein architectures with a nucleophile adjacent to a cationic binding site (**Scheme 2.3**). The monomethyl acyl phosphate warhead of the probe was chosen based on its stability in aqueous solutions and reactivity with nucleophiles relative to its acyl phosphate and dimethyl acyl phosphate counterparts (Di Sabato & Jencks, 1961a, 1961b). Specifically, the acyl phosphate moiety bearing two negative charges is hydrolytically stable and very slow to react with nucleophiles (Di Sabato & Jencks, 1961a, 1961b). In contrast, the dimethyl acyl phosphate moiety bearing a neutral charge is hydrolytically unstable and can react non-specifically, such as through nucleophilic attack by water, since the dimethyl phosphate is a very good leaving group (Di Sabato & Jencks, 1961a, 1961b). Lastly, the monomethyl acyl phosphate bearing a single negative charge remains hydrolytically stable, whereupon reaction with protein nucleophiles arises only when the compound is bound to a cationic site due to the partial neutralization of the negative charge, thereby mimicking the reactivity of a dimethyl acyl phosphate (Di Sabato & Jencks, 1961a, 1961b). Given the structural similarity between the anionic monomethyl acyl phosphate warhead of our probe, SMHP, and MAP (**Figure 2.4**), I anticipated that SHMP would modify 3-HBDH (Kluger & Tsui, 1980, 1986) and hemoglobin (Ueno *et al*., 1986, 1989; Xu *et al*., 1999). I further used SMHP to probe the proteome of *Pseudomonas lemognei* to identify proteins that contained sites with architectures bearing a nucleophile adjacent to a cationic site. Overall, 281 enzymes were

identified, including 3-HBDH. Next, I characterized the interaction of SMHP and MAP with purified 3-HBDH from *Pseudomonas lemognei* and CTP synthase (CTPS) from *E. coli* using fluorescent tagging, LC-MS/MS, and kinetics (UV-based assays).

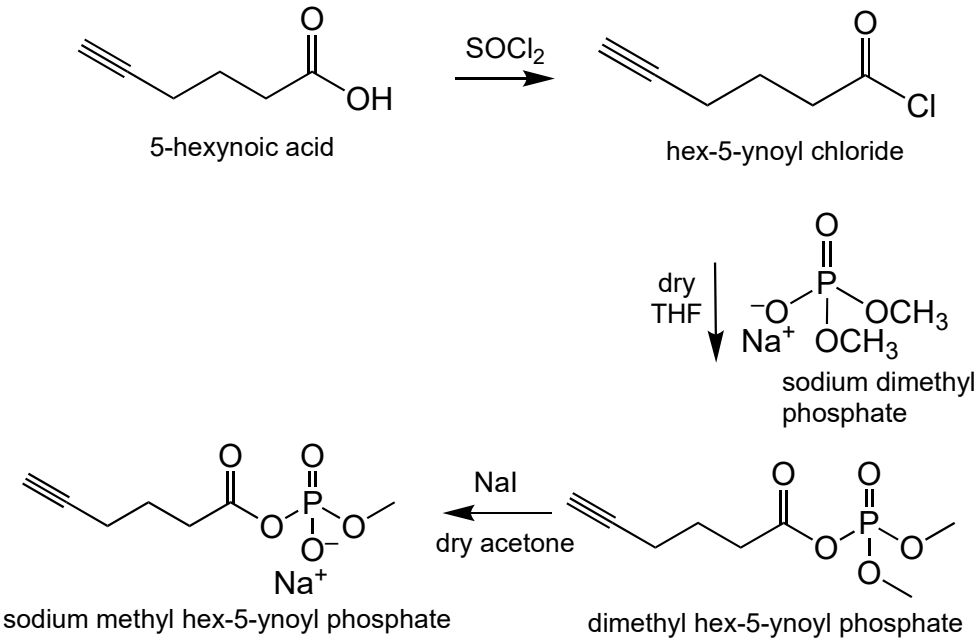

Scheme 2.3 Synthesis of sodium methyl hex-5-ynoyl phosphate (SMHP).

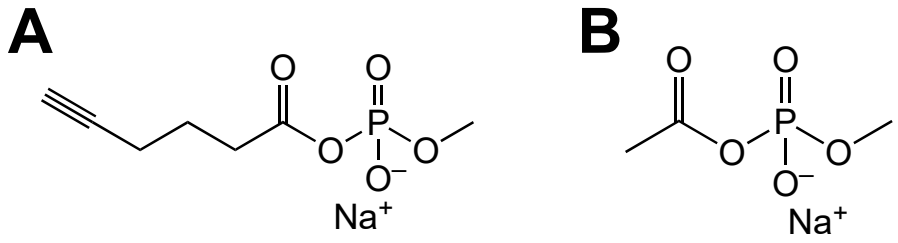

Figure 2.4 Structures of SMHP and MAP. (A) SMHP and (B) MAP both contain an anionic monomethyl acyl phosphate motif that was designed to modify protein architectures with a nucleophile adjacent to a cationic binding site.

2.2 MATERIALS AND METHODS

2.2.1 GENERAL

All reagents were purchased from Sigma-Aldrich Canada Ltd. (Oakville, ON, Canada) unless otherwise stated. His·Bind resin (Novagen) was purchased from EMD Millipore Corp. (Billerica, MA, USA). *Pseudomonas (Paucimonas) lemognei* (DSM 7445) was purchased from DSMZ (Braunschweig, Germany). ®Strata C18-E (55 µm, 70 Å) columns were purchased from Phenomenex **(**Torrance, CA, USA). Streptavidin Agarose (Novagen) was purchased from EMD Chemicals (San Diego, CA, USA). Fluorescein picolyl azide (FPA), tris(hydroxypropyltriazolyl)methylamine (THPTA), and Biotin Azide Plus were purchased from Click Chemistry Tools (Scottsdale, AZ, USA). Pierce™ Trypsin protease (MS-Grade) was purchased from ThermoFischer Scientific (Whitby, ON, Canada). Solid Phase Extraction Disks (ENVI-Disk) was purchased from Supelco (Bellefonte, PA, Canada). OD_{600} values were measured and kinetic studies for 3-HBDH and CTPS were conducted using an HP-8453 UV-visible spectrometer. In-gel fluorescence experiments were carried out using a VersaDoc Imaging System (Bio-Rad). Nuclear magnetic resonance (^{1}H, ^{13}C, and ^{31}P) spectra were obtained using either a Bruker AV 300 or 500 MHz spectrophotometer at the Dalhousie University Nuclear Magnetic Resonance Research Resource Centre (NMR-3). Chemical shifts (δ in ppm) for ^{1}H NMR spectra are reported relative to the residual solvent signal for or HOD (δ 4.79) or $CDCl_3$ (δ 7.26), ^{13}C NMR spectra are reported relative to the residual solvent signal for $CDCl_3$ (δ 77.16) or a secondary reference, DSS (methyl signal), for D_2O, and ^{13}P spectra are reported relative to a secondary reference of 85% phosphoric acid (Gottlieb *et al*., 1997). High resolution mass spectra (HRMS) were obtained using either a Bruker

microTOF mass spectrometer or a Bruker compact QTOF mass spectrophotometer operating in the electrospray ionization (ESI) mode (positive or negative). Intact MS (LC-MS) and LC-MS/MS experiments were carried out at the Faculty of Medicine Biological Mass Spectrometry Core Facility at Dalhousie University. Methods for the synthesis of sodium methyl hex-5-ynoyl phosphate (SMHP) were developed by Gemma Regan (undergraduate student) and Dr. Stephen Bearne in 2014-2015.

2.2.2 SYNTHESES

2.2.2.1 Sodium dimethyl phosphate

Sodium iodide (29.98 g, 0.2 mol, 1 equiv.) and trimethyl phosphate (23.10 mL, 0.2 mol, 1 equiv.) were mixed in dry acetone (250 mL) and refluxed under argon overnight in a round-bottom flask (1 L) (Kluger *et al*., 1990). The product was collected by suction filtration as a white powder (27.86 g, 95% yield) (Kluger *et al*., 1990). ^{1}H NMR (500 MHz, D_2O) δ 3.55 (d, J = 10.7 Hz, 6H) (**Figure 2.5**).

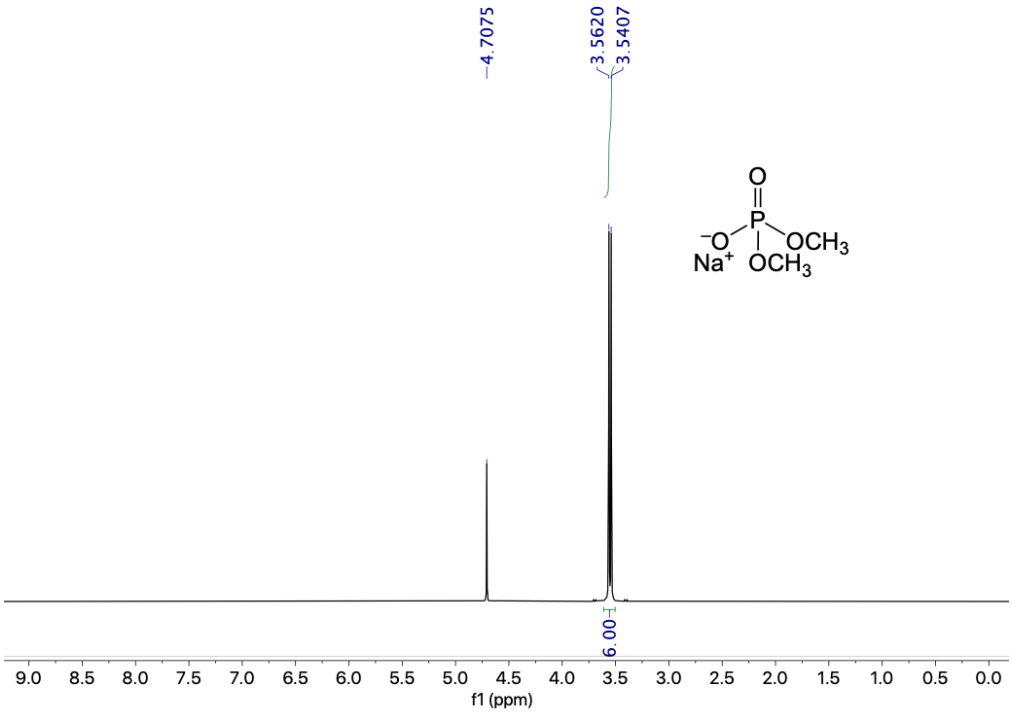

Figure 2.5 ^{1}H NMR spectrum of sodium dimethyl phosphate in D_2O.

2.2.2.2 Hex-5-ynoyl chloride

Freshly distilled thionyl chloride (8.5 mL, 116.5 mmol, 1.2 equiv.) was added to 5-hexynoic acid (10.78 g, 96.1 mmol, 1 equiv.) in a round-bottom flask (50 mL) (Kunzmann *et al*., 2011; Luxenhofer & Jordan, 2006). The mixture was refluxed under argon at 90 °C (oil bath) for ~1 h (Kunzmann *et al*., 2011; Luxenhofer & Jordan, 2006). The resulting dark red/brown solution was subsequently distilled, yielding a colourless liquid (b.p. 165 °C) (9.14 g, 72.8% yield) (Kunzmann *et al*., 2011; Luxenhofer & Jordan, 2006). The ^{1}H NMR spectrum was in agreement with that previously published for hex-5-ynoyl chloride (Kunzmann *et al*., 2011; Luxenhofer & Jordan, 2006).

2.2.2.3 Dimethyl hex-5-ynoyl phosphate

Hex-5-ynoyl chloride (2.30 g, 17.6 mmol, 1 equiv.) was added to a suspension of sodium dimethyl phosphate (2.62 g, 17.6 mmol, 1 equiv.) in dry tetrahydrofuran (THF) (dried over sodium) in a round-bottom flask (50 mL) and stirred overnight under argon at room temperature (Kluger *et al*., 1990). The mixture was filtered through a bed of celite prepared in dry THF, and the solvent was then removed from the resulting filtrate using rotary evaporation (30 °C) to yield the product as a yellow oil (2.65 g, 68.2% yield). ^{1}H NMR (300 MHz, $CDCl_3$) δ 3.91 (d, J = 11.7 Hz, 6H), 2.65 (t, J = 7.3 Hz, 2H), 2.32 (td, J = 6.9, 2.8 Hz, 2H), 2.01 (t, J = 2.7 Hz, 1H), 1.89 (p, J = 6.8 Hz, 2H) (**Figure 2.6**). ^{31}P NMR (122 MHz, $CDCl_3$) δ –5.8903 (**Figure 2.7**). Both NMR spectra are in agreement with the spectra observed by former Bearne lab member, Gemma Regan. ESI-HRMS (positive mode); *m*/*z* calculated for $C_8H_{13}Na_1O_5P_1$ $[M+Na]^+$: 243.0393, found: 243.0384 (**Figure 2.8**).

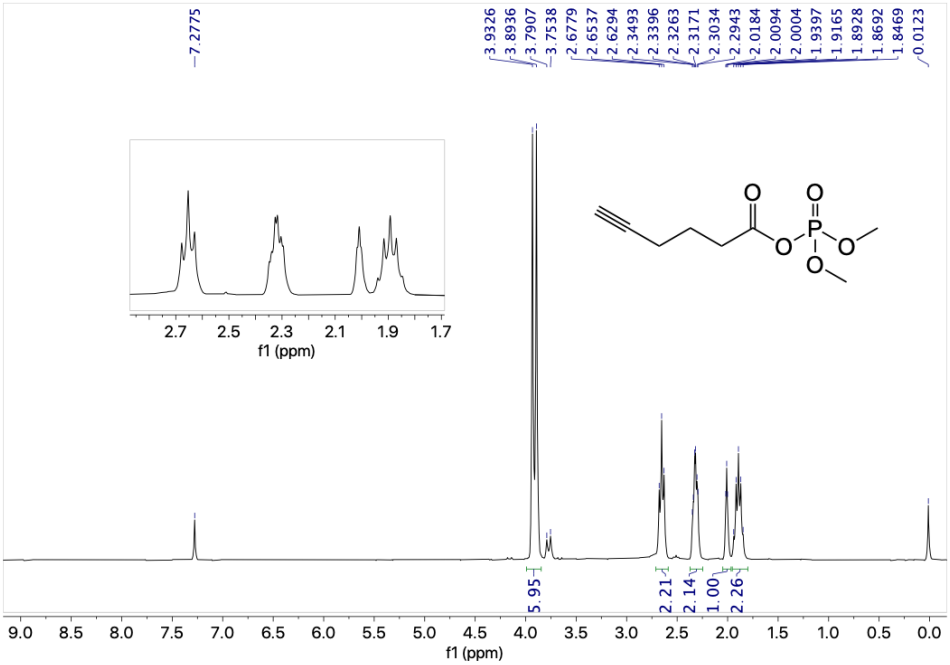

Figure 2.6 ^{1}H NMR spectrum of dimethyl hex-5-ynoyl phosphate in $CDCl_3$.

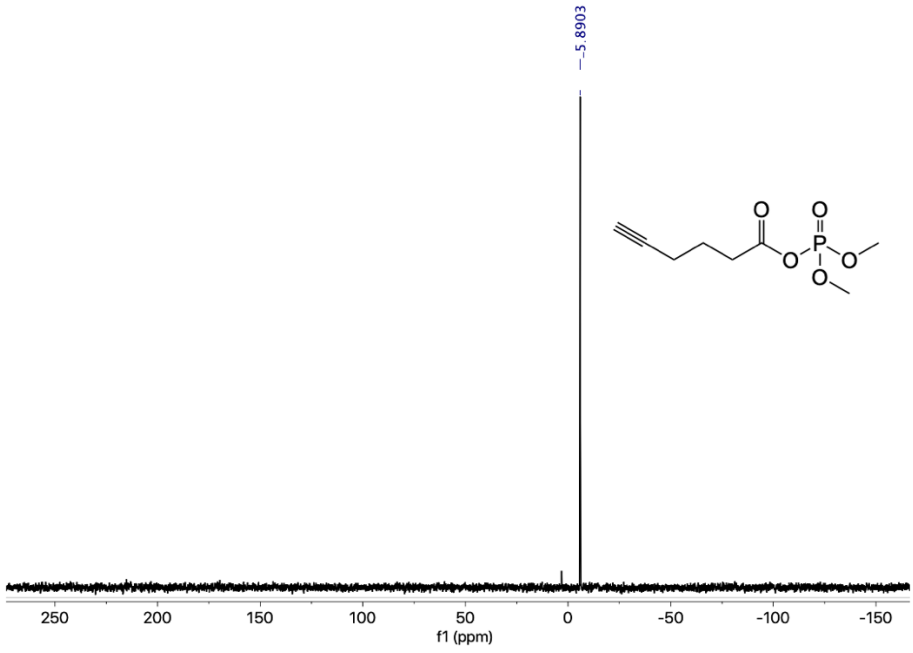

Figure 2.7 ^{31}P NMR spectrum of dimethyl hex-5-ynoyl phosphate in $CDCl_3$.

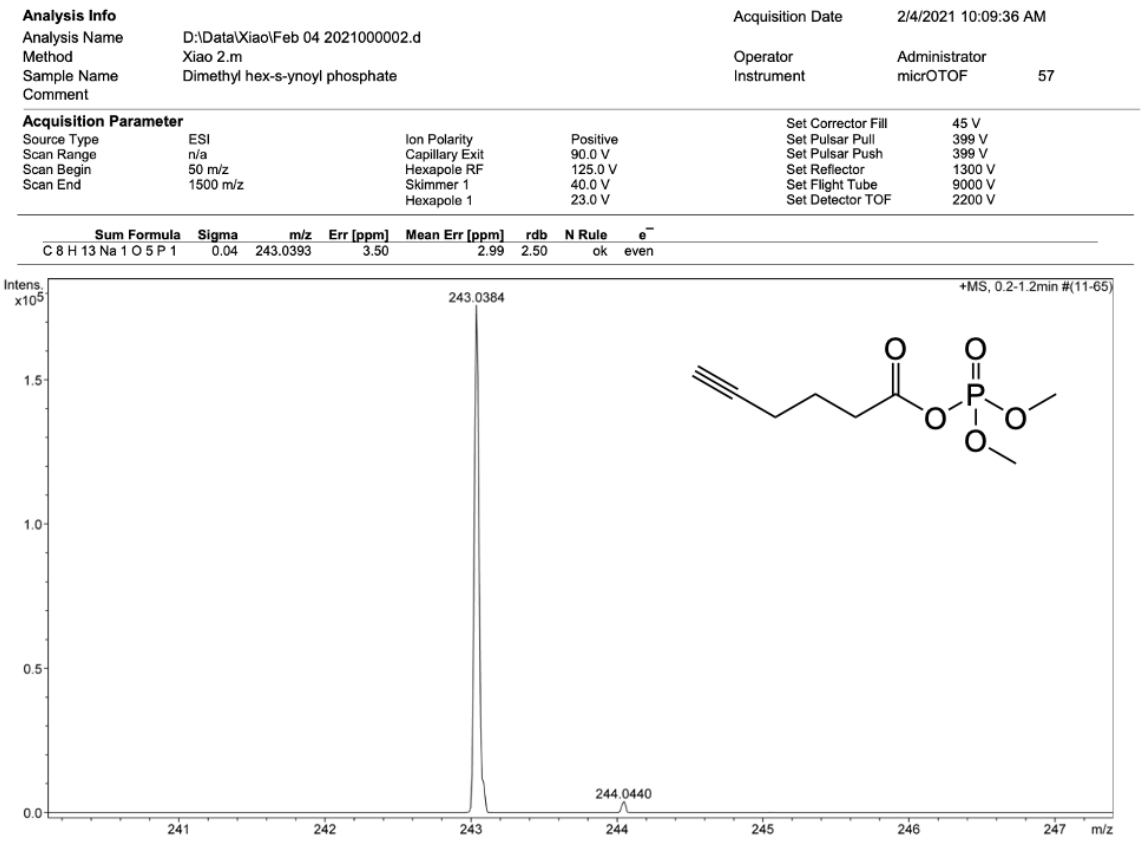

Figure 2.8 ESI-HRMS (positive mode) of dimethyl hex-5-ynoyl phosphate.

2.2.2.4 Sodium methyl hex-5-ynoyl phosphate

A solution of sodium iodide (1.57 g, 10.5 mmol, 1.2 equiv.) in dry acetone (~10 mL) was added to a solution of dimethyl hex-5-ynoyl phosphate (1.97 g, 8.95 mmol, 1 equiv.) and dry acetone (~6.5 mL) (Kluger *et al*., 1990). The mixture was stirred overnight under argon at room temperature. After rotary evaporation (30 °C), the resulting product was dissolved in ddH_2O (2.5 mL) and purified using a 60 mL ®Strata C18-E (55 µm, 70 Å) (2.66 × 3.45 cm) column that was pre-washed with acetonitrile (60 mL) and ddH_2O (120 mL). Fractions (2.5 mL) were collected and analyzed using thin layer chromatography (TLC) on cellulose with a water/isopropanol (30/70) mixture as the

eluent. The TLC plates were sprayed with a spray reagent for phosphates, which was prepared from 5-sulfosalicylic acid (7.0 g) and $FeCl_3$ (0.1 g) dissolved in water (75 mL), which was subsequently added to 95% ethanol (75 mL) as previously described (Clark & Switzer, 1977). Fractions showing the presence of phosphates were lyophilized in separate round-bottom flasks overnight and analyzed by ^{1}H NMR. The earlier collected phosphate fractions appeared as a white power, containing large amounts of starting material, sodium dimethyl phosphate. The later collected fractions appeared as a sticky/jelly-like substance and contained product, sodium methyl hex-5-ynoyl phosphate, with only a very small amount of starting material remaining. These latter fractions were then re-dissolved in ddH_2O (2.5 mL) and passed through an AG ®50W-X8 cation exchange resin (Na^+-form, 2.66 × 13.10 cm) (Bio-Rad Laboratories, Hercules, CA). This resin was pre-washed with 1 M NaCl (1 L) and ddH_2O (1 L). Fractions (2.5 mL) were collected, spotted on cellulose TLC strips, and analyzed using the spray reagent for phosphates. The resulting fractions containing product were lyophilized overnight to yield a colourless sticky/jelly-like product (0.3703 g, 1.6233 mmol, 18% yield). ^{1}H NMR (500 MHz, D_2O) δ 3.64 (d, J = 11.4 Hz, 3H), 2.59 (t, J = 7.3 Hz, 2H), 2.37 (t, J = 2.6 Hz, 1H), 2.28 (td, J = 7.0, 2.6 Hz, 2H), 1.83 (p, J = 7.2 Hz, 2H) (**Figure 2.9**). ^{13}C NMR (126 MHz, D_2O) δ 171.93 (d, J = 9.4 Hz), 84.7431, 70.0191, 53.75 (d, J = 6.4 Hz), 33.69 (d, J = 6.0 Hz), 22.8706, 16.9755 (**Figure 2.10**). ^{31}P NMR (202 MHz, D_2O) δ –5.9721 (**Figure 2.11**). ESI-HRMS (negative mode); m/z calculated for $C_7H_{10}O_5P$ $[M\text{-}H^+]^-$: 205.0271, found: 205.0272 (**Figure 2.12**).

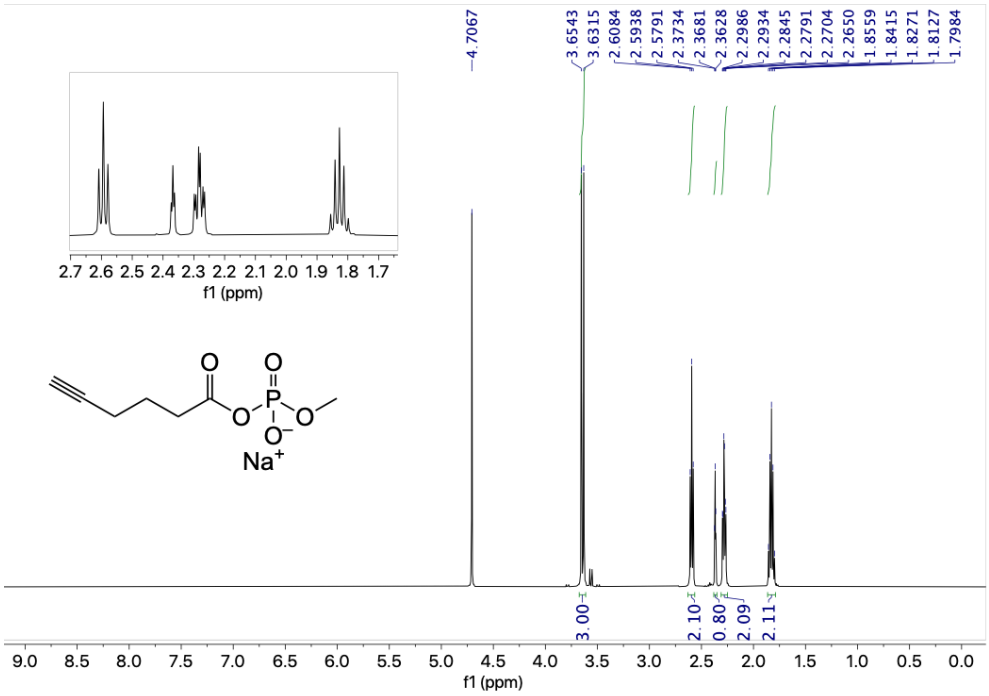

Figure 2.9 ^{1}H NMR spectrum of sodium methyl hex-5-ynoyl phosphate in D_2O.

Figure 2.10 ^{31}P NMR spectrum of sodium methyl hex-5-ynoyl phosphate

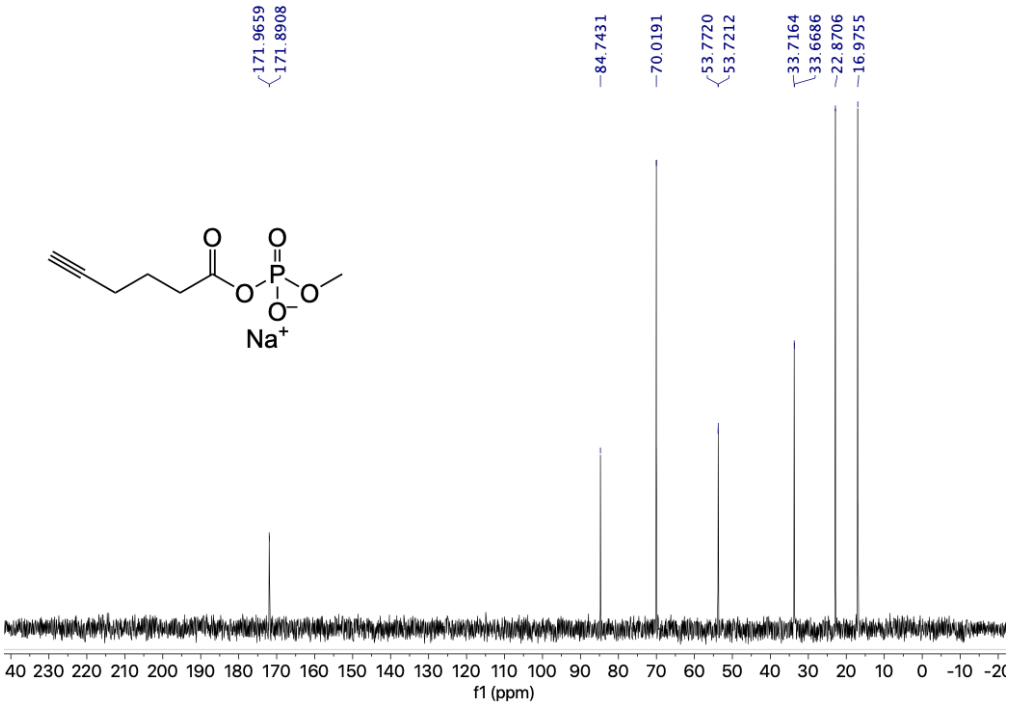

Figure 2.11 ^{13}C NMR spectrum of sodium methyl hex-5-ynoyl phosphate

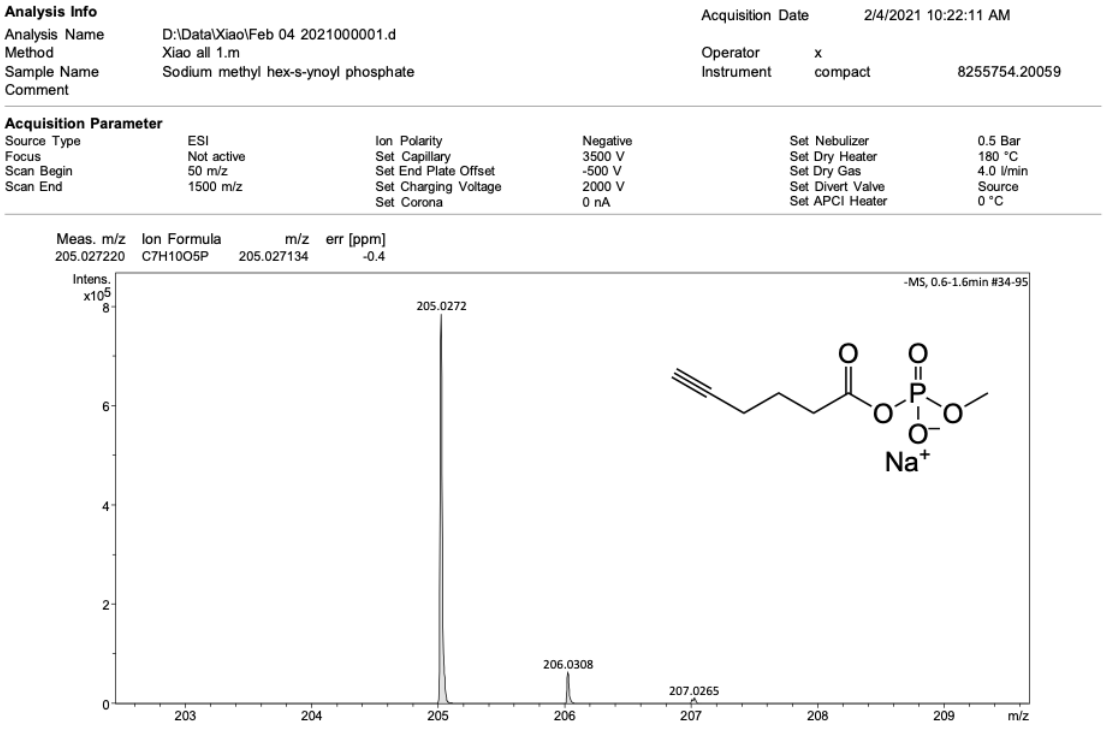

Figure 2.12 ESI-HRMS (negative mode) of sodium methyl hex-5-ynoyl phosphate

2.2.2.5 Methyl acetyl phosphate

MAP was synthesised using methods previously described (Kluger *et al*., 1990). Dimethyl acetyl phosphate was first synthesized from sodium dimethyl phosphate (14.8 g. 0.1 mol) and freshly distilled acetyl chloride (7.8 g, 0.1 mol) in dry THF, which was allowed to stir for 2 days under argon (room temperature) (Kluger *et al*., 1990). The solution was filtered through celite, and the solvent was removed under reduced pressure. The remaining oil was distilled (110 °C, 2 Torr) to yield dimethyl acetyl phosphate as a colourless liquid (9.37 g, 55.76 mmol, 56% yield) (Kluger *et al*., 1990). MAP was synthesized from dimethyl acetyl phosphate (2.4 g, 16 mmol) and sodium iodide (2 g, 16 mmol) in dry acetone as previously described (Kluger *et al*., 1990). The pale-yellow solution stirred overnight at room temperature under argon. After rotary evaporation, MAP was precipitated/crystallized by the addition of 2-propanol. The crude product was filtered, washed with dry acetone, and dried under vacuum to yield sodium methyl acetyl phosphate (MAP) as a white, powder compound (2.06 g, 11.70 mmol, 73% yield). The observed ^{1}H NMR spectrum was in agreement with the ^{1}H NMR spectrum previously reported for MAP (Kluger *et al*., 1990).

2.2.3. EXPRESSION AND PURIFICATION OF 3-HBDH

The open reading frame (EDC30_10172, TCS39122.1) encoding wild-type 3-HBDH from *Pseudomonas lemognei* (ATCC 17989) was synthesized and inserted into a pET-15b(+) vector between restriction sites NdeI and BamHI by BioBasic Inc. (Markham, ON). This construct encodes the wild-type 3-HBDH enzyme as a fusion protein bearing an N-terminal hexahistidine $(His)_6$-tag. Chemically competent *E. coli*

DH5α and *E. coli* BL21 (DE3) cells were transformed using the heat shock method (Sambrook *et al*., 1989) and grown on LB-agar plates containing ampicillin (100 μg/mL) overnight.

Transformants were grown overnight in LB media (5 mL) containing ampicillin (100 μg/mL) and were stored thereafter in 15% glycerol stocks at –80 °C. Starter cultures from the BL21 (DE3) cells from the freshly streaked agar plate or glycerol stocks were prepared and grown overnight (37 °C, 200 rpm) in LB media (5 mL) containing ampicillin (100 μg/mL). Starter cultures (10 mL) were used to inoculate larger expression culture(s) containing 1 L of LB media of the same composition and were grown (37 °C, 200 rpm) until an OD_{600} of ~0.5-0.6 was obtained. Recombinant protein expression was then induced by addition of isopropyl β-D-1-thiogalactopyranoside (IPTG) to a final concentration of 1 mM and the cultures were incubated at 37 °C for an additional 7-8 h (200 rpm). The cells were harvested by centrifugation (3795 × *g*, 10 min, 4 °C) and washed with binding buffer (20 mM Tris-Cl, 500 mM NaCl, 5 mM imidazole, pH 7.9). The cell pellet was stored at –20 °C for future use.

The frozen cell pellet was thawed and resuspended in cold binding buffer (~15 mL). The cell suspension was kept on ice and sonicated (6 × 30 s with 60-s off periods between each 30-s interval) using a Branson Sonifier 250 (setting 5.5, 1-s bursts). The cell lysate was clarified by ultracentrifugation (146 550 × *g*, 35 min, 4 °C) and applied to a column containing His·Bind resin (2.5 mL), pre-charged with Ni^{2+} as per the manufacturer's instructions (Novagen). After washing the column with binding buffer (25 mL), followed by wash buffer (15 mL) (20 mM Tris-Cl, 500 mM NaCl, 60 mM imidazole, pH 7.9), the 3-HBDH was eluted by the addition of strip buffer (10 mL) (20

mM Tris-Cl, 500 mM NaCl, 100 mM EDTA, pH 7.9). Eluted enzyme was dialyzed (MWCO 12 – 14 kDa) for 3 × 8 h (4 °C) against assay buffer (0.1 M Tris-Cl, pH 8.0 for ABPP studies or 0.1 M Tris-Cl, pH 7.8 for kinetic studies). Dialyzed enzyme was aliquoted and stored at –20 °C for future use. Protein concentrations were determined by conducting Bradford assays (Bio-Rad Laboratories, Mississauga, ON, Canada) with BSA standards or by UV absorbance at 280 nm. Using the ExPASy ProtParam web tool (Gasteiger *et al*., 2003), the molecular weight of recombinant wild-type 3-HBDH bearing an N-terminal $(His)_6$-tag was calculated to be 30039.15 Da with an extinction coefficient of 26470 $M^{-1}cm^{-1}$ (under the assumption that all cysteine residues were reduced). Protein purity was assessed using SDS-PAGE (12%) with Coomassie brilliant blue (R-250) staining.

2.2.4 EXPRESSION AND PURIFICATION OF CTPS

Plasmids containing the open reading frame encoding wild-type CTPS from *E. coli* (pET15b-CTPS1) were used to transform BL21 (DE3) cells for protein expression as previously described (Bearne *et al*., 2001). The expression and purification of CTPS was followed exactly as described for 3-HBDH in Section 2.2.3 and as described previously (Bearne *et al*., 2001). Upon elution with strip buffer (10 mL), CTPS was dialyzed (MWCO 12 – 14 kDa) for 3 × 8 h (4 °C) against assay buffer (70 mM HEPES, 10 mM $MgCl_2$, 0.5 mM EGTA, pH 8.0). Dialyzed enzyme was aliquoted and stored at –20 °C for future use. Protein concentrations were determined by conducting Bradford assays (Bio-Rad Laboratories, Mississauga, ON, Canada) with BSA standards. Protein purity was assessed using SDS-PAGE (10%) with Coomassie brilliant blue (R-250) staining.

2.2.5 EXPRESSION OF NATIVE PROTEINS FROM *P. lemognei*

P. lemognei was rehydrated from a dried culture (pellet) with ATCC medium 179 (*Pseudomonas* medium) (Delafield *et al*., 1965) as per the manufacturer's instructions (DSMZ). Agar plates and 50 mL cultures made with the same medium were prepared. Bacteria on agar were grown for ~72 h (30 °C) and those in the 50 mL cultures were grown for ~ 50 h (30 °C, 200 rpm). Glycerol stocks (15%) were prepared from both growth methods and stored at –80 °C. Starter cultures (5 mL) from the freshly streaked agar plate or glycerol stocks were prepared and grown overnight (30 °C, 200 rpm) in the ATCC medium 179. Starter cultures were used to inoculate larger expression culture(s) (15 mL starter culture per 1 L expression culture; 1 L typically used) of the same media composition and were grown (30 °C, 200 rpm) for 24 h until the late exponential growth phase was obtained (OD_{600} of ~1.4-1.6). The cells were harvested by centrifugation (3795 × *g*, 10 min, 4 °C) and resuspended in cold 0.1 M potassium phosphate buffer, pH 8.0 (~ 12 mL). The cell suspension was kept on ice and sonicated (6 × 30 s with 60-s off periods between each 30-s interval) using a Branson Sonifier 250 (setting 5.5, 1-s bursts). The cell lysate was clarified by ultracentrifugation (146 550 × *g*, 35 min, 4 °C). The total protein concentration was determined by conducting Bradford assays (Bio-Rad Laboratories, Mississauga, ON, Canada) with BSA standards.

2.2.6 FLUORESCENT TAGGING AND INTACT MS OF SMHP MODIFIED Hb

The click chemistry conditions for identifying proteins modified by SMHP were initially developed using human Hb. The click-chemistry protocols followed were similar to those described by the manufacturer (Click Chemistry Tools) and reported protocols in

the literature (Presolski *et al*., 2011; Shaw *et al*., 2021; Speers & Cravatt, 2004). Under optimized conditions, Hb (2 mg/mL) in 50 mM Tris-Cl, pH 7.5 buffer was reacted with SMHP (0.5 mM) for 2 h (37 °C). The fluorescein picolyl azide (FPA) tag (Click Chemistry Tools) (100 μM) was then coupled with the SMHP-labelled Hb using a CuAAC reaction, containing tris(hydroxypropyltriazolyl)methylamine (THPTA) (5.0 mM), copper (II) sulfate pentahydrate ($CuSO_4 \bullet 5H_2O$) (1.0 mM) and sodium ascorbate (14.7 mM). Stocks of each click reagent were prepared in ddH_2O. Following a 1-h reaction (room temperature) with gentle rotational mixing, SDS-loading buffer (1× final) was added to each reaction and the Hb-containing samples were subsequently resolved on a 15% SDS-PAGE gel. As described in previously reported protocols, excess click-chemistry reagents were not removed prior to electrophoresis (Speers & Cravatt, 2004). Samples were analyzed using the Versadoc Imaging System with Alexa 488 as the filter setting (FPA λ_{ex} = 490 nm, λ_{em} = 510 nm). Gels were later stained with Coomassie brilliant blue (R-250).

Intact MS (LC-MS) was used to verify the presence of the 94-Da adduct formed upon acylation of Hb by SMHP through the reaction of Hb (2 mg/mL) with SMHP (0.5 mM) (i.e., sample) or no SMHP (i.e., control) for 2 h (37 °C). To demonstrate successful labelling of Hb by the probe, CuAAC reactions were conducted in parallel for both the sample and control, followed by gel-based analysis.

2.2.7 DEVELOPMENT OF A BIOTIN-ABPP PROTOCOL WITH ELUTION OF STREPTAVIDIN ENRICHED BIOTINYLATED PROTEINS

2.2.7.1 Hb

For two 0.5-mL aliquots of Hb sample (2 mg/mL Hb, 0.5 mM SMHP) and control (2 mg/mL Hb, 0 mM SMHP), after reacting for 4 h (37 °C), CuAAC reactions were conducted as described in Section 2.2.6, except that Biotin Azide Plus (BAP) tag (Click Chemistry Tools) (75 μM) instead of FPA was used. Following the CuAAC reaction, three precipitation treatments were explored with Hb, each giving similar recovery yields: no solvent, cold acetone, and methanol/chloroform (MeOH: ddH_2O: $CHCl_3$) (4: 3: 1). For the methanol/chloroform precipitation, which was further used for the precipitation of the *P. lemognei* proteins (Section 2.2.7.2), precipitation was carried out using standard methods previously described (14 000 × g, 4 °C) (Speers & Cravatt, 2009; Staubach *et al*., 2022; Wessel & Flügge, 1984). As previously described by the Cravatt group, pellets were washed with cold MeOH (3×) (500 μL) to remove excess click reagents and the aliquot pairs were combined thereafter (Weerapana *et al*., 2008). The pellets were resolubilized in phosphate buffered saline (PBS) (pH 7.4) containing 1.2% SDS with brief sonication and heating (80 °C, ~5 min) (Weerapana *et al*., 2008). PBS was added to samples to yield a final SDS concentration of 0.2%. (Weerapana *et al*., 2008). To each tube, pre-washed streptavidin-agarose beads (100 μL in a 50% slurry of storage buffer, containing sodium phosphate (10 mM) and sodium azide (0.02%)) (Novagen) was added and the suspension was incubated for 3 h at room temperature with gentle mixing by rotation (Weerapana *et al*., 2008).

After centrifugation (1400 × *g*, 2 min, room temperature) the supernatant was discarded and the streptavidin beads were washed with 0.2% SDS/PBS (3 × 1 mL),

followed by PBS (3 × 1 mL) to remove non-biotinylated Hb (Galmozzi *et al*., 2014; Weerapana *et al*., 2008). To develop the biotin-ABPP protocol, the enriched, biotinylated SMHP-Hb construct was eluted from the streptavidin agarose beads using harsh denaturing conditions. This allowed for the visualization of probe-modified Hb by SDS-PAGE, whereas on-bead trypsin digestion, which will be employed later for biotin-ABPP protocols, does not permit demonstration of labelling of proteins prior to LC-MS/MS analysis. The modified Hb was recovered from the streptavidin-agarose beads upon incubation with a previously reported elution buffer for streptavidin-enriched biotinylated proteins (2% SDS, 6 M urea, 2 M thiourea, 30 mM biotin, in PBS) for 15 min at room temperature, followed by 15 min at 90 °C (Rybak *et al*., 2004). SDS-PAGE gels (15%) were employed to confirm the elution of labelled Hb using both Coomassie brilliant blue (R-250) staining and silver staining (Shevchenko *et al*., 1996).

2.2.7.2 *P. lemognei* proteins

The method described in Section 2.2.7.1 for Hb was also followed for the analysis of the cell lysate containing the soluble proteome of *P. lemognei*. Prior to reacting the lysate proteins with the SMHP probe, however, 4 mL of the clarified lysate was incubated with the streptavidin-agarose beads (400 µL of a 50% slurry) (30 min, 4 °C) in attempt to remove as many non-biotinylated streptavidin-binding proteins as possible. After centrifugation to remove the beads, 2 × 0.5 mL aliquots of the SMHP-treated sample (3.2 mg/mL lysate proteins, 0.5 mM SMHP) and the untreated control (3.2 mg/mL lysate proteins, 0 mM SMHP) were reacted for 4 h (room temperature) in 0.1 M potassium phosphate buffer, pH 8.0. Once reacted, the protein samples were stored at –80 °C overnight as described in Section 2.5.

The protein samples were thawed and CuAAC reactions were conducted as described for Hb. Unlike pure Hb, which could be precipitated and resolubilized effectively in 1.2% SDS using all three methods mentioned above, full recovery of the lysate proteins could only be achieved when they were precipitated with chloroform/methanol (MeOH: ddH_2O: $CHCl_3$) (4: 3: 1). Solubilization of the pellet, as well as the wash steps, streptavidin enrichment, and protein elution were conducted exactly as previously described for Hb. SDS-PAGE with silver staining was used to visualize the eluted proteins, but no proteins were observed, indicating that the modified proteins were present at such low concentrations in the sample that trypsin digestion and LC-MS/MS would be required for the analysis (Section 2.2.8).

2.2.8 BIOTIN-ABPP ANALYSIS OF *P. LEMOGNEI* PROTEINS BY STREPTAVIDIN ENRICHMENT, ON-BEAD DIGESTION, AND IDENTIFICATION BY LC-MS/MS

A similar method to that described in Section 2.2.7.2 for proteins in the *P. lemognei* cell lysate was followed with only minor modifications prior to the streptavidin enrichment steps. To the streptavidin-agarose-treated proteins, 2 × 0.5 mL aliquots of the SMHP-reacted lysate proteins (3.3 mg/mL lysate, 0.5 mM SMHP) and control (3.3 mg/mL lysate, 0 mM SMHP) were reacted for 4 h (room temperature) in 0.1 M potassium phosphate buffer, pH 8.0. CuAAC reactions were conducted as described previously in Section 2.2.6, using the BAP tag (100 μM) instead of the FPA tag. The proteins were pelleted using chloroform/methanol precipitation (MeOH: ddH_2O: $CHCl_3$) (4: 3: 1) and subsequently resolubilized in PBS containing 1.2% SDS as described in Section 2.2.7. PBS was added to give a final concentration of 0.2% SDS (6 mL final volume) to which pre-washed streptavidin-agarose beads (100 μL of a 50% slurry) were

added (conical tubes). The mixture was incubated for 3 h (room temperature) with gentle rotary mixing, as described in Section 2.2.7.

The washing of the streptavidin-agarose beads and on-bead trypsin digestion were conducted using protocols described by Galmozzi *et al*. (2014) and Speers & Cravatt (2009). After discarding the supernatant, the beads were washed sequentially with 1% SDS in PBS (2 × 8 mL), 6 M urea in PBS (2 × 8 mL), and PBS (3 × 8 mL), with gentle rotary mixing for 5 min (room temperature) for each wash prior to pelleting the beads (Galmozzi *et al*., 2014). After removing the supernatant, PBS (1 mL) was added to briefly resuspend the pelleted beads to permit their transfer to screw top microcentrifuge tubes (Galmozzi *et al*., 2014). Upon transfer, beads were centrifuged and the PBS supernatant was removed (Galmozzi *et al*., 2014).

The beads were resuspended in urea (6 M) in PBS (500 µL), DTT was added to give a final concentration of 10 mM, and the mixture was heated at 65 °C for 15 min (Speers & Cravatt, 2009). Iodoacetamide (IAA) was added to yield a final concentration of 25 mM and the solution was mixed by gentle rotation of the foil-covered tubes at room temperature for 30 min (Speers & Cravatt, 2009). Upon centrifugation and removal of supernatant, the beads were washed with PBS (1 mL) (Speers & Cravatt, 2009). Urea (2 M) in PBS (200 µL) was added to beads with a final concentration of 1 mM $CaCl_2$, with 2 mg total trypsin (4 µL from a 0.5 mg/mL stock) (Speers & Cravatt, 2009). The proteins were digested (on-bead) overnight (37 °C) with gentle rotary mixing (Speers & Cravatt, 2009). The beads were pelleted and supernatant was transferred to a fresh microcentrifuge tube, where the reactions were terminated by addition of formic acid to a

final concentration of 5% (Speers & Cravatt, 2009). Samples were stored at –80 °C until LC-MS/MS analysis.

For LC-MS/MS analysis, the samples were thawed and desalted on 'StageTips', using a protocol similar to one previously described (Rappsilber *et al*., 2007). 'StageTips' were prepared using Solid Phase Extraction Disks (ENVI-Disk) (Supelco) consisting of C18-modified silica particles embedded in porous glass fiber membranes. The packed 200-µL tips with ~10 cut disks were conditioned with MeOH (1 × 50 µL), followed by 50% acetonitrile (ACN) (1 × 100 µL) and then 0.1% trifluoroacetic acid (TFA) (2 × 100 µL), centrifuging after each conditioning step. The sample was then added to each column. Following centrifugation, the 'StageTips' were washed with 0.1% TFA (3 × 200 µL). Samples were eluted first with 50% ACN (1 × 100 µL) and then with 70% ACN (1 × 50 µL) to elute the remaining peptides. Desalted samples were then analyzed using LC-MS/MS.

2.2.9 LABELLING OF 3-HBDH AND CTPS BY SHMP USING FLUORESCENT TAGGING

In separate experiments, purified 3-HBDH (Section 2.2.3) and purified CTPS (Section 2.2.4) at concentrations of 0.75 mg/mL in 3-HBDH assay buffer (0.1 M Tris-Cl, pH 8.0) and CTPS assay buffer (70 mM HEPES, 10 mM $MgCl_2$, 0.5 mM EGTA, pH 8.0), respectively, were reacted with 0.5 mM SMHP for 1 h at 37 °C. CuAAC reactions were conducted exactly as described in Section 2.2.6, and the resulting samples were analyzed by SDS-PAGE. As described previously, excess CuAAC reagents were not removed prior to electrophoresis (Speers & Cravatt, 2004). Samples were visualized

using the Versadoc Imaging System with Alexa 488 as the filter setting (FPA λ_{ex} = 490 nm, λ_{em} = 510 nm). Gels were later stained with Coomassie brilliant blue (R-250).

2.2.10 CTPS PROTECTION BY LIGANDS USING FLUORESCENT TAGGING

In separate reaction tubes, CTPS (0.75 mg/mL) in CTPS assay buffer was pre-incubated with either ATP (10 mM), CTP (10 mM), UTP (10 mM), L-glutamine (20 mM), or no ligand (i.e., control) for 1 h (37 °C). SMHP (0.5 mM) was then added and allowed to react for 1 h at 37 °C as described in Section 2.2.9. CuAAC reactions and gel-based analysis were conducted as described in Section 2.2.9.

2.2.11 pH DETERMINATION OF SMHP REACTIVITY USING FLUORESCENT TAGGING

The effect of pH on SMHP-modification of 3-HBDH, CTPS, and Hb was evaluated from pH 6.5 to 9.5. Hb (2 mg/mL) was dissolved in each respective 0.1 M Tris-Cl buffer at pH values of 6.5, 7.0, 7.5, 8.0, 8.5, and 9.5 and reacted with SMHP (0.5 mM) for 2 h at 37 °C. Since 3-HBDH and CTPS were dialyzed and stored in their respective assay buffers at pH 8.0, each enzyme was concentrated using a 10-kDa MW cutoff filter to minimize the volume of enzyme in pH 8.0 buffer, and then diluted into each buffer (Section 2.2.9) from pH 6.5-9.5. 3-HBDH and CTPS, each at concentrations of 0.4 mg/mL, were reacted with SMHP (0.5 mM) for 1 h at 37 °C. CuAAC reactions and gel-based analysis were conducted as described in Section 2.2.9.

2.2.12 PROTECTION BY MAP USING FLUORESCENT TAGGING

The protection against SMHP-labelling by MAP was evaluated using 3-HBDH, CTPS, and Hb. Hb (0.75 mg/mL) was pre-incubated with varying concentrations of MAP: 0 mM, 0.5, 1.0, 2.5, 5.0, 10.0, and 25.0 mM for 2 h at 37 °C. In separate reactions, 3-HBDH (0.75 mg/mL) and CTPS (0.75 mg/mL) were reacted for 1 h at 37 °C with the same concentrations of MAP, ranging from 0 – 25 mM. Thereafter, SMHP (0.5 mM) was added and allowed to react for 2 h at 37 °C for Hb and 1 h at 37 °C for 3-HBDH and CTPS as described in Section 2.2.9. CuAAC reactions and gel-based analysis were conducted as described in Section 2.2.9.

2.2.13 PROTECTION AND pH DEPENDENCY OF ASPIRIN LABELLING USING FLUORESCENT TAGGING

Given the previously described slow rate of acetylation of Hb by aspirin, wherein typically 20 mM aspirin was allowed to react for 12 h at 37 °C with Hb (Klotz & Tam, 1973; Xu *et al*., 1999), the same parameters were used for the present protection study. Hb was pre-incubated with 0 mM (control) and 20 mM aspirin (Alka-Seltzer, acetylsalicylic acid effervescent tablets) (sample) for 12 h at 37 °C, followed by the addition of SMHP (0.5 mM), which reacted for 2 h at 37 °C. CuAAC reactions and gel-based analysis were conducted as described in Section 2.2.6. Once protection was demonstrated, the effect of pH was evaluated wherein Hb was pre-incubated with 0 mM aspirin (control) at pH 6.5, 7.5, and 8.5 or with 20 mM aspirin (sample) at the same pH values for 12 h at 37 °C, followed by the addition of SMHP (0.5 mM) and reacted for 2 h at 37 °C. Again, CuAAC reactions and gel-based analysis were conducted as described in Section 2.2.9.

2.2.14 LC-MS/MS DETERMINATION OF THE MODIFICATION SITES ON 3-HBDH AND CTPS

The sites labelled on 3-HBDH by MAP and SMHP were determined using LC-MS/MS. Three separate reaction tubes were prepared containing 3-HBDH (0.75 mg/mL) and reacted with either SMHP (0.5 mM), MAP (25 mM), or no acyl phosphate (i.e., 0 mM SMHP, 0 mM MAP) for 1 h at 37 °C. Prior to electrophoresis, each reaction solution was incubated at 37 °C for 15 min with SDS-PAGE loading buffer as described by the Biological Mass Spectrometry Core Facility protocols (Cohen, 2022). After subjecting the samples to SDS-PAGE (15 %), staining with Coomassie, followed by de-staining, the protein band for each sample was excised and subjected to reduction by DTT, alkylation by iodiacetamide, and trypsin-catalyzed digestion. The samples were then analyzed using LC-MS/MS. To confirm successful labelling of proteins by SMHP and protection from labelling by MAP, parallel reactions were conducted as described in Sections 2.2.9 and 2.2.12, followed by CuAAC reactions and gel-based analysis.

The sites labelled by SMHP on CTPS were evaluated as follows. In two separate reaction tubes, CTPS (0.75 mg/mL) was treated with SMHP (0.5 mM) or no acyl phosphate (i.e., 0 mM SMHP) for 1 h at 37 °C. As described for 3-HBDH, each reaction solution was incubated at 37 °C for 15 min with SDS-PAGE loading buffer. After subjecting the samples to SDS-PAGE (10 %), staining with Coomassie, followed by de-staining, the protein band for each sample was excised and subjected to reduction, alkylation, trypsin-catalyzed digestion, and analysis using LC-MS/MS. To confirm successful labelling of CTPS by SMHP, parallel reactions were conducted as described in Sections 2.2.9, followed by CuAAC reactions and gel-based analysis.

2.2.15 3-HBDH KINETIC ASSAYS

Assays were conducted using an approach similar to that previously described (Ito *et al*., 2006; Kluger & Bearne, 1994), but conducted under modified conditions of pH and temperature to stabilize the diluted recombinant enzyme. Using a continuous spectrophotometric assay, the conversion of NAD^+ to NADH ($\Delta\varepsilon = 6220\ M^{-1}cm^{-1}$) from the D-3-hydroxybutyrate reaction direction was measured by following the change in absorbance at 340 nm for 120 s at 20 °C. A saturating concentration of NAD^+ (2 mM) was used in all assays with 100 mM potassium phosphate, pH 7.0 as the assay buffer. In all assays, a 1.0-cm quartz cuvette and the total assay volume was of 1.0 mL.

2.2.15.1 Determination of kinetic parameters

The kinetic parameters, k_{cat}, K_m, and k_{cat}/K_m were determined using D-3-hydroxybutyrate concentrations ranging from 0.2 – 18.0 mM, with a final [3-HBDH] of 0.175 μg/mL (5.82 nM). The k_{cat} values were calculated by dividing the V_{max} values by the total enzyme concentration ($[E]_T$) using the molecular weight of 3-HBDH (30 039.15 Da). The Michaelis-Menten equation (eqn 2.1) was used to fit the initial velocities using *KaleidaGraph* software (v. 4.02) (Synergy Software, Reading, PA) for non-linear regression analysis. The assay was conducted in triplicate and average values were reported with the errors corresponding to the standard deviation values.

$$v_i = \frac{V_{max}[S]}{K_m + [S]} \tag{2.1}$$

2.2.15.2 Time-dependent inactivation by MAP

The rate of inactivation of 3-HBDH activity by MAP was assessed by incubating 3-HBDH (3.5 μg/mL) with varying concentrations of MAP (0.0, 2.5, 5.0, 10.0, 25.0, and 65.0 mM) in 3-HBDH assay buffer. Aliquots (50 μL) were diluted twenty-fold to the total assay volume of 1.0 mL, yielding final [3-HBDH] of 0.175 μg/mL (5.82 nM), with NAD^+ (2 mM) and D-3-hydroxybutyrate (7.5 mM). The reaction was followed at each concentration of MAP over varying periods of time. Using eqn 2.2, the observed initial velocities were plotted as ln(% activity) vs. time for each inhibitor concentration and the resulting slopes yielded the observed pseudo-first-order rate constants for inactivation (k_{obs}). Minor enzyme activity losses that occurred over the inactivation assay were corrected for by subtracting the k_{obs} values of the untreated enzyme from those of the MAP-treated enzyme over the same incubation period. Since saturation was observed from the replot of the k_{obs} versus MAP, eqn 2.3 (non-linear regression) was used to fit the data to determine the values of K_I, k_{inact}, and k_{inact}/K_I. The inactivation assay was conducted in triplicate and average values were reported with the errors corresponding to the standard deviation values.

$$\frac{v_i}{v_o} = e^{-k_{obs}t} \tag{2.2}$$

$$k_{obs} = \frac{k_{inact}[I]}{K_I + [I]} \tag{2.3}$$

2.2.16 CTPS KINETIC ASSAYS

Using a continuous spectrophotometric assay, the conversion of UTP to CTP ($\Delta\varepsilon$ = 1338 $M^{-1}cm^{-1}$) was measured by following the change in absorbance at 291 nm for 60 s at 37 °C, as described previously (Bearne *et al.*, 2001). Reactions were conducted in CTPS assay buffer (70 mM HEPES, 10 mM $MgCl_2$, 0.5 mM EGTA, pH 8.0) at saturating concentrations (1 mM) of the nucleotides ATP and UTP. The nucleotides and enzyme were pre-incubated at 37 °C for 2 min to induce tetramerization, followed by the addition of substrate (NH_4Cl) to initiate the reaction. KCl was used to maintain the ionic strength at 0.15 M. At pH 8.0, the final [NH_3] was calculated using a pK_a value of 9.24 for NH_4^+ 9.24 (Iyengar & Bearne, 2003). In all assays, a 0.2-cm quartz cuvette was used with total volume of 0.30 mL.

2.2.16.1 Determination of kinetic parameters

The kinetic parameters, k_{cat}, K_m, and k_{cat}/K_m were determined using free NH_3 ranging from 0.2875 - 8.625 mM (5 - 150 mM NH_4Cl), with the final [CTPS] = 66.67 µg/mL (1.06 µM). The k_{cat} values were calculated by dividing the V_{max} values by the total enzyme concentration ($[E]_T$) using the molecular weight of CTPS (62 911 Da). The Michaelis-Menten equation (eqn 1.1) was used to fit the initial velocity data using *KaleidaGraph* software (v. 4.02) (Synergy Software, Reading, PA) for non-linear regression analysis. The assay was conducted in triplicate and average values were reported with the errors corresponding to the standard deviation values.

2.2.16.2 Time-dependent inactivation by MAP and SMHP

The rate of inactivation of CTPS activity by each MAP and SMHP were assessed individually by incubating CTPS (1.0 mg/mL) with varying concentrations of MAP (0.0, 0.5, 1.0, 2.5, 6.0, and 10.0 mM) and SMHP (0.0, 2.5, 6.0, 10.0, 25.0, 50.0) in CTPS assay buffer. Aliquots (20 μL) were diluted fifteen-fold to the total assay volume of 0.30 mL, yielding final [CTPS] of 66.67 μg/mL (1.06 μM). Saturating concentrations of ATP and UTP (1 mM) were used in the assay tube, wherein the assay reaction was initiated by the addition of NH_4Cl (100 mM) after incubation of the enzyme, MAP or SMHP, and nucleotides for 2 min at 37 °C. The reaction was followed at each concentration of MAP or SMHP over varying periods of time. Using eqn 2.2, the observed initial velocities were plotted as ln(% activity) vs. time for each inhibitor concentration and the resulting slopes yielded the observed pseudo-first-order rate constants for inactivation (k_{obs}). In the MAP-dependent inactivation assays, a replot of the k_{obs} values against the concentration of MAP was used to estimate the apparent second-order rate constant for the efficiency of inactivation (k_{inact}/K_I) in accord with eqn 2.4 since saturation was not observed. In the SMHP-dependent inactivation assays, non-linear regression was used to fit eqn 2.3 to the data from the replot of the k_{obs} values versus [SMHP] since saturation was observed, allowing for the determination of the K_I, k_{inact}, and k_{inact}/K_I values. The inactivation assays were conducted in triplicate and average values were reported with the errors corresponding to the standard deviation values.

$$k_{obs} \approx \frac{k_{inact}\,[MAP]}{K_I} \tag{2.4}$$

2.2.16.3 Protection against MAP-dependent inactivation by ligands

Protection studies against the time-dependent inactivation of CTPS activity by MAP were conducted as described in Section 2.2.16.2, with a [MAP] of 2.5 mM, and varying concentrations of ligands: ATP (0.0, 0.5, 1.0, 1.5, and 2.0 mM), CTP (0.00, 0.05, 0.10, 0.15, 0.15, and 0.20 mM), UTP (0, 1, 2, 3, and 4 mM), and L-Gln (0.0, 0.1, 0.2, 1.0, and 5.0 mM). These ligands were incubated individually with CTPS (1.0 mg/mL) and MAP (2.5 mM) over various times to assess the rate of inactivation in the presence of each ligand. The observed initial velocities were plotted as ln(% activity) vs. time at each protecting ligand concentration and k_{obs} values were determined in accord with eqn 2.2. The values of the inverse of the observed pseudo-first-order rate constants for inactivation ($1/k_{obs}$) were then plotted against the concentration of protecting ligand in accord with eqn 2.5 and 2.6. The apparent dissociation constant for the ligand-mediated protection against inactivation values (K_L) were determined using eqn 2.7. For protection studies with ATP and UTP, where positive co-operativity was observed, the Hill numbers (n) were determined in accord with eqn 2.8 as 2.872 ± 0.116 and 2.870 ± 0.050, respectively. These coefficients were applied to the replot of $1/k_{obs}$ versus [ligand]^n, wherein the $K_L{}^n$ value was determined in accord with eqn 2.9 to permit the determination of the K_L. As these assays were not completed in triplicate, the errors correspond to the uncertainties arising from measurements within the single inactivation experiment.

$$k_{obs} = \frac{k_{inact}[I]}{[I] + [K_I](1 + \frac{[L]}{K_L})} \quad (2.5)$$

$$1/k_{obs} = [L]\frac{K_I}{k_{inact}[I]\,K_L} + \frac{1}{[k_{inact}]}\left(\frac{K_I}{[I]} + 1\right) \quad (2.6)$$

$$K_L = \frac{k_{inact}}{[K_I]\,[I]\,(slope)} \quad (2.7)$$

$$\text{where, slope} = \frac{K_I}{k_{inact}\,[I]\,K_L}$$

$$1/k_{obs} = [L]^n\frac{K_I}{k_{inact}[I]\,K_L{}^n} + \frac{1}{[k_{inact}]}\left(\frac{K_I}{[I]} + 1\right) \quad (2.8)$$

$$K_L{}^n = \frac{k_{inact}}{[K_I]\,[I]\,(slope)} \quad (2.9)$$

2.3 RESULTS AND DISCUSSION

2.3.1 SMHP AS AN ACTIVITY-BASED PROBE: STABILITY AND REACTIVITY

The identity of SMHP was confirmed by ^{1}H NMR, ^{13}C NMR, ^{31}P NMR, and ESI-HRMS (negative mode) as shown in **Figures 2.9-2.12**. To study the reactivity of SMHP towards protein architectures with a nucleophile adjacent to a cationic site, initial studies were conducted using SMHP and human Hb given the previously reported modification of Hb by MAP (Ueno *et al*., 1986, 1989; Xu *et al*., 1999). Furthermore, given the simplicity of the fluorescent tagging approach relative to the biotin-ABPP method, the fluorescein picolyl azide (FPA) tag was used to study the reactivity of SMHP with Hb. Preliminary studies revealed that the probe did indeed modify Hb. The Hb sample (0.5

mM SMHP) and control (0 mM SMHP) were treated in parallel and reacted via click chemistry to verify that the fluorescent labelling of Hb arises solely as a result of the CuAAC reaction between the FPA-tag with the terminal alkyne of SMHP. Consistent among all SMHP-reacted Hb samples, fluorescent bands corresponding to the monomer (~16 kDa) and dimer (~32 kDa) of Hb were observed (**Figure 2.13**). As expected, the control showed no fluorescent bands.

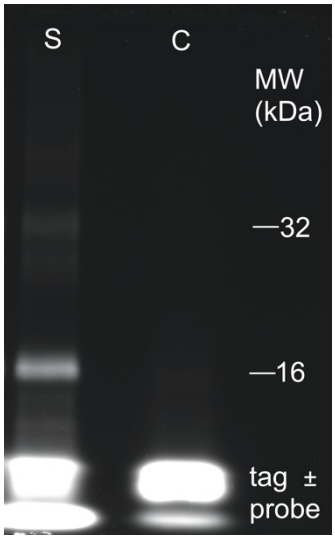

Figure 2.13 Representative SDS-PAGE electrophoretogram of SMHP-modified Hb. Shown in the 15% gel are SMHP-treated Hb (S = sample) and untreated Hb (C= control). Fluorescent bands of SMHP-treated Hb of ~16 kDa (monomer) and ~32 kDa (dimer) are absent in the untreated Hb. Samples were analyzed using the Versadoc Imaging System with Alexa 488 as the filter setting (FPA λ_{ex} = 490 nm, λ_{em} = 510 nm).

Similarly to the design of MAP (Kluger & Tsui, 1980), SMHP was expected to be stable in aqueous solutions and in the absence of non-enzymatic nucleophiles. The high stability of SMHP (stored in H_2O at 4 ºC) was demonstrated over the course of ~8 months since no loss in reactivity with Hb was observed over that period. As previously

described, warheads should exhibit high stability under physiological conditions and yet be highly reactive towards proteins containing the targeted structural motif (Kozarich, 2003; Shindo & Ojida, 2021). Given the stability of SMHP under aqueous conditions and demonstrated high reactivity towards Hb, which contains several cationic residues within the 2,3-DPG binding cleft, this probe afforded the desired characteristics for our investigations of protein architectures.

Intact MS (LC-MS) was then employed to assess the expected 94-Da adducts resulting from the acylation of Hb by SMHP and, as expected, 94-Da adducts were observed in the SMHP-treated Hb sample but not in the untreated Hb control (**Figure 2.14, 2.15**). These adducts were observed with both the α-chains and the β-chains of the Hb tetramer. Interestingly, Ueno *et al*. (1986, 1989) observed acetylation of Hb by MAP only at β-chain residues, specifically βVal 1, βLys 82, and βLys 144. In both studies using HPLC peptide mapping, there were no detectible modified residues within the α-chains (Ueno *et al*., 1986, 1989). Later, Xu *et al*. (1999) confirmed these specific residue modifications using NMR spectroscopy, but also observed acetylation of two residues outside of the 2,3-DPG cleft, including one residue on the α-chain, αLys 90, as well as βLys 59. Given the highly cationic nature of the 2,3-DPG cleft, it is to no surprise that Xu *et al*. (1999) observed a clear preference towards the acetylation of one of the lysine residues within that centre, βLys 82, relative to those found outside of the binding site.

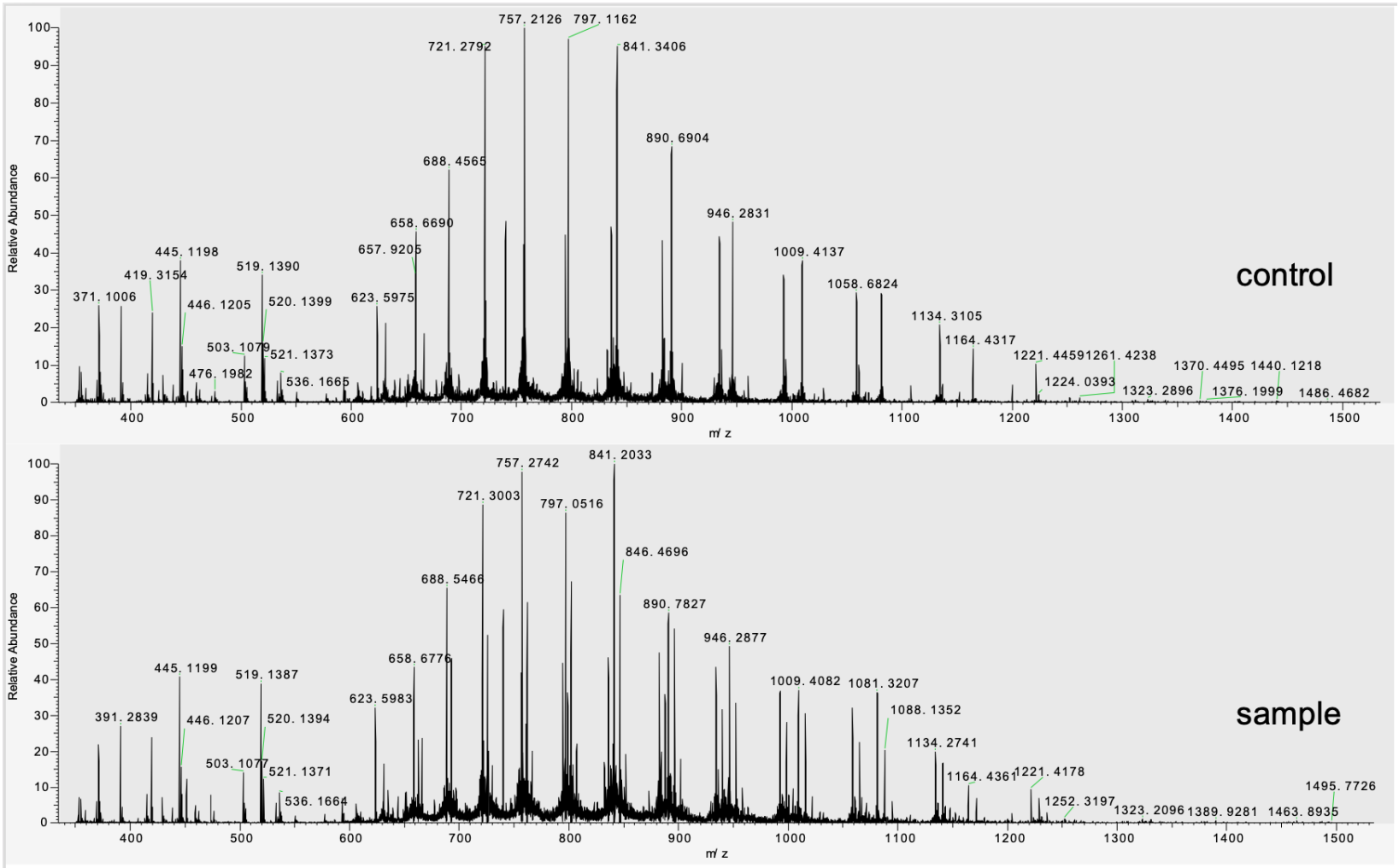

Figure 2.14 Raw *m/z* spectra of SMHP-modified Hb. Shown are the SMHP-treated Hb (sample) spectrum and the untreated Hb (control) spectrum.

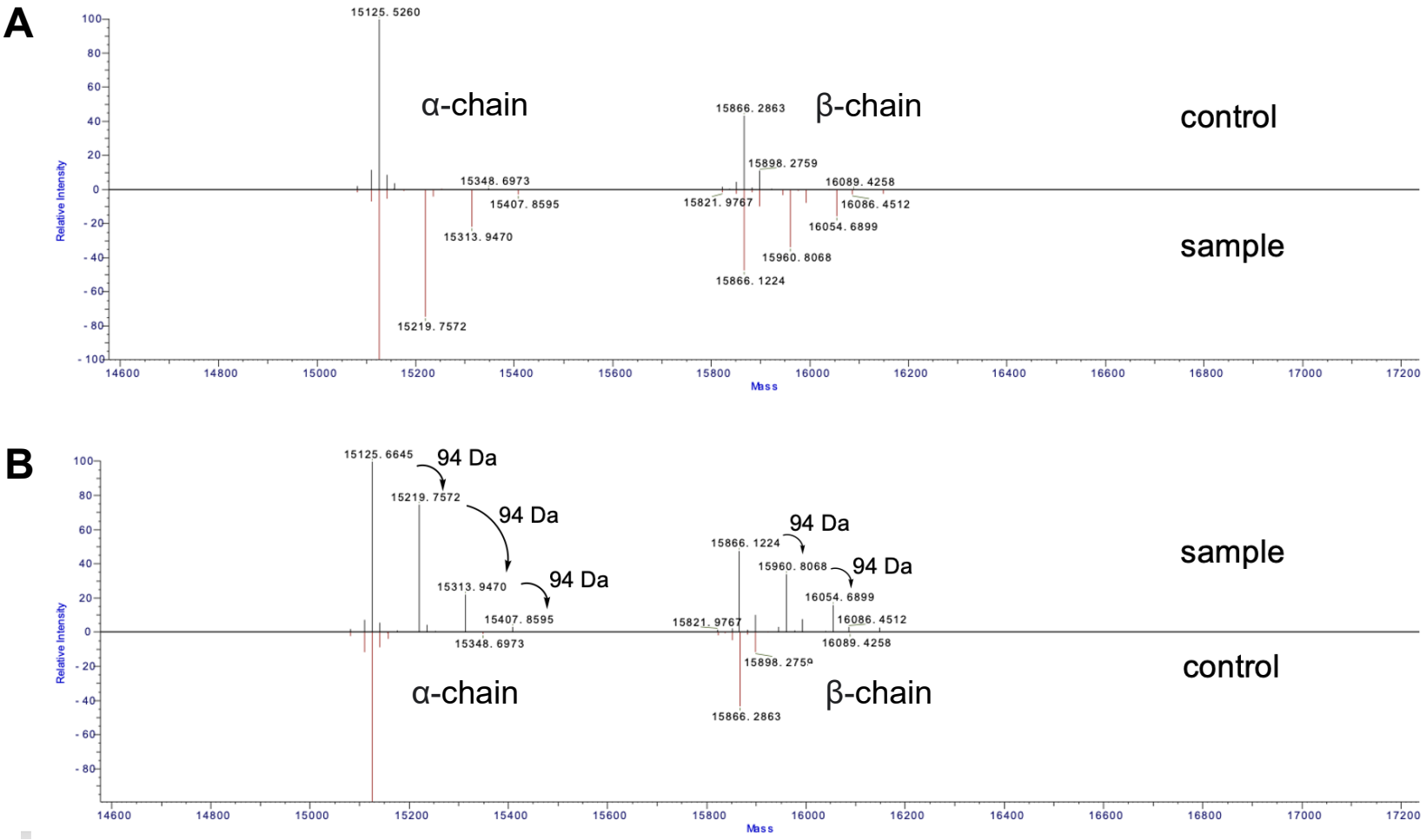

Figure 2.15 Deconvoluted mass spectra of SMHP-modified Hb. Shown are the SMHP-treated Hb (sample) spectrum and the untreated Hb (control) spectrum. Adducts of size 94 Da are observed in both α- and β-chains of the Hb sample, which are absent in the control. Deconvoluted mass spectra for the sample and control Hb are represented as control/sample (A) and (B) reversed representation, sample/control.

2.3.2. ANALYSIS OF SMHP-MODIFIED PROTEINS FROM THE *P. lemognei* PROTEOME

Biotinylated proteins within the proteome of *P. lemognei* were subjected to streptavidin-agarose enrichment, extensive wash steps to remove non-biotinylated proteins, on-bead trypsin digestion, and LC-MS/MS analysis. Upon analysis, 281 SMHP-modified enzymes were identified, from 483 selectively filtered, SMHP-modified proteins, from the *P. lemognei* proteome of 3805 proteins. Identified proteins from the sample that were also observed in the control were only kept if the abundance ratio was ≥ 2.0 (Ting *et al*., 2009; J. Wang *et al*., 2014).

SMHP showed broad-spectrum labelling with evident selectivity towards certain enzyme families, such as kinases, dehydrogenases, and tRNA ligases. The 281 enzymes were grouped by class, subclass, and subsubclass to observe trends in probe specificity towards certain groups (**Figure 2.16**). Proteins modified by the probe were distributed over the seven classes, with transferases (EC 2), oxidoreductases (EC 1), and ligases (EC 6) containing the greatest quantity of enzymes labelled by SMHP. Probe specificity towards certain subclasses was apparent, where the top subclasses with a frequency ≥ 5 were plotted. The most frequent subclass modified by SMHP was the transferase subclass EC 2.7 (transferring phosphorous containing groups) (Bairoch, 2000), which included various kinases, such as histidine kinase, uridylate kinase, and pyruvate kinase. Following EC 2.7, the ligase subclass EC 6.3 (catalyzing C-N bond formation) and EC 6.1 (catalyzing C-O bond formation), the lyase subclass EC 4.2 (C-O lyases), and the oxidoreductase subclass EC 1.1 (acting on the CH-OH group of donors) were the five most frequently labelled subgroups (Bairoch, 2000). Further, examination of the subsubclasses occurring with a frequency of ≥ 5 revealed that four of the subsubclasses

showed frequencies of ≥ 10: EC 6.1.1, EC 1.1.1, EC 2.5.1, and EC 4.2.1. The most frequently modified subsubclass, EC 6.1.1, included ligases catalyzing the formation of aminoacyl-tRNA (Bairoch, 2000), such as glutamate-tRNA ligase, threonine-tRNA ligase, and proline-tRNA ligase. The second most frequently labelled subsubclass, EC 1.1.1, included C-O lyases with NAD(+) or NADP(+) as acceptors (Bairoch, 2000), such as 3-HBDH, isocitrate dehydrogenase, 3-isopropylmalate dehydrogenase, and glutamate dehydrogenase. Next, the third most frequently labelled subsubclass, EC 2.5.1, included transferases; transferring alkyl or aryl groups, other than methyl groups (Bairoch, 2000), such as glutathione S-transferase, cysteine synthase, and 3-phosphoshikimate 1-carboxyvinyltransferase. Lastly, the fourth most frequent subsubclass, EC 4.2.1, included hydro-lyases (Bairoch, 2000), such as phosphogluconate dehydratase, carbonic anhydrase, and ATP phosphoribosyltransferase.

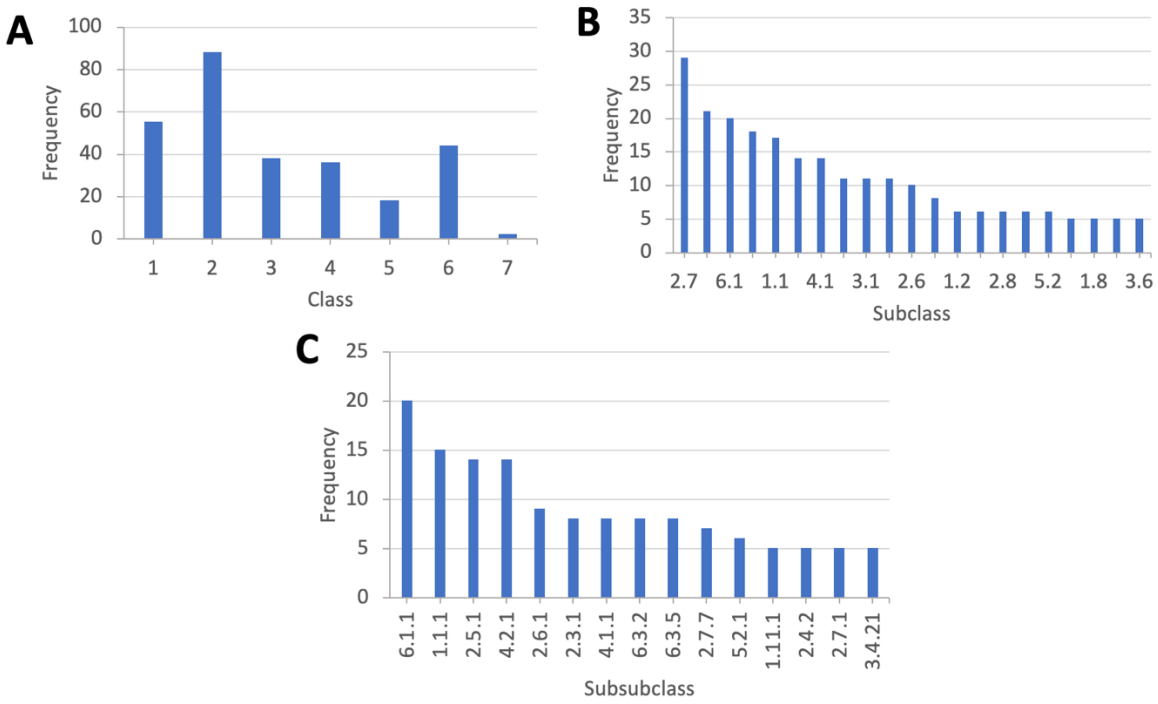

Figure 2.16 Classes of enzymes from the *P. lemognei* proteome modified by SMHP. Enzymes were categorized by their Enzyme Commission (A) class, (B) subclass, and (C) subsubclass based on their frequency (number of times enzymes were observed in each category). All 281 enzymes are grouped by class, where only subclasses and subsubclasses with a frequency of ≥ 5 are represented.

2.3.3 3-HBDH AND CTP SYNTHASE

Within the 281 SMHP-modified enzymes, 3-HBDH and CTP synthase (CTPS) were of particular interest because their X-ray crystal structures are known, they share active-site homology among other organisms, they are therapeutic targets for inhibition, and they are readily available in the Bearne Lab. Thus, these enzymes were subsequently studied in their purified forms to assess their modification by SMHP in greater detail.

2.3.3.1 3-HBDH

3-HBDH served as positive control (proof-of-principle) within the complex *P. lemognei* proteome of 3805 proteins, and thus, its identification confirmed the viability of the biotin-ABPP method. 3-HBDH (EC 1.1.1.30) fell within the second largest subsubclass (EC 1.1.1) by frequency, which primarily consisted of dehydrogenases. Following its identification from the *P. lemognei* proteome, the open reading frame encoding wild-type 3-HBDH from *Pseudomonas lemognei* was synthesized commercially and inserted into a pET-15b(+) vector, wherein this construct encodes the wild-type 3-HBDH enzyme as a fusion protein bearing an N-terminal $(His)_6$-tag. The purity of 3-HBDH was assessed using SDS-PAGE, wherein the monomer (30 kDa), dimer (60 kDa), and tetramer (120 kDa) of the enzyme could be identified (**Figure 2.17**).

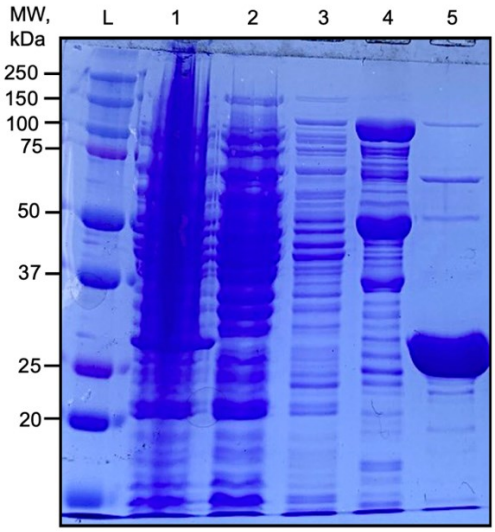

Figure 2.17 Representative SDS-PAGE electrophoretogram showing the purification of wild-type 3-HBDH. The lanes of the 12% gel correspond to: (L) the molecular weight ladder, (1) cell pellet, (2) flow-through of the clarified lysate, (3) wash with binding buffer (i.e., 5 mM imidazole), (4) wash with wash buffer (i.e., 60 mM imidazole), and (5) elution with strip buffer (i.e., 100 mM EDTA). The expected molecular weight of the WT 3-HBDH monomer is 30039 Da.

2.3.3.2 CTPS

While CTPS (EC 6.3.4.2) did not appear in the top few most frequently labeled subsubclasses, it fell within the second largest subclass (6.3) by frequency. CTPS is a universally conserved enzyme that catalyzes the *de novo* biosynthesis of CTP from UTP using either L-glutamine or free ammonia as the nitrogen source (**Scheme 2.4**) (Endrizzi *et al*., 2004; Koshland & Levitzki, 1974; Long & Pardee, 1967). CTPS exists as a homodimer in solution but must undergo tetramerization for catalytic activity (Levitzki & Koshland, 1972b). Specifically, ATP and UTP are required substrates for CTPS that induce tetramerization of the inactive dimer to the active tetramer (Levitzki & Koshland, 1972b). More detailed structural information on ligand binding sites for the multi-domain enzyme will be described in Section 2.3.11 for the analysis of the SMHP-modified sites using LC-MS/MS.

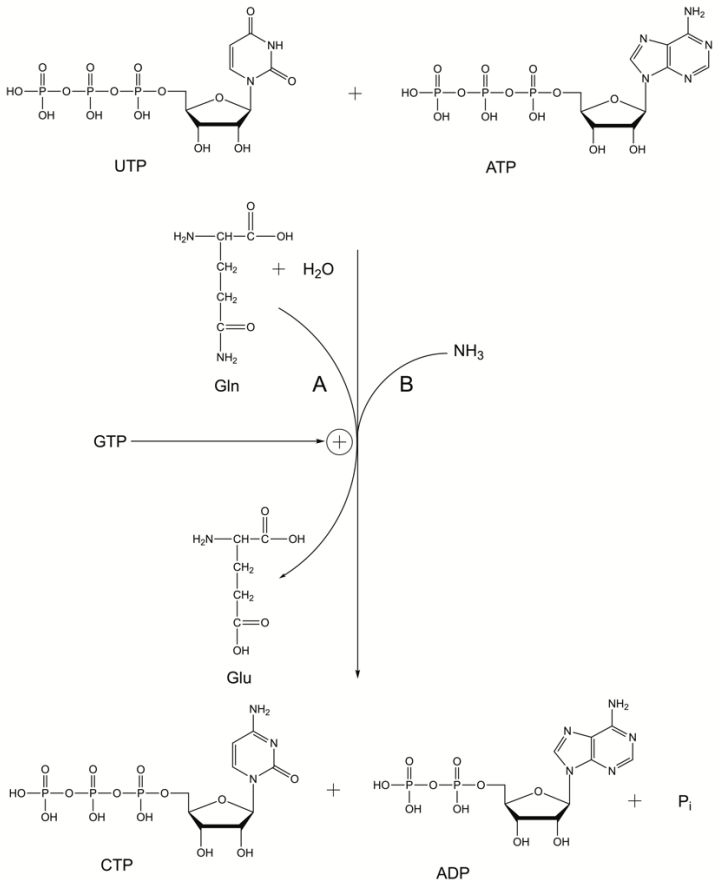

Scheme 2.4 Reaction catalyzed by CTPS to produce CTP from UTP. (A) L-glutamine (Gln) or (B) free (exogenous) ammonia can be used as the nitrogen source.

CTPS plays a critical role in the biosynthesis of DNA, RNA, and phospholipids (P. Y. Wang *et al*., 2015). CTPS catalyzes the final and rate-limiting step in CTP biosynthesis, whereby activity is regulated by product inhibition with CTP acting as a negative feedback inhibitor (Endrizzi *et al*., 2004; Higgins *et al*., 2007; Levitzki & Koshland, 1969). Upregulated CTPS expression and activity have been observed in cancer cells. Hence the enzyme is of therapeutic interest as a target for chemotherapeutic agents (J. C. Williams *et al*., 1978). In addition, CTPS is also recognised as a target for

the development of antiviral (De Clercq, 2009; De Clercq *et al*., 1991), antibacterial (Emami *et al*., 2020; Mori *et al*., 2015), and antiparasitic (Hendriks *et al*., 1998; Narvaez-Ortiz *et al*., 2018) drugs.

2.3.4 IDENTIFICATION OF SMHP-MODIFIED ENZYMES USING FLUORESENT TAGGING

Purified, recombinant wild-type 3-HBDH from *P. lemognei* was modified by SMHP and subsequently reacted with the FPA-tag using the CuAAC reaction. Upon analysis using SDS-PAGE, fluorescent bands corresponding to molecular weights of 30 kDa (monomer) and 60 kDa (dimer) of 3-HBDH were observed in the SMHP-reacted sample but not in the control (**Figure 2.18A**). Similarly, a fluorescent band corresponding to the molecular weight of 63 kDa (monomer) of CTPS was observed in the SMHP-reacted sample but not in the control (**Figure 2.18B**). Thus, fluorescent labelling of the enzyme arises solely as a result of the CuAAC reaction between the FPA-tag with the terminal alkyne of SMHP. Further, as click-chemistry reagents are not removed prior to in-gel analysis, there is a clear reduction in the amount of low molecular weight free tag ± probe that can be observed in the sample relative to the control. Since the ability of SMHP to modify both 3-HBDH and CTPS was clearly demonstrated through both biotin-ABPP in the *P. lemognei* proteome and as purified proteins by fluorescent tagging, the next objective was to investigate the specific sites of modification by SMHP.

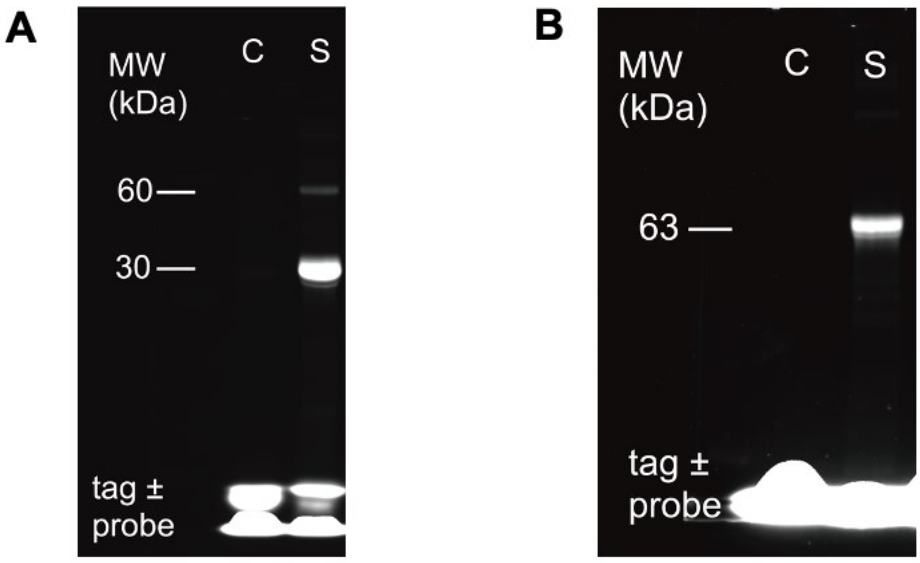

Figure 2.18 Representative SDS-PAGE electrophoretograms of SMHP-modified 3-HBDH and CTPS. (A) SMHP-treated 3-HBDH (S = sample) and untreated 3-HBDH (C = control) (15% gel), and (B) SMHP-treated CTPS (S = sample) and untreated CTPS (C = control) CTPS (10% gel) are shown. SMHP-reacted 3-HBDH showed fluorescent bands corresponding to 30 kDa (monomer) and 60 kDa (dimer). SMHP-reacted CTPS showed a fluorescent band corresponding to 63 kDa (monomer). Samples were analyzed using the Versadoc Imaging System with Alexa 488 as the filter setting (FPA λ_{ex} = 490 nm, λ_{em} = 510 nm).

2.3.5 EVALUATING THE pH-DEPENDENT REACTIVITY OF SMHP

The pH-dependence of the labelling of Hb, 3-HBDH, and CTPS by SMHP was evaluated from pH 6.5-9.5 to determine trends in SMHP-reactivity and to provide some indication as to which nucleophiles(s) could be reacting with SMHP. Consistent among all three proteins, the reactivity between SMHP and the protein nucleophile(s) increased with increasing pH from pH 6.5 to 9.0 as demonstrated by the increasing level of fluorescence with pH (**Figure 2.19**). With 3-HBDH and Hb, the level of fluorescence decreased slightly from pH 9.0-9.5, but continued to increase slightly with CTPS from pH 9.0-9.5. Overall, these findings agree with the pH-dependence reported for the inactivation of 3-HBDH by MAP (Kluger & Tsui, 1986), where the observed first-order

rate constant (k_{obs}) for the inactivation of 3-HBDH by MAP was found to depend on pH, showing a steep increase from pH 6.5 to 8.9 with an estimated pK_a value of 8.2 (Kluger & Tsui, 1986). Consequently, the authors suggested that the reaction might be occurring at a lysine residue, which could be adjacent to a cationic site (Kluger & Tsui, 1986). This proximity to a cationic site would result in the pK_a of the Lys being perturbed downward to the observed value of 8.2 (Kluger & Tsui, 1986), relative to the expected value of ~10.5. Considering the high reactivity of acetyl phosphates towards primary amines (Di Sabato & Jencks, 1961a, 1961b), this conclusion by Kluger and colleagues seemed reasonable. While no further studies were conducted to support this hypothesis, nor to determine the exact lysines being modified, our fluorescence-based pH study using a structurally similar probe (SMHP) follows a similar trend.

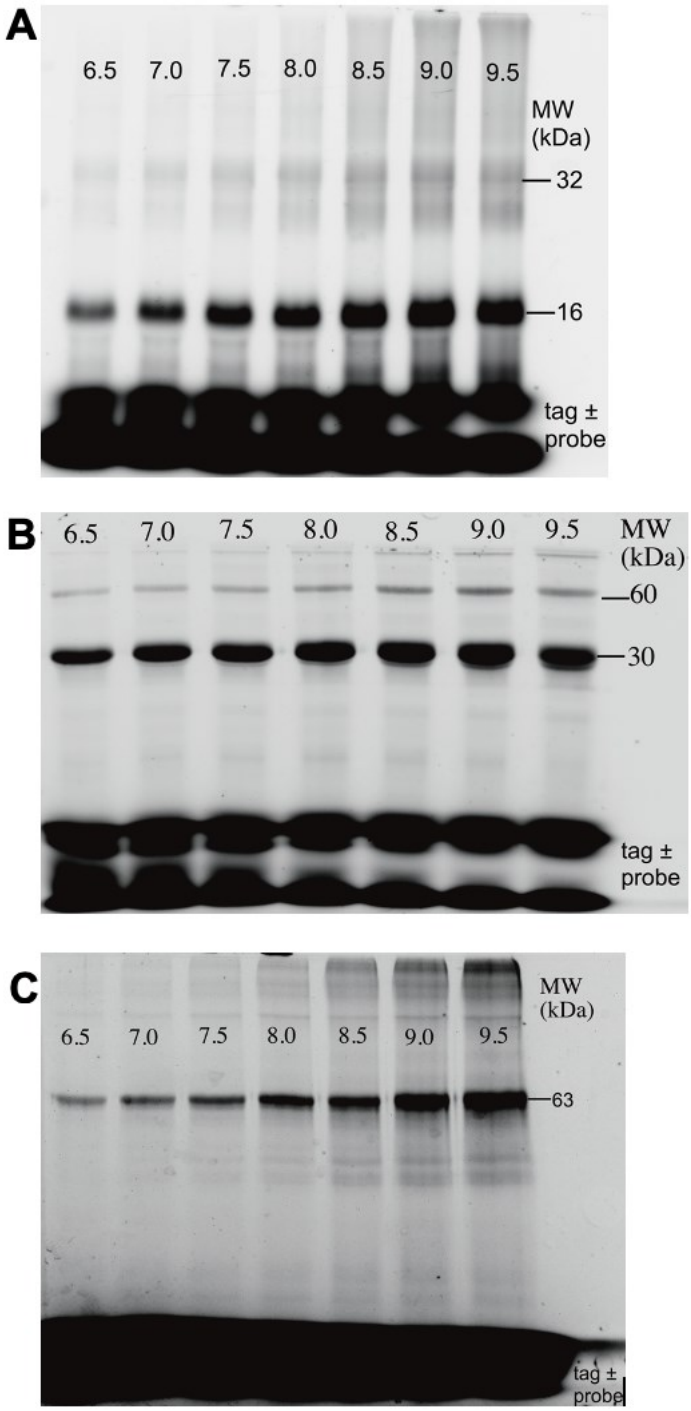

Figure 2.19 SDS-PAGE electrophoretograms of the pH-dependent reactivity of SMHP. Shown are (A) Hb (15% gel), (B) 3-HBDH (15% gel), and (C) CTPS (10% gel). Reactions were conducted from pH 6.5 to 9.5. Samples were analyzed using the Versadoc Imaging System with Alexa 488 as the filter setting (FPA λ_{ex} = 490 nm, λ_{em} = 510 nm). For all proteins, SMHP reactivity was found to be pH-dependent, increasing at higher pH values. The pH values are indicated on each lane.

2.3.6 ASPIRIN-DEPENDENT PROTECTION AGAINST SMHP LABELLING OF Hb

While the structure of aspirin (acetylsalicylate) differs from MAP and SMHP, specifically with respect to the lack of a phosphate group, acetylsalicylate, bearing a single negative charge, was found to acetylate Hb in previous studies (**Figure 2.20A**) (Bridges *et al*., 1975; Klotz & Tam, 1973; Xu *et al*., 1999). The rate of acetylation of Hb by aspirin was found to increase from pH 6.5-8.5, reach a plateau between pH 8.5-9.0, and then decrease at pH 9.5 (Bridges *et al*., 1975). Bridges and colleagues (1975) therefore suggested that the acetylation of Hb is likely to primarily occur at lysine residues, similar to the conclusions made by Kluger & Tsui (1986) for MAP. Xu *et al*. (1999) later confirmed these early findings by conducting protection studies with MAP and aspirin and determined that both compounds modify βLys 82 at the cationic 2,3-DPG binding cleft of Hb.

Given these findings, we first conducted a protection study by pre-incubating Hb in the absence of aspirin (0 mM; 12 h) or with aspirin treatment (20 mM; 12 h), followed by the addition of SMHP (0.5 mM; 2 h). Upon gel-based analysis, there was a clear reduction in the level of fluorescence in the aspirin treated sample relative to the control in the absence of aspirin (**Figure 2.20B**), indicating a reduction in the number of available sites to which SMHP could react and, thus, that the two compounds likely react at the same site(s). The effect of pH on the aspirin-dependent protection was then examined at three pH values: 6.5, 7.5, and 8.5. Hb was pre-incubated in the absence of aspirin (0 mM; 12 h) or with aspirin treatment (20 mM; 12 h), followed by the addition of SMHP (0.5 mM; 2 h). As shown in **Figure 2.20C**, the reduction in the level of

fluorescence from pH 6.5 to 8.5 indicates that both SMHP and aspirin likely react at the same site(s) within the 2,3-DPG binding cleft in a pH-dependent fashion.

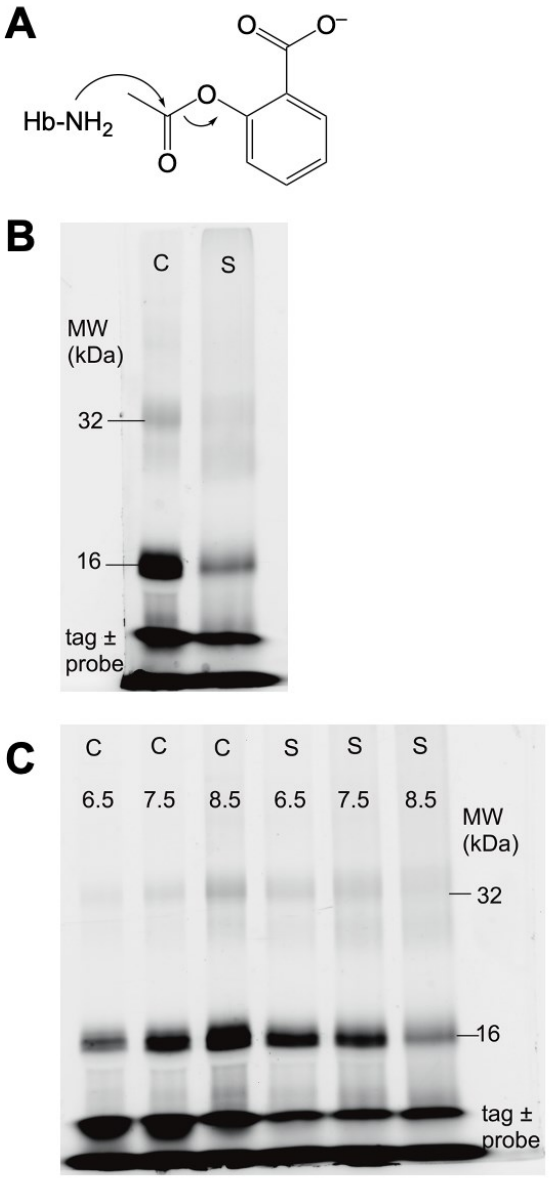

Figure 2.20 Acylation of Hb by aspirin and SMHP. (A) Acylation of Hb by aspirin. (B) Hb was pre-incubated with aspirin (S = sample) or without aspirin (C = control), followed by the addition of SMHP. The reduction in the level of fluorescence with aspirin treatment is likely a result of both SMHP and aspirin modifying the same site(s). (C) Hb was pre-incubated with aspirin (S = sample) or without aspirin (C = control) at pH 6.5, 7.5, and 8.5, yielding modification by both aspirin and SMHP in a pH-dependent manner. Samples were analyzed using the Versadoc Imaging System with Alexa 488 as the filter setting (FPA λ_{ex} = 490 nm, λ_{em} = 510 nm).

2.3.7 MAP-DEPENDENT PROTECTION AGAINST SMHP LABELLING

To evaluate whether SMHP and MAP modify the same sites on Hb, 3-HBDH, and CTPS, a protection study was conducted by pre-incubating each protein with increasing concentrations of MAP (0 – 25 mM) prior to the addition of SMHP. For all three proteins, the level of fluorescence decreased with increasing concentrations of MAP (**Figure 2.21**), consistent with there being a reduction in the number of sites available to react with SMHP. Since the acylation by MAP is irreversible, once the sites are modified, they cannot be later modified by SMHP. This demonstrates that the acyl phosphates likely targeted the same site(s) of each protein, which was anticipated based on SMHP and MAP both containing the reactive monomethyl acyl phosphate moiety. The sites modified by these compounds can be more easily predicted for 3-HBDH and Hb based on literature precedents; however, such a prediction for CTPS is much more difficult due to it possessing multiple ligand binding sites (i.e., for CTP, UTP, ATP/ADP, GTP and L-Gln) (Endrizzi *et al*., 2004, 2005). To further investigate the sites modified by SMHP and MAP on CTPS, fluorescence-based (Section 2.3.8) and kinetic-based (Section 2.3.12.2) protection studies were conducted.

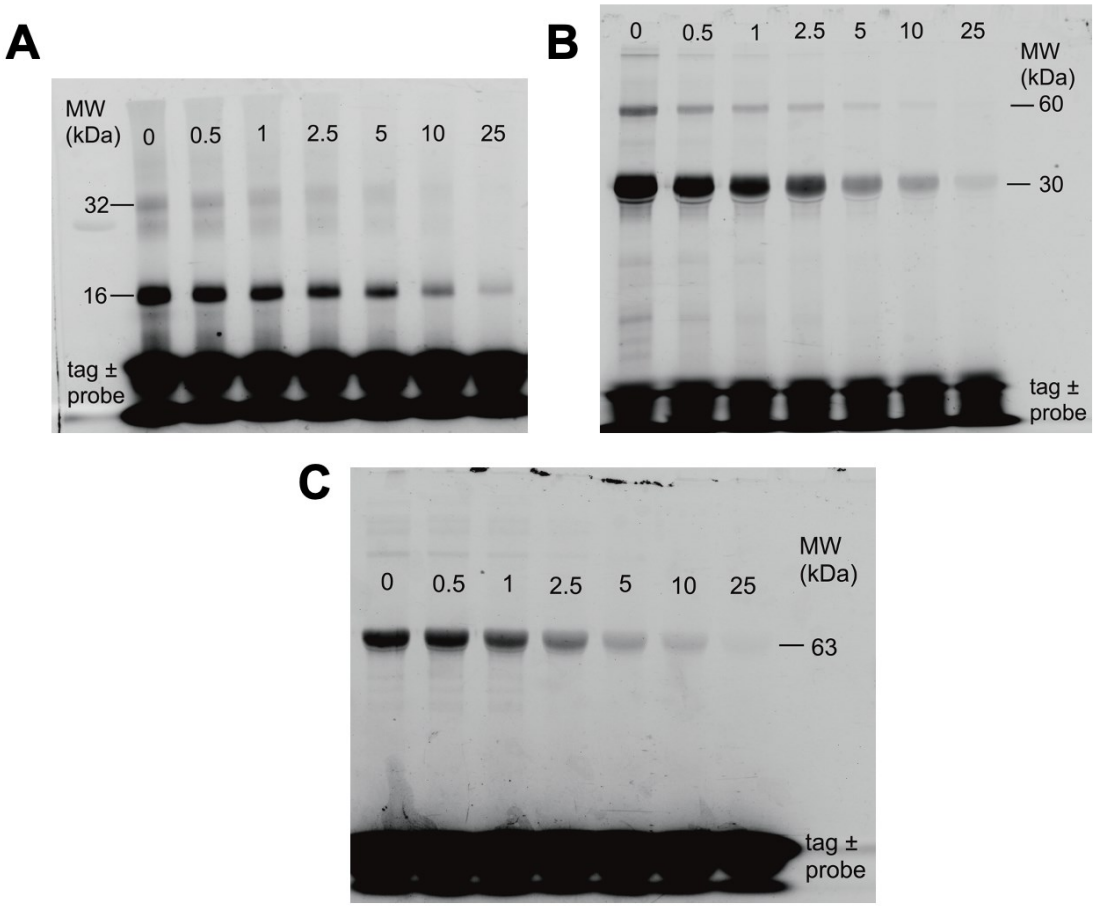

Figure 2.21 SDS-PAGE electrophoretograms of the protection against SMHP-labelling by MAP. Shown are (A) Hb (15% gel), (B) 3-HBDH (15% gel), and (C) CTPS (10% gel). Samples were analyzed using the Versadoc Imaging System with Alexa 488 as the filter setting (FPA λ_{ex} = 490 nm, λ_{em} = 510 nm). The decrease in fluorescence with increasing concentrations of MAP is likely a result of both SMHP and MAP modifying the same sites(s) on each protein.

2.3.8 LIGAND-DEPENDENT PROTECTION AGAINST SMHP LABELLING OF CTPS

In a fluorescence-based protection study to assess the sites on CTPS modified by SMHP, CTPS was pre-incubated with each ligand individually; ATP, CTP, UTP, L-Gln, or with no ligand (control), followed by the addition of SMHP and analyzed using fluorescent tagging. As shown in **Figure 2.22**, pre-incubation of the enzyme with CTP showed the greatest level of protection against labelling by SMHP as illustrated by the faintness of the band relative to the control. ATP and L-Gln showed a modest level of protection and UTP showed either a very minor level or no protection against labelling by SMHP. From this study, SMHP appears to react at multiple ligand binding sites, but predominately at the CTP site. Kinetic-based protection experiments were later conducted to quantitatively assess the protection against MAP-dependent inactivation of CTPS using these same ligands (Section 2.3.12.2).

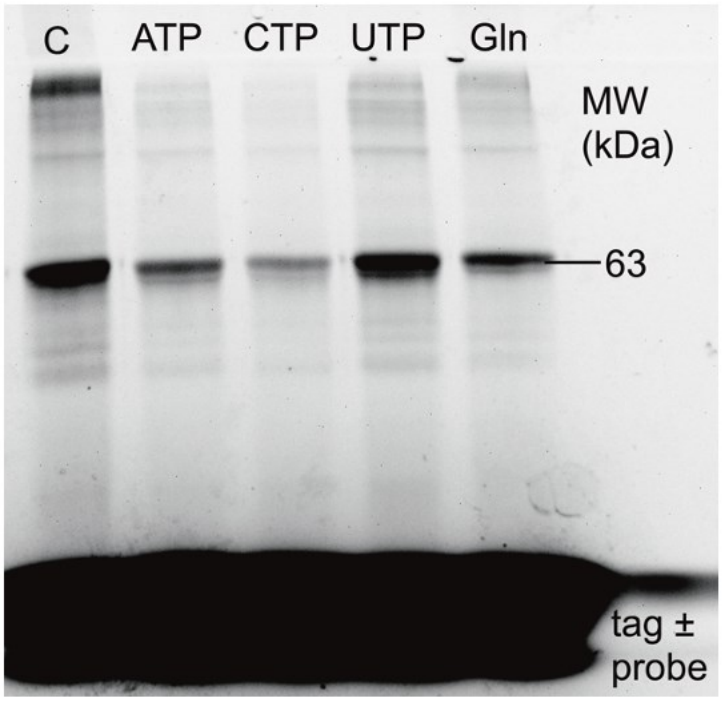

Figure 2.22 SDS-PAGE electrophoretogram of the protection against SMHP-labelling of CTPS by ligands. CTPS was pre-incubated without ligands (C = control) or at saturating concentrations of ATP, CTP, UTP, or L-Gln, followed by the addition of SMHP. Samples were analyzed using the Versadoc Imaging System with Alexa 488 as the filter setting (FPA λ_{ex} = 490 nm, λ_{em} = 510 nm). As shown in the gel (10%), pre-incubation with CTP showed the greatest level of protection against SMHP labelling, but modest protection can be observed when pre-incubated with ATP and L-Gln.

2.3.9 IDENTIFICATION OF 3-HBDH RESIDUES MODIFIED BY SMHP AND MAP

To further assess whether SMHP and MAP targeted the same site(s) within 3-HBDH from *P. lemognei*, each compound was reacted with the enzyme for 1 h, subjected to in-gel trypsin digestion and analyzed by LC-MS/MS. The sequence coverages and LC-MS/MS spectra for the untreated (i.e., control), SMHP-treated, and MAP-treated samples can be found in **Appendix A**. In the SMHP-treated and MAP-treated samples, 94-Da and 42-Da adducts, respectively, were both observed on Ser 142, Lys 156, and Lys 163, which were absent in the untreated samples. As expected, these residues are all located within the conserved active site of 3-HBDH.

While there are no reported crystal structures for 3-HBDH from *P. lemognei*, the amino acid sequences are conserved, especially active-site residues, among 3-HBDHs from other organisms and moreover, among members of the SDR superfamily (Filling *et al*., 2002; Ito *et al*., 2006; Kavanagh *et al*., 2008). 3-HBDH from *P. lemognei* showed the highest amino acid sequence identity (94%) with that of *Oxalobacteraceae bacterium* (accession no. HCY62869.1). Crystal structures for 3-HBDH from: *Alcaligenes faecalis* (PDB: 2YZ7) (Hoque *et al*., 2008), *Pseudomonas fragi* (PDB: 2ZTL) (Nakashima *et al*., 2009), and *Pseudomonas putida* (PDB: 2Q2Q) (Paithankar *et al*., 2007) have been solved and their amino acid sequences share 59, 61, and 67% identity with that of *P. lemognei*, respectfully. A multiple sequence alignment of 3-HBDH from *P. lemognei* with that of *O. bacterium, A. faecalis, P. fragi*, and *P. putida* is shown in **Figure 2.23** to illustrate the conserved residues among 3-HBDH organisms that are modified by SMHP. A crystal structure from *P. fragi* (PDB: 2ZTL) (Nakashima *et al*., 2009) was selected to illustrate those residues of *P. lemognei* modified (**Figure 2.24, 2.25**) because both the coenzyme

NAD^+ and L-3-hydroxybutyrate were bound. The reaction catalyzed by 3-HBDH is highly stereospecific for D-3-hydroxybutyrate (**Scheme 2.2**), with L-3-hydroxybutyrate acting only as a competitive inhibitor with a K_i (1.6 mM) (Ito *et al*., 2006) comparable to the K_m value of D-3-hydroxybutyrate (0.8 mM) (Nakashima *et al*., 2009).

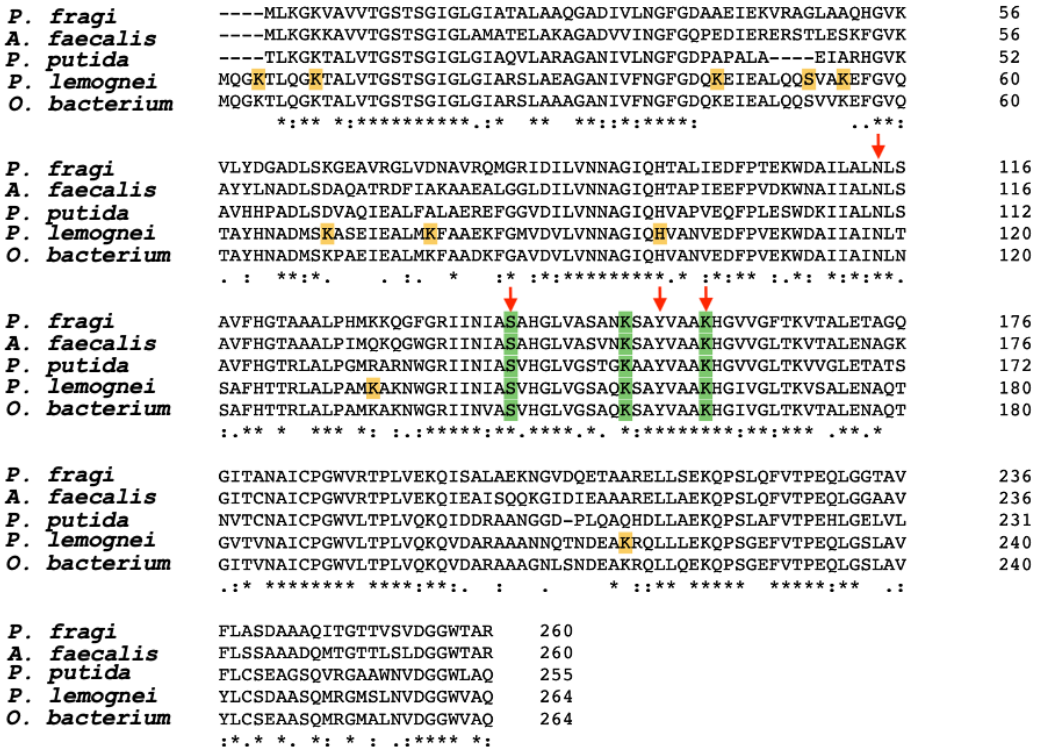

Figure 2.23 Multiple sequence alignment of 3-HBDH. Shown are the aligned amino acid sequences from *P. lemognei* and selected 3-HBDH organisms: *O. bacterium, A. faecalis, P. fragi*, and *P. putida*. Multiple sequence alignments were constructed using Clustal Omega (EMBL-EBI) (Madeira *et al*., 2022). The following residues are indicated: fully conserved (*), conserved between groups of strongly similar properties (:), and conserved between groups of weakly similar properties (.). Residues modified by both SMHP and MAP from *P. lemognei* (Ser 146, Lys 156, and Lys 163) and corresponding residues from the selected 3-HBDH organisms are coloured in green. Additional residues modified by only MAP from *P. lemognei* are coloured in yellow. Conserved catalytic tetrad residues are indicated by a red arrow.

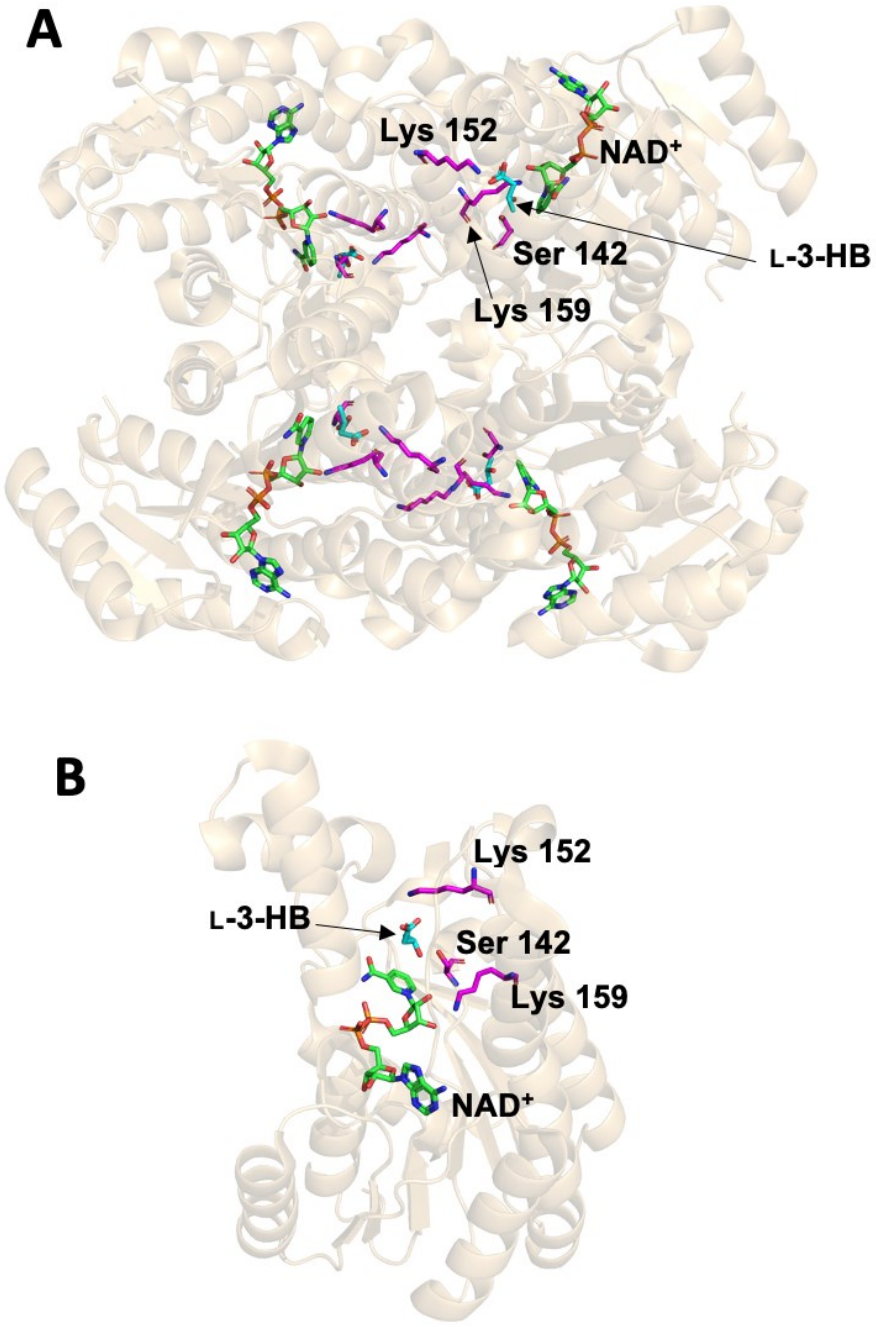

Figure 2.24 Crystal structure of 3-HBDH from *Pseudomonas fragi*. Shown are the (A) homotetramer and (B) monomer enzyme structures. NAD^+ (green), L-3-hydroxybutyrate (L-3-HB) (cyan), and corresponding modified residues (magenta) from the SMHP-modification of 3-HBDH from *Pseudomonas lemognei* are shown. Active site residues: Ser 142, Lys 152, and Lys 159 from *P. fragi* correspond with SMHP-modified residues: Ser 146, Lys 156, and Lys 163 from *P. lemognei* identified by LC-MS/MS. PDB entry: 27TL.

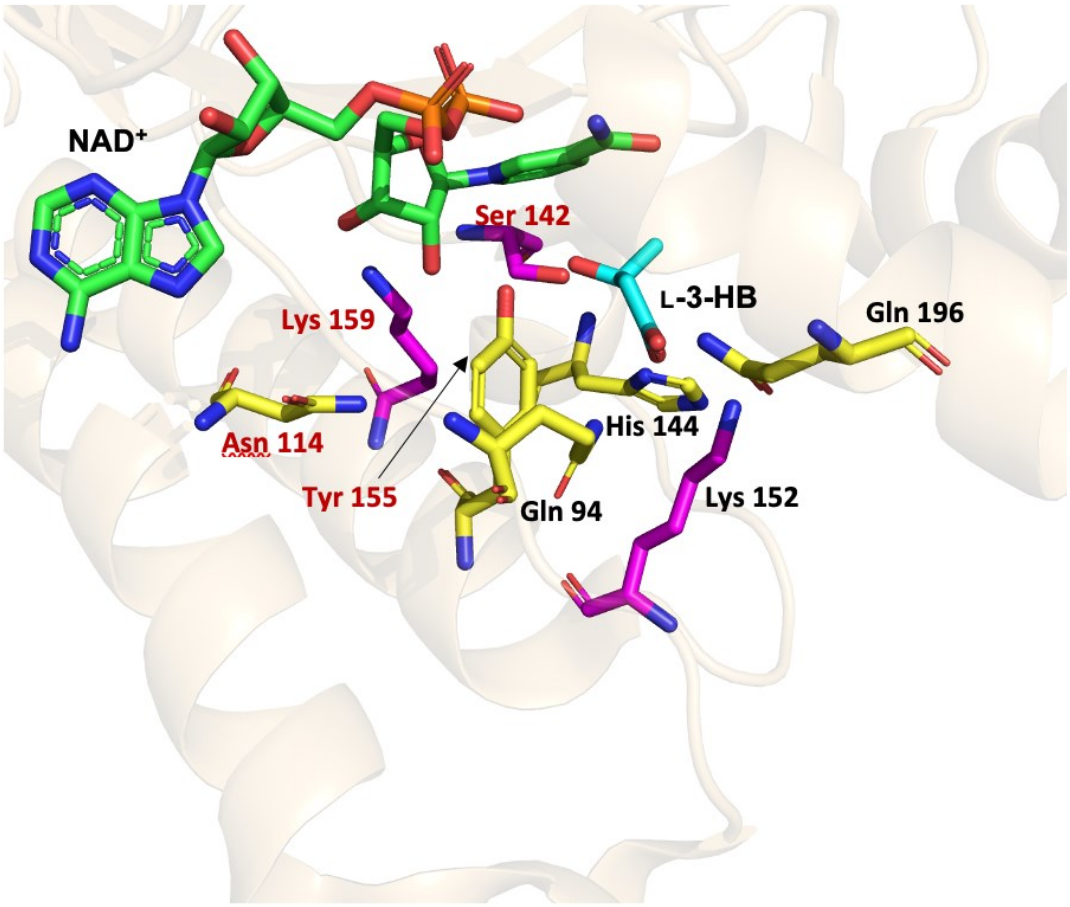

Figure 2.25 Active-site residues of 3-HBDH from *P. fragi.* NAD^+ (green), L-3-hydroxybutyrate (L-3-HB) (cyan), SMHP-modified residues (magenta), and additional active-site residues (yellow) are shown. The conserved residues of the catalytic tetrad are identified in red font. Conserved active site residues: Gln 94, Asn 114, Ser 142, His 144, Lys 152, Tyr 155, and Lys 159 from *P. fragi* are correspond with active-site residues: Gln 98, Asn 118, Ser 146, His 148, Lys 156, Tyr 159, and Lys 163 from *P. lemognei*. PDB entry: 27TL.

These LC-MS/MS findings are consistent with those from the MAP-dependent protection study in which the pre-incubation with MAP, followed by the reaction with SMHP, yielded a reduction in the level of fluorescence in a concentration dependent manner, consistent with MAP and SMHP likely reacting at the same site(s) (Kluger & Tsui, 1986). Given that Ser 146, Lys 156, and Lys 163 were the only residues modified by SMHP, SMHP targeting towards the active site is specific with no off-target modifications.

In addition to targeting the same three residues within the active site as SMHP, (Ser 146, Lys 156, and Lys 163), an additional 10 nucleophiles, mostly lysines, were also modified by MAP (Lys 4, Lys 9, Lys 44, Ser 52, Lys 55, Lys 70, Lys 79, His 99, Lys 134, and Lys 216) as shown in **Figure 2.23**. This was likely a consequence of reacting a high concentration of MAP (25 mM) for a duration of 1 h, thus resulting in off-target labelling.

Within this highly conserved active site are four residues involved in substrate recognition and catalysis, including Gln 196/200, Gln 94/98, His 144/148, and Lys 152/156 (modified by SMHP) in *P. fragi/P. lemognei* 3-HBDH, which form hydrogen bonding interactions with the two oxygen atoms of the carboxylate group of the substrate (Ito *et al*., 2006; Nakashima *et al*., 2009). The residues of the conserved catalytic tetrad in the SDR superfamily include: Tyr 155/159, Ser 142/146, Lys 159/163, and Asn 114/118 in *P. fragi/P. lemognei* 3-HBDH (Ito *et al*., 2006). Thus, two of the three SMHP-modified residues are members of the conserved catalytic tetrad: Ser 142/146, Lys 159/163 in *P. fragi/P. lemognei* 3-HBDH.

Tyr 155/159 in *P. fragi/P. lemognei* 3-HBDH acts as an acid/base catalyst to donate or accept a proton to/from acetoacetate and D-3-hydroxybutyrate, respectively (Hoque *et al*., 2008; Kavanagh *et al*., 2008). Ser 142/146 stabilizes and positions the hydroxyl or carbonyl group of the substrate through hydrogen bonding interactions (Benach *et al*., 1999; Filling *et al*., 2002; Oppermann *et al*., 1997). The two major roles of Lys 159/163 include orientation of the nicotinamide-ribose moiety of the coenzyme through hydrogen bonding and also reduction of the pK_a of Tyr 155/159 through electrostatic interactions to promote proton transfer (Benach *et al*., 1999; Filling *et al*., 2002; Hoque *et al*., 2008). The presence of NAD^+ specifically as the oxidized, positively charged coenzyme further facilitates the reduction in pK_a of the catalytic tyrosine (Benach *et al*., 1999). Lastly, Asn 114/118 establishes a proton relay network, originally proposed by Oppermann and colleagues (2002). As represented in **Figure 2.26**, hydrogen bonding between the catalytic Lys residue (side chain) and the catalytic Asn residue (main chain carbonyl) to a water molecule forms a proton relay network involving the coenzyme ribose (2′-OH), whereby protons are relayed to and from the catalytic Tyr base (Filling *et al*., 2002). This proton relay network provides some indication as to the location of the cationic binding site that may partially neutralize the negative charge of the reactive methyl acyl phosphate species. The relay of protons creates a shift in charge between a positively charged Lys residue and a neutral Lys residue, which could act as both the cationic binding site and the attacking nucleophile throughout the course of the 1 h reaction (Filling *et al*., 2002). While the cationic site cannot be determined with absolute certainty, it is expected that either Lys 159/163 in *P. fragi/P. lemognei* 3-HBDH,

which undergoes a shift in charge to achieve a proton relay network as described above, Lys 152/156 or His 144/148 act as the active-site cation.

Kluger and colleagues (1986) assessed the rate of MAP-dependent inactivation of 3-HBDH from *P. lemognei* in the presence and absence of coenzymes NADH and NAD^+. The rate of inactivation was found to decrease in a concentration-dependent manner in the presence of either NADH or NAD^+, demonstrating protection by the coenzymes (Kluger & Tsui, 1986). Within the active site of 3-HBDH, the hydroxyl groups of the NAD^+/NADH nicotinamide-ribose are known to form hydrogen bonding interactions with Lys 159/163 (modified by SMHP) in *P. fragi/P. lemognei* 3-HBDH, Tyr 155/159, and the main chain carbonyl of Asn 90/94 (Hoque *et al*., 2008; Ito *et al*., 2006). The amide group of the NAD^+/NADH is also anchored by hydrogen bonding interactions with both the main chain amino and carbonyl group of Val 188/192 and the main chain carbonyl of Thr 190/194 (Hoque *et al*., 2008; Ito *et al*., 2006). Thus, given that NAD^+/NADH interacts with several active-site residues, including with Lys 159/163 in *P. fragi/P. lemognei* 3-HBDH, which was modified by both SMHP and MAP in our work, it is not surprising that Kluger and Tsui (1986) observed protection against MAP-dependent inactivation in the presence of these co-enzymes.

Similarly, ADP and the competitive inhibitor methyl acetonylphosphonate have shown protection against MAP-dependent inactivation of 3-HBDH (Kluger & Tsui, 1986). Because of the protection observed by these coenzymes, coenzyme analogues, and substrate analogues, all containing phosphate groups, it is not surprising that kinases were among the most frequently labelled enzyme subclass (EC 2.7) from *P. lemognei* modified by SMHP due to their ATP binding sites (**Figure 2.16**). As kinases typically contain two

active site Lys residues, modification by SMHP and MAP is likely to occur at one of the two active-site lysine residues (Patricelli *et al*., 2007).

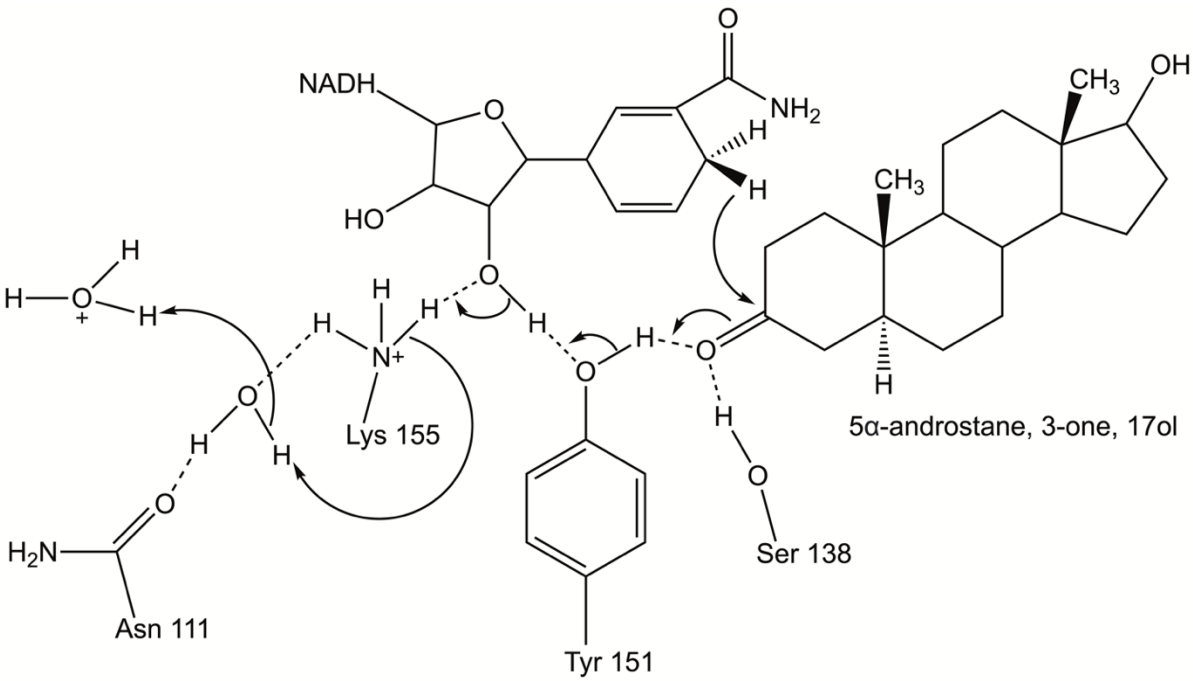

Figure 2.26 Proton relay network in proteins of the SDR superfamily. The proton relay network is established through hydrogen bonding interactions between Asn111, Lys155 and a water molecule. This network is conserved among the SDR superfamily members, whereby conserved active site residues in this figure: Asn 111, Ser 138, Tyr 151, and Lys 155 in 3β/17 β-hydroxysteroid dehydrogenase from *Comamonas testosteroni* are homologous with Asn 114, Ser 142, Tyr 155, and Lys 159 in 3-HBDH from *P. fragi* and, Asn 118, Ser 146, Tyr 159, and Lys 163 from *P. lemognei*. In this representation, NADH is the coenzyme with a steroid substrate (5α-androstane, 3-one, 17ol). Adapted from Filling *et al.,* (2002).

2.3.10 3-HBDH KINETIC ASSAYS

2.3.10.1 Determination of kinetic parameters

The kinetic parameters of 3-HBDH were assessed through non-linear regression analysis for the conversion of NAD^+ to NADH with D-3-hydroxybutyrate as the substrate (**Figure 2.27)**. At pH 7.0 and 20 °C, the kinetic values were determined to be $K_m = 2.61 \pm 0.36$ mM, $k_{cat} = 75.09 \pm 10.35$ s^{-1}, and $k_{cat}/K_m = 28.97 \pm 4.11$ $M^{-1}s^{-1}$.

The optimal pH from the D-3-hydroxybutyrate reaction direction is 8.5 with an optimum temperature of 37 °C (Ito *et al*., 2006; Nasser *et al*., 2002). However, the assay conditions with respect to pH and temperature were adjusted accordingly to 7.0 and 20 °C (with enzyme storage on ice), respectively, to maintain enzyme stability throughout the duration of the assay when the enzyme was diluted (i.e., 0.0035 mg/mL). Instability of 3-HBDH at low concentrations is well-documented across various organisms, such as 3-HBDH from *Myobacterium phlei* (Dhariwal & Venkitasubramanian, 1978), which remained stable at 2.4 mg/mL after 15 min at 37 °C, but when diluted to 0.24 mg/mL, 70% activity was lost over this duration.

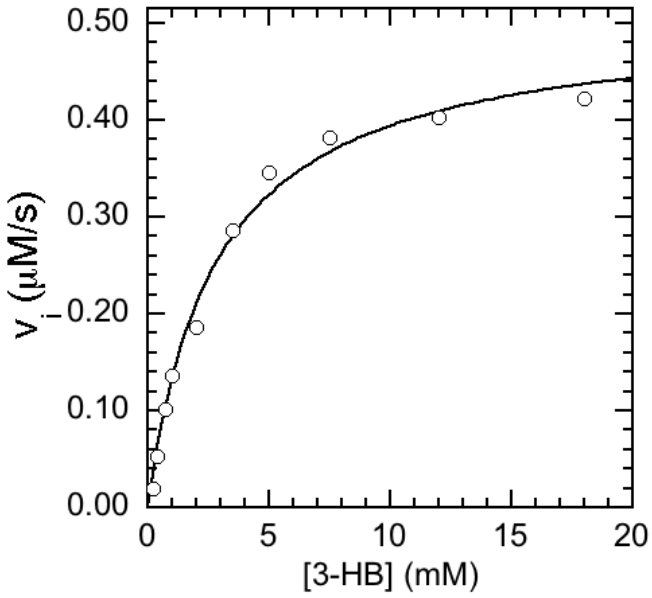

Figure 2.27 Representative Michaelis-Menten plot for the determination of the kinetic parameters for 3-HBDH. The kinetic parameters, k_{cat}, K_m, and k_{cat}/K_m were determined using a saturating concentration of NAD^+ (2 mM), with D-3-hydroxybutyrate (3-HB) concentrations ranging from 0.2-18.0 mM, with a final [3-HBDH] of 0.175 μg/mL (5.82 nM). The kinetic values (determined in triplicate) for 3-HBDH were K_m = 2.61 ± 0.36 mM, k_{cat} = 75.09 ± 10.35 s^{-1}, and k_{cat}/K_m = 28.97 ± 4.11 $M^{-1}s^{-1}$.

2.3.10.2 Inactivation by MAP

The time-dependent inactivation of 3-HBDH (3.5 μg/mL) by MAP was assessed with varying concentrations of MAP (0 – 65.0 mM) under the same pH and temperature conditions described in Section 2.3.10.1. The inactivation of 3-HBDH by MAP was found to occur in a time-dependent manner wherein saturation was observed in the replot of the pseudo-first order rate constants (k_{obs}) as a function of the concentration of MAP (**Figure 2.28**). As shown in **Figure 2.28**, and as described previously in Section 2.2.15.2, minor activity losses that occurred throughout the assay were corrected for by subtracting the pseudo-first-order rate constants (k_{obs} values) obtained from the slopes of the untreated enzyme (i.e., control) from those of the MAP-treated enzyme over the specific reaction period. The kinetic values for the inactivation were determined from the replot of

the k_{obs} values as a function of [MAP] to be K_I = 27.949 ± 0.179 mM, k_{inact} = 0.299 ± 0.012 min^{-1}, and k_{inact}/K_I = 0.178 ± 0.007 $M^{-1}s^{-1}$.

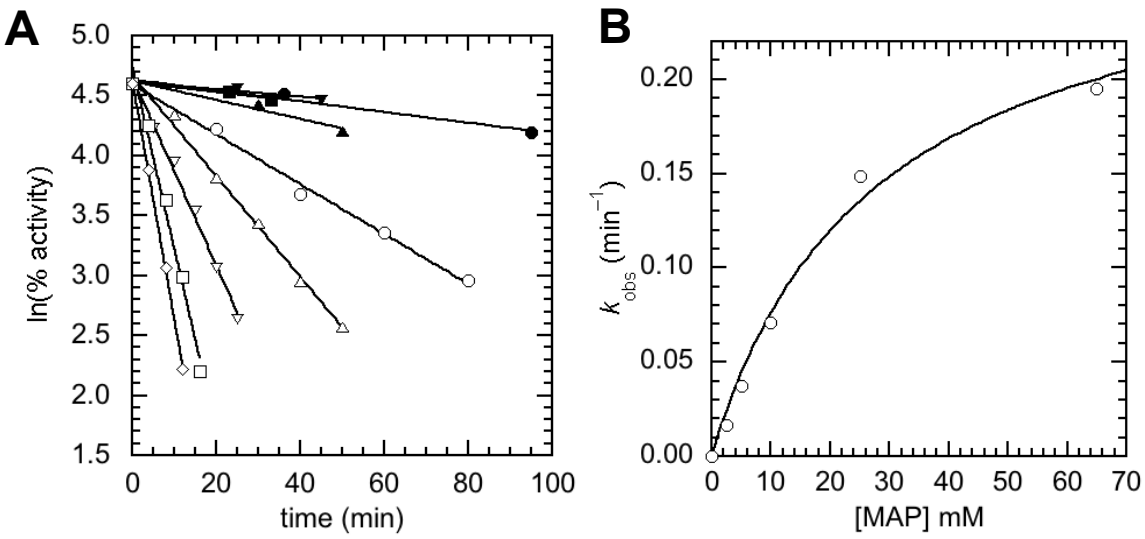

Figure 2.28 Representative plots for the time dependent inactivation of 3-HBDH by MAP. (A) 3-HBDH (3.5 μg/mL) was incubated with varying concentrations of MAP: 2.5 (○), 5.0 (△), 10.0 (▽), 25.0 (□), and 65.0 (◇) mM. Minor enzyme activity losses that occurred over the inactivation assay were corrected for by subtracting the pseudo-first-order rate constants (k_{obs} values) obtained from the slopes of the untreated enzyme (i.e., control) from those of the MAP-treated enzyme over the specific reaction period. The k_{obs} from control 1 (●) was used to correct the k_{obs} values from [MAP] = 2.5 mM (○) and 5.0 mM (△), control 2 (▲) was used to correct the k_{obs} value from [MAP] = 10.0 mM (▽), control 3 (▼) was used to correct the k_{obs} value from [MAP] = 25.0 mM (□), and control 4 (■) was used to correct the k_{obs} value from [MAP] = 65.0 mM (◇). (B) The corrected k_{obs} values from A) were plotted as a function of [MAP] to determine (in triplicate) the K_I, k_{inact}, and k_{inact}/K_I values using non-linear regression analysis since saturation was observed, where K_I = 27.949 ± 0.179 mM, k_{inact} = 0.299 ± 0.012 min^{-1}, and k_{inact}/K_I = 0.178 ± 0.007 $M^{-1}s^{-1}$.

The determined K_I of 27.95 ± 0.18 mM (100 mM potassium phosphate, pH 7.0; 20 °C) for the MAP-dependent inactivation of 3-HBDH with D-3-hydroxybutyrate as the substrate in this work is comparable to the K_i of 10 mM (100 mM potassium phosphate,

pH 6.5; 37 °C) for the inhibition of 3-HBDH by MAP with acetoacetate as the substrate determined by Kluger and Tsui (1986).

SMHP was also found to inactivate 3-HBDH; however, due to the slow rate of inactivation, combined with the spontaneous inactivation of 3-HBDH in the absence of inhibitor, obtaining inactivation kinetics was difficult. Consequently, only the k_{obs} value at a concentration of 5 mM SMHP could be accurately determined. While the inactivation of 3-HBDH by MAP (5 mM) gave a k_{obs} value of 0.0406 ± 0.0033 min^{-1}, the inactivation by SMHP (5 mM) gave a k_{obs} value of 0.0066 ± 0.0005 min^{-1}. Thus, the pseudo-first order rate constant for the inactivation of 3-HBDH by MAP is ~6-fold greater than that of SMHP at a concentration of 5 mM, which is not surprising given that MAP is a smaller compound relative to SMHP. Overall, the inactivation of 3-HBDH by MAP and SMHP provided additional evidence towards the efficiency of reactivity at the active site by the acyl phosphates.

2.3.11 IDENTIFICATION OF CTPS RESIDUES MODIFIED BY SMHP

To assess the specific sites of modification of CTPS from *E. coli*, LC-MS/MS was employed using an approach similar to that used for 3-HBDH. The sequence coverages and LC-MS/MS analysis for the untreated and SMHP-treated samples can be found in **Appendix B**. In the SMHP-treated samples, 94-Da adducts were observed on Lys 223, Lys 233, Lys 239, Lys 246, Lys 252, Lys 342, Lys 479, and Lys 534 (**Figure 2.29**). Unlike with 3-HBDH, however, where each of the three modified residues resided at the active-site, only two of the eight SMHP-modified Lys residues from CTPS were clearly located at the ligand binding sites: Lys 223 at the CTP binding site and Lys 239 the

ATP/ADP binding site. Lys 233, Lys 242, and Lys 252 were located adjacent to the the ATP/ADP binding site, and Lys 342, Lys 479, and Lys 534 were not located near any of the ligand binding sites, including those for the nucleotides and L-Gln.

In the previously conducted fluorescence-based protection study, protection was observed when pre-incubated with each of the ligands, CTP, ATP, L-Gln, and possibly UTP as shown by the reduction in the degree of fluorescence (Section 2.3.8), and thus, these sites were expected to be modified by SMHP using LC-MS/MS. In agreement with the fluorescence-based protection study for CTP and ATP, identification of 94-Da adducts with Lys 223 at the CTP binding site and of Lys 239 at the ATP/ADP by LC-MS/MS provides more conclusive evidence for the site-specific protection. However, the absence of SMHP-modified residues at the L-Gln ligand binding site was surprising given the modest level of protection observed in the fluorescence-based protection study. Since the LC-MS/MS study was conducted in the absence of ligands, it is possible that all potentially reactive residues were accessible; however, upon ligand binding in the fluorescence-based protection study, conformational changes, induced by CTPS ligands, such as L-Gln, could mask the reactivity of some residues. Structural and mechanistic details of CTPS and ligand binding sites are discussed in detail in this Section (2.3.11). To explore the extent of protection in a more quantitative manner, kinetics-based protection studies with MAP were conducted as discussed in Section 2.3.12.2.

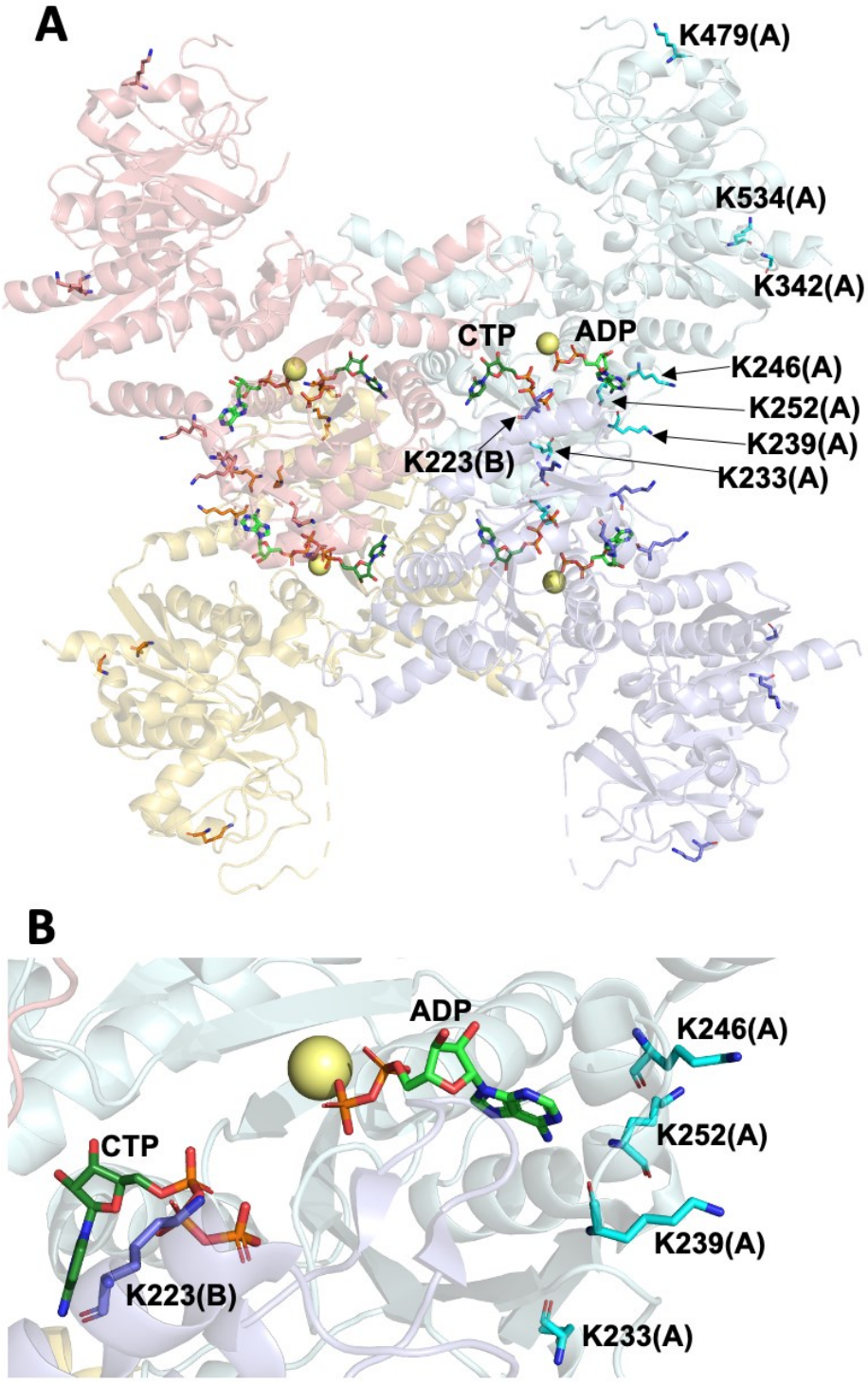
A
K479(A)
K534(A)
K342(A)
CTP
ADP
K246(A)
K252(A)
K239(A)
K223(B)
K233(A)
B
ADP
K246(A)
CTP
K252(A)
K239(A)
K223(B)
K233(A)

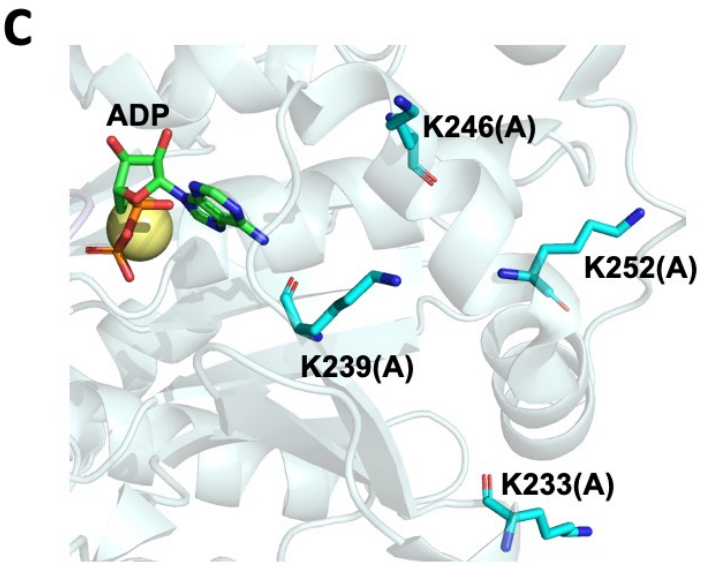

Figure 2.29 Crystal structure of CTPS from *E. coli*. (A, B, C) Shown is the tetramer with the monomers represented in cyan, violet, pink, and orange ribbon representation, with the SMHP-modified residues represented in the same colour as that of their monomer. SMHP-modified Lys residues from the cyan monomer (A- Lys 233, Lys 239, Lys 246, Lys 252, Lys 342, Lys 479, Lys 534) and violet monomer (B- Lys 223) are distinguished beside each labelled residue in parenthesis. Shown in the structures are CTP (forest green), ADP (light green), and the magnesium ion (yellow). PDB entry: 2AD5.

CTPS contains two catalytic domains: a C-terminal glutaminase domain, which catalyzes the hydrolysis of L-Gln and an N-terminal synthase domain, which catalyzes the amination of ATP-activated UTP (4-phospho UTP) to yield CTP (Endrizzi *et al*., 2004; Willemoës, 2004). The NH_3 derived from Gln hydrolysis or from exogenous NH_3 introduced as the substrate is transported from the glutaminase domain to the synthase domain through a 25-Å tunnel that connects the active sites of the two domains (McCluskey & Bearne, 2018).

ATP and UTP act synergistically to induce tetramerization of the inactive homodimer to its catalytically active form, whereby the enzyme displays positive co-operativity for each substrate (Levitzki & Koshland, 1972b; Long & Pardee, 1967). The binding sites for the nucleotide substrates are located in the synthase domain at the

tetramer interfaces (Endrizzi *et al*., 2004, 2005; Weng *et al*., 1986; Weng & Zalkin, 1987). Liu and colleagues (2021) suggested that binding of either substrate, UTP and/or ATP, induces an open-to-closed conformational change. The X-ray crystal structure of CTPS from *E. coli* with bound ADP and CTP was solved by Baldwin and colleagues (2005), as shown in **Figure 2.29** (PDB: 2AD5). The ATP/ADP-binding site with ADP bound showed several hydrogen bonding interactions between the α- and β-phosphates of the ligand and the amide groups of residues Ser 15, Gly 17, Lys 18, Gly 19, and Ile 20 (Endrizzi *et al*., 2005). Furthermore, water-mediated hydrogen bonds facilitated the binding of the ribose O4′ with Arg 211 (guanidinium) and Ser 15 (carbonyl) (Endrizzi *et al*., 2005). Lastly, specificity for the adenine is facilitated by hydrogen bonds between N1 and N6 of the adenine ring with the main chain of Val 241 (amide) and Lys 239 (carbonyl) (modified by SMHP), respectively (Endrizzi *et al*., 2005).

CTP is a feedback inhibitor that is competitive with UTP (Endrizzi *et al*., 2004). Specifically, the triphosphate moiety of CTP and the triphosphate moiety of UTP bind at the same site, leading to the observed competitive feedback inhibition (Endrizzi *et al*., 2004). CTPS from *E. coli* with UTP bound has not been crystallized, but the binding interactions can be easily predicted based on solved structures of CTPS from various species with bound UTP, such as human (PDB: 7MGZ) (Lynch *et al*., 2021) and *Drosophila melanogaster* (PDB: 7DPW) (Zhou *et al*., 2021). Recognition of UTP is highly specific with *E. coli* CTPS with respect to the uracil moiety, ribose and 5′-triphosphate (Scheit & Linke, 1982). Thus very few alternative substrates have been identified to date for UTP, with 2′,2′-difluoro-2′-deoxy-UTP being one of them (McCluskey *et al*., 2016). As described by Baldwin and colleagues (2005), binding of the

cytosine moiety and the ribose of CTP occur through an "induced fit" rearrangement where the Asp 147, Glu 149, Gln 114, and Ile 148 side chains rotate to facilitate binding of the base. Glu 149 (side chain) forms hydrogen bonding interactions with the ribose 2′- and 3′- hydroxyl groups with Val 115 (backbone amide) and Ile 116 (backbone amide) residues providing additional hydrogen bonding interactions with the 2′-hydroxyl (Endrizzi *et al*., 2005). Lastly, the common binding site for the triphosphate moieties of CTP and UTP utilizes extensive hydrogen bonding interactions between the γ-phosphate and Lys 187 (side chain), Thr 188 (side chain and main chain amide) and Lys 189 (main chain amide) in addition to hydrogen bonding interactions between the β-phosphate and the side chains of Lys 189, Gln 192, and Lys 223 (modified by SMHP) (Endrizzi *et al*., 2005).

While it serves a minimal role when exogenous ammonia is used as the substrate, GTP is a positive allosteric activator for the L-Gln-dependent synthesis of CTP (Bearne *et al*., 2001; Levitzki & Koshland, 1972a; Zhou *et al*., 2021). The first crystal structure of CTPS from *D. melanogaster* with GTP bound was recently solved by Liu and colleagues (2021) (PDB: 7DPT) (**Figure 2.30**). The GTP binding site was localized at the cleft between the glutaminase domain and the synthase domain, and more specifically, between the glutaminase active site and the ammonia tunnel (Zhou *et al*., 2021). Tetramerization of the enzyme into its closed state where the glutaminase and synthase domains contract, induced by ATP and UTP binding, is required to form the GTP binding site, thus, the open conformation in the absence of these substrates does not permit binding of GTP (Zhou *et al*., 2021). In addition, this crystal structure of CTPS from *D. melanogaster* also had 6-diazo-5-oxo-L-norleucine (DON) bound, an analogue of L-Gln

and irreversible inactivator of CTPS. In addition to the requirement of both UTP and ATP being bound to facilitate formation of the GTP binding site, it was concluded that binding of DON (L-glutamine) in the GATase domain active-site is also required to stabilize the binding of GTP by facilitating the rotation of Phe 373, which forms a π–π stacking interaction with the guanine ring of GTP (Zhou *et al*., 2021).

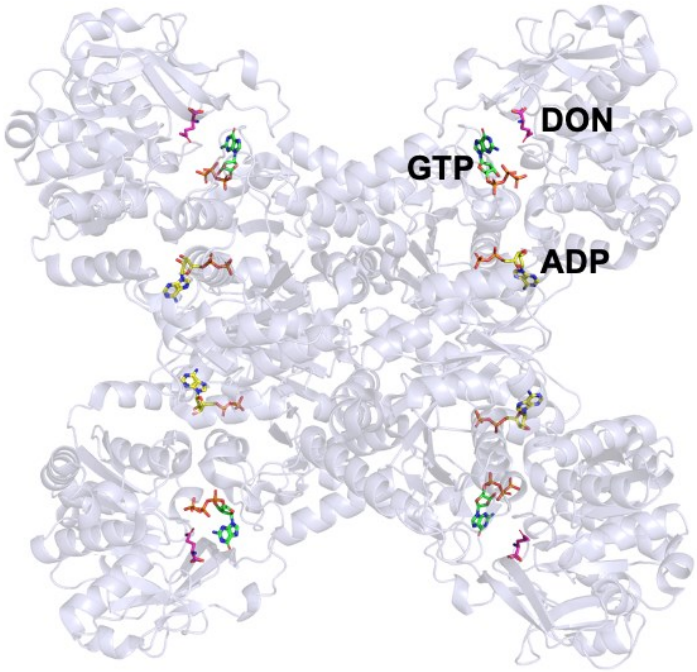

Figure 2.30 Crystal structure of the CTPS tetramer from *D. melanogaster*. Shown in structure are the allosteric activator GTP (green), L-glutamine analogue, 6-diazo-5-oxo-L-norleucine (DON) (magenta), and ADP (yellow). PDB entry: 2DPT.

2.3.12 CTPS KINETIC ASSAYS

2.3.12.1 Inactivation by MAP and SMHP

The time-dependent inactivation of CTPS (1.0 mg/mL) with varying concentrations of MAP (0 – 10 mM) and SMHP (0 – 50 mM) were each found to occur in a time-dependent manner, as shown in **Figures 2.31A**, and **2.32A**. Since saturation was not observed from the replot of the pseudo-first-order rate constant (k_{obs}) values as a function of [MAP] (**Figure 2.31B**) for the MAP-dependent inactivation of CTPS, only the apparent second-order rate constant for the efficiency of inactivation (k_{inact}/K_I) could be determined from the slope of the replot, yielding a k_{inact}/K_I value of 0.613 ± 0.015 $M^{-1}s^{-1}$. As saturation was in fact observed from the replot of the k_{obs} values as a function of [SMHP] (**Figure 2.32B**) for the SMHP-dependent inactivation of CTPS, the kinetic values for the inactivation were determined using non-linear regression analysis as K_I = 10.341 ± 1.347 mM, k_{inact} = 0.110 ± 0.003 min^{-1}, and k_{inact}/K_I = 0.179 ± 0.019 $M^{-1}s^{-1}$.

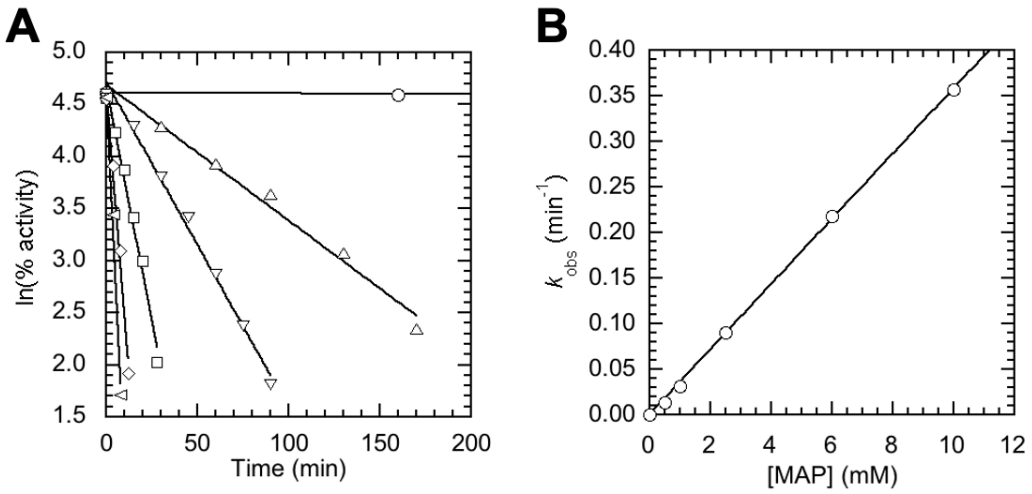

Figure 2.31 Representative plots for the time-dependent inactivation of CTPS by MAP. (A) CTPS (1.0 mg/mL) was incubated with varying concentrations of MAP: 0.0 (○), 0.5 (△), 1.0 (▽), 2.5(□), 6.0 (◇), and 10.0 (◁) mM. (B) The observed pseudo-first-order rate constants (k_{obs} values) obtained as the slopes from (A) were re-plotted as a function of [MAP] to determine (in triplicate) the apparent second-order rate constant for the efficiency of inactivation (k_{inact}/K_I), with a value of 0.613 ± 0.015 $M^{-1}s^{-1}$.

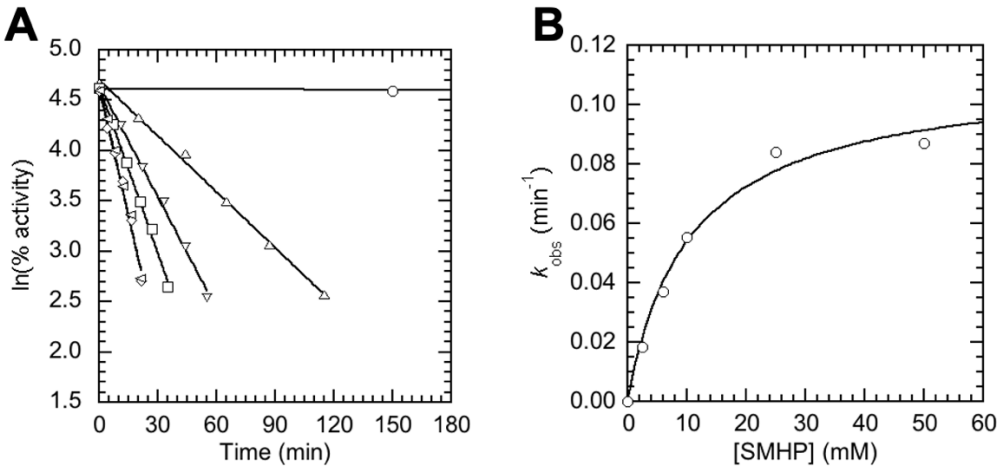

Figure 2.32 Representative plots for the time-dependent inactivation of CTPS by SMHP. (A) CTPS (1.0 mg/mL) was incubated with various concentrations of SMHP: 0.0 (○), 2.5 (△), 6.0 (▽), 10.0 (□), 25.0 (◇), and 50.0 (◁) mM. (B) The observed pseudo-first-order rate constants (k_{obs} values) obtained as the slopes from (A) were re-plotted as a function of [SMHP]. Since saturation was observed, non-linear regression was used to fit the data so that the kinetic constants for K_I, k_{inact}, and k_{inact}/K_I could be determined (in triplicate), where K_I = 10.341 ± 1.347 mM, k_{inact} = 0.110 ± 0.003 min^{-1}, and k_{inact}/K_I = 0.179 ± 0.019 $M^{-1}s^{-1}$.

The efficiency of inactivation (k_{inact}/K_I) for the MAP-dependent inactivation of CTPS was ~ 3-fold greater than that observed for SMHP. Since saturation was observed for the inactivation of CTPS by SMHP, it was interesting that saturation was not also observed for the inactivation of CTPS by MAP. However, as described in Section 2.3.11, while two of the SMHP-modified residues were located at the ATP/ADP and CTP binding sites, the others were surface Lys residues and, thus, such residues could be participating in a bimolecular reaction with MAP. Since SMHP is a larger compound with more binding determinants, it can interact so that a detectible complex formation is observed kinetically. Overall, the inactivation of CTPS by MAP and SMHP provided additional evidence towards the efficiency of reactivity by the acyl phosphates.

2.3.12.2 Protection against MAP-dependent inactivation by ligands

The protection against MAP-dependent inactivation of CTPS was quantitatively assessed by incubating CTPS (1.0 mg/mL) with a fixed concentration of MAP (2.5 mM), with varying concentrations of each ligand (ATP: 0 – 2 mM, CTP: 0 – 0.2 mM, UTP: 0 – 4 mM, and L-glutamine: 0 – 5 mM) (**Figures 2.33** to **2.36**). The calculated K_L values (the apparent dissociation constant for the ligand-mediated protection against inactivation) are given in **Table 2.1** for ATP, CTP, and UTP. All ligands showed protection against inactivation by MAP, with CTP being the most potent protectant as demonstrated by having the highest apparent binding affinity, with a K_L value of 0.075 ± 0.004 mM.

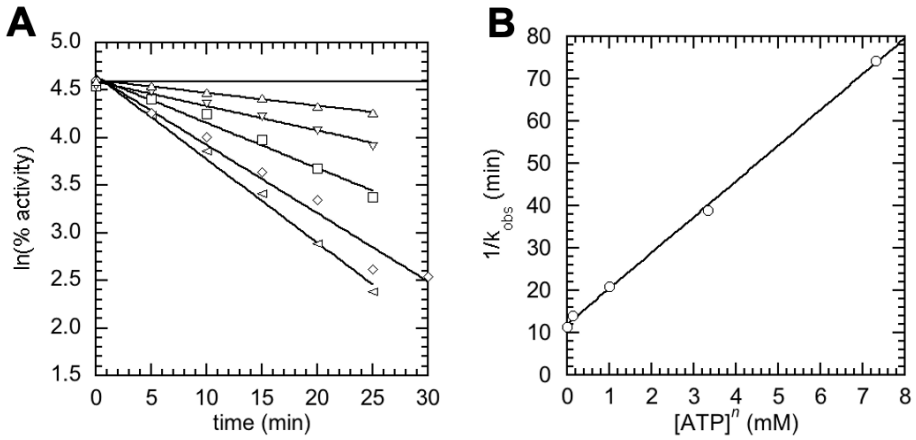

Figure 2.33 Protection against MAP-dependent inactivation of CTPS by ATP. (A) CTPS (1 mg/mL) was incubated with MAP (2.5 mM) with varying concentrations of ATP: 0.0 (◁) 0.5 (◇), 1.0 (□), 1.5 (▽), and 2.0 (△) mM in addition to a control in the absence of MAP and ATP (○). (B) The inverse of the observed pseudo-first-order rate constants ($1/k_{obs}$ values) obtained as the inverse of the slope values from A) were plotted as a function of $[ATP]^n$, where the Hill number (n) = 2.872 ± 0.116, to determine the apparent ligand-mediated dissociation constant for the protection against inactivation (K_L). The slope and y-intercept (determined in singlicate) from the replot were: 8.438 ± 0.171 min mM^{-1} and 11.969 ± 0.622 min, respectively, yielding a K_L value of 1.092 ± 0.100.

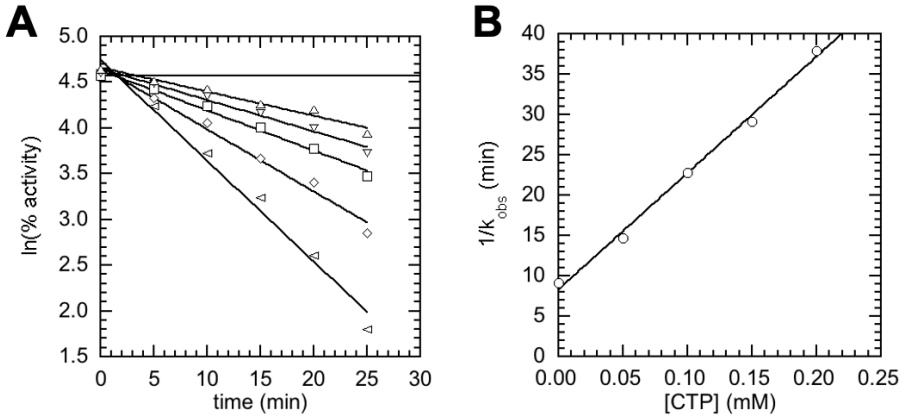

Figure 2.34 Protection against MAP-dependent inactivation of CTPS by CTP. (A) CTPS (1 mg/mL) was incubated with MAP (2.5 mg/mL) with varying concentrations of CTP: 0.00 (◁) 0.05 (◇), 0.10 (□), 0.15 (▽), and 0.20 (△) mM in addition to a control in the absence of MAP and CTP (○). (B) The inverse of the observed pseudo-first-order rate constants ($1/k_{obs}$ values) obtained as the inverse of the slope values from A) were plotted as a function of [CTP] to determine the apparent ligand-mediated dissociation constant for the protection against inactivation (K_L). The slope and y-intercept (determined in singlicate) from the replot were: 144.28 ± 5.75 min mM^{-1} and 8.305 ± 0.704 min, respectively, yielding a K_L value of 0.075 ± 0.004.

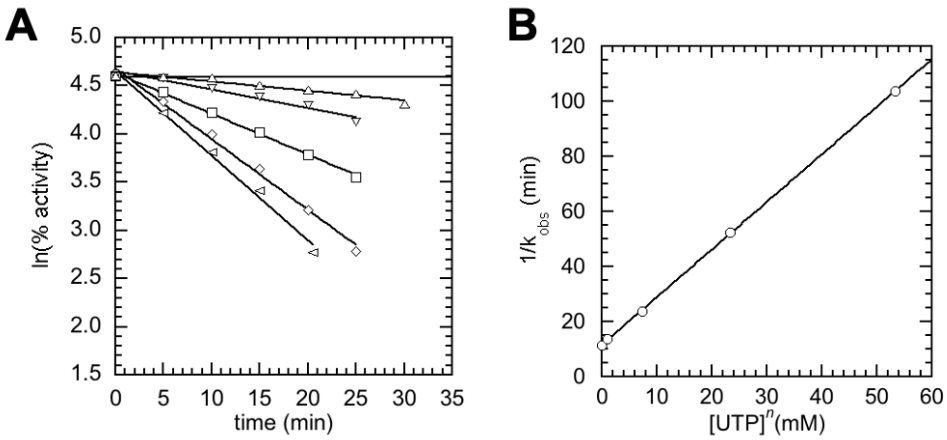

Figure 2.35 Protection against MAP-dependent inactivation of CTPS by UTP. (A) CTPS (1 mg/mL) was incubated with MAP (2.5 mg/mL) with varying concentrations of UTP: 0.0 (◁) 1 (◇), 2 (□), 3 (▽), and 4 (△) mM in addition to a control in the absence of MAP and UTP (○). (B) The inverse of the observed pseudo-first-order rate constants ($1/k_{obs}$ values) obtained as the inverse of the slope values from A) were plotted as a function of $[UTP]^n$, where the Hill number (n) = 2.870 ± 0.050, to determine the apparent ligand-mediated dissociation constant for the protection against inactivation (K_L). The slope and y-intercept (determined in singlicate) from the replot were: 1.728 ± 0.010 min mM^{-1} and 11.505 ± 0.256 min, respectively, yielding a K_L value of 1.897 ± 0.139.

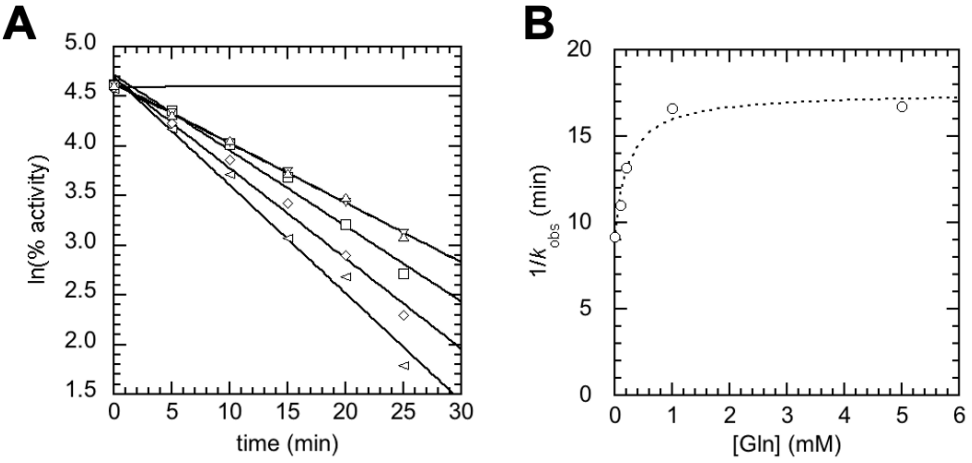

Figure 2.36 Protection against MAP-dependent inactivation of CTPS by Gln. (A) CTPS (1 mg/mL) was incubated with MAP (2.5 mg/mL) with varying concentrations of Gln: 0.0 (◁) 0.1 (◇), 0.2 (□), 1.0 (▽), and 5.0 (△) mM in addition to a control in the absence of MAP and Gln (○). (B) The inverse of the observed pseudo-first-order rate constants ($1/k_{obs}$) obtained as the inverse of the slope values from A) were plotted as a function of [Gln], where the dotted line corresponds to eqn 2.10, which has the general form of eqn 2.11. The K_L value could not be determined due to the observed plateau, which requires a more detailed kinetic analysis.

Table 2.1 K_L values for the protection against MAP-dependent inactivation by CTPS ligands. As these assays were not completed in triplicate, the errors correspond to the uncertainties arising from measurements within the single inactivation experiment.

Ligand	K_L (mM)
ATP	1.092 ± 0.100
CTP	0.075 ± 0.004
UTP	1.897 ± 0.139
Gln	-

These data from the kinetic-based protection assays agree with those observed in the fluorescence-based protection study, where CTP provided the greatest level of protection against both SMHP-modification and MAP-dependent inactivation. Furthermore, the observations are consistent with the identification of Lys 223 as a residue modified by SMHP at the CTP binding site. ATP showed a modest level of protection in both protection studies, which is also consistent with the identification of Lys 239 being modified by SMHP at the ATP/ADP binding site. UTP provided a much weaker level of protection relative to the other ligands, consistent with both protection studies. Although the triphosphate moieties of UTP and CTP overlap with one another, binding of UTP specifically has shown to be highly specific, as mentioned in Section 2.3.11 (Scheit & Linke, 1982). Thus, reaction at the UTP site by SMHP and MAP is likely more challenging than at the CTP site, and hence, a greater degree of protection would be expected in the presence of CTP than UTP as observed experimentally.

Interestingly, protection against MAP-dependent inactivation of CTPS and protection against SMHP-labelling of CTPS was observed in the presence of L-Gln. However, LC-MS/MS analysis revealed that none of the 8 SMHP-modified Lys residues were located near the L-Gln binding site. Given that these two protection studies are in

close agreement with one another, the most plausible explanation for the protection observed in the presence of L-Gln is due to the well-documented ligand-induced conformational changes (Levitzki & Koshland, 1972a, 1972b; Lynch *et al*., 2017; McCluskey & Bearne, 2018; Zhou *et al*., 2021) that in some way reduce the accessibility and thus reactivity of the Lys residues with SMHP and MAP. A few examples of these conformational changes include tetramerization of CTPS by ATP, UTP, and CTP, formation of the ammonia tunnel to facilitate the transfer of nascent ammonia from the glutaminase domain to the synthase domain, open-to-closed structural transition upon UTP and ATP binding to yield the resulting GTP binding site, and closed-to-open transition upon CTP binding (Levitzki & Koshland, 1972b; McCluskey & Bearne, 2018; Zhou *et al*., 2021).

However, in contrast to the ligands CTP, ATP and UTP for which linear replots of $1/k_{obs}$ versus [L] (or $[L]^n$) were obtained, the replot of $1/k_{obs}$ versus [L-Gln] exhibited pronounced curvature, suggesting that the kinetic model giving rise to eqn 2.5 and 2.6 does not adequately describe Gln-dependent protection. While L-Gln does induce conformational changes that likely yield reduced accessibility to the Lys residues as previously described, unlike the other ligands, L-Gln does not induce tetramerization upon binding, and therefore, the MAP-dependent inactivation studies occurred in the presence of the CTPS dimer. Consequently, an alternative mechanism was proposed to describe the protection by L-Gln (**Scheme 2.5**). In this proposed kinetic mechanism and resulting derived equation (eqn 2.10), which has the general form (eqn 2.11) when [I] is constant, a non-linear replot is predicted (certainly, more complex inactivation mechanisms could be proposed). In agreement with **Figure 2.36** wherein pronounced

curvature was observed, the proposed kinetic mechanism describes that full protection against inactivation will not be observed since MAP binding site(s) remain accessible (i.e., open) for inactivation by the acyl phosphate when CTPS is in its dimeric form. Thus, while L-Gln appears to show a modest level of protection as observed through both the fluorescence-based and kinetic-based protection experiments, full protection from SMHP and MAP modification may require tetramerization of the enzyme induced by the binding of nucleotide(s) to limit the accessibility and reactivity of the acyl phosphates with the Lys residues.

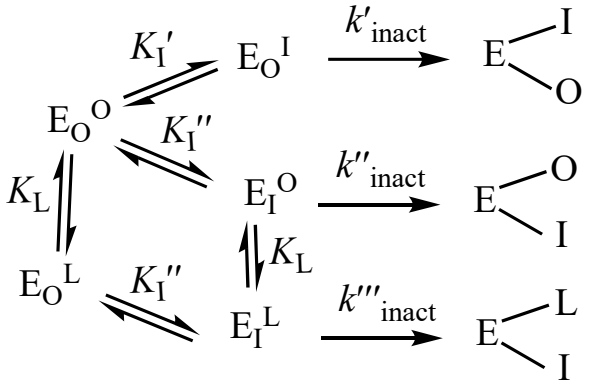

Scheme 2.5 Proposed kinetic scheme for the protection against CTPS inactivation by Gln. In this scheme, (O) represents an empty binding site, (E) is CTPS, (L) is L-Gln, (I) is MAP, and K_L and K_I are dissociation constants for Gln and MAP, respectively. This scheme gives rise to eqn 2.10, which has a general form of eqn 2.11.

$$k_{obs} = \frac{[I]\,(k'_{inact}K_LK_I'' + k''_{inact}K_LK_I' + k'''_{inact}K_I'[L])}{K_LK_I'K_I'' + K_LK_I''[I] + K_LK_I'[I] + K_I'K_I''[L] + K_I'[L][I]} \qquad (2.10)$$

$$k_{obs} = \frac{K + K'[L]}{K'' + K'''[L]} \qquad (2.11)$$

2.4 CONCLUSIONS AND FUTURE DIRECTIONS

A combination of biotin-ABPP and fluorescent tagging were used to investigate proteins that contain a specific architecture: specifically, those containing a nucleophile adjacent to a cationic binding site. Given the structural similarity between the anionic monomethyl acyl phosphate warhead of SMHP and MAP, and the fact that MAP was previously shown to target this type of protein architecture via the irreversible inactivation of 3-HBDH (Kluger & Tsui, 1980, 1986) and modification of Hb, (Ueno *et al*., 1986, 1989; Xu *et al*., 1999), I anticipated that SMHP would modify enzymes with this same architecture.

SMHP was found to modify 281 enzymes from the *P. lemognei* proteome, including 3-HBDH and CTPS, which were then investigated in greater detail to learn more about the sites that were modified by SMHP and MAP. MAP-dependent protection against SMHP labelling was observed using fluorescent tagging, where SMHP and MAP appeared to target the same site(s) within Hb, 3-HBDH, and CTPS. As identified by LC-MS/MS, SMHP and MAP modified the same three catalytic residues within the conserved active site of 3-HBDH: Ser 146, Lys 156, and Lys 163; thus, demonstrating the targeted reactivity of the acyl phosphate warheads with 3-HBDH. For CTPS, LC-MS/MS revealed that 8 Lys residues were modified by SMHP, with Lys 223 and Lys 239 located at the CTP and ATP/ADP sites, respectively. The efficiency of reactivity of the acyl phosphates was explored using kinetics, where SMHP and MAP were both found to inactivate 3-HBDH and CTPS. Lastly, protection against modification of CTPS by the acyl phosphates was explored using fluorescence-based and kinetics-based protection

studies, revealing that the ligands, ATP, UTP, CTP, and L-Gln, protected against the labelling by SMHP and inactivation by MAP, respectively.

In future work, since the conditions for the MAP-dependent inactivation of both 3-HBDH and CTPS have been developed using kinetics, it would be interesting to use these kinetically-controlled conditions to further assess the modification sites in greater detail. By monitoring the inactivation of CTPS and 3-HBDH by MAP and/or SMHP using kinetics, followed by LC-MS/MS after a specified period of time (i.e., percent inactivation), we could determine the primary nucleophile responsible for the inactivation of each enzyme. This investigation would be especially beneficial for CTPS given the increased complexity of SMHP reactivity with there being multiple ligand binding sites. In addition, since kinetics-based studies for the protection of 3-HBDH against inactivation by MAP have been explored with the competitive inhibitor, methyl acetonylphosphonate, in addition to coenzymes NAD^+ and NADH, and ADP (Kluger & Tsui, 1986), it would be valuable to employ such protection studies to assess the protection against the modification of 3-HBDH by SMHP using these same ligands. Furthermore, it would be beneficial to assess the modification site(s) of a third enzyme identified from the *P. lemognei* proteome in its purified form, such as a kinase, wherein various kinases were identified among the most frequent subclass (EC 2.7) modified by SMHP. Lastly, since SMHP exhibited broad-spectrum labelling with proteins from the *P. lemognei* proteome, this ABPP approach could be extended to other cell types to identify additional enzymes that are modified by SMHP.

CHAPTER 3 THE INACTIVATION OF L-FUCONATE DEHYDRATASE BY 3-HYDROXYPYRUVATE AND THE EFFECTS OF TRIS BUFFER

3.1 INTRODUCTION

3.1.1 THE ENOLASE SUPERFAMILY AND THE MANDELATE RACEMASE SUBGROUP

The enolase superfamily (ENS) of enzymes is a structurally similar yet mechanistically diverse superfamily, consisting of ~49 000 members (Akiva *et al*., 2014; Gerlt *et al*., 2005, 2012). There are 12 different reactions catalyzed among the superfamily, including: β-elimination of either a hydroxyl or ammonia group (dehydration/elimination), 1,1-proton transfers (racemization/epimerization), and cycloisomerization (intramolecular addition/elimination) (Babbitt *et al*., 1996; Gerlt *et al*., 2005, 2012; Gerlt & Babbitt, 2001). The superfamily is divided into seven subgroups, including the mandelate racemase (MR) subgroup, where the majority of the members within this subgroup catalyze a β-elimination reaction from acid sugar substrates (Akiva *et al*., 2014; Gerlt *et al*., 2012). While highly diverse in the reactions they catalyze and with their preferred substrates, all members of the ENS superfamily, including those in the MR subgroup, share the same initial reaction wherein an active site base abstracts the α-proton from the carboxylic acid substrate to yield an *aci*-carboxylate intermediate, which is stabilized by an essential Mg^{2+} ion (**Scheme 3.1**) (Babbitt *et al*., 1995, 1996; Gerlt *et al*., 2005). Upon formation of the *aci*-carboxylate intermediate, the vast majority of MR subgroup members, such as L-fuconate dehydratase, D-glucarate dehydratase, D-galactonate dehydratase, and L-rhamnonate dehydratase, catalyze the dehydration of an acid sugar (Gerlt & Babbitt, 2001; Yew *et al*., 2006).

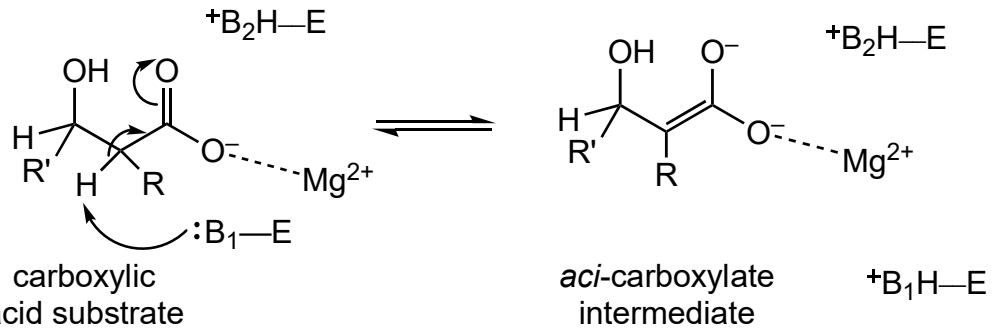

Scheme 3.1 Shared half reaction among the ENS superfamily. This shared reaction involves the abstraction of the α-proton of the carboxylic acid substrate by a catalytic base (B_1) to yield an *aci*-carboxylate intermediate.

Members are assigned to the MR subgroup based on conserved structural features and sequence similarity, yet remain mechanistically diverse (Bearne & St. Maurice, 2017). Two major structural features conserved among the ENS superfamily and thus the MR subgroup are the N-terminal α + β capping domain, which provides side chain determinants for substrate recognition, and the C-terminal $(\beta/\alpha)_7\beta$-barrel domain, which contains residues that coordinate the essential Mg^{2+} ion and catalytic residues that participate in the acid/base chemistry (Gerlt *et al*., 2012; Gerlt & Raushel, 2003; Neidhart *et al*., 1990, 1991). The conserved residues in the MR subgroup that coordinate the Mg^{2+} ion include an Asp residue from β-strand 3, a Glu residue from β-strand 4, and a Glu residue from β-strand 5 (Gerlt *et al*., 2012; Neidhart *et al*., 1990). The carboxylate oxygens of these conserved residues in the C-terminal $(\beta/\alpha)_7\beta$-barrel domain, in addition to the carboxylate oxygen or hydroxyl group of the given substrate, are required for Mg^{2+} coordination (Gerlt *et al*., 2012). Furthermore, Lys and His residues from β-strands 2 and 7, respectively, serve as the conserved Brønsted acid–base catalysts within the MR subgroup (Gerlt *et al*., 2012; Neidhart *et al*., 1991).

3.1.2 STRUCTURE OF L-FUCONATE DEHYDRATASE (FucD)

L-Fuconate dehydratase (FucD) from *Xantomonas campestris* was first assigned to the MR subgroup in 2006 by Gerlt and co-workers. FucD catalyzes the conversion of its primary substrate, L-fuconate, to 2-keto-3-deoxy-L-fuconate via a β-elimination (dehydration) reaction following the initial α-proton abstraction from the acid sugar, which will be discussed in greater detail in Section 3.1.3. Consistent among other MR subgroup members, FucD is comprised of two major domains, including the N-terminal α + β capping domain and the C-terminal $(\beta/\alpha)_7\beta$-barrel domain (Yew *et al*., 2006). Residues Asp 248, Glu 274, and Glu 301 from β-strands 3, 4 and 5, respectively, were identified as the conserved carboxylate ligands that coordinate the essential Mg^{2+} ion (Yew *et al*., 2006). Furthermore, the catalytic residues from β-strands 2 and 7 were identified as Lys 220 and His 351, respectively (Yew *et al*., 2006). Trp 101 from the capping domain serves as a binding determinant for the methyl group of L-fuconate within a hydrophobic pocket, which is analogous to Leu 93 of MR (Bearne & St. Maurice, 2017; Yew *et al*., 2006). While most members of the MR subgroup exist in solution as homooctamers, which is more specifically described as a tetramer of dimers (Neidhart *et al*., 1991), FucD was found to exist as a dimer in solution (**Figure 3.1**) using gel-filtration high-performance liquid chromatography (GF-HPLC) and dynamic light scattering (DLS) by a previous member of the Bearne Lab, Chris Fetter (Fetter, 2019).

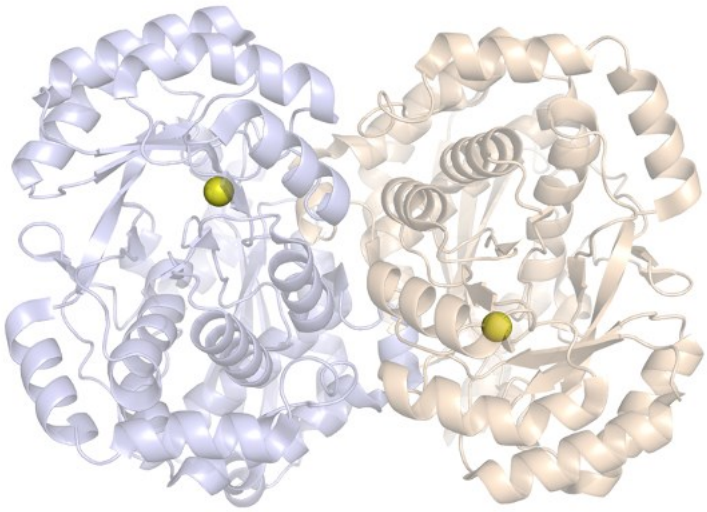

Figure 3.1 Dimeric structure of FucD from *Xantomonas campestris*. Individual monomers are shown in blue and wheat ribbon representation with the essential Mg^{2+} ion represented as a yellow sphere. (PDB entry: 2HXT)

3.1.3 MECHANISM AND SUBSTRATE SPECIFICITY OF FucD

With L-fuconate as the preferred substrate, the mechanism was determined by Gerlt and co-workers (2006) to occur by the abstraction of the α-proton by Lys 220 (Brønsted base) to form the *aci*-carboxylate intermediate (**Scheme 3.2**). Subsequently, the β-elimination is catalyzed, wherein the β-hydroxyl leaving group is protonated by His 351 (conjugate acid) and the resulting dehydrated enol product undergoes stereospecific ketonization catalyzed by Lys 220 (conjugate acid) to yield 2-keto-3-deoxy-L-fuconate as the product.

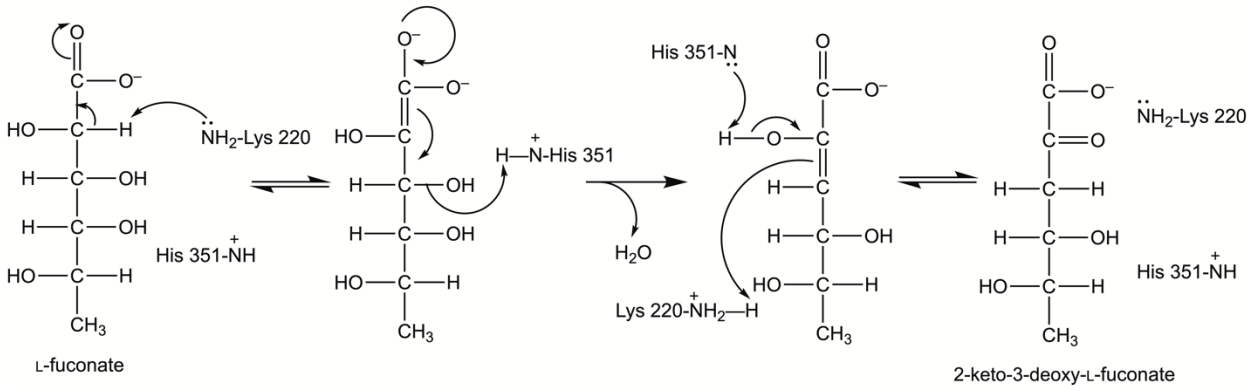

Scheme 3.2 Mechanism for the conversion of L-fuconate to 2-keto-3-deoxy-L-fuconate catalyzed by FucD

Although L-fuconate was determined to be the preferred substrate for FucD based on its kinetic parameters (k_{cat} = 15 ± 0.2 s^{-1}, K_m = 0.33 ± 0.06 mM), FucD also catalyzed the dehydration of other acid sugars: L-galactonate (k_{cat} = 0.9 ± 0.03 s^{-1}, K_m = 6.2 ± 0.4 mM), D-arabinonate (k_{cat} = 2.4 ± 0.07 s^{-1}, K_m = 2.1 ± 0.09 mM), D-altronate (k_{cat} = 0.0064 s^{-1}), L-talonate (k_{cat} = 0.035 s^{-1}), and D-ribonate (k_{cat} = 0.086 s^{-1}) (Yew *et al*., 2006). Interestingly, while the initial α-proton abstraction involves Lys 220 acting as the Brønsted base for substrates L-fuconate, L-galactonate, D-arabinonate, and D-altronate, His 351 acts as the Brønsted base to deprotonate the substrates L-talonate and D-ribonate. Crystal structures of FucD, both in the absence and presence of the ligand D-erythronohydroxamate, an intermediate analogue and competitive inhibitor of the enzyme, were used to further assess the enzyme's preference for L-fuconate. The stereochemistry of the hydroxyl groups from carbons 3-5 were found to be optimal for hydrogen bonding interactions since the 3-OH form an H-bond with His 351, the 4-OH forms an H-bond with Asp 24, and the 5-OH forms an H-bond with Gly 22 (backbone). Lastly, L-fuconate differs from L-galactonate and D-arabinonate only in the presence of a

methyl group on carbon-6, which is recognized by Trp 101 as the binding determinant within a hydrophobic binding pocket at the active site (Yew *et al*., 2006).

3.1.4 INACTIVATION OF MR AND FucD BY 3-HYDROXYPYRUVATE

3-Hydroxypyruvate (3-HP) was previously discovered to irreversibly inactivate MR from *Pseudomonas putida*, where the catalytic residues, Lys 166 and His 297, were identified as binding determinants for the inhibitor (Nagar *et al*., 2015). MR is a minority member within the MR subgroup in that the enzyme catalyzes a racemization reaction upon formation of the *aci*-carboxylate intermediate rather than a dehydration reaction (Bearne & St. Maurice, 2017). The inactivation of MR was shown to occur via a Schiff-base mechanism (**Scheme 3.3**) (Nagar *et al*., 2015). Through this mechanism, the α-carbonyl of 3-HP and the ε-NH_2 group of Lys 166 form a Schiff base, followed by deprotonation of the imine by a Brønsted base, which was presumed to be His 297. The resulting Lys 166-enol(ate) adduct (86 Da) could then tautomerize to yield an aldehyde adduct (86 Da). In addition to observing this 86-Da adduct using LC-MS/MS analysis, the resulting enol(ate)/aldehyde adduct was also observed using X-ray crystallography (PDB 4X2P) (Nagar *et al*., 2015).

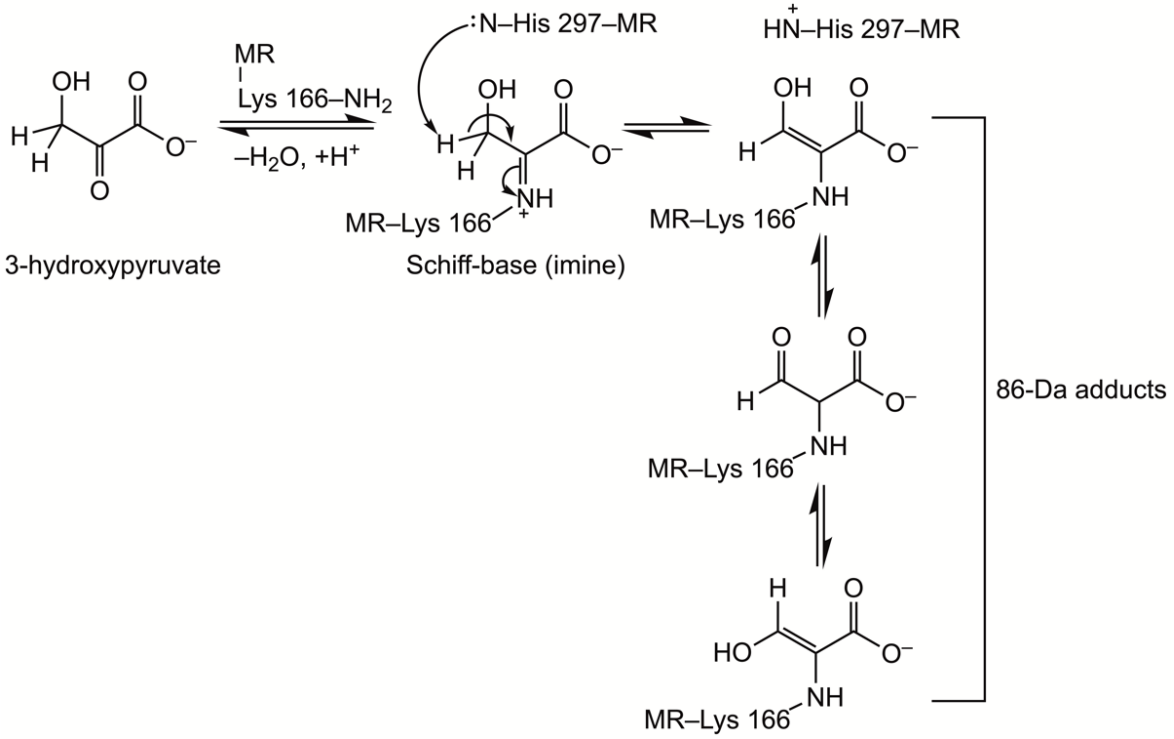

Scheme 3.3 Mechanism for the inactivation of MR by 3-HP. Adapted from Bearne & St. Maurice (2017).

The kinetics of the inactivation of MR by 3-HP were previously assessed through time-dependent inactivation studies, where the second-order rate constant for the efficiency of inactivation (k_{inact}/K_I) was determined to be 83 ± 8 $M^{-1}s^{-1}$ (Nagar *et al*., 2015). Given that members of the MR subgroup share conserved active-site residues and that the catalytic Lys and His residues act as binding determinants for 3-HP, Chris Fetter, a previous M.Sc. student in the Bearne lab, sought to investigate whether 3-HP could also inactivate FucD. Interestingly, Chris Fetter determined that the efficiency of inactivation of FucD by 3-HP was significantly lower (0.023 ± 0.001 $M^{-1}s^{-1}$) than that observed for the inactivation of MR. While Chris Fetter observed 86-Da adducts with Lys 220 using LC-MS/MS analysis, surprisingly, 58-Da adducts were also observed with Lys 220 and

with other nucleophilic residues outside of the active site. The combination of kinetics and LC-MS/MS findings suggested the possibility that FucD was being inactivated by 3-HP through a different mechanism than that found for MR. A pathway was proposed to explain the formation of the observed 58-Da adducts, where 3-HP, either enzymatically or non-enzymatically, is converted to glycolaldehyde (GLH), which had been shown in previous studies to form 58-Da adducts with proteins upon reacting with nucleophilic residues, predominantly Lys and Arg (Glomb & Monnier, 1995; Thorpe & Baynes, 2003). Given the conserved catalytic machinery among MR subgroup members, the vastly different behaviors with respect to the 3-HP-dependent inactivation of MR and FucD was surprising.

3.1.5 OVERVIEW OF THIS WORK

Building on the findings of Chris Fetter, my goal was to investigate whether the reduced rate of inactivation observed for FucD was potentially a consequence of the buffer used, tris(hydroxymethyl)aminomethane (Tris), given the known ability of primary amines to form Schiff-base products with carbonyl groups, such as aldehydes and ketones. In this chapter, time-dependent inactivation studies of FucD by 3-HP were conducted at varying concentrations of Tris. Interestingly, Tris was found to protect against the inactivation of FucD in a concentration-dependent manner, where the k_{inact}^{app} and K_I^{app} values decreased with respect to increasing Tris-Cl concentrations, but the overall $k_{inact}^{app}/K_I^{app}$ remained unchanged. Given these observations, in addition to evaluating the inactivation of FucD by 3-HP, I sought to investigate the effect of Tris specifically on the 3-HP-dependent inactivation of FucD.

Furthermore, protection studies with L-fuconate were conducted to assess whether the 3-HP-dependent inactivation of FucD occurs at the active site. Next, intact ESI-MS studies are described that assess the size and number of adducts formed when 3-HP-dependent inactivation of FucD was conducted in 5 mM versus 50 mM Tris-Cl buffer.

3.2 MATERIALS AND METHODS

3.2.1 GENERAL

All reagents were purchased from Sigma-Aldrich Canada Ltd. (Oakville, ON, Canada) unless otherwise stated. Nuclear magnetic resonance (^{1}H and ^{13}C) spectra were obtained using either a Bruker AV 300 or 500 MHz spectrophotometer at the Dalhousie University Nuclear Magnetic Resonance Research Resource Centre (NMR-3). Chemical shifts (δ in ppm) for the ^{1}H NMR spectrum are reported relative to the residual solvent signal for HOD (δ 4.79) (Gottlieb *et al*., 1997) and for the ^{13}C NMR spectrum they are reported relative to the secondary reference, DSS (methyl signal). Kinetic studies were conducted using a circular dichroism (CD)-based assay with a JASCO J-810 spectropolarimeter. High resolution mass spectra (HRMS) were obtained using a Bruker compact QTOF mass spectrophotometer operating in the electrospray ionization (ESI) mode (negative). Intact MS (LC-MS) experiments were carried out at the Faculty of Medicine Biological Mass Spectrometry Core Facility at Dalhousie University.

3.2.2 SYNTHESIS OF L-FUCONATE

The first half of the synthesis to prepare barium L-fuconate from L-fucose was conducted by Dr. Stephen Bearne. L-Fucose (1.5 g, 9.14 mmol) was dissolved in water (7.5 mL) in a round-bottom flask (25 mL). Br_2 (0.5 mL, 9.4 mmol) was added, and the

solution was covered in aluminum foil, sealed with a stopper, and stirred for two days (room temperature). Thereafter, air was blown into the solution to remove excess Br_2 until the solution became colourless. NaOH (6 M) was added dropwise until the pH of the solution was 7 (pH paper). In a minimum volume of water, $BaCl_2$ (1.2 g, 5.76 mmol) was added to the reaction mixture to precipitate barium L-fuconate, which was collected by suction filtration.

The barium L-fuconate was subsequently converted to its sodium salt by addition of dilute H_2SO_4 (1 mL, 2.675 mmol) to the barium L-fuconate (1.325 g, 2.675 mmol) in H_2O (~20 mL) followed by stirring for ~2 h. The precipitated $BaSO_4$ was then removed by filtration through a bed of celite. The pH of the filtrate was adjusted to 12 (pH paper) by dropwise addition of NaOH (6 M), which was mixed for ~2 h at 70 °C in excess water to hydrolyze the lactone. The solution was then passed through a AG ®50W-X8 cation exchange resin (H^+ form, 2.66 × 13.10 cm) (Bio-Rad Laboratories, Hercules, CA). The L-fuconic acid was subsequently converted to sodium L-fuconate by dropwise addition of NaOH (6 M), which was brought to pH 8.5-9 (pH paper). The product was subjected to rotary evaporation for ~2 h at 40 °C to reduce the volume to ~100 mL, and the remaining solvent was removed by lyophilization (~40 h) to yield sodium L-fuconate as a white powder (1.23 g, 66.6% yield); ^{1}H NMR (500 MHz, D_2O) δ 4.24-4.21 (m, 1H), 4.06 (qd, J = 6.6, 1.9 Hz, 1H), 3.93-3.86 (m, 1H), 3.42 (ddd, J = 9.4, 1.9, 1.0 Hz, 1H), 1.22 (d, J = 6.6 Hz, 3H) (**Figure 3.2**); ^{13}C NMR (126 MHz, D_2O) δ 179.52, 73.32, 71.87, 71.75, 66.04, 18.76 (**Figure 3.3**). ESI-HRMS (negative mode); m/z calculated for $C_6H_{11}O_6$ [M-H^+]$^-$: 179.0561, found: 179.0564 (**Figure 3.4**).

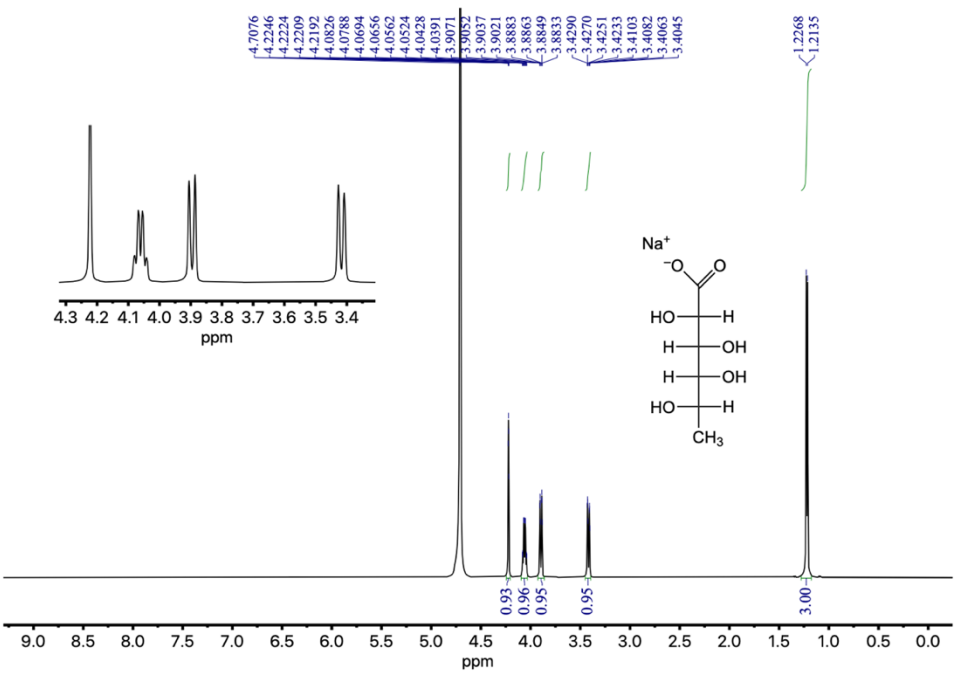

Figure 3.2 ^{1}H NMR spectrum of sodium L-fuconate in D_2O.

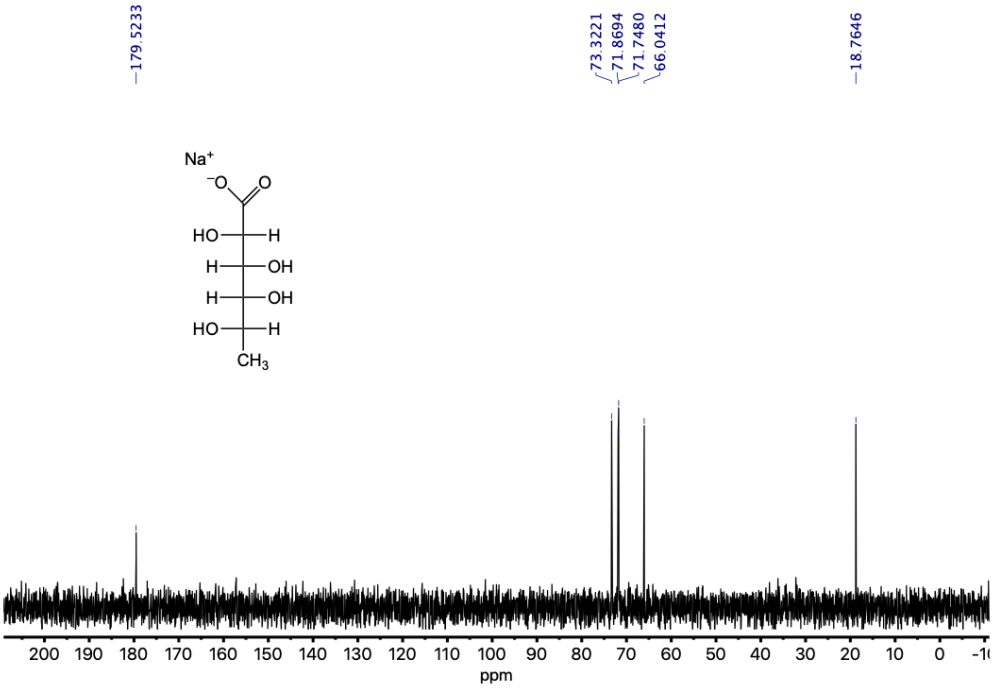

Figure 3.3 ^{13}C NMR spectrum of sodium L-fuconate in D_2O.

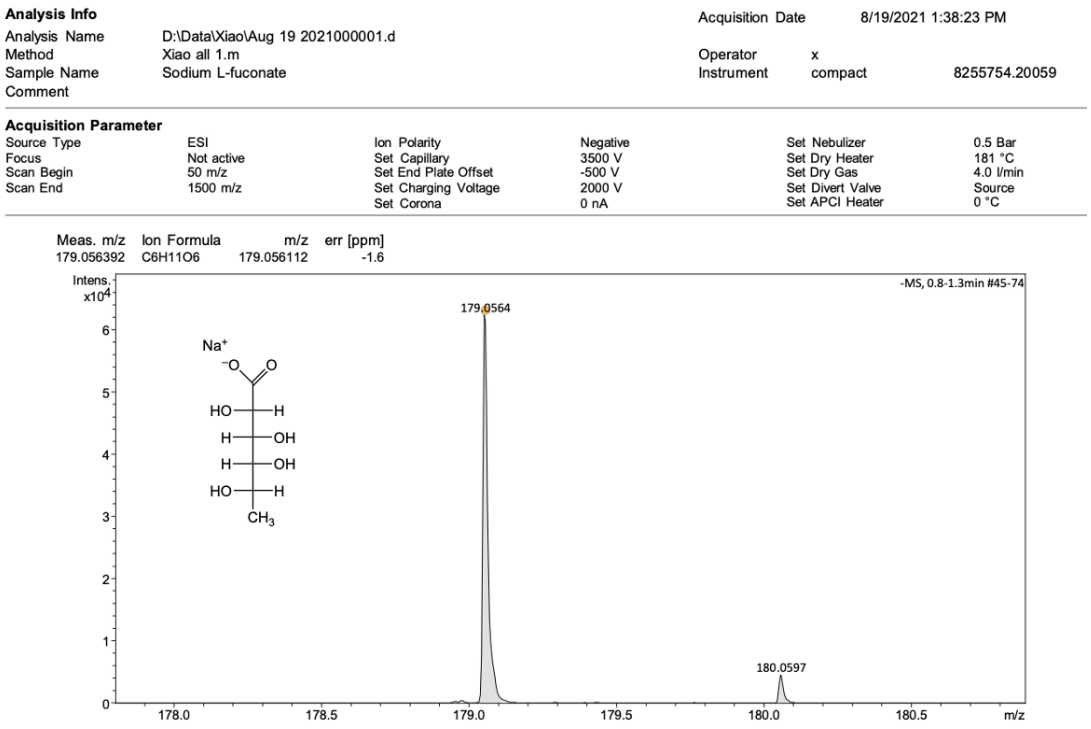

Figure 3.4 ESI-HRMS (negative mode) of sodium L-fuconate.

3.2.3 EXPRESSION AND PURIFICATION OF FucD

The open reading frame (GI:21233491) encoding wild-type FucD from *Xanthomonas campestris* was synthesized and inserted into a pET-52b(+) vector by BioBasic Inc. (Markham, ON). This construct encodes the wild-type FucD enzyme as a fusion protein bearing an N-terminal StrepII-tag (Markham, ON). Chemically competent *E. coli* BL21 (DE3) cells were transformed using the heat shock method (Sambrook *et al*., 1989) and plated on LB-agar plates containing ampicillin (100 μg/mL) overnight.

Transformants were grown overnight in LB media (5 mL) containing ampicillin (100 μg/mL) (37 °C, 200 rpm) and were stored thereafter in 15% glycerol stocks at –80 °C. Starter cultures of the *E. coli* BL21 (DE3) cells from freshly streaked LB-agar plates

were grown overnight in LB media containing ampicillin (100 μg/mL) (37 °C, 200 rpm). Starter cultures (10 mL) were used to inoculate larger expression culture(s) containing 1 L of the same media composition and were grown (37 °C, 200 rpm) until an OD_{600} of ~0.5-0.6 was obtained. Recombinant protein expression was then induced by addition of IPTG to a final concentration of 0.1 mM and the cultures were incubated at 16 °C for 24 h (175 rpm). The cells were harvested by centrifugation (3795 × *g*, 10 min, 4 °C) and the cell pellets were stored at –20 °C for future use.

Frozen cell pellets were thawed and resuspended in ice-cold sonication buffer (~ 35 mL) (100 mM Tris-Cl, 5 mM $MgCl_2$, pH 7.5). The cell suspension was kept on ice and sonicated (6 × 30 s with 60-s off periods between each 30-s interval) with a Branson Sonifier 250 (setting 5.5, 1-s bursts). The cell lysate was clarified by ultracentrifugation (146 550 × *g*, 35 min, 4 °C) and applied to a column containing StrepTactin XT Superflow affinity resin (IBA GmbH, Göttingen, Germany), and purified using an ÄKTA fast protein liquid chromatography (FPLC) system (GE Healthcare, Baie d'Urfé, QC) as per the manufacturer's instructions (IBA). After washing the column with wash buffer (100 mM Tris-Cl, 150 mM NaCl, 1 mM EDTA, pH 7.5), FucD was eluted by the addition of elution buffer (100 mM Tris-Cl, 150 mM NaCl, 1 mM EDTA, 50 mM biotin, pH 7.5). Eluted enzyme was dialyzed (MWCO 12 – 14 kDa) for 3 × 8 h (4 °C) against storage buffer (5 mM Tris-Cl, 10 mM $MgCl_2$, 10% glycerol, pH 7.5). However, for studies on the effects of Tris buffer, described in Sections 3.2.4 and 3.2.5, FucD was dialyzed into the desired Tris-Cl buffer concentration (5 – 50 mM), containing 10 mM $MgCl_2$ and 10% glycerol at pH 7.5. Dialyzed enzyme was aliquoted and stored at –20 °C for future use.

Protein concentrations were determined by conducting Bradford assays (Bio-Rad Laboratories, Mississauga, ON, Canada) with BSA standards or by UV absorbance at 280 nm. Using the ExPASy ProtParam web tool (Gasteiger *et al*., 2003), the molecular weight of wild-type FucD fusion protein bearing the N-terminal StrepII-tag was calculated to be 50 813.83 Da with an extinction coefficient of 64400 $M^{-1}cm^{-1}$ (under the assumption that all cysteine residues were reduced). Protein purity was assessed using SDS-PAGE (10%) with Coomassie brilliant blue (R-250) staining.

3.2.4 FucD KINETIC ASSAYS

3.2.4.1 Determination of kinetic parameters

The kinetic parameters for FucD were determined using CD spectroscopy by monitoring the conversion L-fuconate to 2-keto-3-deoxy- L-fuconate. Initial velocity values were obtained from the linear slopes by following the change in ellipticity at 216 nm over a period of 300 s at 25 °C using a molar ellipticity of 8985 deg cm^2 mol^{-1} (Fetter, 2019). In a 0.5-cm pathlength quartz cuvette with a total volume of 1.0 mL, reactions were initiated by the addition of FucD to a final concentration of 9.5 µg/mL (0.19 µM) with 0.005 % BSA and L-fuconate (0.2–6.0 mM) in 5 mM Tris-Cl and and 50 mM Tris-Cl, pH 7.5 assay buffers containing 10 mM $MgCl_2$. The Michaelis-Menten equation (eqn 2.1) was fit to the initial velocity data using *KaleidaGraph* software (v. 4.02) (Synergy Software, Reading, PA) for non-linear regression analysis. The k_{cat} values were calculated by dividing the V_{max} values by the total enzyme concentration ($[E]_T$) using the molecular weight of FucD (50 813.83 Da). The kinetic assays in both the 5 mM

Tris-Cl and 50 mM Tris-Cl buffers were performed in triplicate and the average values were reported with the errors corresponding to the standard deviation values.

3.2.4.2 Time-dependent inactivation by 3-HP

The rate of inactivation of FucD by 3-HP at 25 °C was assessed by incubating FucD (475 μg/mL) with BSA (0.05%) at varying concentrations of 3-HP (0.00, 1.60, 3.19, 6.38, and 12.76 mM) in FucD assay buffer at varying concentrations of Tris-Cl (5.0, 7.5, 10.0, 20.0, and 50.0 mM) buffer containing 10 mM $MgCl_2$ at pH 7.5. At various time points, aliquots (20 μL) were diluted fifty-fold to the total assay volume of 1.0 mL, yielding final [FucD] of 9.5 μg/mL (0.19 μM) with L-fuconate (2.5 mM). The reaction was followed at 216 nm using a 0.2-cm pathlength quartz cuvette for each concentration of 3-HP. For the triplicate determinations conducted in 5 mM Tris-Cl buffer, the observed initial velocities were plotted as ln(% activity) vs. time for each inhibitor concentration using eqn 2.2, and the resulting slopes yielded the observed pseudo-first-order rate constants for inactivation (k_{obs}). A replot of the k_{obs} values against the concentration of 3-HP was used to estimate the apparent second-order rate constant for the efficiency of inactivation (k_{inact}/K_I) in accord with eqn. 3.1 since saturation was not observed. For the single inactivation assays conducted at the higher concentrations of Tris-Cl buffer (7.5, 10, 20, and 50 mM), non-linear regression was used to fit eqn 3.2 to the data from the ln(% activity) vs. time plot (using eqn 2.2) since saturation was observed, allowing for the determination of the apparent values of K_I, k_{inact}, and k_{inact}/K_I at various concentrations of Tris-Cl.

$$k_{obs} \approx \frac{k_{inact}[\text{3-HP}]}{K_I} \tag{3.1}$$

$$k_{obs} = \frac{k_{inact}[\text{3-HP}]}{K_I + [\text{3-HP}](1 + \frac{[T]}{K_T})} \tag{3.2}$$

where T = Tris-Cl buffer

3.2.4.3 Protection assays with L-fuconate

Given that the competitive inhibitor of FucD, D-erythronohydroxamate, was not readily available, protection against 3-HP-dependent inactivation by the substrate L-fuconate was used to assess whether the inactivation by 3-HP occurs at the active site. Protection studies against the time-dependent inactivation of FucD were conducted as described in Section 3.2.4.2, where assays were conducted in both 5 mM and 50 mM Tris-Cl assay buffers. FucD (475 μg/mL) with BSA (0.05%) was incubated with 3-HP (12.76 mM) and varying concentrations of L-fuconate (0, 1, and 5 mM). Aliquots (20 μL) were diluted fifty-fold to a total volume of 1.0 mL, with a final FucD concentration of 9.5 μg/mL (0.19 μM), and assayed for activity with L-fuconate (2.5 mM). The observed initial velocities were plotted as ln(% activity) vs. time for each L-fuconate concentration using eqn 2.2 as previously described.

3.2.5 INTACT MS SAMPLE PREPARATION

Intact MS (LC-MS) was used to compare the adducts formed from the inactivation of FucD by 3-HP conducted in 5 mM versus 50 mM Tris-Cl assay buffer

containing 10 mM $MgCl_2$, pH 7.5. FucD (475 μg/mL) was incubated with 0 mM 3-HP (control) or with 12.76 mM 3-HP (sample) for 1 h at 25 °C. No BSA was used for stabilization. To confirm the expected loss in activity after 1 h, aliquots (20 μL) were diluted fifty-fold to a total volume of 1.0 mL, yielding a final FucD concentration of 9.5 μg/mL (0.19 μM). Upon initiation of the reaction by addition of FucD to the assay tube, which contained L-fuconate (2.5 mM) in the respective Tris-Cl buffer, the reaction velocity was determined. A total of four FucD samples were prepared for LC-MS, including: (1) 3-HP (0 mM) in 5 mM Tris-Cl buffer, (2) 3-HP (12.76 mM) in 5 mM Tris-Cl buffer, (3) 3-HP (0 mM) in 50 mM Tris-Cl buffer, and (4) 3-HP (12.76 mM) in 50 mM Tris-Cl buffer.

3.2.6 ^{1}H NMR SPECTROSCOPY OF 3-HP IN TRIS BUFFER

Assay buffer containing 50 mM Tris-Cl, 10 mM $MgCl_2$, pH 7.5 was lyophilized, followed by 3 rounds of lyophilization from D_2O. 3-HP was lyophilized from D_2O three times and added to the deuterated assay buffer, with a 3-HP concentration of 79.75 mM. The pD was adjusted to 7.5 using DCl and allowed to incubate at room temperature for 0 h and 12 h prior to conducting ^{1}H NMR spectroscopy to determine whether glycolaldehyde (GLH) was formed non-enzymatically from Mg^{2+} over this period. In addition, GLH (100 mM) was dissolved in D_2O and the chemical shifts were assessed using ^{1}H NMR spectroscopy to be used as a standard for the determination of the expected chemical shifts of the un-hydrated and hydrated species of GLH.

3.3. RESULTS AND DISCUSSION

3.3.1 FucD KINETIC ASSAYS

3.3.1.1 Determination of kinetic parameters

The kinetic parameters of FucD were first assessed in 5 mM Tris-Cl assay buffer (5 mM Tris-Cl, 10 mM $MgCl_2$, pH 7.5). While the resulting k_{cat} and K_m values were greater than those previously found by Gerlt and co-workers (2006) by ~2.5-fold and ~2.9-fold, respectively, the overall catalytic efficiency (k_{cat}/K_m) was in good agreement with their value as shown in **Table 3.1**. Since the kinetics for inactivation of FucD by 3-HP differed greatly with respect to the concentration of Tris-Cl used, which is described in Section 3.3.1.2, the kinetic parameters were also assessed in 50 mM Tris-Cl assay buffer (50 mM Tris-Cl, 10 mM $MgCl_2$, pH 7.5) to determine if the Tris concentration could affect the kinetic parameters in the absence of 3-HP. However, the kinetic parameters obtained in 50 mM Tris-Cl were experimentally equal to those obtained using 5 mM Tris-Cl as shown in **Table 3.1** and **Figure 3.4**. Thus, these data suggested that the reduced rate of inactivation of FucD by 3-HP with increasing concentrations of Tris-Cl (Section 3.3.1.2) does not result from the buffer altering the kinetic parameters of FucD in the absence of 3-HP.

Table 3.1 Kinetic parameters for the conversion of L-fuconate to 2-keto-3-deoxy-L-fuconate by FucD. The kinetic parameters were determined in triplicate, with errors corresponding to the standard deviation values.

	This work 5 mM Tris-Cl, 10 mM $MgCl_2$, pH 7.5	**This work** 50 mM Tris-Cl, 10 mM $MgCl_2$, pH 7.5	**Yew *et al*. (2006)** 50 mM HEPES, 10 mM $MgCl_2$, pH 7.5
K_m (mM)	0.970 ± 0.032	0.949 ± 0.117	0.33 ± 0.06
k_{cat} (s^{-1})	37.618 ± 0.535	38.404 ± 0.504	15 ± 0.2
k_{cat}/K_m ($M^{-1}s^{-1}$)	38823 ± 1527	40928 ± 5821	45000

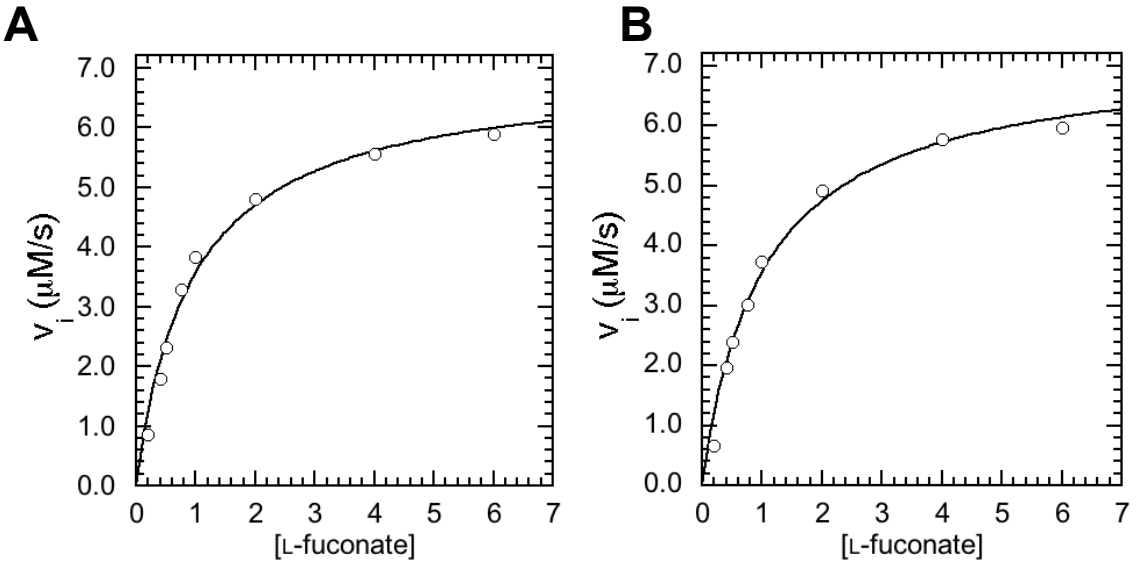

Figure 3.4 Representative Michaelis-Menten plots for the determination of the kinetic parameters for FucD. The kinetic parameters were determined (in triplicate) in each (A) 5 mM and (B) 50 mM Tris-Cl assay buffer. The kinetic parameters, k_{cat}, K_m, and k_{cat}/K_m, were determined using L-fuconate concentrations ranging from 0.2 to 6.0 mM and a FucD concentration of 9.5 μg/mL (0.19 μM).

Although the kinetic parameters remained unchanged when the assay was conducted in 5 mM versus 50 mM Tris-Cl, Tris buffer has been shown to affect enzyme activity through interactions with divalent cations in numerous studies (Amsler & Sigel, 1976; Babel *et al*., 2020; Crow & Pritchard, 1976; Desmarais *et al*., 2002; Fischer *et al*.,

1979; Neumann *et al*., 1975; Wever *et al*., 1977) and, thus, caution should be observed when studying enzymes that require divalent cations for catalysis, such as FucD. Sigel and co-workers (1979), using spectrophotometry and potentiometry, found that Tris formed complexes with many divalent cations in solution, especially Cu^{2+}, with evident involvement of both the amine group of Tris and at least one hydroxyl group of Tris in the complex. Lai and co-workers (2020) used isothermal titration calorimetry (ITC) to compare the interactions between common buffers and several divalent metals in solution in the absence of protein. While 4-(2-hydroxyethyl)-1-piperazineethanesulfonic acid (HEPES), 2-(*N*-morpholino)ethane sulfonic acid (MES), and 3-(*N*-morpholino)propane sulfonic acid (MOPS) either formed no complexes, or extremely weak complexes, with the various metals under study, Tris showed strong interactions, predominately with Cu^{2+} and Pb^{2+} (Xiao *et al*., 2020). Contrarily, the interactions between Tris and Cd^{2+}, Ca^{2+}, Co^{2+}, Mn^{2+}, Ni^{+}, Zn^{2+}, and Mg^{2+} (used in this study) were much less prominent, as evidenced by their exhibiting lower calorimetric outputs (Xiao *et al*., 2020). In addition, a study by Desmarais *et al.* (2002) using X-ray crystallography revealed that Tris formed strong complexes with two active site Zn^{2+} ions of the bimetallic enzyme, aminopeptidase. Specifically, electron density maps showed this chelation occurring with the amine and two of the oxygen atoms of Tris (Desmarais *et al*., 2002). Similarly, the amine of Tris chelated one of the three active site zinc ions of phospholipase C as determined by X-ray crystallography, which consequently resulted in the inhibition of the enzymatic activity (Hansen *et al*., 1993).

Since the Mg^{2+} ion is essential for catalysis by FucD, any changes in the kinetic parameters between the varying Tris concentrations would have indicated this possible

phenomenon; however, given that the kinetic parameters remained unchanged, and that Mg^{2+} does not appear to be a primary divalent metal involved in Tris complex formation based on a literature survey, Tris-Cl buffer was used for all FucD experiments conducted. Unfortunately, Tris-Cl is one of the few buffers compatible with the CD-based assay because it exhibits little absorbance at 216 nm, unlike HEPES for which the high absorbance at this wavelength makes it unsuitable for use in the assay.

3.3.1.2 Inactivation by 3-HP

The time-dependent inactivation of FucD by 3-HP was assessed with varying concentrations of 3-HP (0.00, 1.60, 3.19, 6.38, and 12.76 mM) and with varying concentrations of Tris-Cl buffer (5.0, 7.5, 10.0, 20.0, and 50.0 mM). The inactivation of FucD by 3-HP was found to occur in a time-dependent manner, however, the rates of inactivation of FucD were found to decrease with increasing concentrations of Tris as shown in **Figure 3.5**. The replot of the k_{obs} values against the concentration of 3-HP (**Figure 3.6**) did not show saturation in the presence of 5 mM Tris-Cl buffer, and thus, only the apparent second-order rate constant for the efficiency of inactivation ($k_{inact}^{app}/K_I^{app}$) could be determined (eqn 3.1) (**Table 3.2**). In contrast, saturation was observed at the higher concentrations of Tris-Cl buffer (7.5, 10, 20, and 50 mM), and therefore, non-linear regression was used to fit eqn 3.2 to the data so that the K_I^{app}, k_{inact}^{app}, and $k_{inact}^{app}/K_I^{app}$ values could be determined (**Table 3.2**).

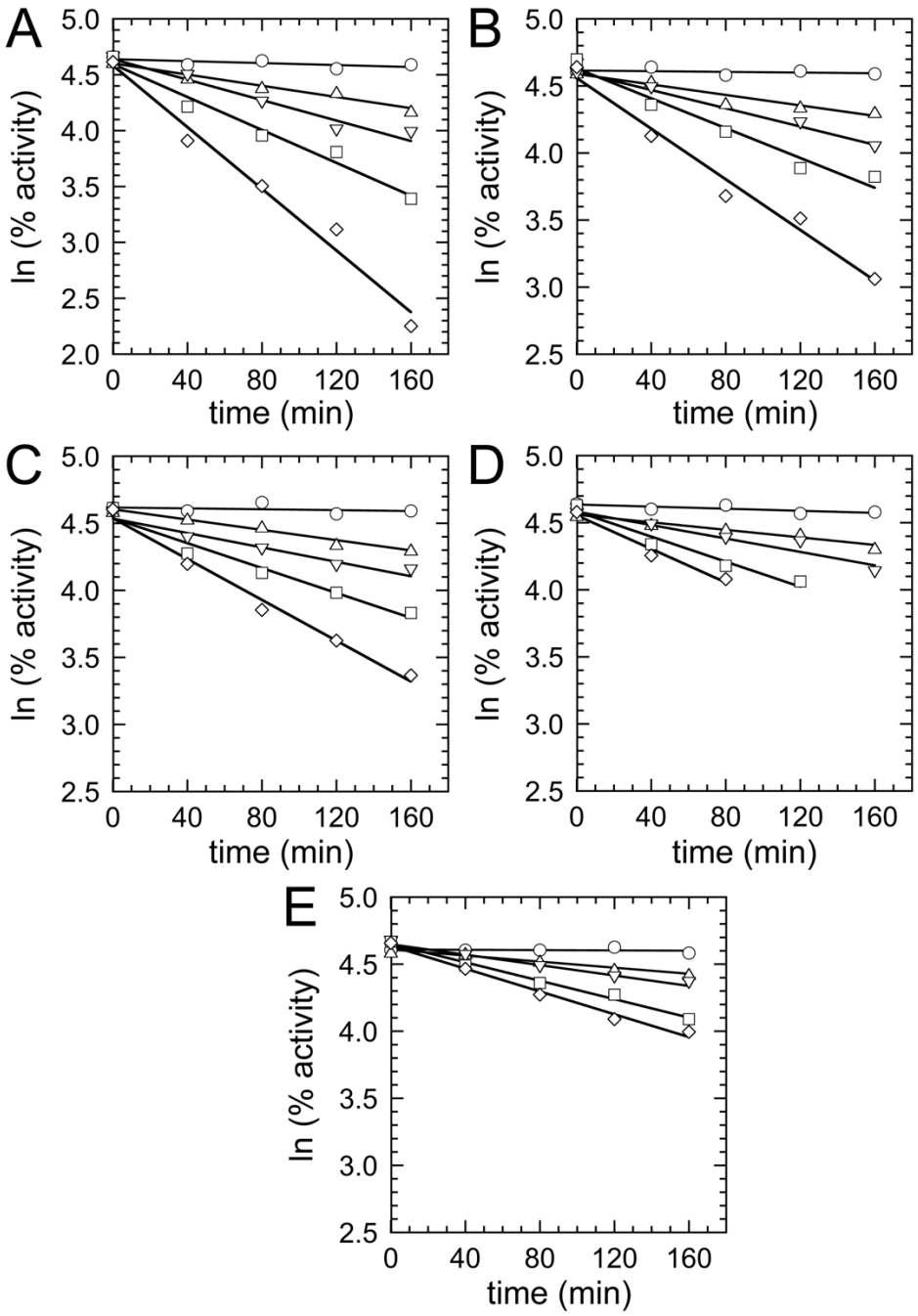

Figure 3.5 Time-dependent inactivation of FucD by 3-HP at varying concentrations of Tris-Cl. FucD (0.475 mg/mL) was incubated with various concentrations of 3-HP: 0.00 (○), 1.60 (△), 3.19 (▽), 6.38 (□), and 12.76 mM (◇), wherein the inactivation assays were conducted with various concentrations of Tris-Cl buffer: (A) 5.0 mM, (B) 7.5 mM, (C) 10 mM, (D) 20 mM, and (E) 50 mM. Assays were conducted in triplicate for the 5.0 mM Tris-Cl concentration and conducted in singlicate for each the 7.5, 10, 20, and 50 mM Tris-Cl concentrations.

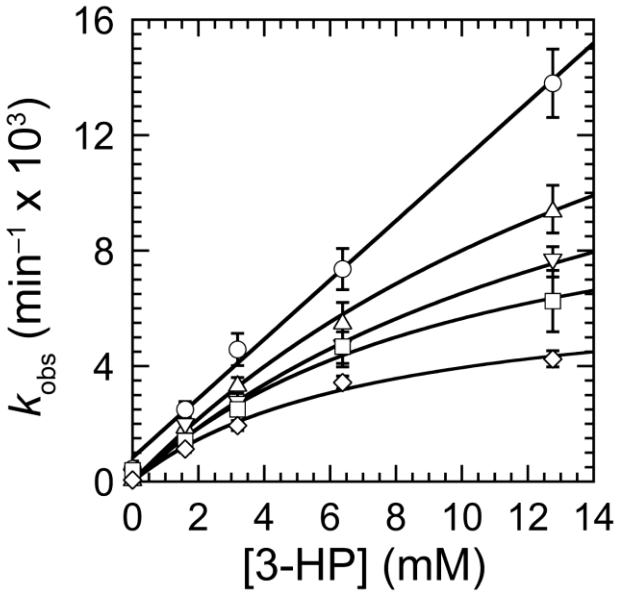

Figure 3.6 Replot of the observed pseudo-first order rate constants (k_{obs}) for the inactivation of FucD as a function of [3-HP]. Assays were conducted with varying concentrations of Tris-Cl: 5.0 mM (○), 7.5 mM (△), 10.0 mM (▽), 20.0 mM (□), and 50 mM (◇).

Table 3.2 Kinetic parameters for the 3-HP-dependent inactivation of FucD at varying concentrations of Tris-Cl.

[Tris] (mM)	K_I^{app} (mM)	k_{inact}^{app} (min^{-1})	$k_{inact}^{app}/K_I^{app}$ (M^{-1}s^{-1})
5.0[a]	-	-	0.0167 ± 0.0021
7.5[b]	20.640 ± 3.912	0.0245 ± 0.0032	0.0198 ± 0.0046
10.0[b]	16.849 ± 4.752	0.0175 ± 0.0032	0.0173 ± 0.0058
20.0[b]	10.666 ± 3.300	0.0117 ± 0.0020	0.0182 ± 0.0064
50.0[b]	7.431 ± 1.682	0.00688 ± 0.00077	0.0154 ± 0.0039

[a]Assay conducted in triplicate
[b]Assay conducted in singlicate

As indicated in **Table 3.2**, both the K_I^{app} and k_{inact}^{app} values decreased with increasing concentrations of Tris, whereas the overall $k_{inact}^{app}/K_I^{app}$ values remained largely unchanged (~0.018 ± 0.002 M^{-1}s^{-1}), which is in good agreement with the value determined by Chris Fetter conducted in 50 mM Tris-HCl buffer (0.023 ± 0.001 M^{-1}s^{-1}) (Fetter, 2019). Overall, in agreement with previous findings by Chris Fetter, 3-HP irreversibly inactivates FucD, but with a significantly reduced efficiency of inactivation

relative to that of MR (83 ± $M^{-1}s^{-1}$) (Nagar *et al*., 2015). These data suggested that Tris protects against the inactivation of FucD by 3-HP in an uncompetitive manner (**Scheme 3.4**) since higher concentrations of Tris reduced the K_I^{app} and k_{inact}^{app} values to the same degree in accord with eqns 3.3 and 3.4 (derived from eqn 3.2). In agreement with the uncompetitive kinetic mechanism, the replots of $1/K_I^{app}$ versus [Tris] and $1/k_{inact}^{app}$ versus [Tris] appeared to exhibit linearity within the errors of the experiment (**Figure 3.7**). It is certainly possible that alternative mechanisms that account for this protection against 3-HP-dependent inactivation could exist.

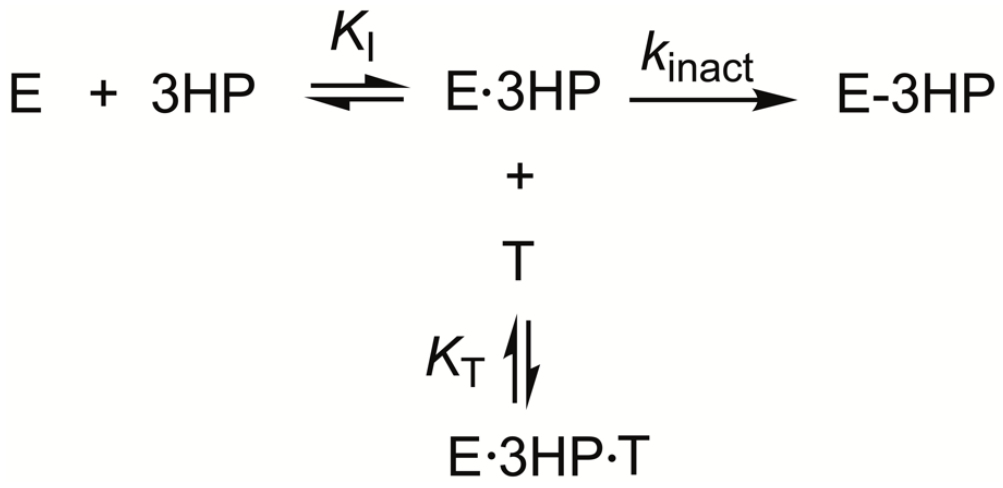

Scheme 3.4 Proposed uncompetitive kinetic mechanism for the protection against 3-HP-dependent inactivation of FucD by Tris (T).

$$K_I^{app} = \frac{K_I}{(1+\frac{[T]}{K_T})} \tag{3.3}$$

$$k_{inact}^{app} = \frac{k_{inact}}{(1+\frac{[T]}{K_T})} \tag{3.4}$$

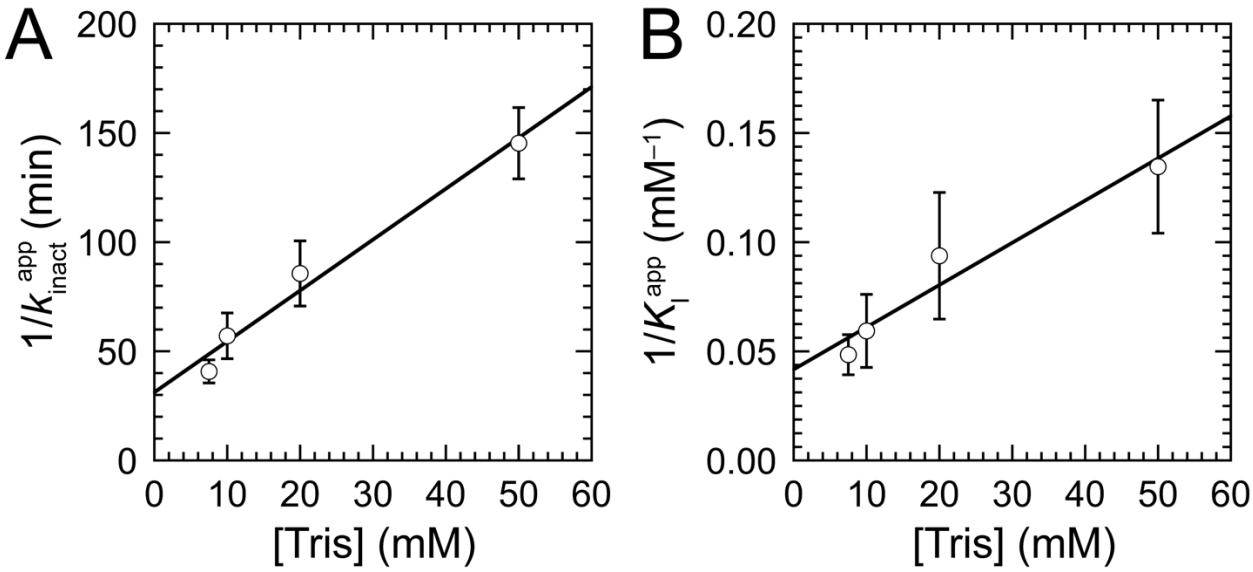

Figure 3.7 Replot of the inverse values of k_{inact}^{app} and K_I^{app} as a function of [Tris]. (A) $1/k_{inact}^{app}$ versus [Tris] and (B) $1/K_I^{app}$ versus [Tris] replots include the assays conducted in 7.5, 10, 20, and 50 mM Tris-Cl. A dotted line through 7.5, 10, and 20 mM Tris-Cl was included to show the failure of the predicted linear relationship in accord with eqns 3.3 and 3.4.

Numerous studies have reported the inhibition of enzymes by Tris and the vast majority of these studies found the mode of inhibition to be competitive. A few examples of such enzymes, including several glycosidases, that were inhibited by Tris in a competitive manner, include isomaltase (Larner & Gillespie, 1956), oligo-1,6-glucosidase

(Larner & Gillespie, 1956), α-galactosidase (Grossmann & Terra, 2001), dextransucrase (Miller & Robyt, 1986), sucrase (Vasseur *et al*., 1990), α-amylase (Ghalanbor *et al*., 2008), aminopeptidase (Desmarais *et al*., 2002), and ornithine carbamyl transferase (Carunchio *et al*., 1999).

Most of the inhibitory effects caused by Tris are either a consequence of interactions between the buffer and carbonyl-containing substrates or cofactors, or, due to the chelation of divalent metal ions that are essential for catalysis. However, Tris is a known competitive inhibitor of glycosidases. Indeed, Tris protected against the inactivation of β-glucosidase and β-fucosidase from *Dalbergia cochinchinenis* by conduritol B epoxide (CBE), with a concentration of 300 mM Tris affording complete protection against the inactivation of both enzymes by CBE (6.0 mM) (Surarit *et al*., 1996). Similarly, protection from CBE-dependent inactivation of β-glucosidase from *Aspergillus niger* by Tris was found to occur in a concentration-dependent manner, where the rate of inactivation decreased with respect to increasing concentrations of Tris, from 50 to 200 mM Tris ([CBE] = 3.0 mM), with almost complete protection observed in the presence of 200 mM Tris (Kimura *et al*., 1997).

Interestingly, Tris was found to protect against heat-inactivation of alkaline phosphatase from *Neurospora crassa* in a concentration-dependent manner (Morales *et al*., 2000). Tris (0.3 M) protected against the heat inactivation when alkaline phosphatase was incubated at 70 ºC, yielding a half-life of 19 min. In contrast, when alkaline phosphatase was incubated at 70 ºC with 2-(cyclohexylamino)ethanesulfonic acid (CHES) buffer (0.3 M), the resulting half-life of 2.3 min was significantly shorter than that in the presence of Tris.

3.3.1.3 Absence of protection against inactivation by L-fuconate

Given that D-erythronohydroxamate, a known competitive inhibitor of FucD, (Yew *et al*., 2006), was not readily available, protection by the substrate L-fuconate was employed to assess whether the inactivation by 3-HP occurs at the active site. Surprisingly, at Tris-Cl concentrations of 5 and 50 mM, L-fuconate provided no protection against the rate of inactivation by 3-HP (**Figure 3.8**).

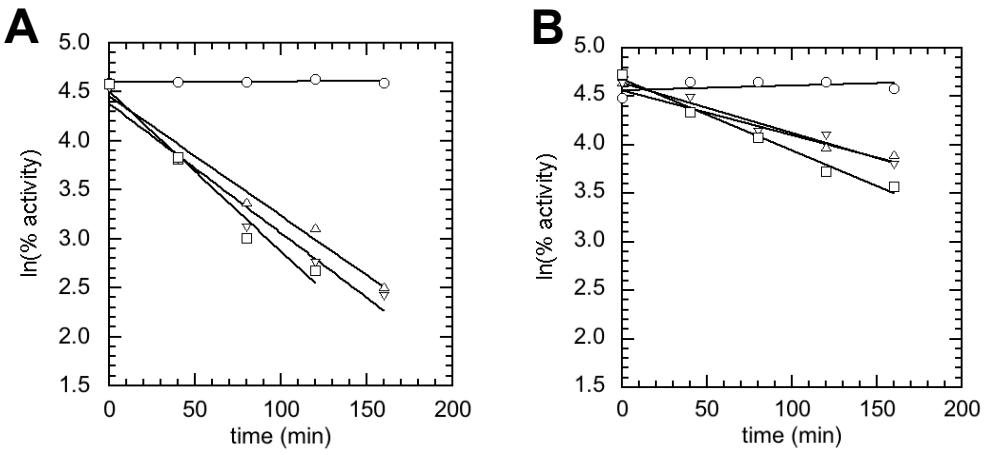

Figure 3.8 Plots for the 3-HP-dependent inactivation of FucD in the presence of L-fuconate. In (A) 5 mM and (B) 50 mM Tris-Cl assay buffer, FucD (0.475 mg/mL) was incubated in the absence of 3-HP and L-fuconate (○), and in the presence of a fixed 3-HP concentration of 12.76 mM, with L-fuconate concentrations of: 0.0 (△), 1.0 (▽), and 5.0 mM (□). Assays were conducted in singlicate.

The absence of protection against 3-HP-dependent inactivation of FucD in the presence of L-fuconate was surprising given that benzohydroxymate, a competitive inhibitor of MR, protected against the 3-HP-dependent inactivation of MR in a concentration-dependent manner (Nagar *et al*., 2015). The benzohydroxymate-dependent protection study provided further evidence, along with X-ray crystallography and MS/MS studies, that inactivation of MR by 3-HP occurs via reaction at the active site (Nagar *et al*., 2015). Considering that Lys 166 and His 297 of MR act to form a Schiff base with 3-

HP and catalyze its deprotonation, respectively (Nagar *et al*., 2015), that these conserved catalytic residues at the active site of FucD (Lys 220 and His 351) do not appear to behave in a similar fashion despite their similar positioning at the active site of FucD suggests that differences must arise, in part, due to subtle differences in the active site architectures. This is especially true since the catalytic mechanisms of these enzymes differ, β-elimination (FucD) versus racemization (MR), and thus, the mechanism for inactivation of FucD may occur differently than that of MR. Consequently, the reaction of 3-HP at allosteric sites may account for why the efficiency of inactivation of FucD by 3-HP is significantly lower (0.0167 ± 0.0021 $M^{-1}s^{-1}$ in 5 mM Tris-Cl, 10 mM $MgCl_2$, pH 7.5) than that observed for MR (83 ± 8 $M^{-1}s^{-1}$ in 100 mM HEPES, 3.3 mM $MgCl_2$, pH 7.5) (Nagar *et al*., 2015). Furthermore, while Chris Fetter (Fetter, 2019) and I observed both 86-Da and 58-Da adducts at Lys 220 using LC-MS/MS analysis, we also identified 58-Da adducts on multiple additional polar residues that were not within the active site. These findings could suggest that although 3-HP, and possibly GLH (see Section 3.3.2) modify the active site FucD, the inactivation of the enzyme itself may occur at a non-active site location.

Alternatively, the lack of protection against inactivation by L-fuconate could arise from dimer asymmetry. Dimer asymmetry was described by Pai and colleagues (2017) for fluoroacetate dehalogenase using freeze-trapping X-ray crystallography, NMR, and computational techniques (rigidity-based transition models and molecular dynamics simulations). They showed that only one protomer of the enzyme dimer could bind substrate at any given time. In this model, one protomer exists in the open state that could bind and therefore catalyze the turnover of substrate, whereas the other protomer exists in

a closed state that is unable to bind substrate (Kim *et al*., 2017). The conformational exchanges between the two protomers to afford such asymmetry was found to occur on the millisecond timescale, where the rate of conformational exchange is enhanced once substrate is bound (Kim *et al*., 2017). Given this phenomenon of dimer asymmetry, the possibility exists that if this were true for FucD, protection against 3-HP-dependent inactivation by L-fuconate may not provide full protection if the binding of L-fuconate at the active site of one protomer of the dimer results in the active site of the other protomer being available to undergo reaction with 3-HP, and, consequently, lead to inactivation in the presence of substrate binding. Thus, even with high concentrations of L-fuconate present, the substrate could only ever occupy one protomer at any given time, leaving the other protomer free for inactivation by 3-HP. However, if this were the case, L-fuconate would still be anticipated to provide half the level of protection, wherein the rate of inactivation would be half of that observed in the absence of substrate, which was not observed in our protection studies.

Overall, these protection studies conducted with L-fuconate provide further evidence, along with the low efficiency of inactivation, and MS/MS findings (Fetter, 2019) that the mechanisms of inactivation for both MR subgroup members, FucD and MR, appear to be different despite their similar catalytic machinery.

3.3.2 LC-MS ANALYSIS OF THE INACTIVATION OF FucD BY 3-HP

To explore the origin of the inactivating effect of 3-HP on FucD, intact MS (LC-MS) was employed to determine the size and number of adducts formed when 3-HP-dependent inactivation of FucD by 3-HP was conducted in 5 mM versus 50 mM Tris-Cl

buffer. As shown in **Figures 3.9**, **3.10**, and **Table 3.3**, a combination of both 58- and 86-Da adducts were observed in both 3-HP-treated samples (i.e., in 5 mM Tris and 50 mM Tris-Cl), which were also previously observed in LC-MS/MS experiments (Fetter, 2019). Shown in **Table 3.3** are the predicted adducts from each 3-HP-treated FucD sample, which were determined by subtracting the average mass of the sample peak (i.e., 3-HP-treated FucD) by that of the control peak (i.e., untreated FucD). Due to the abundance of average masses detected by LC-MS, only those with a relative abundance of ≥10% to that of the base peak (100%) (most abundant ion) are presented in **Table 3.3**.

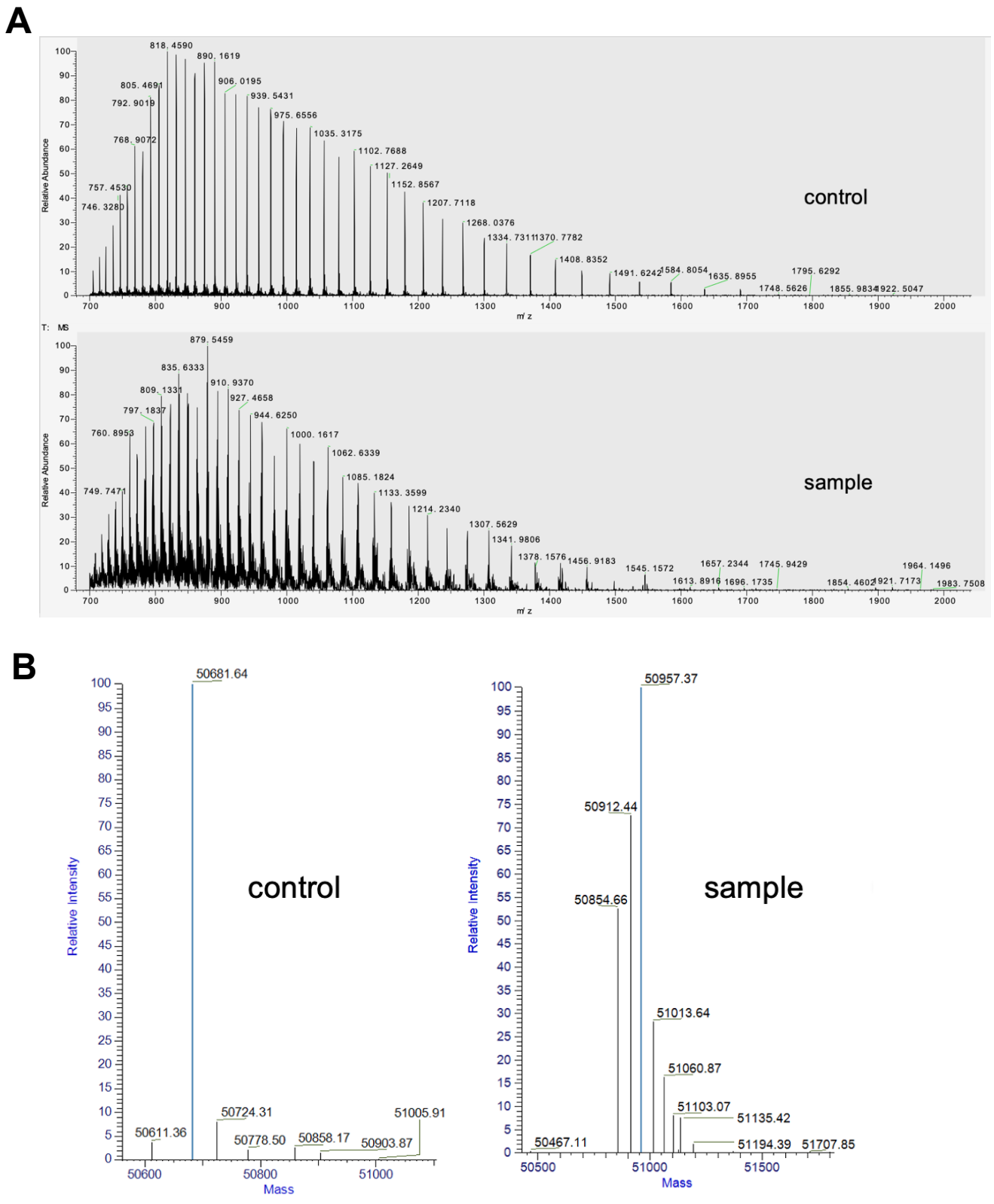

Figure 3.9 LC-MS spectra of 3-HP-inactivated FucD in 5 mM Tris-Cl assay buffer. (A) Raw *m*/*z* and (B) deconvoluted mass spectra of 3-HP-treated FucD (sample) and untreated FucD (control) are shown.

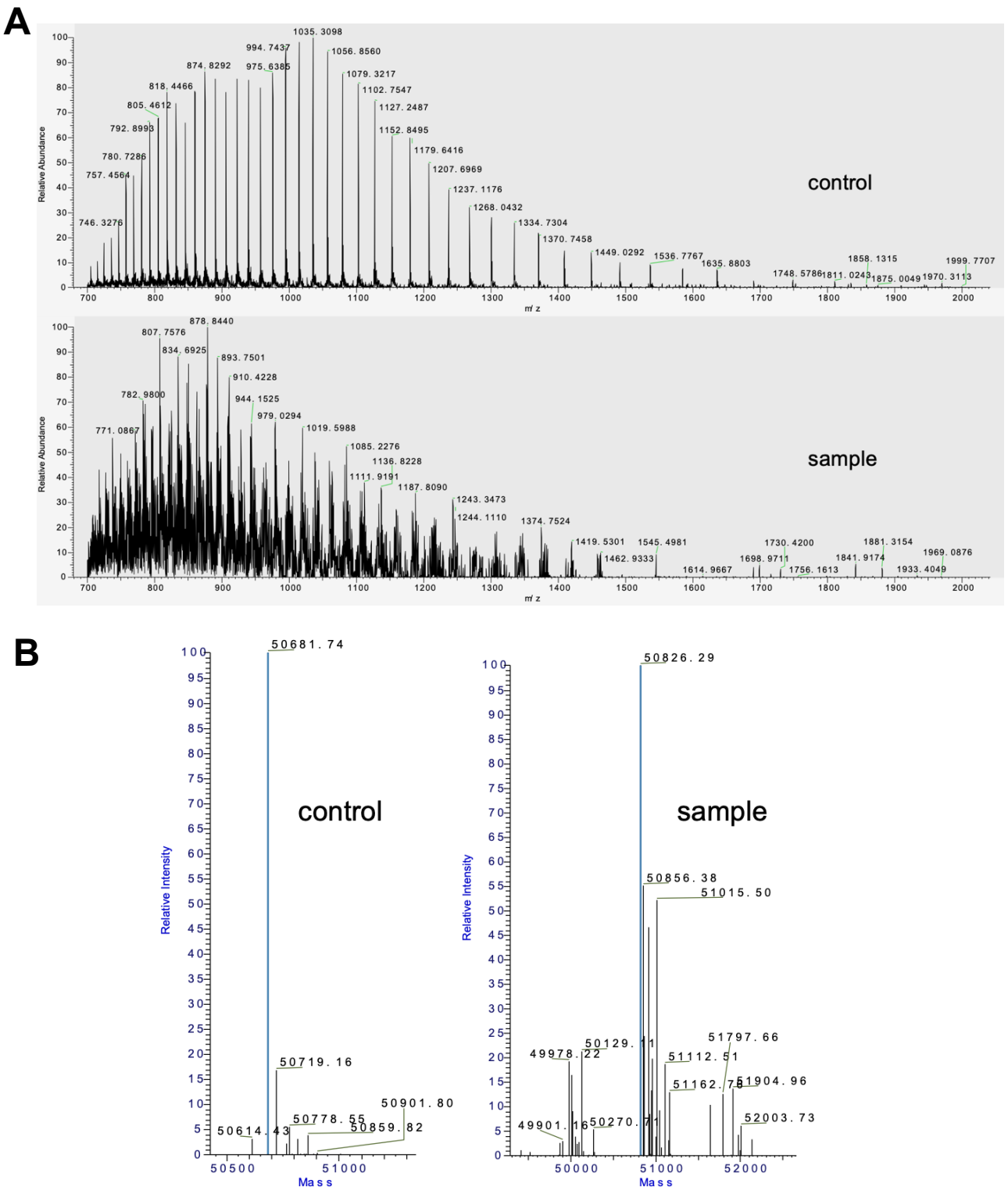

Figure 3.10 LC-MS spectra of 3-HP-inactivated FucD in 50 mM Tris-Cl assay buffer. (A) Raw *m*/*z* and (B) deconvoluted mass spectra of 3-HP-treated FucD (sample) and untreated FucD (control) are shown.

Table 3.3 Observed masses from LC-MS deconvoluted spectra and predicted adducts resulting from the inactivation of FucD by 3-HP in 5 mM and 50 mM Tris-Cl assay buffer. In both samples, 58-Da, 86-Da, and 44-Da (tryptophan oxidation to hydroxy-bis-tryptophandione) adducts were observed. Adducts that could not be predicted from the observed mass were indicated as "undetermined". The adducts are ranked in order (highest to lowest) by their relative abundance to the base peak (most abundant ion). Only those peaks with a relative abundance of ≥10% are presented.

relative abundance	observed mass (Da) **5 mM Tris**	observed mass shift (Da) **5 mM Tris**	predicted adducts (Da) **5 mM Tris**	observed mass (Da) **50 mM Tris**	observed mass shift (Da) **50 mM Tris**	predicted adducts (Da) **50 mM Tris**
highest	50957	+275	+86, +86, +58, +44	50826	+144	+86, +58
	50912	+230	+86, +86, +58 or +58, +58, +58, +58	50856	+174	+86, +86
	50855	+173	+86, +86	51016	+334	+86, +86, +58, +58, +44
	51014	+332	+86, +86, +58, +58, +44	50922	+240	undetermined
	51061	+379	+86, +58, +58, +58, +58, +58	50864	+182	undetermined
	-	-	-	50958	+276	+86, +86, +58, +44
	-	-	-	51113	+431	86, +86, +86, +58, +58, +58
	-	-	-	50952	+270	undetermined
	-	-	-	51163	+481	undetermined
lowest	-	-	-	51798	+1116	undetermined

Consistent with both 3-HP-treated FucD samples in 5 mM and 50 mM Tris-Cl buffer, a combination of both 58- and 86-Da adducts were observed, with their proposed structures illustrated in **Figure 3.11**. The formation of the 86-Da adduct was described in Section 3.1.4 as the Schiff base formed between the ε-NH_2 group of catalytic Lys 166 for MR (equivalent to Lys 220 of FucD) and 3-HP, which is subsequently deprotonated by a Brønsted base, to yield the enol(ate)/aldehyde adduct (86 Da). A similar mechanism is proposed for the 3-HP-dependent inactivation of FucD. A proposed reaction scheme for the 58-Da adduct was described by Chris Fetter (**Scheme 3.5**) (Fetter, 2019), wherein FucD catalyzes the tautomerization of 3-HP to yield tartronate semialdehyde, which is then decarboxylated to yield GLH. Alternatively, GLH could be formed non-enzymatically from 3-HP in the presence of Mg^{2+}, as previously described in the literature for 3-HP in the presence of divalent metals (Hedrick & Sallach, 1961), wherein 3-HP is tautomerized to yield tartronate semialdehyde, which could then be spontaneously decarboxylated. Subsequently, GLH could react with nucleophilic residues, predominantly Lys and Arg, to form a Schiff base (Glomb & Monnier, 1995; Thorpe & Baynes, 2003). The imine is then deprotonated by a Brønsted base, which could undergo a Cannizzaro reaction with GLH to yield the carboxylic acid adduct (58 Da) with Lys 220 or other nucleophilic residues.

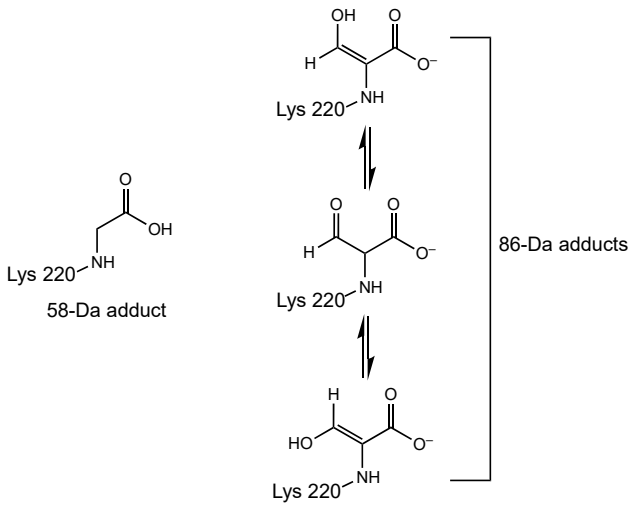

Figure 3.11 Proposed structures for the observed 86- and 58-Da adducts formed from the 3-HP-dependent inactivation of FucD.

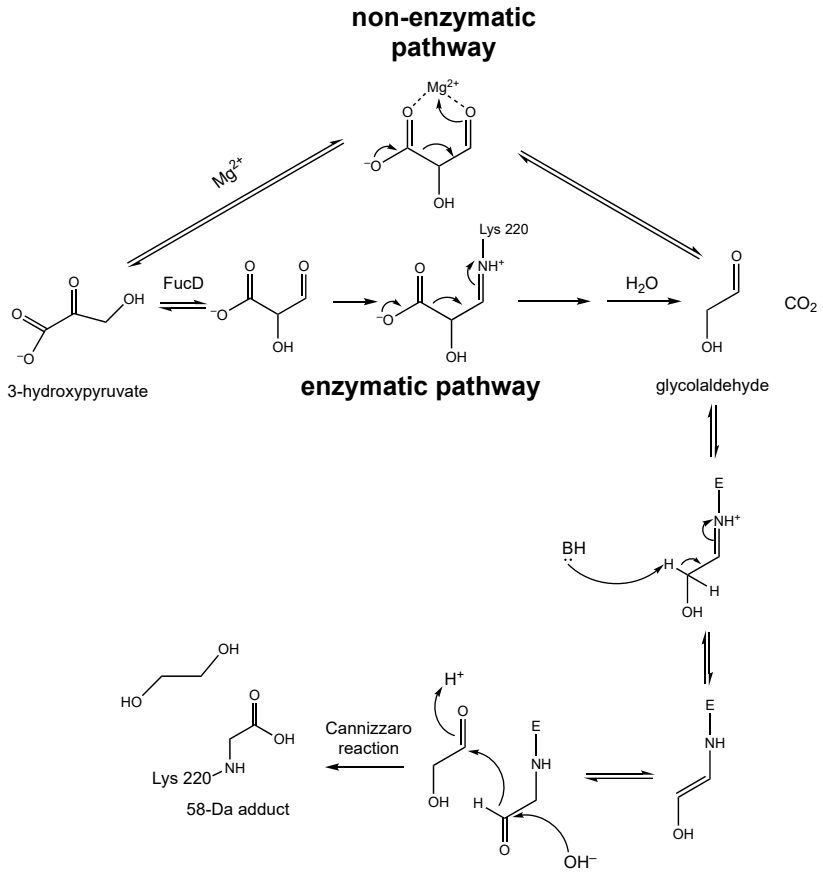

Scheme 3.5 Proposed pathways for the non-enzymatic and enzymatic formation of GLH from 3-HP to yield the 58-Da adducts. Adapted from Fetter, 2019.

However, while the 58- and 86-Da adducts were observed in both 3-HP-inactivated FucD samples, the 3-HP-treated FucD in 50 mM Tris-Cl sample (**Figure 3.10)** contained a significantly greater number of peaks as shown in the raw *m/z* and deconvoluted mass spectra, corresponding to distinct average masses, than the 3-HP-treated FucD in 5 mM Tris-Cl sample (**Figure 3.9)**. In addition, the presence of unknown adducts were observed only in the 3-HP-treated FucD in 50 mM Tris-Cl sample as indicated in **Table 3.3**. Thus, while the story remains unclear with respect to the exact mechanism responsible for the protection against 3-HP-dependent inactivation by Tris, these LC-MS data show clear differences in the abundance of adducts formed from the inactivation of FucD by 3-HP in the presence of a high concentration of Tris-Cl (50 mM) versus in a low concentration of Tris-Cl (5 mM).

3.3.3 ^{1}H NMR ANALYSIS OF 3-HP IN TRIS BUFFER

^{1}H NMR spectroscopy was employed to determine whether GLH is formed non-enzymatically by spontaneous decarboxylation of 3-HP (79.75 mM) in the presence of Mg^{2+} from assay buffer containing 50 mM Tris-Cl, 10 mM $MgCl_2$ after a 12 h incubation period at room temperature. First, the chemical shifts of the un-hydrated and hydrated species of GLH were determined: un-hydrated GLH ^{1}H NMR (500 MHz, D_2O) δ 9.59 (s, 1H), 4.40 (s, 2H); hydrated GLH ^{1}H NMR (500 MHz, D_2O) δ 5.01 (t, J = 5.1 Hz, 1H), 3.47 (d, J = 5.1 Hz, 2H) (**Figure 3.12**). The ^{1}H NMR spectrum agreed with those previously published for GLH (Amyes & Richard, 2007; Kua *et al*., 2013).

As shown in **Figure**s **3.13**, the signals arising from the hydrated and un-hydrated forms of 3-HP were observed and remained stable over 12 h. After 0 h of incubation: un-

hydrated 3-HP ^{1}H NMR (300 MHz, D_2O) δ 4.64 (s, 2H); hydrated 3-HP ^{1}H NMR (300 MHz, D_2O) δ 3.59 (s, 2H), after 12 h of incubation: 3-HP ^{1}H NMR (300 MHz, D_2O) δ 4.64 (s, 2H); hydrated 3-HP ^{1}H NMR (300 MHz, D_2O) δ 3.60 (s, 2H). Neither the signals corresponding to the hydrated nor the un-hydrated GLH species were observed in the 3-HP samples initially or after 12 h of incubation. Thus, GLH is not formed from 3-HP in the presence of Mg^{2+} under these conditions, i.e., the non-enzymatic decarboxylation of 3-HP as described in the literature for 3-HP in the presence of divalent metals (Hedrick & Sallach, 1961) does not appear to contribute to GLH formation in the presence of 10 mM Mg^{2+}.

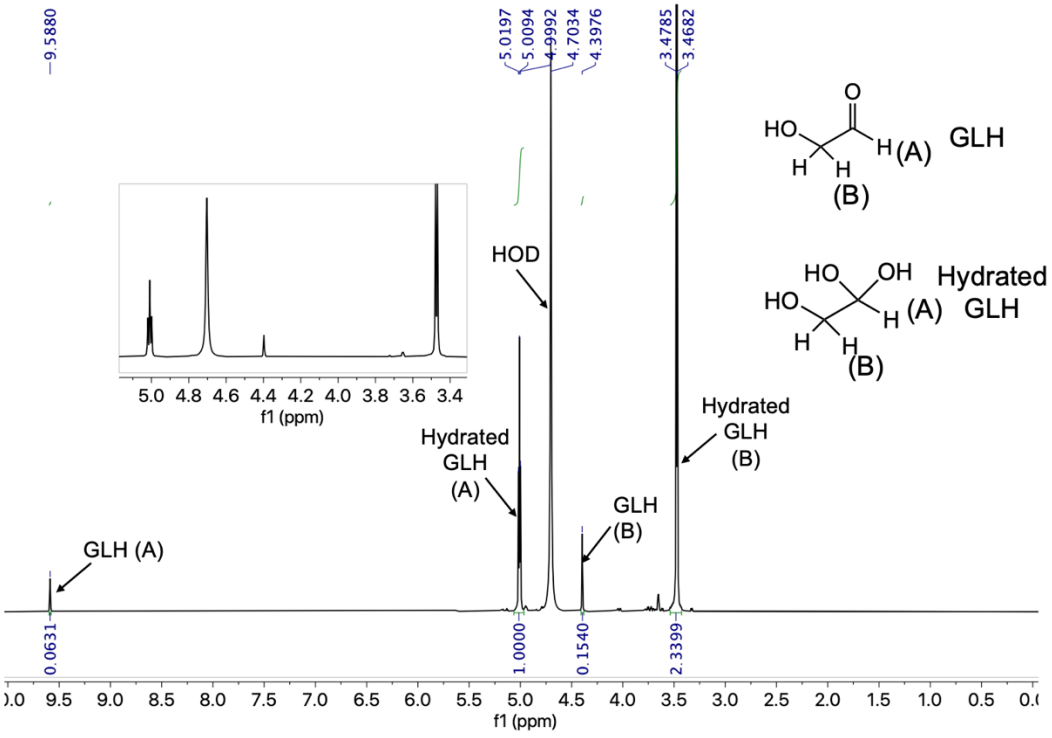

Figure 3.12 ^{1}H NMR spectrum of glycolaldehyde. GLH (100 mM) was dissolved in D_2O to determine the chemical shifts of its un-hydrated and hydrated species.

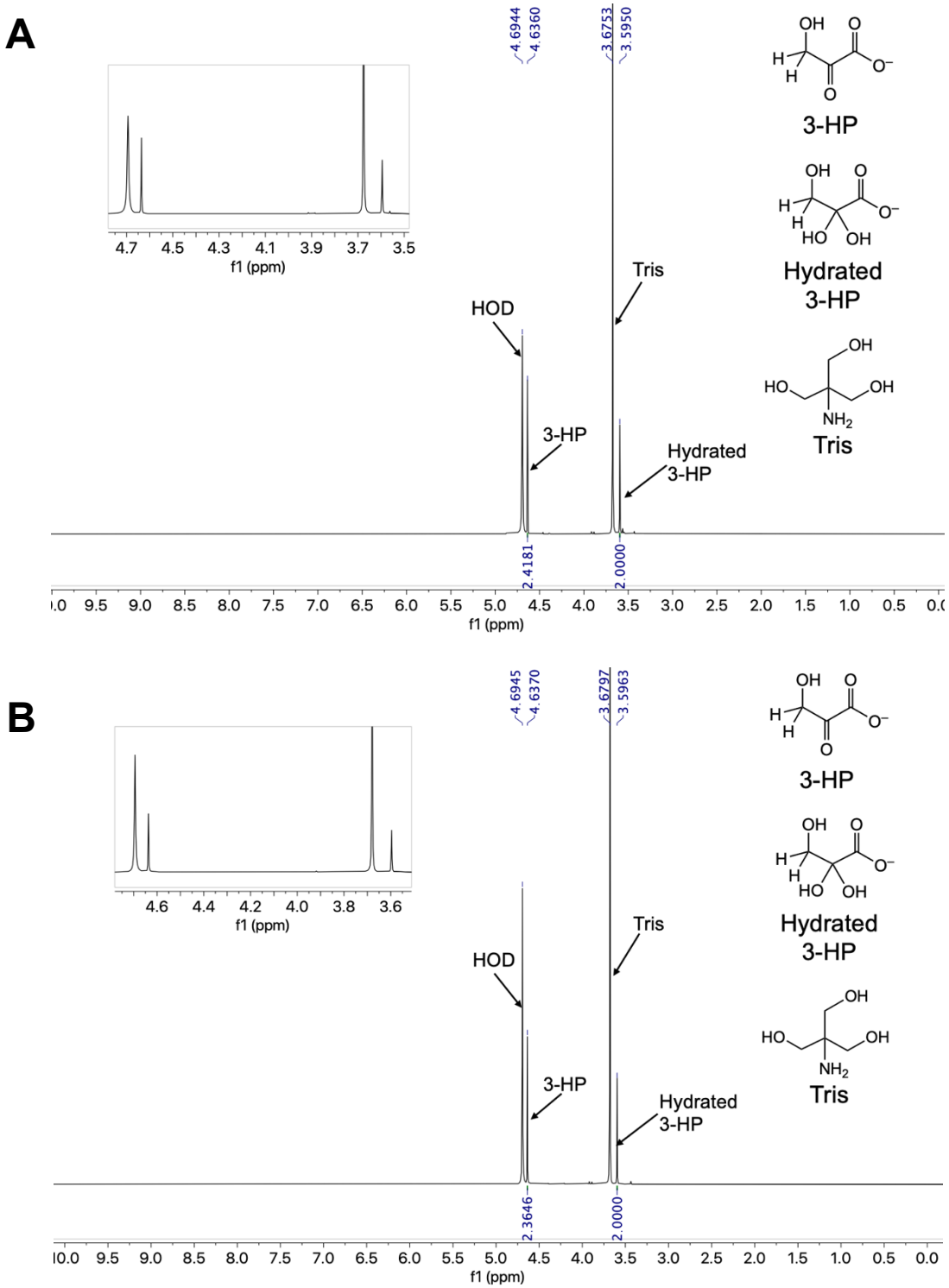

Figure 3.13 ^{1}H NMR spectra of 3-HP in deuterated Tris-Cl assay buffer after 12 h incubation. 3-HP (79.75 mM) in deuterated assay buffer containing 50 mM Tris-Cl, 10 mM $MgCl_2$ was incubated for (A) 0 h and (B) 12 h at room temperature. Signals corresponding to the un-hydrated and hydrated 3-HP species are shown. No evidence of non-enzymatic formation of GLH was detected for up to 12 h.

3.4 CONCLUSIONS AND FUTURE WORK

The inactivation of MR by 3-hydroxypyruvate (3-HP) was previously discovered to occur through a Schiff-base mechanism with Lys 166, yielding a k_{inact}/K_I value of 83 ± 8 $M^{-1}s^{-1}$ (Nagar *et al*., 2015). Given that members of the MR subgroup share conserved active-site residues and that the catalytic Lys and His residues act as binding determinants for 3-HP, we investigated whether 3-HP could also inactivate FucD. Time-dependent inactivation studies of FucD by 3-HP revealed that the efficiency of inactivation was much lower than that reported for MR, and that Tris protected FucD from 3-HP-dependent inactivation. The k_{inact}^{app} and K_I^{app} values decreased with respect to increasing Tris concentrations from 5 to 50 mM, but the $k_{inact}^{app}/K_I^{app}$ remained unchanged over this range of Tris concentrations (~0.018 ± 0.002 $M^{-1}s^{-1}$).

Furthermore, unlike with MR where protection against 3-HP-dependent inactivation was observed using benzohydroxymate, the substrate L-fuconate did not afford protection against the 3-HP-dependent inactivation of FucD. Hence, unlike with MR, inactivation does not appear to occur at the active site. While 3-HP-treated FucD samples conducted in both 5 mM and 50 mM Tris-Cl buffers showed the presence 58- and 86-Da adducts, the 50 mM Tris-Cl sample showed the presence of a greater abundance of adducts, many of which could not be identified.

Overall, it is evident that, despite the conserved active-site residues between the MR subgroup members, 3-HP likely inactivates FucD through a different mechanism than that previously determined for MR. In addition, while Tris remains one of the most commonly used biochemical buffers to date, it has been well-reported to chelate divalent metal ions, form Schiff-base adducts with carbonyl compounds, and to inhibit various

enzymes, predominantly via competitive inhibition. In this work, I identified a much less commonly reported phenomenon where Tris acts as a protectant against enzyme inactivation, again, emphasizing that caution should be observed when using this buffer for enzyme-based studies. In future work, since GLH is not formed non-enzymatically in the presence of Mg^{2+} under the assay conditions, it remains to determine if GLH is formed in the presence of FucD. While ^{1}H NMR spectroscopy could be used to detect GLH generated enzymatically, the experiment may not be conclusive if the enzyme rapidly traps the GLH as it is formed and is inactivated.

CHAPTER 4 CAN THE BIDIRECTIONAL ACTIVITY OF GLUTAMATE RACEMASE BE RE-ENGINEERED TO BECOME PREFERENTIALLY 'UNIDIRECTIONAL'?

4.1 INTRODUCTION

4.1.1 GLUTAMATE-RACEMASE

Glutamate racemase is a cofactor-independent amino acid racemase that catalyzes the interconversion of L-glutamate (L-Glu) and D-glutamate (D-Glu) via a two-base mechanism (Glavas & Tanner, 1999). Glutamate racemase plays a critical role in the biosynthesis of bacterial cell walls, wherein D-Glu, in addition to D-alanine, is an essential component of peptidoglycan, which protects bacteria from osmotic rupture (Fisher, 2008; Lundqvist *et al*., 2007; Van Heijenoort, 2001). Since glutamate racemase is conserved across the bacterial domain, developing inhibitors as antibacterial drugs of glutamate racemase activity is of therapeutic interest (Fisher, 2008; Lundqvist *et al*., 2007).

Two active-site cysteine residues serve as the acid/base catalysts in the 1,1-proton transfer mechanism between L-Glu and D-Glu, which are conserved among the GR family **(Scheme 4.1)** (Glavas & Tanner, 1999; Glaves & Tanner, 2001). Specifically, in the case of GR from *Lactobacillus fermenti* (*Lf*GR), the thiolate of Cys 73 acts as a Brønsted base to abstract the α-proton from D-Glu to form the planar carbanionic intermediate (Glavas & Tanner, 2001). The intermediate is subsequently re-protonated by the thiol of Cys 184, which serves as the conjugate acid, to yield L-Glu (Glavas & Tanner, 2001). With L-Glu as the substrate, Cys 184 abstracts the α-proton to form the carbanionic intermediate, which is subsequently re-protonated by Cys 73 to yield D-Glu (Glavas & Tanner, 2001).

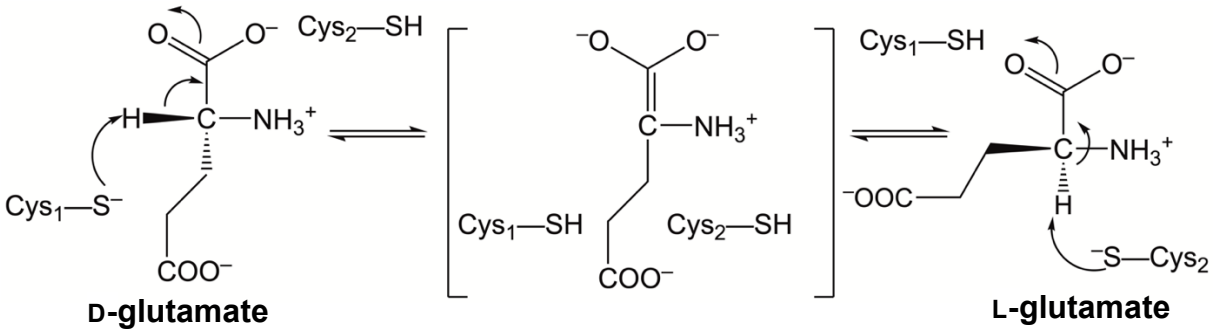

Scheme 4.1 Racemization reaction of D-Glu and L-Glu catalyzed by GR. Cys_1 and Cys_2 represent the two active-site acid/base catalysts. In the cases of GR from *Lactobacillus fermenti*, Cys_1 = Cys 73 and Cys_2 = Cys 184 and from *Fusobacterium nucleatum* Cys_1 = Cys 76 and Cys_2 = Cys 186.

While not all GRs exhibit a stereochemical preference for L- or D-Glu, GR from *Lactobacillus fermenti* (Glavas & Tanner, 1999, 2001) and GR from *Fusobacterium nucleatum* (Potrykus *et al*., 2009) are pseudosymmetric enzymes, whereby the k_{cat} and K_m values are approximately equal in both the D→L and L→D reaction directions. The ratio of the catalytic efficiencies (k_{cat}/K_m) in the D→L and L→D reaction directions for racemases yields the equilibrium constant (K_{eq}) as dictated by the Haldane relationship (eqn 4.1) and is unity.

$$K_{eq} = \frac{(k_{cat} / K_m)^{L\rightarrow D}}{(k_{cat} / K_m)^{D\rightarrow L}} \qquad (4.1)$$

4.1.2 SUBSTITUTION OF CATALYTIC CYS RESIDUES

In 1993, Knowles and co-workers constructed single substitutions of the catalytic Cys residues to Ala residues in *Lf*GR, C73A and C184A, which resulted in complete loss in enzymatic activity (Tanner *et al*., 1993). However, given that a Brønsted base is required for substrate deprotonation, a more isosteric substitution of the Cys residues to Ser residues, C73S and C184S, was later explored by Glaves and Tanner (1999), since, unlike Ala, the alkoxide/hydroxyl of Ser could potentially serve as base/acid catalysts similarly to the thiolate/thiol of Cys. These authors observed that the catalytic efficiencies (k_{cat}/K_m) were greatly reduced relative to the wild-type GR enzyme by ~600-fold for C184S and ~1200-fold for C73S in both reaction directions when the reaction was conducted at pH 8.0. The K_m values were increased ~10-fold for both variants in both reaction directions. Thus, while significant activity was lost with the Ser variants, these data indicated that Ser could act as enzymatic acid/base catalysts for this reaction despite the pK_a of the Ser hydroxyl (~16) being considerably greater than that of the Cys thiol (~10). Furthermore, like wild-type *Lf*GR, both variants exhibited pseudosymmetric behavior at pH 8.0 since the K_m and k_{cat} values were similar in both the L→D and D→L reaction directions.

Glaves and Tanner (1999) further investigated the pH-dependence of the k_{cat}/K_m values for the D→L reaction direction from pH 7.0 to 9.0. Interestingly, the k_{cat}/K_m values for the C73S variant increased ~10-fold over this pH range, but the k_{cat}/K_m for the C184S variant remained largely unchanged. The authors suggested that this trend was observed since Ser 73 must act as a Brønsted base in the D→L reaction direction but is predominately protonated, and thus, with increasing pH, greater amounts of alkoxide

became available to deprotonate D-Glu. Contrarily, Ser 184, which acts as a general acid catalyst in this reaction direction and is already predominately protonated in its hydroxyl form over this pH range, there is little change in the catalytic efficiency. Since the coupled assay using NADH diaphorase was not amenable to assaying *Lf*GR in the reverse reaction direction, the effect of pH on the catalytic efficiency of *Lf*GR in the L→D reaction direction was not examined, but Glaves and Tanner (1999) proposed that the opposite trend would be observed in the L→D reaction direction, where the k_{cat}/K_m values for the C184S variant would increase with pH but would remain largely unchanged for the C73S variant.

4.1.3 GR FROM *Fusobacterium nucleatum*

GR from *Fusobacterium nucleatum* (*Fn*GR) was previously purified and characterized by Potrykus *et al*. (2009). *F. nucleatum* is an oral pathogen that promotes periodontal disease through its coaggregation with other fusobacterial strains to form dental plaque (Kolenbrander *et al*., 1990; Kolenbrander & London, 1993). While the oligomeric state of GR can differ greatly between organisms (Lundqvist *et al*., 2007; Taal *et al*., 2004), *Fn*GR was found to exist primarily as a dimer in solution using a combination of blue native-polyacrylamide gel electrophoresis, Ferguson plot analysis, and chemical cross-linking studies (Potrykus *et al*., 2009). With Cys 76 and Cys 186 as the active site acid/base catalysts for *Fn*GR (analogous to Cys 73 and Cys 184 from *Lf*GR, respectively), the kinetic parameters for wild-type *Fn*GR were determined in both the L→D and D→L reaction directions for the substrates L-Glu (K_m = 1.04 ± 0.07 mM; k_{cat} = 17.4 ± 0.8 s^{-1}; k_{cat}/K_m = 17 ± 1 $mM^{-1}s^{-1}$) and D-Glu (K_m = 1.7 ± 0.1 mM; k_{cat} = 26 ± 1 s^{-}

[1]; k_{cat}/K_m = 15 ± 1 $mM^{-1}s^{-1}$) (Potrykus *et al*., 2009). As the catalytic efficiencies were approximately equal, the resulting K_{eq} value was 1.1 ± 0.1 in accord with eqn 4.1 (Potrykus *et al*., 2009).

4.1.4 OVERVIEW OF THIS WORK

My objective was to construct *Fn*GR Cys to Ser variants, C76S and C186S, to determine whether, like *Lf*GR, residual activity would be observed despite the increased pK_a value of Ser by ~6 units relative to Cys. Herein, I show that, in agreement with the findings of Glaves and Tanner (1999), the thiol to hydroxyl substituted variants for *Fn*GR were significantly less active than the wild-type enzyme, but still retained some residual activity at pH 8.0. The next objective was to determine whether the variants would exhibit 'unidirectional' activity at increased pH values, which was anticipated based on findings by Glaves and Tanner (1999) in the D→L reaction direction. Given the findings for *Lf*GR, it was reasonable to anticipate that C76S of *Fn*GR would exhibit greater catalytic efficiency turning over D-Glu relative to L-Glu at higher pH values, and that C186S would exhibit greater catalytic efficiency turning over L-Glu relative to D-Glu at higher pH values. The catalytic efficiencies of both variants were examined at pH 8.0, 8.5, and 9.0 in both the D→L and L→D reaction directions, where, due to the extremely low activity of the variants, the pH effect below 8.0 could not be accurately assessed using the CD-based assay. Furthermore, the variants were not examined above pH 9.0 since previous studies with wild-type *Fn*GR showed that there was a significant drop in the catalytic efficiency above pH 9.0 (Potrykus *et al*., 2009).

4.2 MATERIALS AND METHODS

4.2.1 GENERAL

All reagents were purchased from Sigma-Aldrich Canada Ltd. (Oakville, ON, Canada) unless otherwise stated. The primers used for site-directed mutagenesis were purchased from Integrated DNA Technologies (IDT) (Coralville, IA, USA). The QIAprep Spin Miniprep Kit was purchased from Qiagen (Toronto, ON, Canada). Phusion high fidelity polymerase was purchased from New England Biolabs (Ipswich, MA, USA). Kinetic studies were conducted using a CD-based assay with a JASCO J-810 spectropolarimeter. Sanger sequencing was carried out commercially by Robarts Research Institute (London, ON, Canada).

4.2.2 SITE-DIRECTED MUTAGENESIS

The pET15b(+) plasmids containing the open reading frame encoding wild-type GR from *F. nucleatum* from the *murI* gene (locus FN116, SWISS-PROT accession number Q8REE6) (Potrykus et al., 2009) were extracted from *E. coli* DH5α cells using a QIAprep Spin Miniprep Kit (Qiagen) following the manufacturer's instructions. The *Fn*GR mutant, C76S, was constructed by mutagenesis using deoxyoligonucleotide primers: 5′-AATAGT**AGC**TAGCAATACAGCTTC-3′ (forward) and 5′-ACTAATTTACAATTATTTTTGACAAAAAAATC-3′ (reverse), where the altered codon encoding residue 76 is underlined and the altered base is showed in boldface. The *Fn*GR mutant, C186S, was constructed by mutagenesis using deoxyoligonucleotide primers: 5′- AGTATTAGGT**AGC**ACTCATTATCCACTTATAAG-3′ (forward) and 5′-AAGGTATCAGCATTTTTAGGAATTTCAG -3′ (reverse), where the altered codon

encoding residue 186 is underlined and the altered base is showed in boldface. Phusion high-fidelity polymerase was used for the amplification of DNA from the extracted template DNA according to the manufacturer's instructions (New England Biolabs). Amplification was conducted with the initial denaturation at 98 °C for 5 min, followed by 30 cycles for 30 s at 98 °C, 30 s at the annealing temperature (48°C for C76S and 52°C for C186S), and 3 min at 72 °C for elongation. After the temperatures were cycled 30 times, a final extension was conducted for 10 min at 72 °C. The reaction product was treated with DpnI restriction enzyme overnight at 25 °C to remove methylated template DNA. Chemically competent *E. coli* DH5α cells were transformed using the heat shock method with the PCR products (Sambrook *et al*., 1989) and the cells were plated on LB-agar plates containing ampicillin (100 μg/mL) followed by incubation overnight at 37 °C. Transformants were grown overnight in LB media (5 mL) containing ampicillin (100 μg/mL) and plasmids were then extracted using a QIAprep Spin Miniprep Kit (Qiagen) as previously described. Glycerol stocks (15) of the *E. coli* DH5α cells were also prepared and stored at –80 °C. The open reading frames were commercially sequenced (Robarts Research Institute) using Sanger sequencing to verify only selected mutations to the *Fn*GR open reading frame were introduced.

4.2.3 EXPRESSION AND PURIFICATION OF WT, C76S, AND C186S *Fn*GR

Plasmids containing the open reading frame encoding wild-type GR from *F. nucleatum* from the *murI* gene and constructed *Fn*GR variants, C76S and C186S, were used to transform BL21 (DE3) cells for protein expression as previously described (Potrykus *et al*., 2009). The expression and purification of *Fn*GR was followed exactly as

described for 3-HBDH in Section 2.2.3 and as described previously (Potrykus *et al*., 2009). The same binding, wash, and strip buffers were used as described in Section 2.2.3, with the addition of D,L-glutamate (1 mM) in each buffer for stabilization of the enzyme during the purification. Upon elution with strip buffer (10 mL), *Fn*GR was dialyzed (MWCO 12 – 14 kDa) for 3 × 8 h (4 °C) against storage buffer (10 mM potassium phosphate, 0.2 mM DTT, pH 8.0). The dialyzed enzyme was aliquoted and stored at –80 °C for future use. Protein concentrations were determined by conducting Bradford assays (Bio-Rad Laboratories, Mississauga, ON, Canada) with BSA standards. Protein purity was assessed using SDS-PAGE (12%) with Coomassie brilliant blue (R-250) staining.

4.2.4 DETERMINATION OF KINETIC PARAMETERS FOR WT *Fn*GR

The kinetic parameters for WT *Fn*GR in both the L→D and D→L reaction directions were determined using CD spectroscopy as previously described (Potrykus *et al*., 2009). Initial velocity values were obtained from the linear slopes by following the change in ellipticity at 204 nm over a period of 300 s at 30 °C, using a molar ellipticity of 31 000 deg cm^2 mol^{-1} (31 mdeg $mM^{-1}cm^{-1}$). In a 0.5-cm pathlength quartz cuvette with a total volume of 1.0 mL, reactions were initiated by the addition of WT *Fn*GR to a final concentration of 6.25 μg/mL (0.195 μM) with L- or D-Glu (0.15–5.0 mM) in 10 mM potassium phosphate, pH 8.0, assay buffer. The Michaelis-Menten equation was fitted to the initial velocity data using *KaleidaGraph* software (v. 4.02) (Synergy Software, Reading, PA) for non-linear regression analysis (eqn 2.1). The k_{cat} values were calculated by dividing the V_{max} values by the total enzyme concentration ($[E]_T$) using the molecular weight of the recombinant WT *Fn*GR bearing a $(His)_6$-tag (32 045.86 Da). The kinetic

assays in both reaction directions were performed in triplicate and the average values were reported with the errors corresponding to the standard deviation values.

4.2.4 pH-STUDY FOR C76S and C186S *Fn*GR VARIANTS

The kinetic parameters for the *Fn*GR variants, C76S and C186S, were determined in both reaction directions for the substrates D- and L-Glu using CD spectroscopy. Initial velocity values were obtained from the linear slopes by following the change in ellipticity at 204 nm over a period of 300 s at 30 °C. In a 0.1-cm pathlength quartz cuvette with a total volume of 0.30 mL, reactions were initiated by the addition of C76S or C186S *Fn*GR to a final concentration of 0.10 mg/mL (3.12 μM) with L- or D-Glu (5.0–20.0 mM) in assay buffer. Assays were conducted at pH 8.0, 8.5, and 9.0 using the following buffers: 10 mM potassium phosphate (pH 8.0) and 10 mM boric acid (pH 8.5, 9.0). Substrate concentrations were limited by the high absorbance at 204 nm observed at high concentrations of substrate and the high concentration of enzyme required to observe catalytic activity. Hence, high concentrations of substrate could not be employed and saturation was not observed. Eqn 4.2 was fitted to the initial velocity data and the k_{cat}/K_m values were estimated by dividing the slope (V_{max}/K_m) by the total enzyme concentration ($[E]_T$), using the molecular weight of $(His)_6$-tagged *Fn*GR variants C76S and C186S of 32 029.80 Da. The kinetic assays in both reaction directions were performed in triplicate and the average values were reported with the errors corresponding to the standard deviation values.

$$v_i = \frac{V_{max}}{K_m}[S] \tag{4.2}$$

4.3 RESULTS AND DISCUSSION

4.3.1. KINETIC PARAMETERS AND PSEUDOSYMMETRY OF WT FnGR

The kinetic parameters of wild-type *Fn*GR were determined with both L- and D-Glu substrates at pH 8.0, wherein the pH optimum for wild-type *Fn*GR was previously determined to be 8.0-8.5 (Potrykus *et al*., 2009). Using non-linear regression analysis, the values of K_m, k_{cat}, and k_{cat}/K_m were found to be similar to those previously determined for WT *Fn*GR (**Figure 4.1, Table 4.1**) (Potrykus *et al*., 2009). Furthermore, the values of K_m, k_{cat}, and k_{cat}/K_m were similar in both L→D and D→L reaction directions, yielding a K_{eq} value of 0.956 ± 0.082 based on the Haldane equation (eqn 4.1). Hence, like *Lf*GR, *Fn*GR exhibits pseudosymmetry. However, not all GRs characterized to date are pseudosymmetric, and thus the kinetic parameters for each enantiomer can be quite different, for example, such as those observed for the GR from *Enterococcus faecalis* (L-Glu: K_m = 1200 ± 12 μM, k_{cat} = 1500 ± 40 min^{-1}; D-Glu: K_m = 250 ± 20 μM, k_{cat} = 704 ± 14 min^{-1}) (Lundqvist *et al*., 2007).

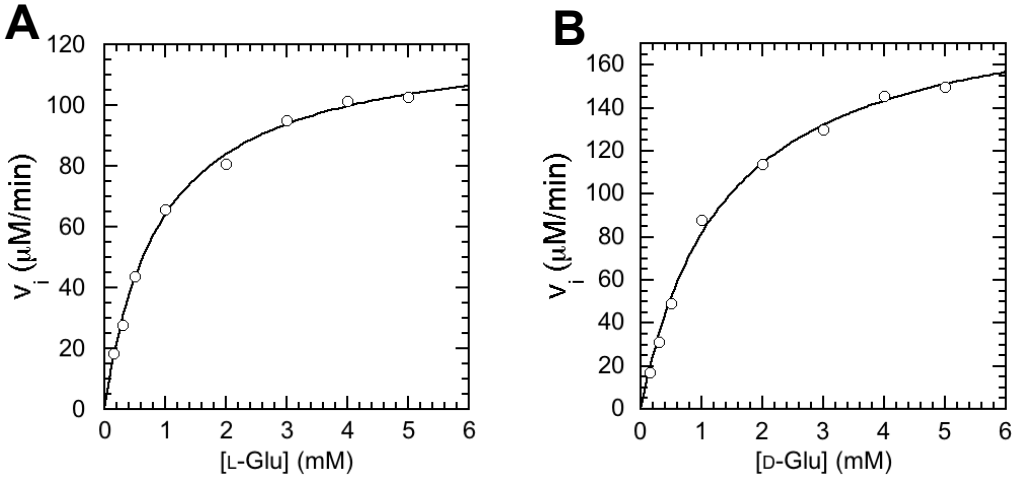

Figure 4.1 Representative Michaelis-Menten plots for the determination of the kinetic parameters for WT *Fn*GR with L-Glu and D-Glu at pH 8.0. (A) L-Glu and (B) D-Glu concentrations ranged from 0.15–5.0 mM with a WT *Fn*GR concentration of 6.25 μg/mL (0.195 μM). The kinetic parameters (determined in triplicate) were: L-Glu: k_{cat} = 10.176 ± 0.316 s^{-1}, K_m = 0.933 ± 0.025, and k_{cat}/K_m = 10.917 ± 0.544 $mM^{-1}s^{-1}$, and D-Glu: k_{cat} = 17.067 ± 0.554 s^{-1}, K_m = 1.501 ± 0.149, and k_{cat}/K_m = 11.419 ± 0.793 $mM^{-1}s^{-1}$.

Table 4.1 Kinetic parameters for the racemization of L- and D-Glu by wild-type *Fn*GR. The kinetic parameters were determined in triplicate with errors corresponding to the standard deviation values.

	This work	**This work**	**Potrykus *et al.* (2009)**	**Potrykus *et al.* (2009)**
	L-Glu	D-Glu	L-Glu	D-Glu
K_m (mM)	0.933 ± 0.025	1.501 ± 0.149	1.04 ± 0.07	1.7 ± 0.1
k_{cat} (s^{-1})	10.176 ± 0.316	17.067 ± 0.554	17.4 ± 0.2	26 ± 1
k_{cat}/K_m ($mM^{-1}s^{-1}$)	10.917 ± 0.544	11.419 ± 0.793	17 ± 1	15 ± 1

4.3.2 pH-DEPENDENCIES OF THE k_{cat}/K_m VALUES FOR C76S AND C186S *Fn*GRs

Upon constructing the C76S and C186S *Fn*GR variants, they were expressed, purified, and their purity was assessed by SDS-PAGE (**Figure 4.2**).

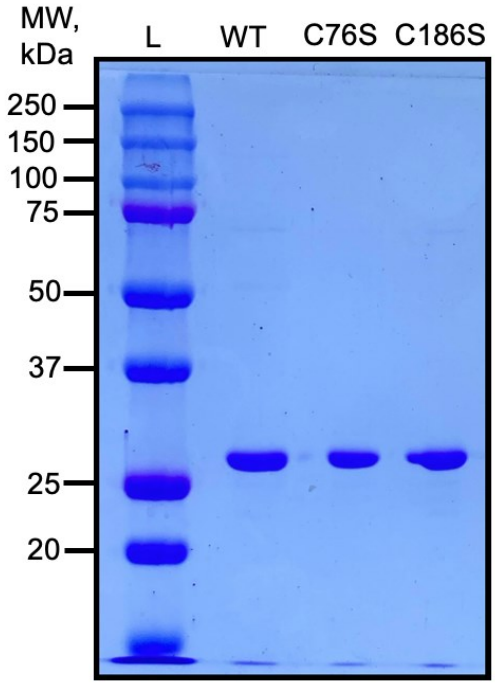

Figure 4.2 Representative SDS-PAGE electrophoretogram showing purified WT, C76S, and C186S *Fn*GR variants. Shown is a 12% gel stained with Coomassie brilliant blue (R-250), where lane "L" corresponds to the molecular weight ladder. The expected molecular weight of the wild-type, C76S, and C186S *Fn*GR variants are 32 046 Da, 32 030 Da, and 32 030 Da, respectively.

The kinetic parameters of the C76S and C186S *Fn*GR variants were determined in both the L→D and D→L reaction directions at pH 8.0, 8.5, and 9.0 (**Figures 4.3** and **4.4**; **Tables 4.2**, **4.3**, and **4.4**). At pH 8.0, the catalytic efficiencies of the variants were reduced by ~180-fold to ~420-fold from the WT enzyme depending on the variant and reaction direction. The C76S *Fn*GR variant exhibited greater catalytic efficiency, turning over D-Glu relative to L-Glu as the pH was increased, thus exhibiting evidence of a preferred 'unidirectional' behavior at higher pH values. Surprisingly, this trend was not observed for C186S *Fn*GR in the L→D reaction direction. While there was a slight increase in the catalytic efficiency of C186S *Fn*GR in the L→D reaction direction from pH 8.0 to 9.0, overall, minimal pH-dependency was observed and the resulting catalytic efficiency for turning over L-Glu was not greater than that of D-Glu as anticipated with increasing pH.

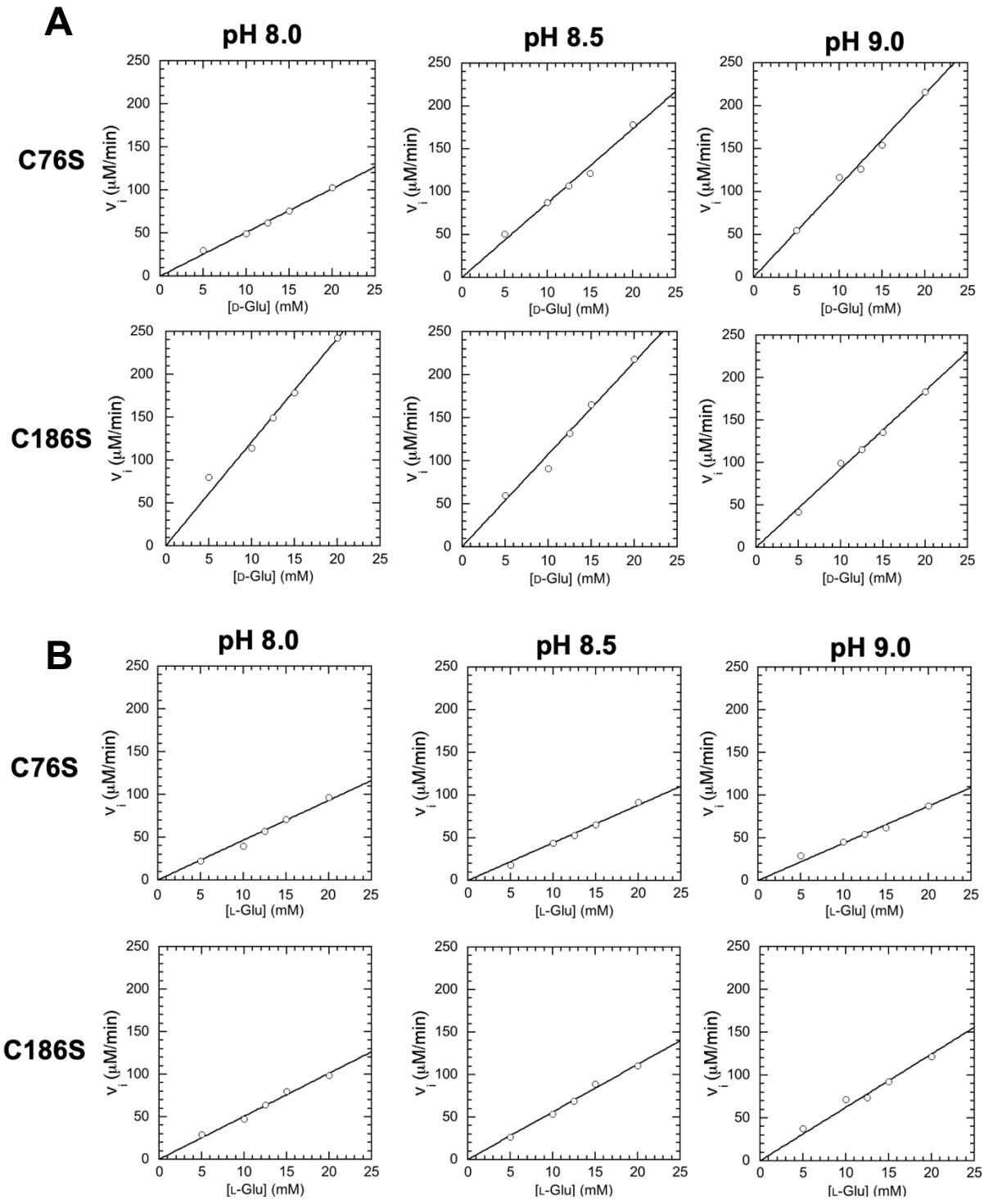

Figure 4.3 Representative plots for the determination of the catalytic efficiency (k_{cat}/K_m) for the C76S and C186S *Fn*GR variants at pH 8.0, 8.5, and 9.0. Assays were conducted (in triplicate) in both reaction directions, with (A) D-Glu and (B) L-Glu concentrations ranging from 5–20 mM and with a final enzyme concentration of 0.10 mg/mL (3.12 μM).

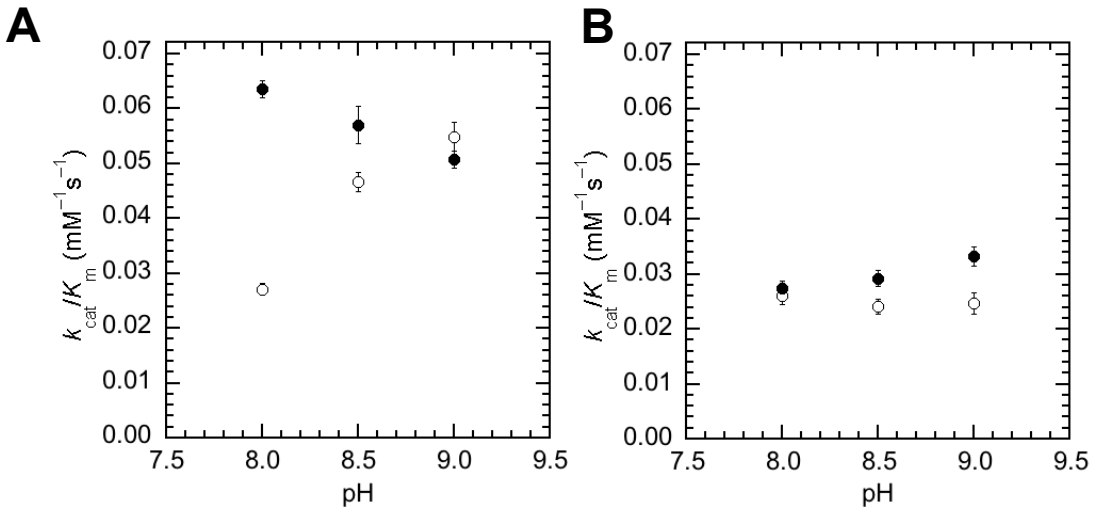

Figure 4.4 Comparison of the catalytic efficiencies (k_{cat}/K_m) between the C76S and C186S *Fn*GR variants at pH 8.0, 8.5, and 9.0. Assays for the C76S (○) and C186S (●) *Fn*GR variants were conducted in both reaction directions, with (A) D-Glu and (B) L-Glu concentrations ranged from 5–20 mM and with a final enzyme concentration of 0.10 mg/mL (3.12 μM). The error bars correspond to the standard deviations of each triplicate assay.

Table 4.2 Catalytic efficiencies of WT, C76S, and C186S *Fn*GR with D-Glu at pH 8.0, 8.5, and 9.0.

	k_{cat}/K_m (mM^{-1}s^{-1})		
*Fn*GR variant	**pH 8.0**	**pH 8.5**	**pH 9.0**
WT	11.419 ± 0.793	-	-
C76S	0.0271 ± 0.0011	0.0467 ± 0.0018	0.0549 ± 0.0026
C186S	0.0636 ± 0.0015	0.0570 ± 0.0034	0.0507 ± 0.0015

Table 4.3 Catalytic efficiencies of WT, C76S, and C186S *Fn*GR with L-Glu at pH 8.0, 8.5, and 9.0.

	k_{cat}/K_m (mM^{-1}s^{-1})		
*Fn*GR variant	**pH 8.0**	**pH 8.5**	**pH 9.0**
WT	10.917 ± 0.544	-	-
C76S	0.0261 ± 0.0016	0.0242 ± 0.0014	0.0247 ± 0.0020
C186S	0.0274 ± 0.0013	0.0293 ± 0.0014	0.0332 ± 0.0018

Table 4.4 K_{eq} values for WT, C76S, and C186S *Fn*GR at pH 8.0, 8.5, and 9.0. K_{eq} values were calculated in accord with the Haldane relation: $K_{eq} = (k_{cat}/K_m)^{L\rightarrow D}/(k_{cat}/K_m)^{D\rightarrow L}$.

	K_{eq}		
*Fn*GR variant	**pH 8.0**	**pH 8.5**	**pH 9.0**
WT	0.956 ± 0.082	-	-
C76S	0.963 ± 0.071	0.517 ± 0.036	0.450 ± 0.042
C186S	0.432 ± 0.023	0.513 ± 0.039	0.655 ± 0.096

Despite significant losses of activity for both the C76S and C186S *Fn*GR variants, relative to the WT enzyme at pH 8.0, the residual catalytic activity indicates that the Ser residues can act as acid/base catalysts for the racemization of L- and D-Glu despite the pK_a of Ser (~16) being ~6 units greater than that of Cys (~10). Interestingly at pH 8.0 the values of k_{cat}/K_m were approximately equal in both reaction directions for the C76S *Fn*GR variant (K_{eq} = 0.963 ± 0.071) in agreement with the expected equilibrium constant for a racemization reaction; however, the values differed for C186S (K_{eq} = 0.432 ± 0.023). In the L→D reaction direction, Ser 186 of C186S *Fn*GR must act as a Brønsted base while in the D→L reaction direction, Ser 186 acts as a general acid catalyst. Given that the pK_a of the Ser hydroxyl is greater than that of the Cys thiol by ~6 units and thus predominately exists in its protonated, hydroxyl form, the higher catalytic efficiency in the D→L direction could be explained by the fact that Cys 76 of C186S *Fn*GR, which is the better nucleophile, acts as the Brønsted base in this reaction direction and that Ser 186 acts as the general acid. However, it is surprising that this phenomenon was not observed for the C76S variant at pH 8.0, wherein the K_{eq} value was approximately unity, similarly to the WT enzyme.

In the D→L reaction direction, the catalytic efficiency of C76S *Fn*GR increased by ~2-fold from pH 8.0 to 9.0, but decreased slightly for C186S *Fn*GR over this pH range,

thereby following a trend similar to the pH-rate profile in the D→L reaction direction observed by Glaves and Tanner (1999) with *Lf*GR. Ser 76 of C76S *Fn*GR acts as the Brønsted base in the D→L reaction direction, but is largely protonated due to its high pK_a value. Hence, with increasing pH values from 8.0 to 9.0, more alkoxide becomes available to deprotonate D-Glu and the catalytic efficiency increased over this range. Also, as expected, a minimal change in the catalytic efficiency of the C186S *Fn*GR was observed over this pH range despite a slight decrease in efficiency from pH 8.0 to 9.0, which was also observed for C184S *Lf*GR (Glavas & Tanner, 1999). Since Ser 186 of C186S *Fn*GR acts as the general acid catalyst in the D→L reaction direction and the hydroxyl is largely protonated over this pH range, there is little change in the variant's catalytic efficiency. Therefore, in the D→L reaction direction, the catalytic efficiencies of the C76S variant of *Fn*GR and the C73S variant of *Lf*GR (Glavas & Tanner, 1999) are both pH-dependent.

Although a pH study of the serine variants of *Lf*GR in the L→D reaction direction was not explored since the coupled assay did not operate in this reaction direction, Glaves and Tanner (1999) postulated that the opposite trend would be observed in the L→D reaction direction, wherein the catalytic efficiencies of the C184S variant would increase with increasing pH values and that the C73S *Lf*GR would show little pH-dependence. If this were true, then C184S *Lf*GR would exhibit greater catalytic efficiency for L-Glu over D-Glu as the pH was increased (Glavas & Tanner, 1999). While there was a slight increase in the catalytic efficiency of the C186S *Fn*GR variant in the L→D reaction direction from pH 8.0 to 9.0, overall, the catalytic efficiency of C186S *Fn*GR did not exhibit much variation with pH in contrast to C76S *Fn*GR in the D→L reaction direction.

With the two catalytic Cys residues of GRs being located at opposite sides of the active site, these differences in the efficiencies for catalysis in the L→D versus D→L reaction directions could be explained by different effects of the microenvironment near the catalytic Cys/Ser residues. Neighbouring residues, such as those of a catalytic dyad if present, could reduce the pK_a of the catalytic Cys residues in WT *Fn*GR to yield approximately equal catalytic efficiencies in both reaction directions; however, since the pK_a of Ser is ~6 units higher, perturbing the pK_a downwards may become more difficult in the variants. For example, in *Lf*GR, Asp 10 and His 186 were suggested to assist Cys 73 and Cys 184, respectively, in their roles as acid/base catalysis (Glaves & Tanner, 2001). Therefore, subtle differences in the neighbouring residues of the Ser residues acting as the Brønsted base (Ser 76 for D-Glu and Ser 186 for L-Glu) could explain why Ser 76 of C76S *Fn*GR exhibits pH-dependence of the k_{cat}/K_m but Ser 186 of C186S *Fn*GR does not. For example, if the pK_a of Ser 76 is lowered to ~7 at pH 9.0 but the pK_a of Ser 186 is only lowered to ~12, the increased abundance of Ser 76 alkoxide will facilitate the deprotonation of D-Glu with an increased catalytic efficiency, but, since much of the Ser 186 remains in hydroxyl form, the catalytic efficiency would consequently be less affected at higher pH values.

4.4 CONCLUSIONS AND FUTURE WORK

The C76S and C186S variants of GR from the oral pathogen *F. nucleatum* were assessed to determine whether, like the C73S and C184S *Lf*GR variants, residual activity would be observed (Glavas & Tanner, 1999). In agreement with findings by Glaves and Tanner (1999), the thiol to hydroxyl substituted variants for *Fn*GR were significantly less

active, yet retained some level of activity at pH 8.0 (decreased ~180- to ~420-fold from that of the wild-type enzyme, depending on the variant and reaction direction). The C76S *Fn*GR variant exhibited greater catalytic efficiency turning over D-Glu relative to L-Glu as the pH was increased, thus exhibiting evidence of a preferred 'unidirectional' behavior at higher pH values; however, this trend was not observed for C186S *Fn*GR in the L→D reaction direction.

Previous work in the Bearne lab found that, unlike *Fn*GR and *Lf*GR, for GR from *Bacillus subtilis* (*Bs*GR) is not pseudosymmetric since the catalytic parameters, K_m and k_{cat}, (L-Glu: $K_m = 14 \pm 2$ mM, $k_{cat} = 63 \pm 4$ s^{-1}; D-Glu: $K_m = 1.7 \pm 0.4$ mM, $k_{cat} = 8.3 \pm 0.5$ min^{-1}), were quite different in both reaction directions, but had similar k_{cat}/K_m values (L-Glu: $k_{cat}/K_m = 4.6 \pm 0.6$ $s^{-1}mM^{-1}$; D-Glu: $k_{cat}/K_m = 5 \pm 1$ $s^{-1}mM^{-1}$) (Potrykus *et al*., 2009). It would be interesting to examine whether substitutions of the catalytic Cys residues to Ser residues of *Bs*GR would yield a preferred 'unidirectional' behavior at higher pH values for both variants, or, like *Fn*GR, 'unidirectional' behavior would only be observed for the C74S *Bs*GR variant (analogous to C76S for *Fn*GR).

CHAPTER 5 CONCLUSIONS AND FUTURE WORK

This thesis focused on three major topics: (i) investigations of protein architectures using an activity-based probe (Chapter 2), (ii) evaluation of the 3-HP-dependent inactivation of FucD and the effects of Tris buffer (Chapter 3), and (iii) the possibility of engineering preferential 'unidirectional' activity of glutamate racemase from *Fusobacterium nucleatum* (Chapter 4).

Investigations of active-site architectures using an activity-based probe

ABPP is becoming an increasingly employed strategy in the field of proteomics due to its large diversity of applications and ability to profile proteins in highly complex proteomes. Using this strategy, I synthesized SMHP, a small-molecule probe, designed to target protein architectures with a nucleophile adjacent to a cationic binding site. Given the structural similarity between the anionic monomethyl acyl phosphate warhead of SMHP and MAP, and the fact that MAP was previously shown to target this type of protein architecture via the irreversible inactivation of 3-HBDH (Kluger & Tsui, 1980, 1986) and modification of Hb, (Ueno *et al*., 1986, 1989; Xu *et al*., 1999), I anticipated that SMHP would modify enzymes with this architecture.

SMHP modified 281 enzymes from the *P. lemognei* proteome of 3805 proteins, including 3-HBDH and CTPS. I used a combined experimental approach of fluorescent tagging, LC-MS/MS, and inactivation-based kinetics to investigate the specific sites that were modified by SMHP and MAP. As determined through fluorescent tagging, MAP provided protection against SMHP labelling, indicating that SMHP and MAP targeted similar site(s) within Hb, 3-HBDH, and CTPS. As identified by LC-MS/MS, SMHP and

MAP modified the same three catalytic residues within the conserved active site of 3-HBDH: Ser 146, Lys 156, and Lys 163; thus, demonstrating the targeted reactivity of the acyl phosphate warheads with 3-HBDH. For CTPS, 8 Lys residues were modified by SMHP, with Lys 223 and Lys 239 located at the CTP and ATP/ADP ligand binding sites, respectively. The efficiency of reactivity of the acyl phosphates was explored using kinetics, where both MAP and SMHP inactivated 3-HBDH and CTPS. Lastly, protection against modification of CTPS by the acyl phosphates was explored using fluorescence-based and kinetics-based protection studies, wherein the ligands, ATP, UTP, CTP, and L-Glu, protected against the labelling by SMHP and inactivation by MAP, respectively.

In the future, since the conditions for the MAP-dependent inactivation of both 3-HBDH and CTPS have been developed, it would be interesting to use these kinetically-controlled conditions to further assess the modification sites in greater detail. By monitoring the inactivation of CTPS and 3-HBDH by MAP and/or SMHP using kinetics, followed by LC-MS/MS after a specified period of time (i.e., percent inactivation), we could determine the primary nucleophile responsible for the inactivation of each enzyme. In addition, since kinetics-based studies for the protection of 3-HBDH against inactivation by MAP have been explored with the competitive inhibitor, methyl acetonylphosphonate, in addition to coenzymes NAD^+ and NADH, and also with ADP, it would be valuable to employ such protection studies to assess the protection against the modification of 3-HBDH by SMHP using these same ligands. Furthermore, it would be beneficial to assess the modification site(s) of a third enzyme identified from the *P. lemognei* proteome in its purified form, such as a kinase, wherein various kinases were identified among the most frequent subclass (EC 2.7) modified by SMHP. Lastly, since

SMHP exhibited broad-spectrum reactivity with proteins from the *P. lemognei* proteome, our ABPP approach could be extended to other cell types to identify additional enzymes that are modified by SMHP.

Evaluating the inactivation of L-fuconate dehydratase by 3-hydroxypyruvate and the effects of Tris buffer

Members of the MR subgroup are structurally similar yet mechanistically diverse in the reactions they catalyze (Akiva *et al*., 2014; Gerlt *et al*., 2005, 2012). The inactivation of MR by 3-HP was previously shown to occur through a Schiff-base mechanism with Lys 166, yielding a k_{inact}/K_I value of 83 ± 8 $M^{-1}s^{-1}$ (Nagar *et al*., 2015). Since members of the MR subgroup share conserved active-site residues, we investigated whether 3-HP could also inactivate FucD. Time-dependent inactivation studies of FucD by 3-HP revealed that the efficiency of inactivation was much lower than that reported for MR, and that Tris protected FucD from 3-HP-dependent inactivation. The k_{inact}^{app} and K_I^{app} values decreased with respect to increasing Tris concentrations from 5 to 50 mM, but the $k_{inact}^{app}/K_I^{app}$ remained unchanged over this range of Tris concentrations (~0.018 ± 0.002 $M^{-1}s^{-1}$).

The substrate L-fuconate did not afford protection against the 3-HP-dependent inactivation of FucD. Hence, unlike with MR, inactivation does not appear occur at the active site. While FucD inactivated by 3-HP in both 5 mM and 50 mM Tris-Cl buffers showed the presence 58- and 86-Da adducts, the 50 mM Tris-Cl sample showed the presence of a greater abundance of adducts, many of which could not be identified. Overall, it is evident that, despite the conserved active-site residues between the MR subgroup members, 3-HP likely inactivates FucD through a different mechanism than

that previously determined for MR. In addition, while Tris remains one of the most commonly used biochemical buffers to date, it has been well-reported to chelate divalent metal ions, form Schiff-base adducts with carbonyl compounds, and to inhibit various enzymes, predominantly via competitive inhibition. In this work, I identified a much less commonly reported phenomenon where Tris acts to protect the enzyme against inactivation.

In future work, since GLH is not formed non-enzymatically in the presence of Mg^{2+} under the assay conditions, it remains to determine whether GLH is formed in the presence of FucD. While ^{1}H NMR spectroscopy could be used to detect GLH generated enzymatically, the experiment may not be conclusive if the enzyme rapidly traps the GLH as it is formed and is inactivated.

Can the bidirectional activity of glutamate racemase be re-engineered to become 'unidirectional'?

Glutamate racemase catalyzes the interconversion of L-Glu and D-Glu using two Cys residues as acid/base catalysts, where D-Glu is essential for the biosynthesis of peptidoglycan found in bacterial cell walls (Fisher, 2008; Lundqvist *et al*., 2007; Van Heijenoort, 2001). The C76S and C186S variants of GR from oral pathogen *F. nucleatum* were assessed to determine whether, like the C73S and C184S *Lf*GR variants, residual activity would be observed (Glavas & Tanner, 1999). In agreement with findings by Glaves and Tanner (1999), the thiol to hydroxyl substituted variants for *Fn*GR were significantly less active, but still retained some level of activity at pH 8.0 (decreased ~180 - ~420-fold from the wild-type depending on the variant and reaction direction). Despite the significant loss of activity relative to the wild-type enzyme, the residual

activity observed for the variants demonstrated that the Ser residues can act as acid/base catalysts for the racemization of L- and D-Glu despite the pK_a of Ser (~16) being ~6 units greater than that of Cys (~10). The C76S *Fn*GR variant exhibited greater catalytic efficiency turning over D-Glu relative to L-Glu as the pH was increased, thus exhibiting evidence of a preferred 'unidirectional' behavior at higher pH values; however, this trend was not observed for C186S *Fn*GR in the L→D reaction direction. In future work, it would be interesting to examine the pH-dependencies of the catalytic efficiencies for the Cys→Ser variants of GR from *Bacillus subtilis* (*Bs*GR). Unlike *Lf*GR and *Fn*GR, *Bs*GR is not pseudosymmetric and hence it is of interest to know if a preferred 'unidirectional' behavior at higher pH values for both variants would be observed and how it might differ from the results obtained for the pseudosymmetic enzymes.

REFERENCES

Adibekian, A., Martin, B. R., Chang, J. W., Hsu, K.-L., Tsuboi, K., Bachovchin, D. A., Speers, A. E., Brown, S. J., Spicer, T., Fernandez-Vega, V., Ferguson, J., Hodder, P. S., Rosen, H., & Cravatt, B. F. (2012). Confirming target engagement for reversible inhibitors *in vivo* by kinetically tuned activity-based probes. *Journal of the American Chemical Society*, *134*, 31. https://doi.org/10.1021/ja303400u

Akiva, E., Brown, S., Almonacid, D. E., Barber, A. E., Custer, A. F., Hicks, M. A., Huang, C. C., Lauck, F., Mashiyama, S. T., Meng, E. C., Mischel, D., Morris, J. H., Ojha, S., Schnoes, A. M., Stryke, D., Yunes, J. M., Ferrin, T. E., Holliday, G. L., & Babbitt, P. C. (2014). The structure-function linkage database. *Nucleic Acids Research*, *42*(D1), D521–D530. https://doi.org/10.1093/nar/gkt1130

Amsler, P. E., & Sigel, H. (1976). Comparison of the metal-ion-promoted dephosphorylation of the 5'-triphosphates of adenosine, inosine, guanosine and cytidine by Mn^{2+}, Ni^{2+} and Zn^{2+} in binary and ternary complexes. *European Journal of Biochemistry*, *63*(2), 569–581. https://doi.org/10.1111/J.1432-1033.1976.TB10261.X

Amyes, T. L., & Richard, J. P. (2007). Enzymatic catalysis of proton transfer at carbon: Activation of triosephosphate isomerase by phosphite dianion. *Biochemistry*, *46*(19), 5841–5854. https://doi.org/https://doi.org/10.1021/bi700409b

Aneja, P., Dziak, R., Cai, G. Q., & Charles, T. C. (2002). Identification of an acetoacetyl coenzyme A synthetase-dependent pathway for utilization of L-(+)-3-hydroxybutyrate in *Sinorhizobium meliloti*. *Journal of Bacteriology*, *184*(6), 1571–1577. https://doi.org/10.1128/JB.184.6.1571-1577.2002

Babbitt, P. C., Hasson, M. S., Wedekind, J. E., Palmer, D. R. J., Barrett, W. C., Reed, G. H., Rayment, I., Ringe, D., Kenyon, G. L., & Gerlt, J. A. (1996). The enolase superfamily: A general strategy for enzyme-catalyzed abstraction of the α-Protons of Carboxylic Acids. *Biochemistry*, *35*, 16489–16501. https://doi.org/10.1021/bi9616413

Babbitt, P. C., Mrachko, G. T., Hasson, M. S., Huisman, G. W., Kolter, R., Ringe, D., Petsko, G. A., Kenyon, G. L., & Gerlt, J. A. (1995). A functionally diverse enzyme superfamily that abstracts the alpha protons of carboxylic acids. *Science* , *267*(5201), 1159–1161. https://doi.org/10.1126/SCIENCE.7855594

Babel, L., Bonnet-Gómez, S., & Fromm, K. (2020). Appropriate buffers for studying the bioinorganic chemistry of silver(I). *Chemistry*, *2*(1), 193–202. https://doi.org/10.3390/chemistry2010012

Bairoch, A. (2000). The ENZYME database in 2000. *Nucleic Acids Research*, *28*(1), 304–305. https://doi.org/10.1093/NAR/28.1.304

Bearne, S. L., Hekmat, O., & MacDonnell, J. E. (2001). Inhibition of *Escherichia coli* CTP synthase by glutamate γ-semialdehyde and the role of the allosteric effector GTP in glutamine hydrolysis. *Biochemical Journal*, *356*(Pt 1), 232. https://doi.org/10.1042/0264-6021:3560223

Bearne, S. L., & St. Maurice, M. (2017). A Paradigm for C-H Bond Cleavage: Structural and functional aspects of transition state stabilization by mandelate racemase. In *Advances in protein chemistry and structural biology* (Vol. 109, pp. 113–160). Academic Press Inc. https://doi.org/10.1016/BS.APCSB.2017.04.007

Benach, J., Atrian, S., Gonzàlez-Duarte, R., & Ladenstein, R. (1999). The catalytic reaction and inhibition mechanism of *Drosophila* alcohol dehydrogenase: observation of an enzyme-bound NAD-ketone adduct at 1.4 Å resolution by X-ray crystallography. *Journal of Molecular Biology*, *289*(2), 335–355. https://doi.org/10.1006/JMBI.1999.2765

Bridges, K. R., Schmidt, G. J., Jensen, M., Cerami, A., & Bunn, H. F. (1975). The acetylation of hemoglobin by aspirin: *in vitro* and *in vivo*. *Journal of Clinical Investigation*, *56*(1), 201–207. https://doi.org/10.1172/JCI108068

Cahill, G. F. (2006). Fuel metabolism in starvation. *Annual Review of Nutrition*, *26*, 1–22. https://doi.org/10.1146/ANNUREV.NUTR.26.061505.111258

Carunchio, V., Girelli, A. M., & Messina, A. (1999). Buffer effect on the kinetics of ornithine carbamyl transferase by hplc. *Biomedical Chromatography*, *13*(1), 65–69. https://doi.org/10.1002/(SICI)1099-0801(199902)13:1<65::AID-BMC813>3.0.CO;2-J

Clark, J. M., & Switzer, R. L. (1977). *Experimental Biochemistry* (2nd ed.). W.H. Freeman and Company.

Cohen, A. (2022). *Biological Mass Spectrometry Core Facility - Dalhousie University*. Retrieved July 14, 2022, from https://medicine.dal.ca/research/biological-mass-spectrometry.html

Cravatt, B. F., Wright, A. T., & Kozarich, J. W. (2008). Activity-based protein profiling: From enzyme chemistry to proteomic chemistry. *Annual Review of Biochemistry*, *77*, 383–414. https://doi.org/10.1146/annurev.biochem.75.101304.124125

Crow, V. L., & Pritchard, G. G. (1976). Purification and properties of pyruvate kinase from *Streptococcus lactis*. *Biochimica et Biophysica Acta*, *438*(1), 90–101. https://doi.org/10.1016/0005-2744(76)90225-4

Custer, E. M., Myers, J. L., Poffenbarger, P. L., & Schoen, I. (1983). The storage stability of 3-hydroxybutyrate in serum, plasma, and whole blood. *American Journal of Clinical Pathology*, *80*(3), 375–380. https://doi.org/10.1093/ajcp/80.3.375

De Clercq, E. (2009). Another ten stories in antiviral drug discovery (part C): "Old" and "new" antivirals, strategies, and perspectives. *Medicinal Research Reviews*, *29*(4), 611–645. https://doi.org/10.1002/MED.20153

De Clercq, E., Murase, J., & Marquez, V. E. (1991). Broad-spectrum antiviral and cytocidal activity of cyclopentenylcytosine, a carbocyclic nucleoside targeted at CTP synthetase. *Biochemical Pharmacology*, *41*(12), 1821–1829. https://doi.org/10.1016/0006-2952(91)90120-T

Delafield, F. P., Cooksey, K. E., & Doudoroff, M. (1965). β-Hydroxybutyric dehydrogenase and dimer hydrolase of *Pseudomonas lemoignei*. *Journal of Biological Chemistry*, *240*(10), 4023–4028. https://doi.org/10.1016/S0021-9258(18)97145-0

Deng, H., Lei, Q., Wu, Y., He, Y., & Li, W. (2020). Activity-based protein profiling: Recent advances in medicinal chemistry. *European Journal of Medicinal Chemistry*, *191*, 112151. https://doi.org/10.1016/j.ejmech.2020.112151

Desmarais, W. T., Bienvenue, D. L., Bzymek, K. P., Holz, R. C., Petsko, G. A., & Ringe, D. (2002). The 1.20 Å resolution crystal structure of the aminopeptidase from A*eromonas proteolytica* complexed with Tris: A tale of buffer inhibition. *Structure*, *10*(8), 1063–1072. https://doi.org/10.1016/S0969-2126(02)00810-9

Dhariwal, K. R., & Venkitasubramanian, T. A. (1978). Purification and properties of 3-hydroxybutyrate dehydrogenase from *Mycobacterium phlei* ATCC354. *Journal of General Microbiology*, *104*, 123–126.

Di Sabato, G., & Jencks, W. P. (1961a). Mechanism and catalysis of reactions of acyl phosphates. II. Hydrolysis. *J. Am. Chem. Soc.*, *83*(2), 4400–4405. https://doi.org/10.1021/ja01482a024

Di Sabato, G., & Jencks, W. P. (1961b). Nucleophilic reactions of acyl phosphates mechanism and catalysis of reactions of acyl phosphates. I. Nucleophilic reactions. *J. Am. Chem. Soc*, *83*(2), 4393–4400. https://doi.org/10.1021/ja01482a024

Emami, K., Wu, L. J., & Errington, J. (2020). A small molecule inhibitor of CTP synthetase identified by differential activity on a *Bacillus subtilis* mutant deficient in class A penicillin-binding proteins. *Frontiers in Microbiology*, *11*, 1–12. https://doi.org/10.3389/FMICB.2020.02001

Endrizzi, J. A., Kim, H., Anderson, P. M., & Baldwin, E. P. (2004). Crystal structure of *Escherichia coli* cytidine triphosphate synthetase, a nucleotide-regulated glutamine amidotransferase/ATP-dependent amidoligase fusion protein and homologue of anticancer and antiparasitic drug targets. *Biochemistry*, *43*(21), 6447–6463. https://doi.org/10.1021/BI0496945

Endrizzi, J. A., Kim, H., Anderson, P. M., & Baldwin, E. P. (2005). Mechanisms of product feedback regulation and drug resistance in cytidine triphosphate synthetases from the structure of a CTP-inhibited complex. *Biochemistry*, *44*(41), 13491–13499. https://doi.org/10.1021/bi051282o

Fetter, C. M. (2019). *Exploring Catalysis in the Mandelate Racemase Subgroup of the Enolase Superfamily: Subtle Differences in the Catalytic Machinery* (Issue August). Dalhousie University.

Filling, C., Berndt, K. D., Benach, J., Knapp, S., Prozorovski, T., Nordling, E., Ladenstein, R., Jörnvall, H., & Oppermann, U. (2002). Critical residues for structure and catalysis in short-chain dehydrogenases/reductases. *The Journal of Biological Chemistry*, *277*(28), 25677–25684. https://doi.org/10.1074/JBC.M202160200

Fischer, B. E., Häring, U. K., Tribolet, R., & Sigel, H. (1979). Metal ion/buffer interactions. *European Journal of Biochemistry*, *94*(2), 523–530. https://doi.org/10.1111/J.1432-1033.1979.TB12921.X

Fisher, S. L. (2008). Glutamate racemase as a target for drug discovery. *Microbial Biotechnology*, *1*(5), 360. https://doi.org/10.1111/J.1751-7915.2008.00031.X

Galmozzi, A., Dominguez, E., Cravatt, B. F., & Saez, E. (2014). Application of activity-based protein profiling to study enzyme function in adipocytes. *Methods in Enzymology*, *538*, 151–169. https://doi.org/10.1016/B978-0-12-800280-3.00009-8

Gasteiger, E., Gattiker, A., Hoogland, C., Ivanyi, I., Appel, R. D., & Bairoch, A. (2003). ExPASy: The proteomics server for in-depth protein knowledge and analysis. *Nucleic Acids Research*, *31*(13), 3784–3788. https://doi.org/10.1093/NAR/GKG563

Gerlt, J. A., & Babbitt, P. C. (2001). Divergent evolution of enzymatic function: mechanistically diverse superfamilies and functionally distinct suprafamilies. *Annual Review of Biochemistry*, *70*, 209–246. https://doi.org/10.1146/annurev.biochem.70.1.209

Gerlt, J. A., Babbitt, P. C., Jacobson, M. P., & Almo, S. C. (2012). Divergent evolution in enolase superfamily: Strategies for assigning functions. *The Journal of Biological Chemistry*, *287*(1), 29–34. https://doi.org/10.1074/JBC.R111.240945

Gerlt, J. A., Babbitt, P. C., & Rayment, I. (2005). Divergent evolution in the enolase superfamily: The interplay of mechanism and specificity. *Archives of Biochemistry and Biophysics*, *433*(1), 59–70. https://doi.org/10.1016/J.ABB.2004.07.034

Gerlt, J. A., & Raushel, F. M. (2003). Evolution of function in $(\beta/\alpha)_8$-barrel enzymes. *Current Opinion in Chemical Biology*, *7*(2), 252–264. https://doi.org/10.1016/S1367-5931(03)00019-X

Ghalanbor, Z., Ghaemi, N., Marashi, S., Amanlou, M., Habibi-Rezaei, M., Khajeh, K., & Ranjbar, B. (2008). Binding of Tris to *Bacillus licheniformis* α-amylase can affect its starch hydrolysis activity. *Protein and Peptide Letters*, *15*(2), 212–214. https://doi.org/10.2174/092986608783489616

Glavas, S., & Tanner, M. E. (1999). Catalytic acid/base residues of glutamate racemase. *Biochemistry*, *38*(13), 4106–4113. https://doi.org/10.1021/bi982663n

Glavas, S., & Tanner, M. E. (2001). Active site residues of glutamate racemase. *Biochemistry*, *40*(21), 6199–6204. https://doi.org/10.1021/bi002703z

Glomb, M. A., & Monnier, V. M. (1995). Mechanism of protein modification by glyoxal and glycolaldehyde, reactive intermediates of the Maillard reaction. *Journal of Biological Chemistry*, *270*(17), 10017–10026. https://doi.org/10.1074/JBC.270.17.10017

Gottlieb, H. E., Kotlyar, V., & Nudelman, A. (1997). NMR chemical shifts of common laboratory solvents as trace impurities. *The Journal of Organic Chemistry*, *62*, 7512–7515. https://doi.org/10.1021/jo971176v

Green, N. M. (1963a). Avidin. 1. The use of [^{14}C] biotin for kinetic studies and for assay. *The Biochemical Journal*, *89*(3), 585–591. https://doi.org/10.1042/BJ0890585

Green, N. M. (1963b). Avidin. 3. The nature of the biotin binding site. *Biochem. J*, *89*, 609. 10.1042/bj0890599

Green, N. M. (1990). [5] Avidin and streptavidin. *Methods in Enzymology*, *184*, 51–67. https://doi.org/10.1016/0076-6879(90)84259-J

Grossmann, G. A., & Terra, W. R. (2001). α-Galactosidases from the larval midgut of *Tenebrio molitor* (Coleoptera) and *Spodoptera frugiperda* (Lepidoptera). *Comparative Biochemistry and Physiology Part B: Biochemistry and Molecular Biology*, *128*(1), 109–122. https://doi.org/https://doi.org/10.1016/S1096-4959(00)00306-7

Hansen, S., Hansen, L. K., & Hough, E. (1993). The crystal structure of Tris-inhibited phospholipase C from *Bacillus cereus* at 1.9 Å resolution. The nature of the metal ion in site 2. *Journal of Molecular Biology*, *231*(3), 870–876. https://doi.org/10.1006/JMBI.1993.1333

Hedrick, J. L., & Sallach, H. J. (1961). The metabolism of hydroxypyruvate. *Journal of Biological Chemistry*, *236*(7), 1867–1871. https://doi.org/10.1016/S0021-9258(18)64096-7

Hendriks, E. F., O'Sullivan, W. J., & Stewart, T. S. (1998). Molecular cloning and characterization of the *Plasmodium falciparum* cytidine triphosphate synthetase gene. *Biochimica et Biophysica Acta*, *1399*(2), 213–218. https://doi.org/10.1016/S0167-4781(98)00108-0

Higgins, M. J., Graves, P. R., & Graves, L. M. (2007). Regulation of human cytidine triphosphate synthetase 1 by glycogen synthase kinase 3. *Journal of Biological Chemistry*, *282*(40), 29493–29503. https://doi.org/10.1074/JBC.M703948200

Hong, V., Steinmetz, N. F., Manchester, M., & Finn, M. G. (2010). Labeling live cells by copper-catalyzed alkyne−azide click chemistry. *Bioconjugate Chemistry*, *21*(10), 1912–1916. https://doi.org/10.1021/BC100272Z

Hoque, M., Shimizu, S., Czarina, E., Juan, M., Sato, Y., Hossain, M. T., Yamamoto, T., Imamura, S., Suzuki, K., Amano, H., Sekiguchi, T., Tsunoda, M., & Takénaka, A. (2009). Structure of D-3-hydroxybutyrate dehydrogenase prepared in the presence of the substrate D-3-hydroxybutyrate and NAD^+. *Acta Crystallographica Section F*, *65*, 331–335. https://doi.org/10.1107/S1744309109008537

Hoque, M., Shimizu, S., Hossain, M. T., Yamamoto, T., Imamura, S., Suzuki, K., Tsunoda, M., Amano, H., Sekiguchi, T., & Takénaka, A. (2008). The structures of *Alcaligenes faecalis* D--3-hydroxybutyrate dehydrogenase before and after NAD^+ and acetate binding suggest a dynamical reaction mechanism as a member of the SDR family. *Acta Crystallographica Section D*, *64*(5), 496–505. https://doi.org/10.1107/S0907444908004009

Ito, K., Nakajima, Y., Ichihara, E., Ogawa, K., Katayama, N., Nakashima, K., & Yoshimoto, T. (2006). D-3-Hydroxybutyrate dehydrogenase from *Pseudomonas fragi*: Molecular cloning of the enzyme gene and crystal structure of the enzyme. *Journal of Molecular Biology*, *355*(4), 722–733. https://doi.org/10.1016/J.JMB.2005.10.072

Iyengar, A., & Bearne, S. L. (2003). Aspartate-107 and leucine-109 facilitate efficient coupling of glutamine hydrolysis to CTP synthesis by *Escherichia coli* CTP synthase. *Biochemical Journal*, *369*(Pt 3), 497–507. https://doi.org/10.1042/BJ20021110

Jessani, N., Young, J. A., Diaz, S. L., Patricelli, M. P., Varki, A., Cravatt, B. F., Jessani, N., Young, J. A., Cravatt, B. F., Diaz, S. L., Varki, A., & Patricelli, M. P. (2005). Class assignment of sequence-unrelated members of enzyme superfamilies by activity-based protein profiling. *Angewandte Chemie, 44*, 2400–2403. https://doi.org/10.1002/anie.200463098

Kanazawa, H., Hoque, M., Tsunoda, M., Suzuki, K., Yamamoto, T., Kawai, G., Kondo, J., & Takénaka, A. (2016). Structural insights into the catalytic reaction trigger and inhibition of D-3-hydroxybutyrate dehydrogenase. *Acta Crystallographica Section F*, *72*, 507–515. https://doi.org/10.1107/S2053230X16007767

Kavanagh, K. L., Jörnvall, H., Persson, B., & Oppermann, U. (2008). The SDR superfamily: functional and structural diversity within a family of metabolic and regulatory enzymes. *Cellular and Molecular Life Sciences : CMLS*, *65*(24), 3895–3906. https://doi.org/10.1007/S00018-008-8588-Y

Kim, T. H., Mehrabi, P., Ren, Z., Sljoka, A., Ing, C., Bezginov, A., Ye, L., Pomès, R., Prosser, R. S., & Pai, E. F. (2017). The role of dimer asymmetry and protomer dynamics in enzyme catalysis. *Science* , *355*(6322), 1–11. https://doi.org/10.1126/SCIENCE.AAG2355

Kimura, A., Takata, M., Fukushi, Y., Mori, H., Matsui, H., & Chiba, S. (1997). A Catalytic amino acid and primary structure of active site in *Aspevgillus niger* α-glucosidase. *Bioscience, Biotechnology, and Biochemistry*, *61*(7), 1091–1098. https://doi.org/10.1271/BBB.61.1091

Klotz, I. M., & Tam, J. W. (1973). Acetylation of sickle cell hemoglobin by aspirin. *Proceedings of the National Academy of Sciences of the United States of America*, *70*(5), 1313–1315. https://doi.org/10.1073/pnas.70.5.1313

Kluger, R., & Bearne, S. L. (1994). Inactivation of D-3-hydroxybutyrate dehydrogenase by fumaroyl bis(methyl phosphate). *Bioorganic and Medicinal Chemistry*, *2*(6), 379–385. https://doi.org/10.1016/0968-0896(94)80004-9

Kluger, R., Grant, A. S., Bearne, S. L., & Trachsel, M. R. (1990). Dicarboxylic acid bis(methyl phosphates): Anionic biomimetic cross-linking reagents. *Journal of Organic Chemistry*, *55*(9), 2864–2868. https://doi.org/10.1021/jo00296a056

Kluger, R., Nakaoka, K., & Tsui, W. C. (1978). Substrate analog studies of the specificity and catalytic mechanism of D-3-hydroxybutyrate dehydrogenase. *Journal of the American Chemical Society*, *100*(23), 7388–7392. https://doi.org/10.1021/JA00491A041

Kluger, R., & Tsui, W. C. (1980). Methyl Acetyl Phosphate. A Small Anionic Acetylating Agent. *Journal of Organic Chemistry*, *45*(13), 2723–2724. https://doi.org/10.1021/jo01301a039

Kluger, R., & Tsui, W. C. (1981). Inhibition of bacterial D-3-hydroxybutyrate dehydrogenase by substrates and substrate analogues. *Canadian Journal of Biochemistry*, *59*(10), 810–815. https://doi.org/10.1139/O81-112

Kluger, R., & Tsui, W. C. (1986). Reaction of the anionic acetylation agent methyl acetyl phosphate with D-3-hydroxybutyrate dehydrogenase. *Biochemistry and Cell Biology*, *64*(5), 434–440. https://doi.org/10.1139/o86-061

Koch, D. D., & Feldbruegge, D. H. (1987). Optimized kinetic method for automated determination of β-hydroxybutyrate. *Clinical Chemistry*, *33*(10), 1761–1766. https://doi.org/10.1093/clinchem/33.10.1761

Kolb, H. C., & Sharpless, K. B. (2003). The growing impact of click chemistry on drug discovery. *Drug Discovery Today*, *8*(24), 1128–1137. https://doi.org/10.1016/S1359-6446(03)02933-7

Kolenbrander, P. E., Andersen, R. N., & Moore, L. V. H. (1990). Intrageneric coaggregation among strains of human oral bacteria: potential role in primary colonization of the tooth surface. *Applied and Environmental Microbiology*, *56*(12), 3894. https://doi.org/10.1128/AEM.56.12.3890-3894.1990

Kolenbrander, P. E., & London, J. (1993). Adhere today, here tomorrow: oral bacterial adherence. *Journal of Bacteriology*, *175*(11), 3252. https://doi.org/10.1128/JB.175.11.3247-3252.1993

Koshland, D. E., & Levitzki, A. (1974). 16. CTP synthetase and related enzymes. In *The Enzymes* (p. vol 10. pp. 539-559). Elsevier Inc. https://doi.org/https://doi.org/10.1016/S1874-6047(08)60148-1

Kozarich, J. W. (2003). Activity-based proteomics: Enzyme chemistry redux. *Current Opinion in Chemical Biology*, *7*(1), 78–83. https://doi.org/10.1016/S1367-5931(02)00013-3

Krishnakumar, A. M., Sliwa, D., Endrizzi, J. A., Boyd, E. S., Ensign, S. A., & Peters, J. W. (2008). Getting a handle on the role of coenzyme M in alkene metabolism. *Microbiology and Molecular Biology Reviews : MMBR*, *72*(3), 456. https://doi.org/10.1128/MMBR.00005-08

Kua, J., Galloway, M. M., Millage, K. D., Avila, J. E., & De Haan, D. O. (2013). Glycolaldehyde monomer and oligomer equilibria in aqueous solution: Comparing computational chemistry and NMR data. *Journal of Physical Chemistry A*, *117*(14), 2997–3008. https://doi.org/https://doi.org/10.1021/jp312202j

Kumar, S., Zhou, B., Liang, F., Wang, W. Q., Huang, Z., & Zhang, Z. Y. (2004). Activity-based probes for protein tyrosine phosphatases. *Proceedings of the National Academy of Sciences of the United States of America*, *101*(21), 7943–7948. https://doi.org/10.1073/pnas.0402323101

Kunzmann, M. H., Staub, I., Böttcher, T., & Sieber, S. A. (2011). Protein reactivity of natural product-derived γ-butyrolactones. *Biochemistry*, *50*(5), 910–916. https://doi.org/10.1021/bi101858g

Kwan, R. C. H., Hon, P. Y. T., Mak, W. C., Law, L. Y., Hu, J., & Renneberg, R. (2006). Biosensor for rapid determination of 3-hydroxybutyrate using bi-enzyme system. *Biosensors & Bioelectronics*, *21*(7), 1101–1106. https://doi.org/10.1016/J.BIOS.2005.04.005

Larner, J., & Gillespie, R. E. (1956). Gastrointestinal digestion of starch. II. Properties of the intestinal carbohydrases. *The Journal of Biological Chemistry*, *223*(2), 709–726. https://doi.org/10.1016/S0021-9258(18)65071-9

Leung, D., Hardouin, C., Boger, D. L., & Cravatt, B. F. (2003). Discovering potent and selective reversible inhibitors of enzymes in complex proteomes. *Nature Biotechnology*, *21*(6), 687–691. https://doi.org/10.1038/NBT826

Levitzki, A., & Koshland, D. E. (1969). Negative cooperativity in regulatory enzymes. *Proceedings of the National Academy of Sciences of the United States of America*, *62*(4), 1121–1128. https://doi.org/10.1073/PNAS.62.4.1121

Levitzki, A., & Koshland, D. E. (1972a). Role of an allosteric effector. Guanosine triphosphate activation in cytosine triphosphate synthetase. *Biochemistry*, *11*(2), 241–246. https://doi.org/10.1021/bi00752a015

Levitzki, A., & Koshland, D. E. (1972b). Ligand-induced dimer-to-tetramer transformation in cytosine triphosphate synthetase. *Biochemistry*, *11*(2), 247–253. https://doi.org/10.1021/bi00752a015

Li, L., & Zhang, Z. (2016). Development and applications of the copper-catalyzed azide-alkyne cycloaddition (CuAAC) as a bioorthogonal reaction. *Molecules*, *21*(10), 1–22. https://doi.org/10.3390/molecules21101393

Liu, Y., Fredrickson, J. K., Sadler, N. C., Nandhikonda, P., Smith, R. D., & Wright, A. T. (2015). Advancing understanding of microbial bioenergy conversion processes by activity-based protein profiling. *Biotechnology for Biofuels*, *8*(1). https://doi.org/10.1186/s13068-015-0343-7

Liu, Y., Patricelli, M. P., & Cravatt, B. F. (1999). Activity-based protein profiling: The serine hydrolases. *Proceedings of the National Academy of Sciences of the United States of America*, *96*(26), 14694–14699. https://doi.org/10.1073/pnas.96.26.14694

Long, C. W., & Pardee, A. B. (1967). Cytidine triphosphate synthetase of *Escherichia coli* B. I. Purification and Kinetics. *The Journal of Biological Chemistry*, *242*(20), 4715–4721. https://doi.org/10.1016/S0021-9258(18)99515-3

Lundqvist, T., Fisher, S. L., Kern, G., Folmer, R. H. A., Xue, Y., Newton, D. T., Keating, T. A., Alm, R. A., & De Jonge, B. L. M. (2007). Exploitation of structural and regulatory diversity in glutamate racemases. *Nature*, *447*(7146), 817–822. https://doi.org/10.1038/NATURE05689

Luxenhofer, R., & Jordan, R. (2006). Click Chemistry with poly(2-oxazoline)s. *Macromolecules*, *39*(10), 3509–3516. https://doi.org/10.1021/MA052515M

Lynch, E. M., DiMattia, M. A., Albanese, S., van Zundert, G. C. P., Hansen, J. M., Quispe, J. D., Kennedy, M. A., Verras, A., Borrelli, K., Toms, A. V., Kaila, N., Kreutter, K. D., McElwee, J. J., & Kollman, J. M. (2021). Structural basis for isoform-specific inhibition of human CTPS1. *Proceedings of the National Academy of Sciences of the United States of America*, *118*(40), e2107968118. https://doi.org/10.1073/PNAS.2107968118

Lynch, E. M., Hicks, D. R., Shepherd, M., Endrizzi, J. A., Maker, A., Hansen, J. M., Barry, R. M., Gitai, Z., Baldwin, E. P., & Kollman, J. M. (2017). Human CTP synthase filament structure reveals the active enzyme conformation. *Nature Structural & Molecular Biology*, *24*(6), 507–514. https://doi.org/10.1038/NSMB.3407

Machado, T. F. G., Purg, M., McMahon, S. A., Read, B. J., Oehler, V., Åqvist, J., Gloster, T. M., & da Silva, R. G. (2020). Dissecting the mechanism of (R)-3-hydroxybutyrate dehydrogenase by kinetic isotope effects, protein crystallography, and computational chemistry. *ACS Catalysis*, *10*(24), 15019–15032. https://doi.org/10.1021/acscatal.0c04736

Madeira, F., Pearce, M., Tivey, A. R. N., Basutkar, P., Lee, J., Edbali, O., Madhusoodanan, N., Kolesnikov, A., & Lopez, R. (2022). Search and sequence analysis tools services from EMBL-EBI in 2022. *Nucleic Acids Research*. https://doi.org/10.1093/NAR/GKAC240

McCluskey, G. D., & Bearne, S. L. (2018). "Pinching" the ammonia tunnel of CTP synthase unveils coordinated catalytic and allosteric-dependent control of ammonia passage. *Biochimica et Biophysica Acta. General Subjects*, *1862*(12), 2714–2727. https://doi.org/10.1016/J.BBAGEN.2018.08.008

McCluskey, G. D., Mohamady, S., Taylor, S. D., & Bearne, S. L. (2016). Exploring the potent inhibition of CTP Synthase by gemcitabine-5′-triphosphate. *ChemBioChem*, *17*(23), 2240–2249. https://doi.org/10.1002/CBIC.201600405

McKenna, S. M., Fay, E. M., & McGouran, J. F. (2021). Flipping the switch: Innovations in inducible probes for protein profiling. *ACS Chemical Biology*, *16*(12), 2719–2730. https://doi.org/10.1021/ACSCHEMBIO.1C00572

Miller, A. W., & Robyt, J. F. (1986). Inhibition of dextransucrase by Zn^{2+}, Ni^{2+}, Co^{2+}, and tris(hydroxymethyl)aminomethane (Tris). *Archives of Biochemistry and Biophysics*, *248*(2), 579–586. https://doi.org/10.1016/0003-9861(86)90511-4

Morales, A. C., Nozawa, S. R., Thedei, G., Maccheroni, W., & Rossi, A. (2000). Properties of a constitutive alkaline phosphatase from strain 74A of the mold *Neurospora crassa*. *Brazilian Journal of Medical and Biological Research*, *33*(8), 905–912.

Mori, G., Chiarelli, L. R., Esposito, M., Makarov, V., Bellinzoni, M., Hartkoorn, R. C., Degiacomi, G., Boldrin, F., Ekins, S., De jesus lopes ribeiro, A. L., Marino, L. B., Centárová, I., Svetlíková, Z., Blaško, J., Kazakova, E., Lepioshkin, A., Barilone, N., Zanoni, G., Porta, A., … Pasca, M. R. (2015). Thiophenecarboxamide derivatives Activated by EthA kill *Mycobacterium tuberculosis* by inhibiting the CTP Synthetase PyrG. *Chemistry & Biology*, *22*(7), 917. https://doi.org/10.1016/J.CHEMBIOL.2015.05.016

Nagar, M., Wyatt, B. N., St. Maurice, M., & Bearne, S. L. (2015). Inactivation of mandelate racemase by 3-hydroxypyruvate reveals a potential mechanistic link between enzyme superfamilies. *Biochemistry*, *54*(17), 2747–2757. https://doi.org/10.1021/acs.biochem.5b00221

Nakashima, K., Ito, K., Nakajima, Y., Yamazawa, R., Miyakawa, S., & Yoshimoto, T. (2009). Closed complex of the D-3-hydroxybutyrate dehydrogenase induced by an enantiomeric competitive inhibitor. *The Journal of Biochemistry*, *145*(4), 467–479. https://doi.org/10.1093/JB/MVN186

Narvaez-Ortiz, H. Y., Lopez, A. J., Gupta, N., & Zimmermann, B. H. (2018). A CTP synthase undergoing stage-specific spatial expression is essential for the survival of the intracellular parasite *Toxoplasma gondii*. *Frontiers in Cellular and Infection Microbiology*, *8*, 83. https://doi.org/10.3389/fcimb.2018.00083

Nasser, B., El Kebbaj, M. S., Cottin, P., & Latruffe, N. (2002). Purification and characterization of the D-β-hydroxybutyrate dehydrogenase from dromedary liver mitochondria. *Comparative Biochemistry and Physiology Part B: Biochemistry and Molecular Biology*, *131*(1), 9–18. https://doi.org/10.1016/S1096-4959(01)00461-4

Neidhart, D. J., Howell, P. L., Petsko, G. A., Powers, V. M., Li, R., Kenyon, G. L., & Gerlt, J. A. (1991). Mechanism of the reaction catalyzed by mandelate racemase. 2. Crystal structure of mandelate racemase at 2.5-Å resolution: Identification of the active site and possible catalytic residues. *Biochemistry*, *30*(38), 9264–9273. https://doi.org/10.1021/bi00102a019

Neidhart, D. J., Kenyon, G. L., Gerlt, J. A., & Petsko, G. A. (1990). Mandelate racemase and muconate lactonizing enzyme are mechanistically distinct and structurally homologous. *Nature* , *347*(6294), 692–694. https://doi.org/10.1038/347692a0

Neumann, H., Kezdy, F., Hsu, J., & Rosenberg, I. H. (1975). The reaction of tris (hydroxymethyl)aminomethane with calf intestinal alkaline phosphatase. *Biochimica et Biophysica Acta*, *391*(2), 292–300. https://doi.org/10.1016/0005-2744(75)90253-3

Newman, J. C., & Verdin, E. (2014). Ketone bodies as signaling metabolites. *Trends in Endocrinology & Metabolism*, *25*(1), 42–52. https://doi.org/10.1016/j.tem.2013.09.002

Niphakis, M. J., & Cravatt, B. F. (2014). Enzyme inhibitor discovery by activity-based protein profiling. *Annual Review of Biochemistry*, *83*, 341–377. https://doi.org/10.1146/annurev-biochem-060713-035708

Nomura, D. K., Dix, M. M., & Cravatt, B. F. (2010). Activity-based protein profiling for biochemical pathway discovery in cancer. *Nature Reviews Cancer*, *10*(9), 630–638. https://doi.org/10.1038/nrc2901

Oppermann, U. C. T., Filling, C., Berndt, K. D., Persson, B., Benach, J., Ladenstein, R., & Jörnvall, H. (1997). Active site directed mutagenesis of 3/17-hydroxysteroid dehydrogenase establishes differential effects on short-chain dehydrogenase/reductase reactions. *Biochemistry*, *36*(1), 34–40. https://doi.org/10.1021/bi961803v

Paithankar, K. S., Feller, C., Kuettner, E. B., Keim, A., Grunow, M., & Sträter, N. (2007). Cosubstrate-induced dynamics of D-3-hydroxybutyrate dehydrogenase from *Pseudomonas putida*. *The FEBS Journal*, *274*(21), 5767–5779. https://doi.org/10.1111/J.1742-4658.2007.06102.X

Patricelli, M. P., Szardenings, A. K., Liyanage, M., Nomanbhoy, T. K., Wu, M., Weissig, H., Aban, A., Chun, D., Tanner, S., & Kozarich, J. W. (2007). Functional interrogation of the kinome using nucleotide acyl phosphates. *Biochemistry*, *46*(2), 350–358. https://doi.org/10.1021/bi062142x

Peng, H., & Hulleman, J. D. (2019). Prospective application of activity-based proteomic profiling in vision research-potential unique insights into ocular protease biology and pathology. *International Journal of Molecular Sciences*, *20*(16), 3855. https://doi.org/10.3390/ijms20163855

Potrykus, J., Flemming, J., & Bearne, S. L. (2009). Kinetic characterization and quaternary structure of glutamate racemase from the periodontal anaerobe *Fusobacterium nucleatum*. *Archives of Biochemistry and Biophysics*, *491*(1–2), 16–24. https://doi.org/10.1016/j.abb.2009.09.009

Presolski, S. I., Hong, V. P., & Finn, M. G. (2011). Copper-catalyzed azide–alkyne click chemistry for bioconjugation. *Current Protocols in Chemical Biology*, *3*(4), 162. https://doi.org/10.1002/9780470559277.CH110148

Rappsilber, J., Mann, M., & Ishihama, Y. (2007). Protocol for micro-purification, enrichment, pre-fractionation and storage of peptides for proteomics using StageTips. *Nature Protocols*, *2*(8), 1896–1906. https://doi.org/10.1038/NPROT.2007.261

Rodionov, V. O., Presolski, S. I., Díaz Díaz, D., Fokin, V. V, & Finn, M. G. (2007). Ligand-accelerated Cu-catalyzed azide-alkyne cycloaddition: A mechanistic report. *Journal of the American Chemical Society*, *129*(42), 12705–12712. https://doi.org/10.1021/ja072679d

Rostovtsev, V. V, Green, L. G., Fokin, V. V, Barry Sharpless, K., A C Coolen, H. K., N M van Leeuwen, P. W., & M Nolte, R. J. (2002). A stepwise Huisgen cycloaddition process: copper(I)-catalyzed regioselective "ligation" of azides and terminal alkynes. *Journal* of the *Chemical Society*, *Chemical Communications*, *41*(14), 2596–2599. https://doi.org/10.1002/1521-3773

Rybak, J. N., Scheurer, S. B., Neri, D., & Elia, G. (2004). Purification of biotinylated proteins on streptavidin resin: A protocol for quantitative elution. *Proteomics*, *4*(8), 2296–2299. https://doi.org/10.1002/pmic.200300780

Saghatelian, A., Jessani, N., Joseph, A., Humphrey, M., & Cravatt, B. F. (2004). Activity-based probes for the proteomic profiling of metalloproteases. *Proceedings of the National Academy of Sciences of the United States of America*, *101*(27), 10000–10005. https://doi.org/10.1073/pnas.0402784101

Sambrook, J., Fritsch, E. F., & Maniatis, T. (1989). *Molecular cloning : a laboratory manual* (2nd ed.). Cold Spring Harbor Laboratory Press.

Scheit, K. H., & Linke, H. J. (1982). Substrate specificity of CTP synthetase from *Escherichia coli*. *European Journal of Biochemistry*, *126*(1), 57–60. https://doi.org/10.1111/j.1432-1033.1982.tb06745.x

Shaw, T. A., Powdrill, M. H., Sherratt, A. R., Garland, K., Li, B. J., Beauchemin, A. M., & Pezacki, J. P. (2021). Reactivity of *N*-acyl hydrazone probes with the mammalian proteome. *RSC Medicinal Chemistry*, *12*(5), 797–803. https://doi.org/10.1039/D1MD00027F

Shevchenko, A., Wilm, M., Vorm, O., & Mann, M. (1996). Mass spectrometric sequencing of proteins from silver-stained polyacrylamide gels. *Analytical Chemistry*, *68*(5), 858. https://doi.org/10.1021/ac950914h

Shimomura, T., Sumiya, T., Ono, M., Ito, T., & Hanaoka, T. A. (2013). A novel, disposable, screen-printed amperometric biosensor for ketone 3-β-hydroxybutyrate fabricated using a 3-β-hydroxybutyrate dehydrogenase-mesoporous silica conjugate. *Analytical and Bioanalytical Chemistry*, *405*(1), 297–305. https://doi.org/10.1007/S00216-012-6494-5

Shindo, N., & Ojida, A. (2021). Recent progress in covalent warheads for *in vivo* targeting of endogenous proteins. *Bioorganic & Medicinal Chemistry*, *47*(1), 116386. https://doi.org/10.1016/J.BMC.2021.116386

Speers, A. E., & Cravatt, B. F. (2004). Profiling enzyme activities *in vivo* using click chemistry methods. *Chemistry and Biology*, *11*(4), 535–546. https://doi.org/10.1016/J.CHEMBIOL.2004.03.012

Speers, A. E., & Cravatt, B. F. (2009). Activity-based protein profiling (ABPP) and click chemistry (CC)–ABPP by MudPIT mass spectrometry. *Current Protocols in Chemical Biology*, *1*(1), 29–41. https://doi.org/10.1002/9780470559277.ch090138

Staubach, S., Tertel, T., Walkenfort, B., Buschmann, D., Pfaffl, M. W., Weber, G., & Giebel, B. (2022). Free flow electrophoresis allows quick and reproducible preparation of extracellular vesicles from conditioned cell culture media. *Extracellular Vesicles and Circulating Nucleic Acids*, *3*(1), 31–48. https://doi.org/10.20517/EVCNA.2021.26

Surarit, R., Matsui, H., Chiba, S., Svasti, J., & Srisomsap, C. (1996). Chemical Modification of β-Glucosidase/ β-Fucosidase from *Dalbergia cochinchinensis* Pierre by Conduritol B Epoxide. *Bioscience, Biotechnology, and Biochemistry*, *60*(8), 1265–1268. https://doi.org/10.1271/BBB.60.1265

Taal, M. A., Sedelnikova, S. E., Ruzheinikov, S. N., Baker, P. J., & Rice, D. W. (2004). Expression, purification and preliminary X-ray analysis of crystals of *Bacillus subtilis* glutamate racemase. *Acta Crystallographica. Section D, Biological Crystallography*, *60*(Pt 11), 2031–2034. https://doi.org/10.1107/S0907444904021134

Tan, A. W. H., Smith, C. M., Aogaichi, T., & Plaut, G. W. E. (1975). Inhibition of D-(-)-3-hydroxybutyrate dehydrogenase by malonate analogues. *Archives of Biochemistry and Biophysics*, *166*(1), 164–173. https://doi.org/10.1016/0003-9861(75)90376-8

Tanner, M. E., Knowles, J. R., & Gallo, K. A. (1993). Isotope effects and the identification of catalytic residues in the reaction catalyzed by glutamate racemase. *Biochemistry*, *32*(15), 3998–4006. https://doi.org/10.1021/BI00066A021

Thorpe, S. R., & Baynes, J. W. (2003). Maillard reaction products in tissue proteins: New products and new perspectives. *Amino Acids*, *25*(3), 275–281. https://doi.org/10.1007/S00726-003-0017-9

Ting, L., Cowley, M. J., Hoon, S. L., Guilhaus, M., Raftery, M. J., & Cavicchioli, R. (2009). Normalization and Statistical Analysis of Quantitative Proteomics Data Generated by Metabolic Labeling. *Molecular & Cellular Proteomics : MCP*, *8*(10), 2227. https://doi.org/10.1074/MCP.M800462-MCP200

Ueno, H., Pospischil, M. A., & Manning, J. M. (1989). Methyl acetyl phosphate as a covalent probe for anion-binding sites in human and bovine hemoglobins. *Journal of Biological Chemistry*, *264*(21), 12344–12351. https://doi.org/10.1016/S0021-9258(18)63864-5

Ueno, H., Pospischil, M. A., Manning, J. M., & Kluger, R. (1986). Site specific modification of hemoglobin by methyl acetyl phosphate. *Archives of Biochemistry and Biophysics*, *244*(2), 795–800.

Van Heijenoort, J. (2001). Recent advances in the formation of the bacterial peptidoglycan monomer unit. *Natural Product Reports*, *18*(5), 503–519. https://doi.org/10.1039/A804532A

Vasseur, M., Frangne, R., Caüzac, M., Mahmood, A., & Alvarado, F. (1990). pH-dependent inhibitory effects of tris and lithium ion on intestinal brush-border sucrase. *Journal of Enzyme Inhibition*, *4*(1), 15–26. https://doi.org/10.3109/14756369009030384

Wang, J., Tan, X. F., Nguyen, V. S., Yang, P., Zhou, J., Gao, M., Li, Z., Lim, T. K., He, Y., Ong, C. S., Lay, Y., Zhang, J., Zhu, G., Lai, S. L., Ghosh, D., Mok, Y. K., Shen, H. M., & Lin, Q. (2014). A Quantitative Chemical Proteomics Approach to Profile the Specific Cellular Targets of Andrographolide, a Promising Anticancer Agent That Suppresses Tumor Metastasis. *Molecular & Cellular Proteomics*, *13*(3), 876–886. https://doi.org/10.1074/MCP.M113.029793

Wang, P. Y., Lin, W. C., Tsai, Y. C., Cheng, M. L., Lin, Y. H., Tseng, S. H., Chakraborty, A., & Pai, L. M. (2015). Regulation of CTP synthase filament formation during DNA endoreplication in *Drosophila*. *Genetics*, *201*(4), 1511–1523. https://doi.org/10.1534/GENETICS.115.180737/-/DC1

Wang, S., Tian, Y., Wang, M., Sun, G., & Sun, X. (2018). Advanced activity-based protein profiling application strategies for drug development. *Frontiers in Pharmacology*, *9*(353), 1–9. https://doi.org/10.3389/fphar.2018.00353

Weerapana, E., Simon, G. M., & Cravatt, B. F. (2008). Disparate proteome reactivity profiles of carbon electrophiles. *Nature Chemical Biology*, *4*(7), 405–407. https://doi.org/10.1038/nchembio.91

Weng, M., Makaroff, C. A., & Zalkin, H. (1986). Nucleotide sequence of *Escherichia coli* pyrG encoding CTP synthetase. *Journal of Biological Chemistry*, *261*(12), 5568–5574. https://doi.org/10.1016/S0021-9258(19)57252-0

Weng, M., & Zalkin, H. (1987). Structural role for a conserved region in the CTP synthetase glutamine amide transfer domain. *Journal of Bacteriology*, *169*(7), 3023–2028. https://doi.org/10.1128/JB.169.7.3023-3028.1987

Wessel, D., & Flügge, U. I. (1984). A method for the quantitative recovery of protein in dilute solution in the presence of detergents and lipids. *Analytical Biochemistry*, *138*(1), 141–143. https://doi.org/10.1016/0003-2697(84)90782-6

Wever, R., Van Ark, G., & Van Gelder, B. F. (1977). Low-spin forms of cytochrome c oxidase. *FEBS Letters*, *84*(2), 388–390. https://doi.org/10.1016/0014-5793(77)80731-X

Willemoës, M. (2004). Competition between ammonia derived from internal glutamine hydrolysis and hydroxylamine present in the solution for incorporation into UTP as catalysed by *Lactococcus lactis* CTP synthase. *Archives of Biochemistry and Biophysics*, *424*(1), 105–111. https://doi.org/10.1016/J.ABB.2004.01.018

Willems, L. I., Overkleeft, H. S., & Van Kasteren, S. I. (2014). Current developments in activity-based protein profiling. *Bioconjugate Chemistry*, *25*(7), 1181–1191. https://doi.org/10.1021/bc500208y

Williams, J. C., Kizaki, H., Weber, G., & Morris, H. P. (1978). Increased CTP synthetase activity in cancer cells. *Nature*, *271*(5640), 71–73. https://doi.org/10.1038/271071A0

Williams, S. J., Hekmat, O., & Withers, S. G. (2006). Synthesis and testing of mechanism-based protein-profiling probes for retaining endoglycosidases. *ChemBioChem*, *7*(1), 116–124. https://doi.org/10.1002/cbic.200500279

Wright, A. T., & Cravatt, B. F. (2007). Chemical proteomic probes for profiling cytochrome P450 activities and drug interactions *in vivo*. *Chemistry and Biology*, *14*(9), 1043–1051. https://doi.org/10.1016/j.chembiol.2007.08.008

Wright, A. T., Song, J. D., & Cravatt, B. F. (2009). A suite of activity-based probes for human cytochrome P450 enzymes. *Journal of the American Chemical Society*, *131*(30), 10692–10700. https://doi.org/10.1021/ja9037609

Xiao, C.-Q., Huang, Q., Zhang, Y., Zhang, H.-Q., & Lai, L. (2020). Binding thermodynamics of divalent metal ions to several biological buffers. *Thermochimica Acta*, *691*, 1–8. https://doi.org/10.1016/j.tca.2020.178721

Xu, A. S. L., Labotka, R. J., & London, R. E. (1999). Acetylation of human hemoglobin by methyl acetylphosphate. Evidence of broad regio-selectivity revealed by NMR studies. *Journal of Biological Chemistry*, *274*(38), 26629–26632. https://doi.org/10.1074/jbc.274.38.26629

Yew, W. S., Fedorov, A. A., Fedorov, E. V., Rakus, J. F., Pierce, R. W., Almo, S. C., & Gerlt, J. A. (2006). Evolution of enzymatic activities in the enolase superfamily: L-fuconate dehydratase from *Xanthomonas campestris*. *Biochemistry*, *45*(49), 14582–14597. https://doi.org/10.1021/bi061687o

Zhou, X., Guo, C. J., Chang, C. C., Zhong, J., Hu, H. H., Lu, G. M., & Liu, J. L. (2021). Structural basis for ligand binding modes of CTP synthase. *Proceedings of the National Academy of Sciences of the United States of America*, *118*(30), 1–11. https://doi.org/10.1073/pnas.2026621118

APPENDIX A

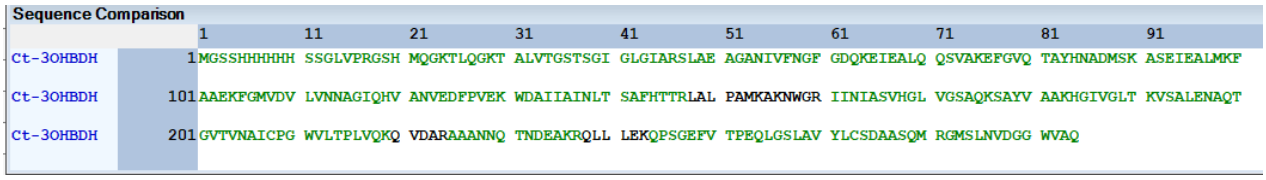

Figure 1A Sequence coverage (91.55%) of untreated 3-HBDH

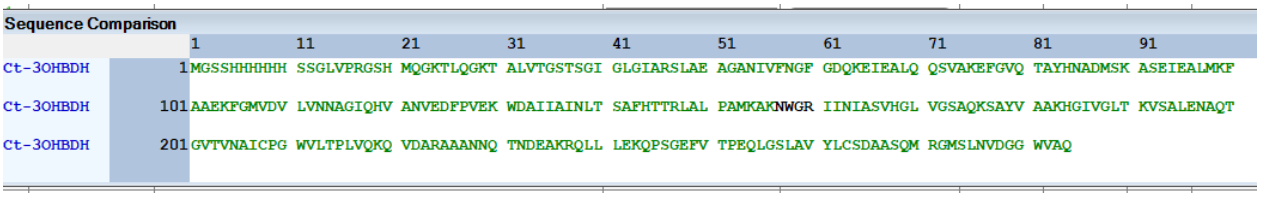

Figure 2A Sequence coverage (98.59%) of SMHP-treated 3-HBDH

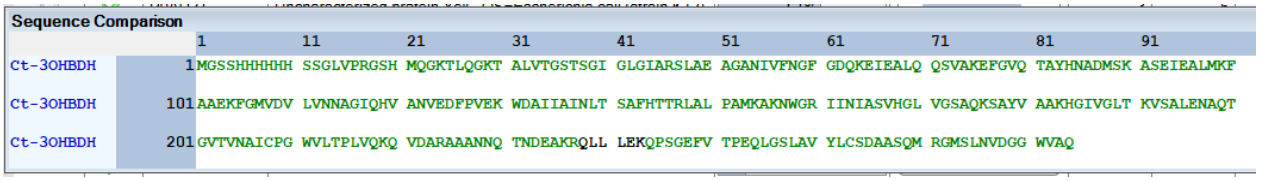

Figure 3A Sequence coverage (97.89%) of MAP-treated 3-HBDH

A

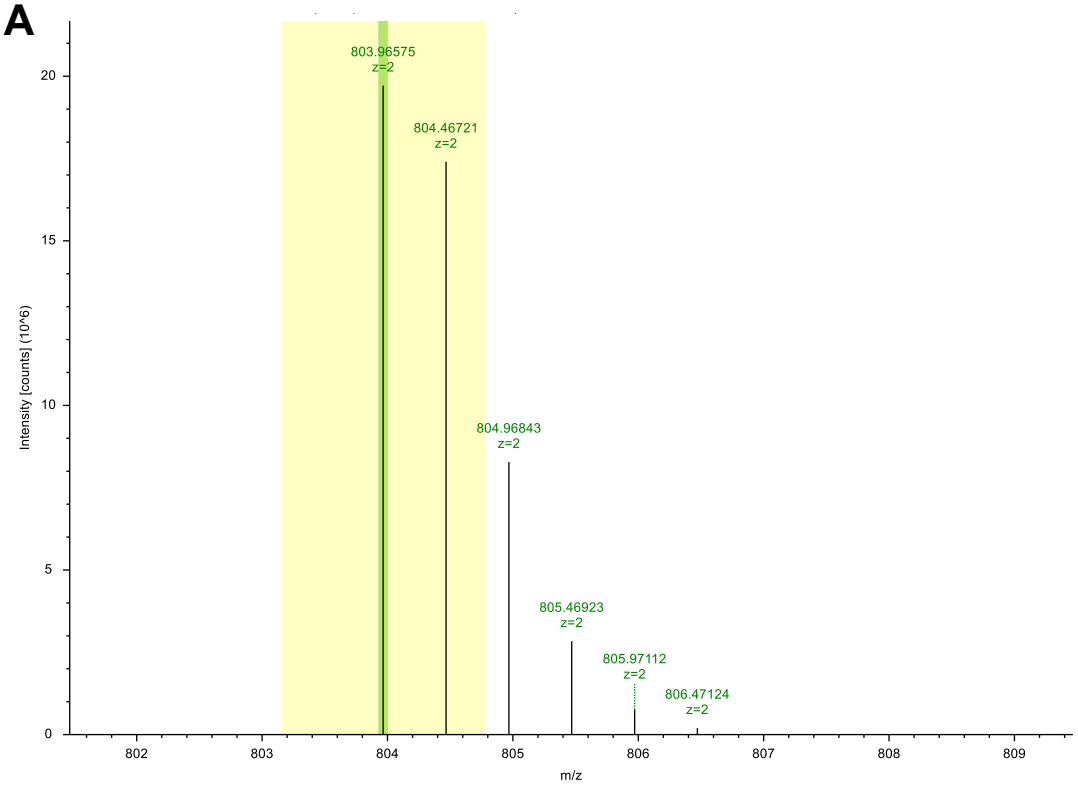

B

Fragment Matches

Value Type: Theo. Mass [Da]

Ion Series | Neutral Losses | Precursor Ions | Internal Fragments

#1	b^+	b^{2+}	Seq.	y^+	y^{2+}	#2
1	114.09134	57.54931	I			16
2	227.17540	114.09134	I	1493.84345	747.42536	15
3	341.21833	171.11280	N	1380.75939	690.88333	14
4	454.30240	227.65484	I	1266.71646	633.86187	13
5	525.33951	263.17339	A	1153.63240	577.31984	12
6	612.37154	306.68941	S	1082.59528	541.80128	11
7	711.43995	356.22361	V	995.56325	498.28527	10
8	848.49886	424.75307	H	896.49484	448.75106	9
9	905.52033	453.26380	G	759.43593	380.22160	8
10	1018.60439	509.80583	L	702.41447	351.71087	7
11	1117.67281	559.34004	V	589.33040	295.16884	6
12	1174.69427	587.85077	G	490.26199	245.63463	5
13	1261.72630	631.36679	S	433.24052	217.12390	4
14	1332.76341	666.88534	A	346.20850	173.60789	3
15	1460.82199	730.91463	Q	275.17138	138.08933	2
16			K	147.11280	74.06004	1

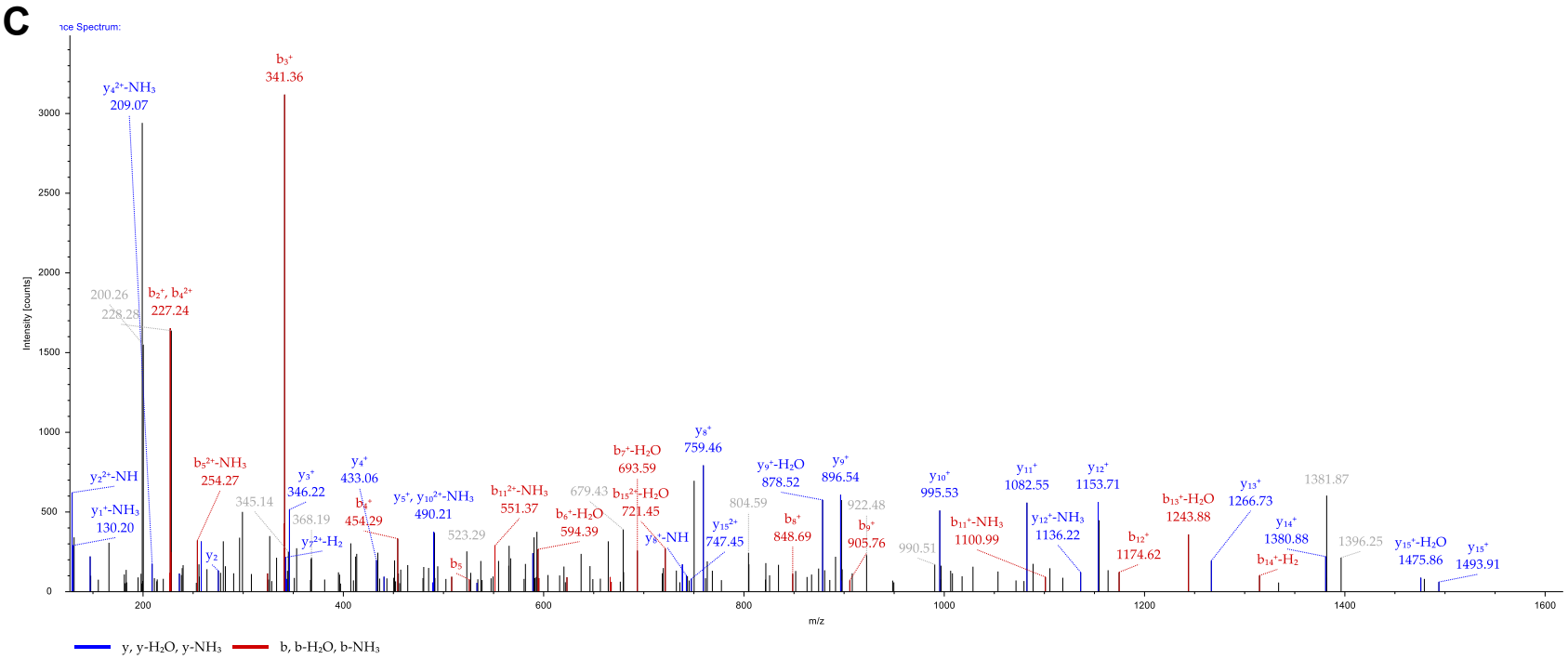

Figure 4A LC-MS/MS analysis showing no adducts with Ser 146 from peptide: IINIASVHGLVGSAQK in untreated 3-HBDH. The precursor isotope pattern spectrum (MS1) (A), and MS/MS spectrum for the doubly charged ion of the II-peptide (*m*/*z* 803.966 Da; MH^+ = 1606.924 Da) reveal no 94-Da (SMHP modification) or 42-Da (MAP modification) adducts with the b_6^+ ion corresponding to Ser 146 (with 0 missed cleavages) (B, C).

A

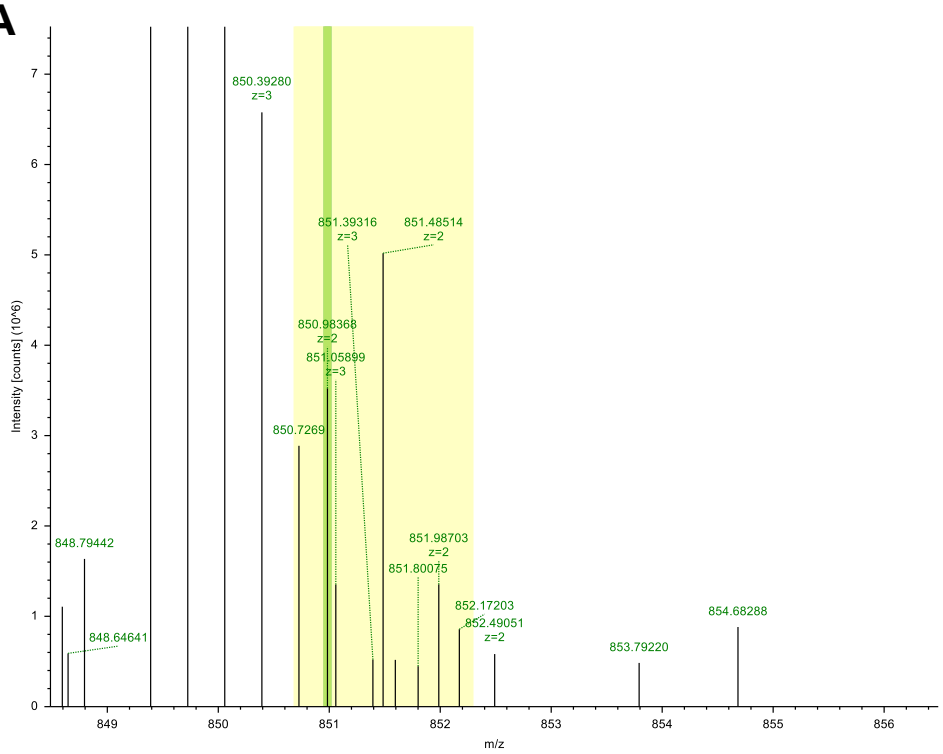

B

Fragment Matches

Value Type: Theo. Mass [Da]

Ion Series | Neutral Losses | Precursor Ions | Internal Fragments

#1	b⁺	b²⁺	Seq.	y⁺	y²⁺	#2
1	114.09134	57.54931	I			16
2	227.17540	114.09134	I	1587.88531	794.44630	15
3	341.21833	171.11280	N	1474.80125	737.90426	14
4	454.30240	227.65484	I	1360.75832	680.88280	13
5	525.33951	263.17339	A	1247.67426	624.34077	12
6	706.41340	353.71034	S-Hex-5-...	1176.63715	588.82221	11
7	805.48181	403.24455	V	995.56325	498.28527	10
8	942.54073	471.77400	H	896.49484	448.75106	9
9	999.56219	500.28473	G	759.43593	380.22160	8
10	1112.64625	556.82677	L	702.41447	351.71087	7
11	1211.71467	606.36097	V	589.33040	295.16884	6
12	1268.73613	634.87170	G	490.26199	245.63463	5
13	1355.76816	678.38772	S	433.24052	217.12390	4
14	1426.80527	713.90628	A	346.20850	173.60789	3
15	1554.86385	777.93556	Q	275.17138	138.08933	2
16			K	147.11280	74.06004	1

C

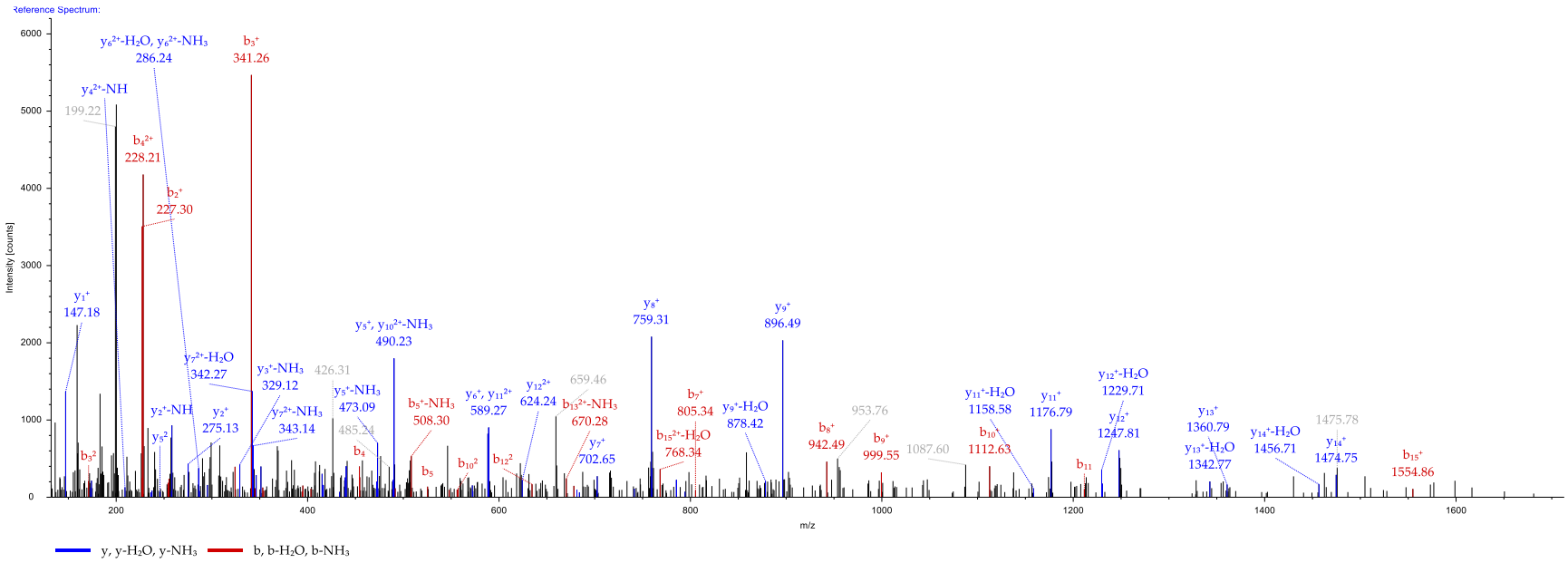

Figure 5A LC-MS/MS analysis showing 94-Da adducts with Ser 146 from peptide: IINIASVHGLVGSAQK in SMHP-treated 3-HBDH. The precursor isotope pattern spectrum (MS1) (A), and MS/MS spectrum for the doubly charged ion of the II-peptide (*m/z* 850.984 Da; MH^+ = 1700.960 Da) reveal an increase in mass of the b_6^+ ion by 94 Da corresponding to Ser 146 (with 0 missed cleavages) (B, C). Identical II-peptides were found in the control and SMHP-treated samples and showed a mass increase of 94 Da between the b_6^+ ions arising from the SMHP-modified (706.413 Da) and unmodified peptide (612.372 Da).

A

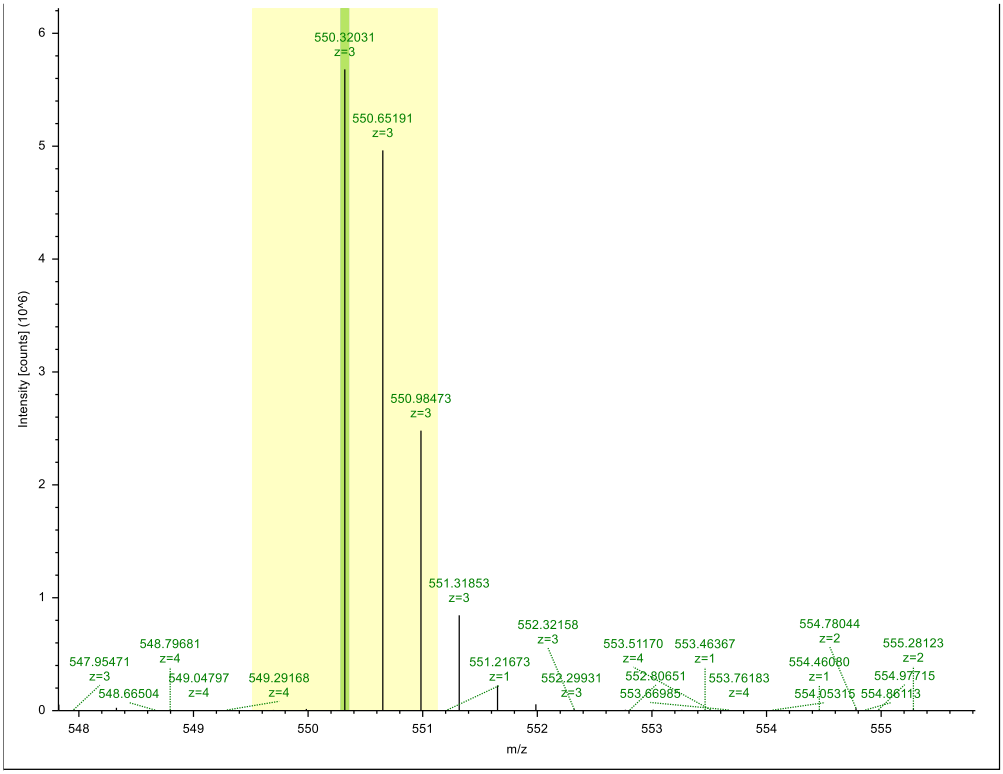

B

Fragment Matches

Value Type: Theo. Mass [Da]

Ion Series | Neutral Losses | Precursor Ions | Internal Fragments

#1	b^{+}	b^{2+}	b^{3+}	Seq.	y^{+}	y^{2+}	y^{3+}	#2
1	114.09134	57.54931	38.70196	I				16
2	227.17540	114.09134	76.39665	I	1535.85402	768.43065	512.62286	15
3	341.21833	171.11280	114.41096	N	1422.76995	711.88861	474.92817	14
4	454.30240	227.65484	152.10565	I	1308.72703	654.86715	436.91386	13
5	525.33951	263.17339	175.78469	A	1195.64296	598.32512	399.21917	12
6	654.38210	327.69469	218.79889	S-Acetyl	1124.60585	562.80656	375.54013	11
7	753.45052	377.22890	251.82169	V	995.56325	498.28527	332.52594	10
8	890.50943	445.75835	297.50799	H	896.49484	448.75106	299.50313	9
9	947.53089	474.26908	316.51515	G	759.43593	380.22160	253.81683	8
10	1060.61496	530.81112	354.20984	L	702.41447	351.71087	234.80967	7
11	1159.68337	580.34532	387.23264	V	589.33040	295.16884	197.11498	6
12	1216.70483	608.85606	406.23980	G	490.26199	245.63463	164.09218	5
13	1303.73686	652.37207	435.25047	S	433.24052	217.12390	145.08503	4
14	1374.77398	687.89063	458.92951	A	346.20850	173.60789	116.07435	3
15	1502.83255	751.91991	501.61570	Q	275.17138	138.08933	92.39531	2
16				K	147.11280	74.06004	49.70912	1

C

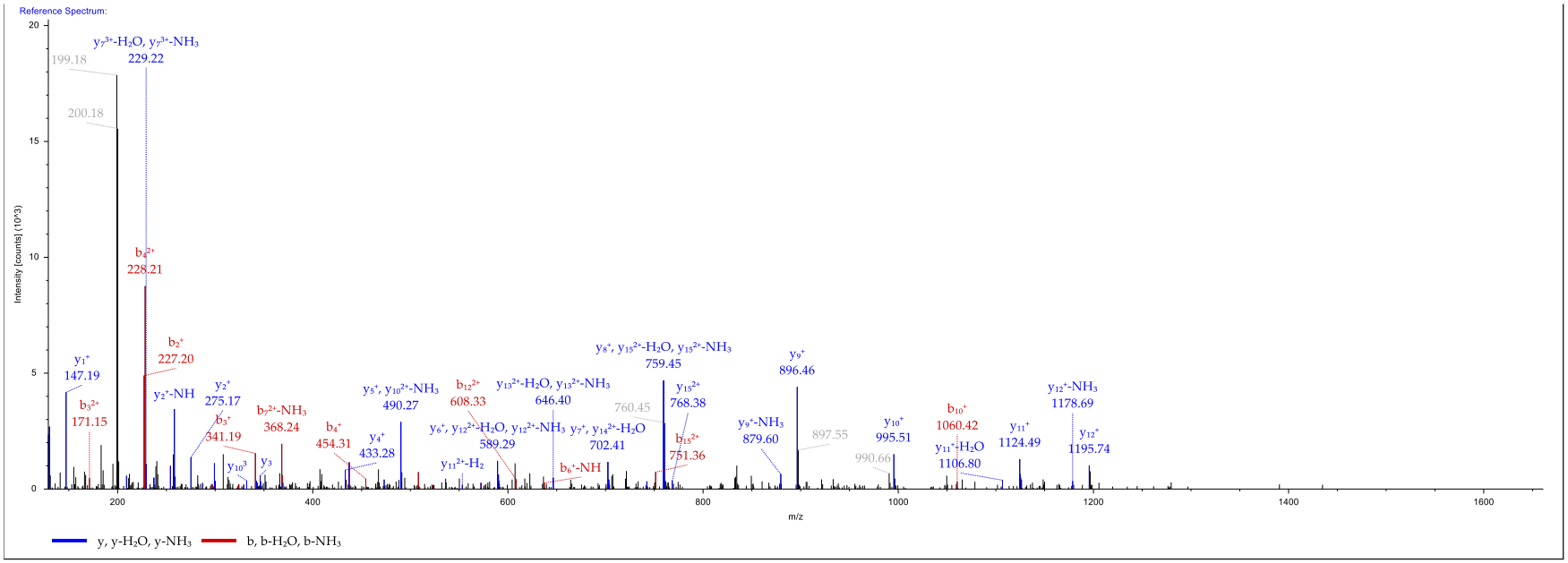

Figure 6A LC-MS/MS analysis showing a 42-Da adduct with Ser 146 from peptide: IINIASVHGLVGSAQK in MAP-treated 3-HBDH. The precursor isotope pattern spectrum (MS1) (A), and MS/MS spectrum for the triply charged ion of the II-peptide (*m/z* 550.320 Da; MH^+ = 1648.946 Da) reveal an increase in mass of the b_6^+ ion by 42 Da corresponding to Ser 146 (with 0 missed cleavages) (B, C). Identical II-peptides were found in the control and SMHP-treated samples and showed a mass increase of 42 Da between the b_6^+ ions arising from the MAP-modified (654.382 Da) and unmodified peptide (612.372 Da).

A

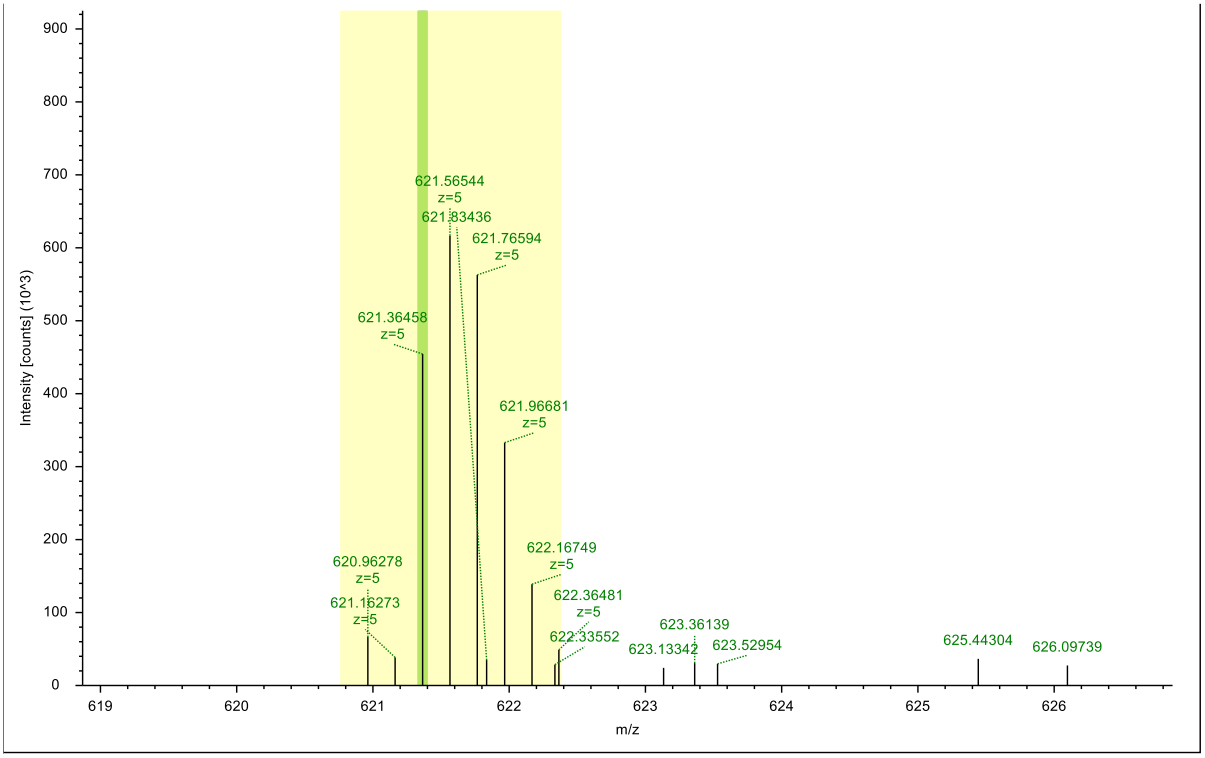

B

Fragment Matches

Value Type: Theo. Mass [Da]

Ion Series | Neutral Losses | Precursor Ions | Internal Fragments

#1	b⁺	b²⁺	b³⁺	b⁴⁺	b⁵⁺	Seq.	y⁺	y²⁺	y³⁺	y⁴⁺	y⁵⁺	#2
1	114.09134	57.54931	38.70196	29.27829	23.62409	I						31
2	227.17540	114.09134	76.39665	57.54931	46.24090	I	2989.69455	1495.35091	997.23637	748.17909	598.74473	30
3	341.21833	171.11280	114.41096	86.06004	69.04949	N	2876.61049	1438.80888	959.54168	719.90808	576.12792	29
4	454.30240	227.65484	152.10565	114.33106	91.66630	I	2762.56756	1381.78742	921.52737	691.39735	553.31933	28
5	525.33951	263.17339	175.78469	132.09033	105.87372	A	2649.48349	1325.24539	883.83268	663.12633	530.70252	27
6	612.37154	306.68941	204.79536	153.84834	123.28013	S	2578.44638	1289.72683	860.15364	645.36705	516.49510	26
7	711.43995	356.22361	237.81817	178.61545	143.09381	V	2491.41435	1246.21081	831.14297	623.60905	499.08869	25
8	848.49886	424.75307	283.50447	212.88017	170.50559	H	2392.34594	1196.67661	798.12016	598.84194	479.27501	24
9	905.52033	453.26380	302.51163	227.13554	181.90989	G	2255.28703	1128.14715	752.43386	564.57721	451.86323	23
10	1018.60439	509.80583	340.20631	255.40656	204.52670	L	2198.26556	1099.63642	733.42671	550.32185	440.45893	22
11	1117.67281	559.34004	373.22912	280.17366	224.34038	V	2085.18150	1043.09439	695.73202	522.05083	417.84212	21
12	1174.69427	587.85077	392.23627	294.42902	235.74468	G	1986.11308	993.56018	662.70921	497.28373	398.02844	20
13	1261.72630	631.36679	421.24695	316.18703	253.15108	S	1929.09162	965.04945	643.70206	483.02836	386.62415	19
14	1332.76341	666.88534	444.92599	333.94631	267.35850	A	1842.05959	921.53343	614.69138	461.27036	369.21774	18
15	1460.82199	730.91463	487.61218	365.96095	292.97022	Q	1771.02248	886.01488	591.01234	443.51108	355.01032	17
16	1588.91695	794.96211	530.31050	397.98470	318.58921	K	1642.96390	821.98559	548.32615	411.49643	329.39860	16
17	1675.94898	838.47813	559.32118	419.74270	335.99562	S	1514.86894	757.93811	505.62783	379.47269	303.77961	15
18	1746.98609	873.99668	583.00022	437.50198	350.20304	A	1427.83691	714.42209	476.61715	357.71469	286.37320	14
19	1910.04942	955.52835	637.35466	478.26781	382.81571	Y	1356.79980	678.90354	452.93812	339.95541	272.16578	13
20	2009.11784	1005.06256	670.37746	503.03492	402.62939	V	1193.73647	597.37187	398.58367	299.18957	239.55311	12
21	2080.15495	1040.58111	694.05650	520.79419	416.83681	A	1094.66805	547.83767	365.56087	274.42247	219.73943	11
22	2151.19206	1076.09967	717.73554	538.55347	431.04423	A	1023.63094	512.31911	341.88183	256.66319	205.53201	10
23	2279.28703	1140.14715	760.43386	570.57721	456.66323	K	952.59383	476.80055	318.20279	238.90391	191.32459	9
24	2416.34594	1208.67661	806.12016	604.84194	484.07501	H	824.49886	412.75307	275.50447	206.88017	165.70559	8
25	2473.36740	1237.18734	825.12732	619.09731	495.47930	G	687.43995	344.22361	229.81817	172.61545	138.29381	7
26	2586.45147	1293.72937	862.82201	647.36832	518.09611	I	630.41849	315.71288	210.81101	158.36008	126.88952	6
27	2685.51988	1343.26358	895.84481	672.13543	537.90980	V	517.33442	259.17085	173.11633	130.08906	104.27271	5
28	2742.54134	1371.77431	914.85197	686.39079	549.31409	G	418.26601	209.63664	140.09352	105.32196	84.45902	4
29	2855.62541	1428.31634	952.54665	714.66181	571.93090	L	361.24455	181.12591	121.08637	91.06659	73.05473	3
30	2956.67309	1478.84018	986.22921	739.92373	592.14044	T	248.16048	124.58388	83.39168	62.79558	50.43792	2
31						K	147.11280	74.06004	49.70912	37.53366	30.22838	1

C

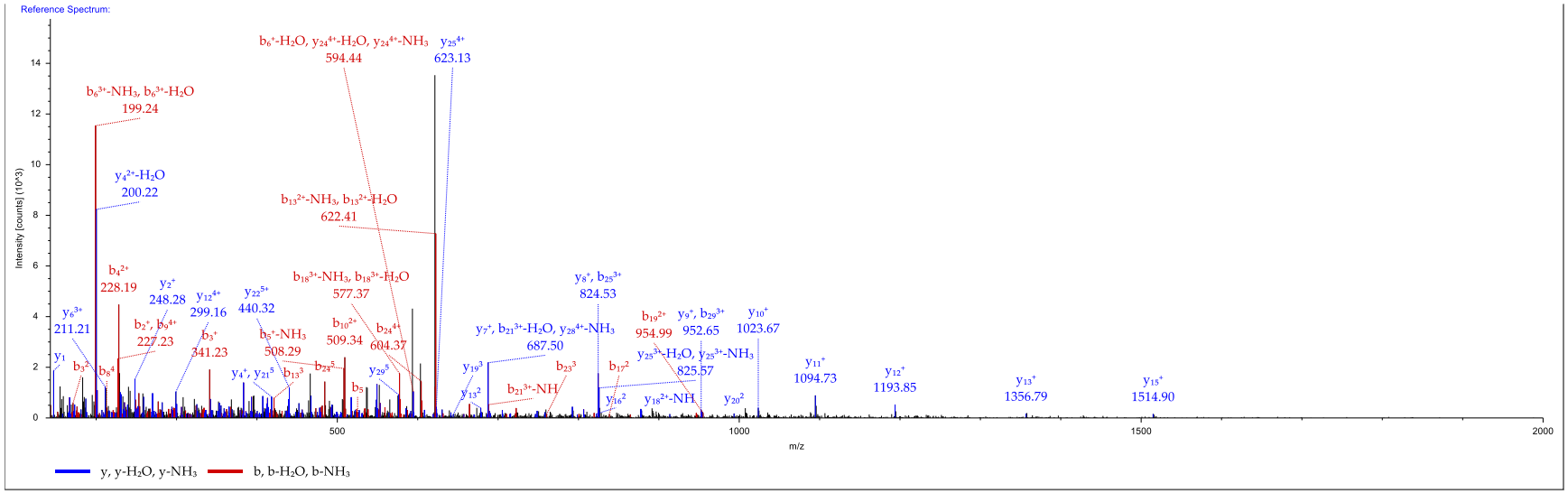

Figure 7A LC-MS/MS analysis showing no adducts with Ser 146, Lys 156, or Lys 163 from peptide: IINIASVHGLVGSAQKSAYVAAKHGIVGLTK in untreated 3-HBDH. The precursor isotope pattern spectrum (MS1) (A), and MS/MS spectrum for the +5 charged ion of the II-peptide (*m/z* 621.365 Da; MH^+ = 3102.793 Da) reveal no 94-Da (SMHP modification) or 42-Da (MAP modification) adducts with Ser 146, Lys 156, or Lys 163 (b_6^+, b_{16}^+, b_{23}^+ ions) (with 2 missed cleavages) (B, C).

A

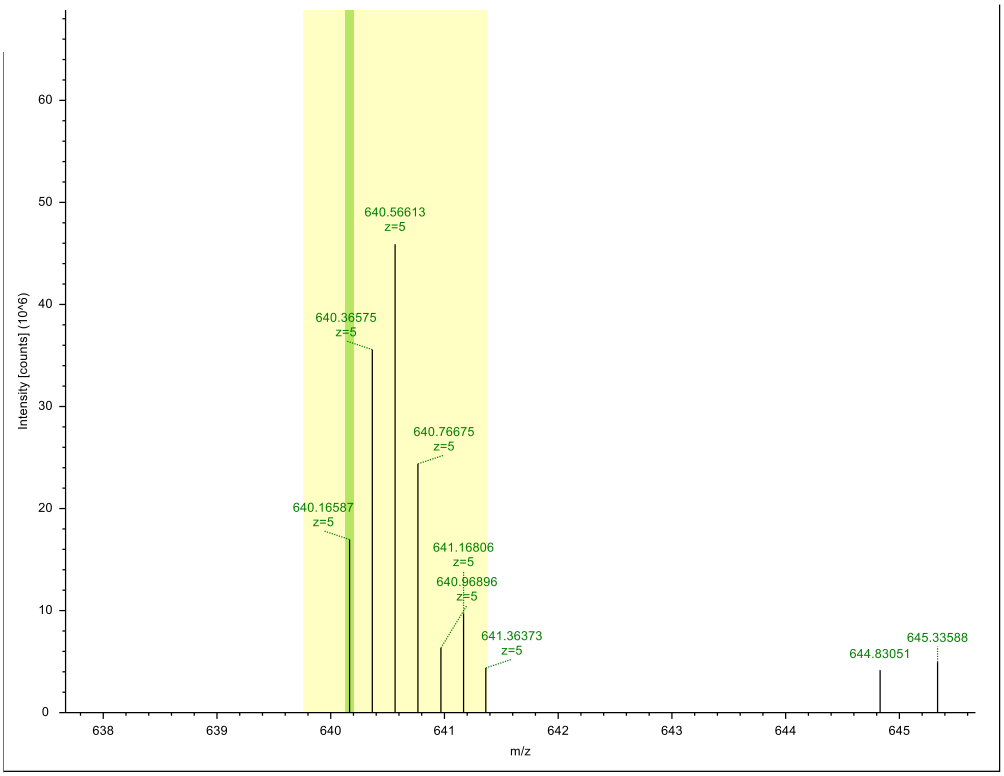

B

Fragment Matches

Value Type: Theo. Mass [Da]

Ion Series | Neutral Losses | Precursor Ions | Internal Fragments

#1	b+	b2+	b3+	b4+	b5+	Seq.	y+	y2+	y3+	y4+	y5+	#2
1	114.09134	57.54931	38.70196	29.27829	23.62409	I						31
2	227.17540	114.09134	76.39665	57.54931	46.24090	I	3083.73641	1542.37184	1028.58366	771.68956	617.55310	30
3	341.21833	171.11280	114.41096	86.06004	69.04949	N	2970.65235	1485.82981	990.88897	743.41854	594.93629	29
4	454.30240	227.65484	152.10565	114.33106	91.66630	I	2856.60942	1428.80835	952.87466	714.90781	572.12771	28
5	525.33951	263.17339	175.78469	132.09033	105.87372	A	2743.52536	1372.26632	915.17997	686.63680	549.51089	27
6	612.37154	306.68941	204.79536	153.84834	123.28013	S	2672.48824	1336.74776	891.50093	668.87752	535.30347	26
7	711.43995	356.22361	237.81817	178.61545	143.09381	V	2585.45621	1293.23175	862.49026	647.11951	517.89706	25
8	848.49886	424.75307	283.50447	212.88017	170.50559	H	2486.38780	1243.69754	829.46745	622.35241	498.08338	24
9	905.52033	453.26380	302.51163	227.13554	181.90989	G	2349.32889	1175.16808	783.78115	588.08768	470.67160	23
10	1018.60439	509.80583	340.20631	255.40656	204.52670	L	2292.30743	1146.65735	764.77399	573.83231	459.26731	22
11	1117.67281	559.34004	373.22912	280.17366	224.34038	V	2179.22336	1090.11532	727.07930	545.56130	436.65049	21
12	1174.69427	587.85077	392.23627	294.42902	235.74468	G	2080.15495	1040.58111	694.05650	520.79419	416.83681	20
13	1261.72630	631.36679	421.24695	316.18703	253.15108	S	2023.13348	1012.07038	675.04935	506.53883	405.43252	19
14	1332.76341	666.88534	444.92599	333.94631	267.35850	A	1936.10146	968.55437	646.03867	484.78082	388.02611	18
15	1460.82199	730.91463	487.61218	365.96095	292.97022	Q	1865.06434	933.03581	622.35963	467.02154	373.81869	17
16	1682.95881	841.98305	561.65779	421.49516	337.39758	K-Hex-5-...	1737.00576	869.00652	579.67344	435.00690	348.20697	16
17	1769.99084	885.49906	590.66847	443.25317	354.80399	S	1514.86894	757.93811	505.62783	379.47269	303.77961	15
18	1841.02796	921.01762	614.34750	461.01245	369.01141	A	1427.83691	714.42209	476.61715	357.71469	286.37320	14
19	2004.09128	1002.54928	668.70195	501.77828	401.62408	Y	1356.79980	678.90354	452.93812	339.95541	272.16578	13
20	2103.15970	1052.08349	701.72475	526.54538	421.43776	V	1193.73647	597.37187	398.58367	299.18957	239.55311	12
21	2174.19681	1087.60204	725.40379	544.30466	435.64518	A	1094.66805	547.83767	365.56087	274.42247	219.73943	11
22	2245.23393	1123.12060	749.08283	562.06394	449.85261	A	1023.63094	512.31911	341.88183	256.66319	205.53201	10
23	2373.32889	1187.16808	791.78115	594.08768	475.47160	K	952.59383	476.80055	318.20279	238.90391	191.32459	9
24	2510.38780	1255.69754	837.46745	628.35241	502.88338	H	824.49886	412.75307	275.50447	206.88017	165.70559	8
25	2567.40926	1284.20827	856.47461	642.60777	514.28767	G	687.43995	344.22361	229.81817	172.61545	138.29381	7
26	2680.49333	1340.75030	894.16929	670.87879	536.90449	I	630.41849	315.71288	210.81101	158.36008	126.88952	6
27	2779.56174	1390.28451	927.19210	695.64589	556.71817	V	517.33442	259.17085	173.11633	130.08906	104.27271	5
28	2836.58321	1418.79524	946.19925	709.90126	568.12246	G	418.26601	209.63664	140.09352	105.32196	84.45902	4
29	2949.66727	1475.33727	983.89394	738.17227	590.73928	L	361.24455	181.12591	121.08637	91.06659	73.05473	3
30	3050.71495	1525.86111	1017.57650	763.43419	610.94881	T	248.16048	124.58388	83.39168	62.79558	50.43792	2
31						K	147.11280	74.06004	49.70912	37.53366	30.22838	1

C

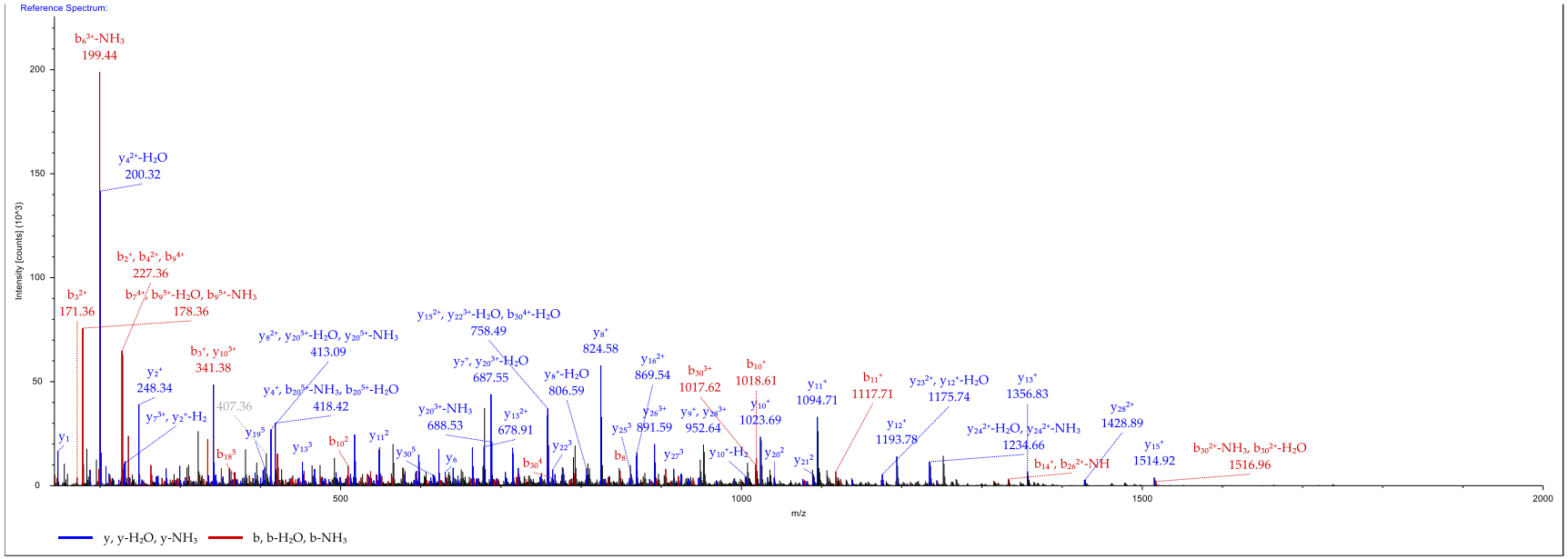

Figure 8A LC-MS/MS analysis showing a 94-Da adduct with Lys 156 from peptide: IINIASVHGLVGSAQKSAYVAAKHGIVGLTK in SMHP-treated 3-HBDH. The precursor isotope pattern spectrum (MS1) (A), and MS/MS spectrum for the +5 charged ion of the II-peptide (*m/z* 640.166 Da; MH^+ = 3196.800 Da) reveal an increase in mass of the b_{16}^+ ion by 94 Da corresponding to Lys 156 (with 2 missed cleavages) (B, C). Identical II-peptides were found in the control and SMHP-treated samples and showed a mass increase of 94 Da between the b_{16}^+ ions arising from the SMHP-modified (1682.956 Da) and unmodified peptide (1588.917 Da).

A

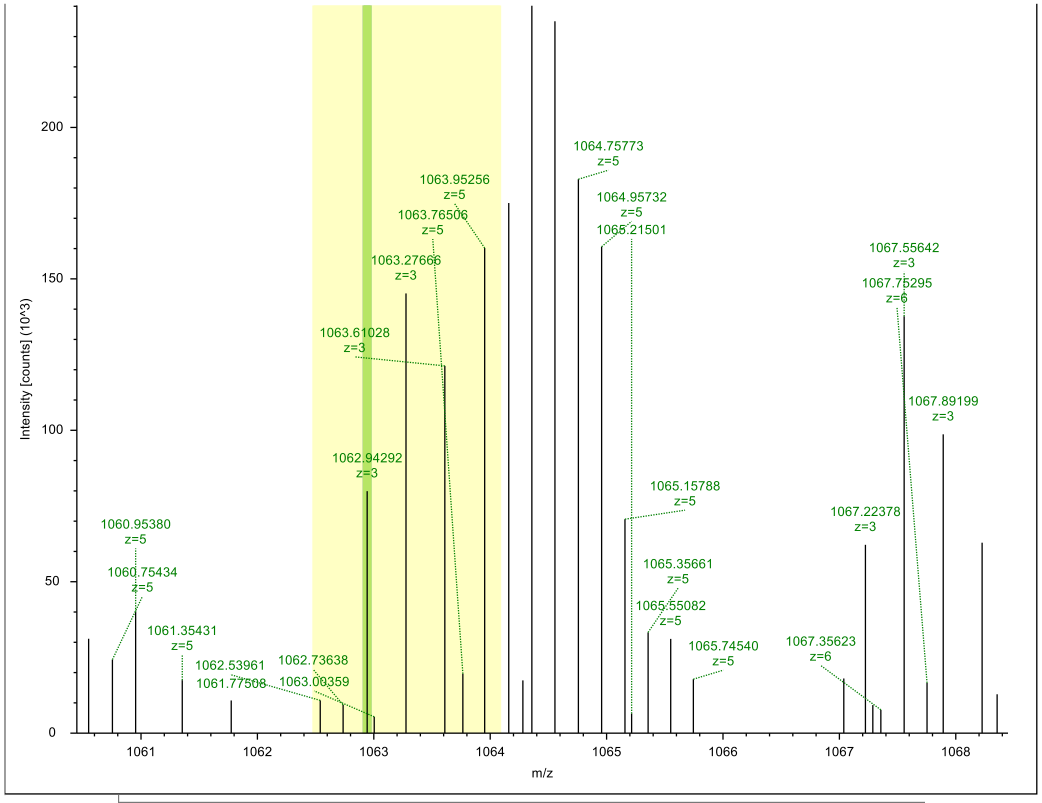

B

Fragment Matches

Value Type: Theo. Mass [Da]

Ion Series | Neutral Losses | Precursor Ions | Internal Fragments

#1	b⁺	b²⁺	b³⁺	Seq.	y⁺	y²⁺	y³⁺	#2
1	114.09134	57.54931	38.70196	I				31
2	227.17540	114.09134	76.39665	I	3073.71568	1537.36148	1025.24341	30
3	341.21833	171.11280	114.41096	N	2960.63162	1480.81945	987.54872	29
4	454.30240	227.65484	152.10565	I	2846.58869	1423.79798	949.53441	28
5	525.33951	263.17339	175.78469	A	2733.50462	1367.25595	911.83973	27
6	612.37154	306.68941	204.79536	S	2662.46751	1331.73739	888.16069	26
7	711.43995	356.22361	237.81817	V	2575.43548	1288.22138	859.15001	25
8	848.49886	424.75307	283.50447	H	2476.36707	1238.68717	826.12721	24
9	905.52033	453.26380	302.51163	G	2339.30816	1170.15772	780.44090	23
10	1018.60439	509.80583	340.20631	L	2282.28669	1141.64698	761.43375	22
11	1117.67281	559.34004	373.22912	V	2169.20263	1085.10495	723.73906	21
12	1174.69427	587.85077	392.23627	G	2070.13421	1035.57075	690.71626	20
13	1261.72630	631.36679	421.24695	S	2013.11275	1007.06001	671.70910	19
14	1332.76341	666.88534	444.92599	A	1926.08072	963.54400	642.69843	18
15	1460.82199	730.91463	487.61218	Q	1855.04361	928.02544	619.01939	17
16	1630.92752	815.96740	544.31402	K-Acetyl	1726.98503	863.99615	576.33319	16
17	1717.95954	859.48341	573.32470	S	1556.87950	778.94339	519.63135	15
18	1788.99666	895.00197	597.00374	A	1469.84748	735.42738	490.62068	14
19	1952.05999	976.53363	651.35818	Y	1398.81036	699.90882	466.94164	13
20	2051.12840	1026.06784	684.38098	V	1235.74703	618.37715	412.58720	12
21	2122.16551	1061.58640	708.06002	A	1136.67862	568.84295	379.56439	11
22	2193.20263	1097.10495	731.73906	A	1065.64151	533.32439	355.88535	10
23	2363.30816	1182.15772	788.44090	K-Acetyl	994.60439	497.80583	332.20631	9
24	2500.36707	1250.68717	834.12721	H	824.49886	412.75307	275.50447	8
25	2557.38853	1279.19790	853.13436	G	687.43995	344.22361	229.81817	7
26	2670.47260	1335.73994	890.82905	I	630.41849	315.71288	210.81101	6
27	2769.54101	1385.27414	923.85185	V	517.33442	259.17085	173.11633	5
28	2826.56247	1413.78487	942.85901	G	418.26601	209.63664	140.09352	4
29	2939.64654	1470.32691	980.55370	L	361.24455	181.12591	121.08637	3
30	3040.69422	1520.85075	1014.23626	T	248.16048	124.58388	83.39168	2
31				K	147.11280	74.06004	49.70912	1

C

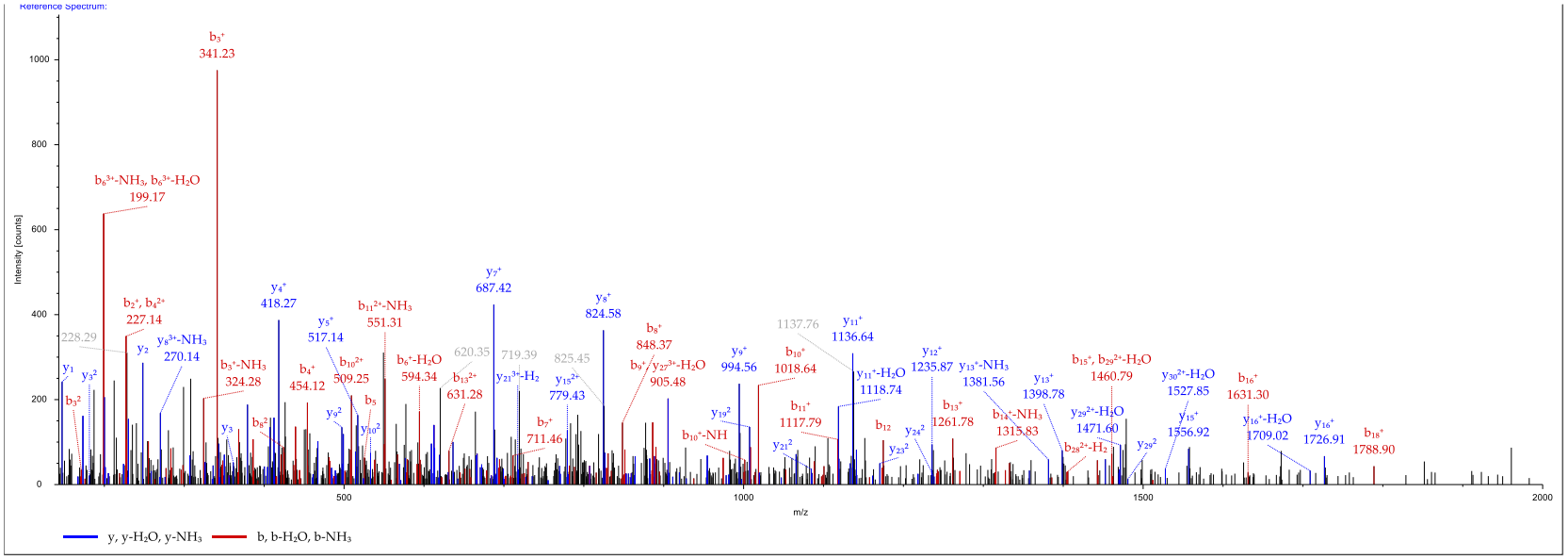

Figure 9A LC-MS/MS analysis showing a 42-Da adduct with Lys 156 and Lys 163 from peptide: IINIASVHGLVGSAQKSAYVAAKHGIVGLTK in SMHP-treated 3-HBDH. The precursor isotope pattern spectrum (MS1) (A), and MS/MS spectrum for the triply charged ion of the II-peptide (*m/z* 1062.943 Da; MH^+ = 3186.814 Da) reveal an increase in mass of the b_{16}^+ and b_{23}^+ ions by 42 Da corresponding to Lys 156 and Lys 163 (with 2 missed cleavages) (B, C). Identical II-peptides were found in the control and SMHP-treated samples and showed a mass increase of 42 Da between the b_{16}^+ and b_{23}^+ ions arising from the SMHP-modified (b_{16}^+1630.928 Da; b_{23}^+ 2363. 308 Da) and unmodified peptide (b_{16}^+1682.956 Da; b_{23}^+ 2279.287 Da).

A

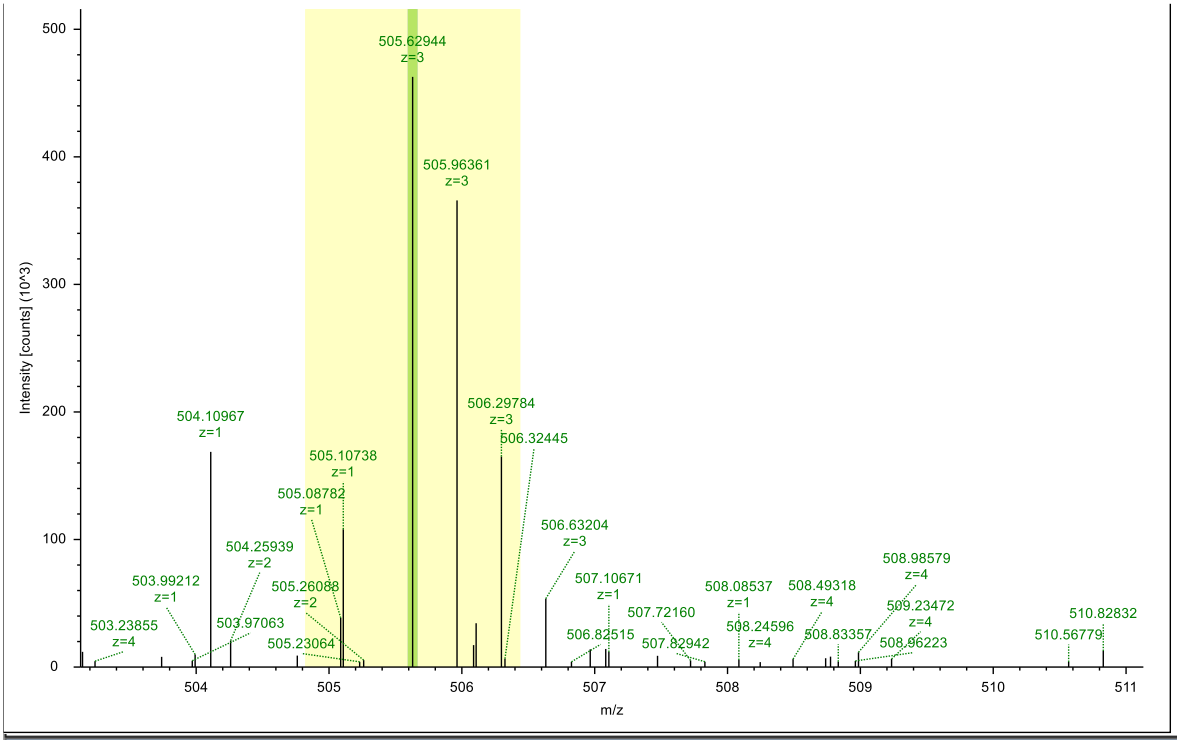

B

Fragment Matches

Value Type: Theo. Mass [Da]

Ion Series | Neutral Losses | Precursor Ions | Internal Fragments

#1	b⁺	b²⁺	b³⁺	Seq.	y⁺	y²⁺	y³⁺	#2
1	88.03930	44.52329	30.01795	S				15
2	159.07642	80.04185	53.69699	A	1427.83691	714.42209	476.61715	14
3	322.13975	161.57351	108.05143	Y	1356.79980	678.90354	452.93812	13
4	421.20816	211.10772	141.07424	V	1193.73647	597.37187	398.58367	12
5	492.24527	246.62628	164.75328	A	1094.66805	547.83767	365.56087	11
6	563.28239	282.14483	188.43231	A	1023.63094	512.31911	341.88183	10
7	691.37735	346.19231	231.13063	K	952.59383	476.80055	318.20279	9
8	828.43626	414.72177	276.81694	H	824.49886	412.75307	275.50447	8
9	885.45773	443.23250	295.82409	G	687.43995	344.22361	229.81817	7
10	998.54179	499.77453	333.51878	I	630.41849	315.71288	210.81101	6
11	1097.61020	549.30874	366.54159	V	517.33442	259.17085	173.11633	5
12	1154.63167	577.81947	385.54874	G	418.26601	209.63664	140.09352	4
13	1267.71573	634.36150	423.24343	L	361.24455	181.12591	121.08637	3
14	1368.76341	684.88534	456.92599	T	248.16048	124.58388	83.39168	2
15				K	147.11280	74.06004	49.70912	1

C

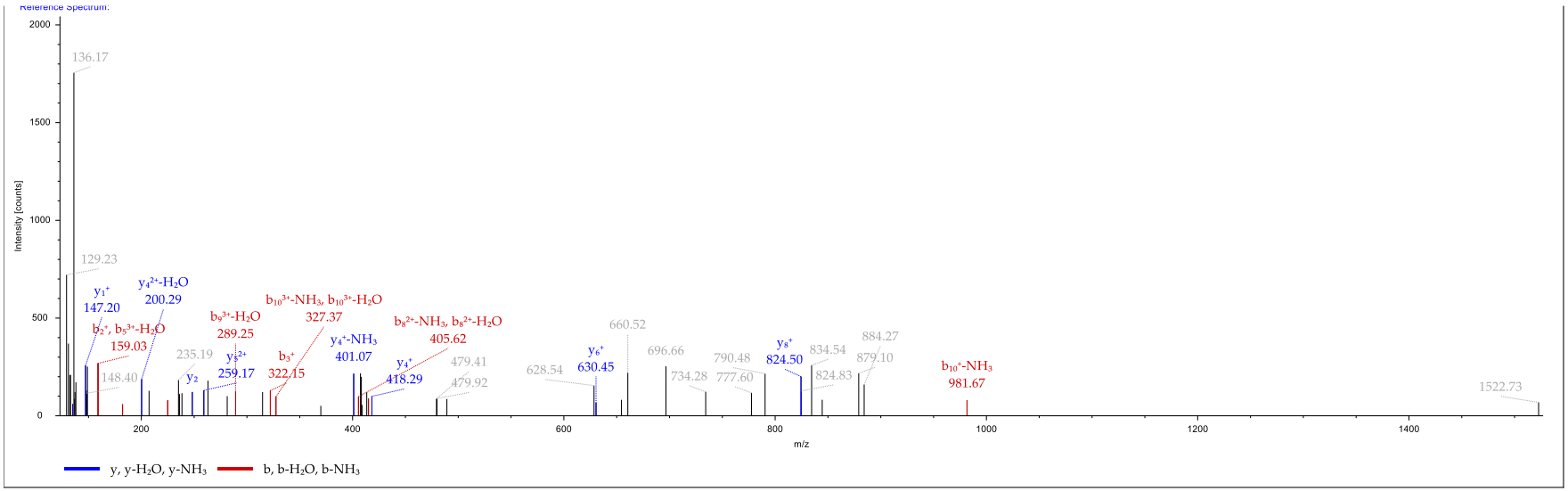

Figure 10A LC-MS/MS analysis showing no adducts with Lys 163 from peptide: SAYVAAKHGIVGLTK in untreated 3-HBDH. The precursor isotope pattern spectrum (MS1) (A), and MS/MS spectrum for the triply charged ion of the SA-peptide (*m/z* 505.629 Da; MH^+ = 1514.874 Da) reveal no 94-Da (SMHP modification) or 42-Da (MAP modification) adducts with the b_7^+ ion corresponding to Lys 163 (with 1 missed cleavage) (B, C).

A

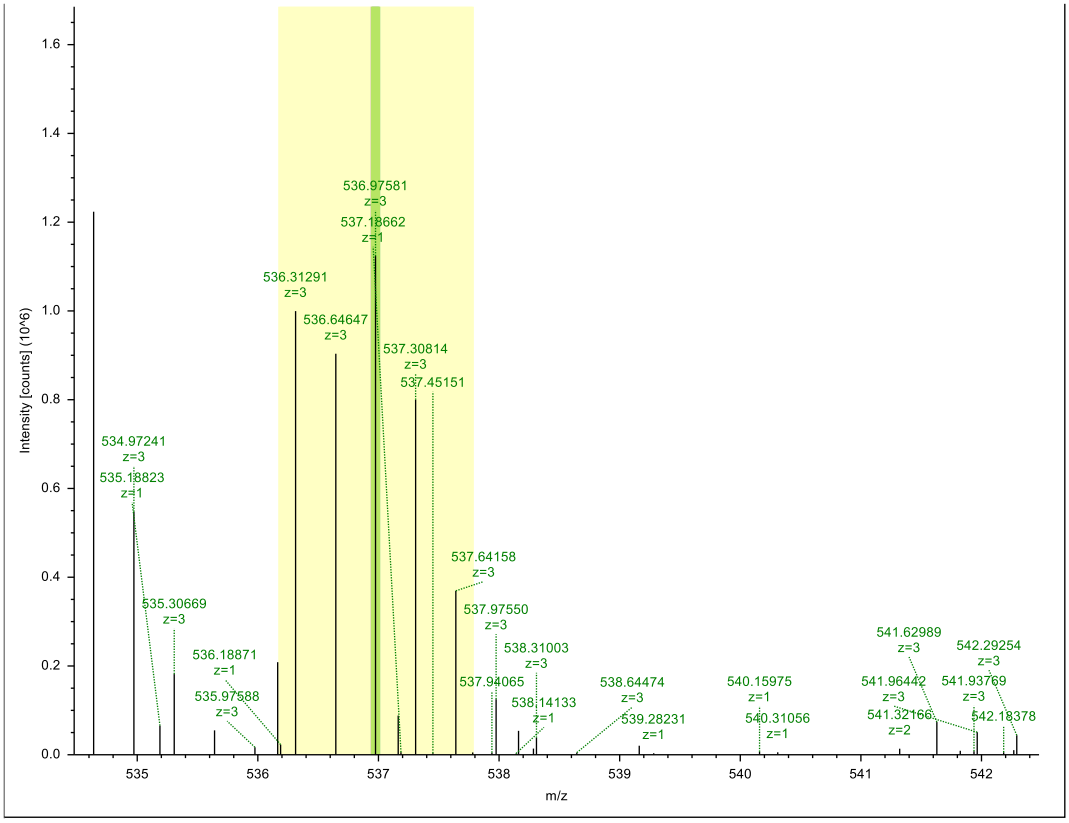

B

Fragment Matches

Value Type: Theo. Mass [Da]

Ion Series | Neutral Losses | Precursor Ions | Internal Fragments

#1	b^+	b^{2+}	b^{3+}	Seq.	y^+	y^{2+}	y^{3+}	#2
1	88.03930	44.52329	30.01795	S				15
2	159.07642	80.04185	53.69699	A	1521.87877	761.44302	507.96444	14
3	322.13975	161.57351	108.05143	Y	1450.84166	725.92447	484.28540	13
4	421.20816	211.10772	141.07424	V	1287.77833	644.39280	429.93096	12
5	492.24527	246.62628	164.75328	A	1188.70992	594.85860	396.90816	11
6	563.28239	282.14483	188.43231	A	1117.67280	559.34004	373.22912	10
7	785.41921	393.21325	262.47792	K-Hex-5-...	1046.63569	523.82148	349.55008	9
8	922.47813	461.74270	308.16423	H	824.49886	412.75307	275.50447	8
9	979.49959	490.25343	327.17138	G	687.43995	344.22361	229.81817	7
10	1092.58365	546.79547	364.86607	I	630.41849	315.71288	210.81101	6
11	1191.65207	596.32967	397.88887	V	517.33442	259.17085	173.11633	5
12	1248.67353	624.84040	416.89603	G	418.26601	209.63664	140.09352	4
13	1361.75760	681.38244	454.59072	L	361.24455	181.12591	121.08637	3
14	1462.80527	731.90628	488.27328	T	248.16048	124.58388	83.39168	2
15				K	147.11280	74.06004	49.70912	1

C

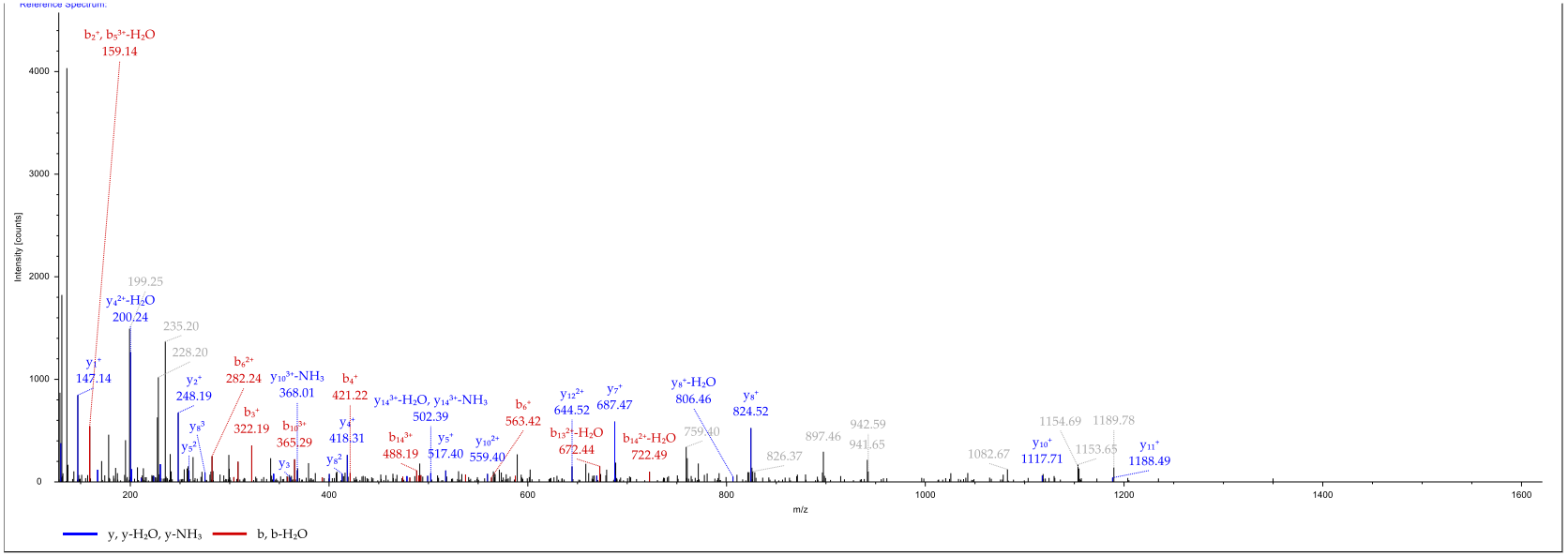

Figure 11A LC-MS/MS analysis showing a 94-Da adduct with Lys 163 from peptide: SAYVAAKHGIVGLTK in SMHP-treated 3-HBDH. The precursor isotope pattern spectrum (MS1) (A), and MS/MS spectrum for the triply charged ion of the SA-peptide (*m/z* 536.976 Da; MH^+ = 1608.913 Da) reveal an increase in mass of the b_7^+ ion by 94 Da corresponding to Lys 163 (with 1 missed cleavage) (B, C). Identical II-peptides were found in the control and SMHP-treated samples and showed a mass increase of 94 Da between the b_7^+ ions arising from the SMHP-modified (785.419 Da) and unmodified peptide (691.377 Da)

APPENDIX B

Figure 1B Sequence coverage (81.34%) of untreated CTPS

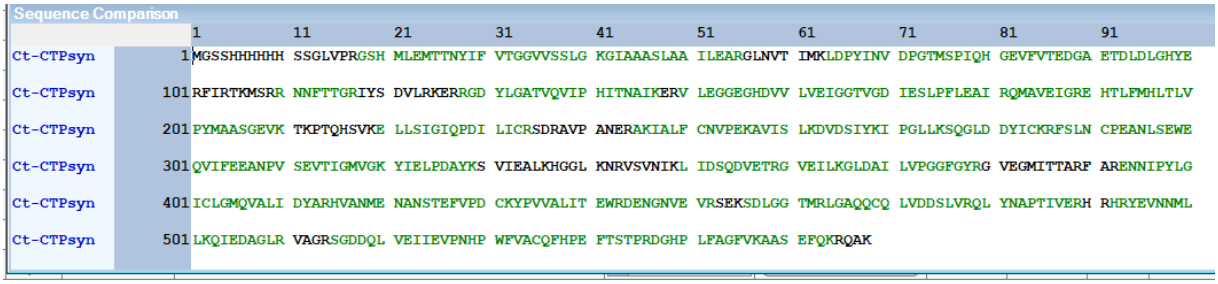

Figure 2B Sequence coverage (80.63%) of SMHP-treated CTPS

A

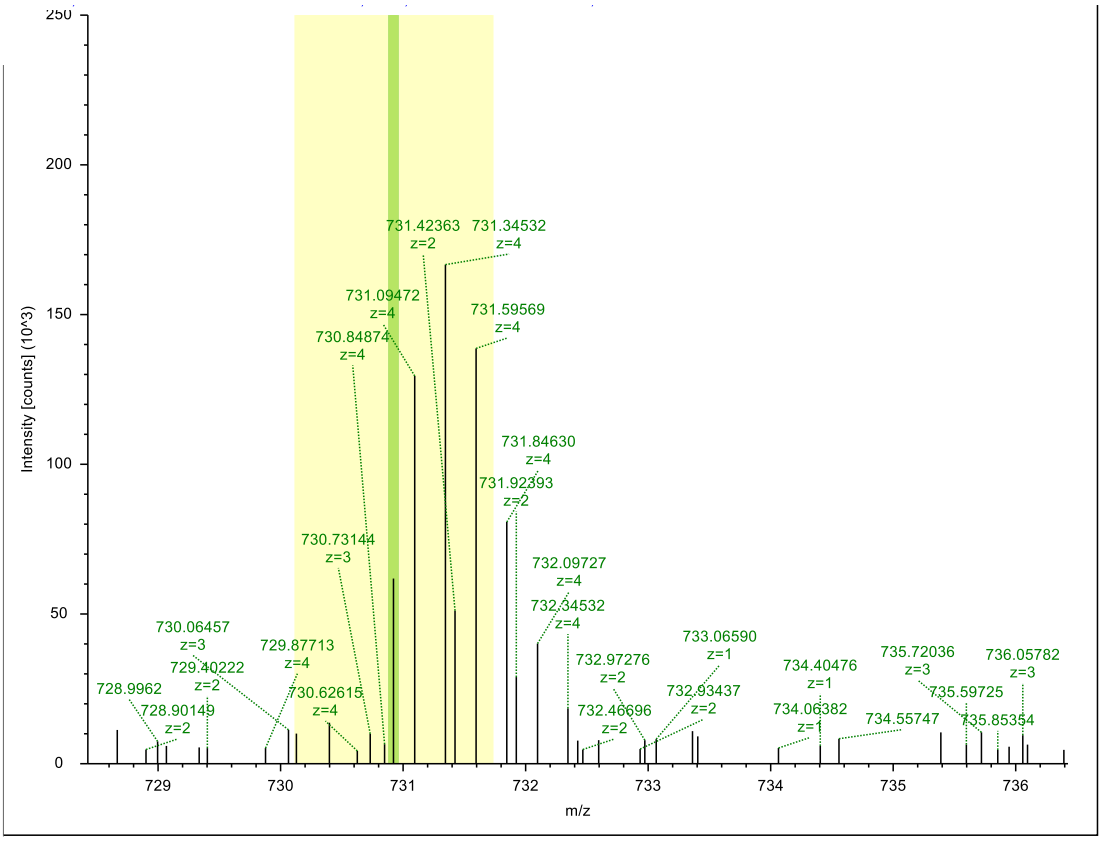

B

Fragment Matches

Value Type: Theo. Mass [Da]

Ion Series | Neutral Losses | Precursor Ions | Internal Fragments

#1	b^+	b^{2+}	Seq.	y^+	y^{2+}	#2
1	116.03422	58.52075	D			13
2	215.10263	108.05496	V	1345.80896	673.40812	12
3	330.12958	165.56843	D	1246.74055	623.87391	11
4	417.16160	209.08444	S	1131.71361	566.36044	10
5	530.24567	265.62647	I	1044.68158	522.84443	9
6	693.30900	347.15814	Y	931.59751	466.30240	8
7	821.40396	411.20562	K	768.53419	384.77073	7
8	934.48802	467.74765	I	640.43922	320.72325	6
9	1031.54079	516.27403	P	527.35516	264.18122	5
10	1088.56225	544.78476	G	430.30240	215.65484	4
11	1201.64632	601.32680	L	373.28093	187.14410	3
12	1314.73038	657.86883	L	260.19687	130.60207	2
13			K	147.11280	74.06004	1

C

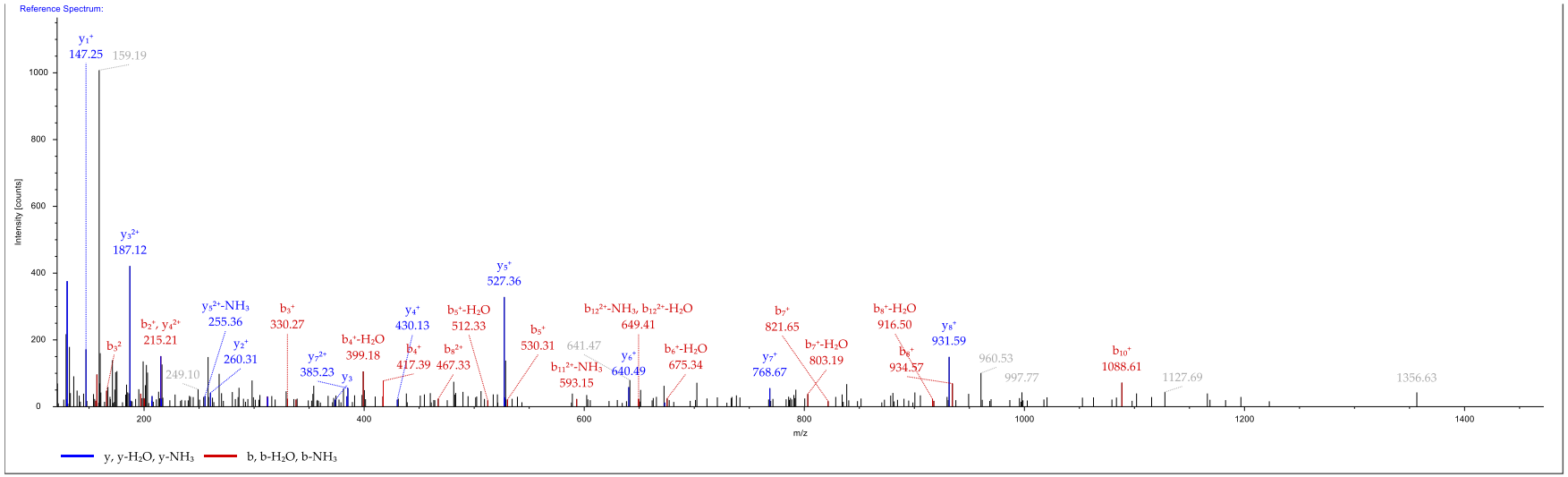

Figure 3B LC-MS/MS analysis showing no adducts with Lys 246 from peptide: DVDSIYKIPGLLK in untreated CTPS. The precursor isotope pattern spectrum (MS1) (A), and MS/MS spectrum for the doubly charged ion of the DV-peptide (*m*/*z* 730.922 Da; MH^+ = 1460.836 Da) reveal no 94-Da (SMHP modification) adducts with the b_7^+ ion corresponding to Lys 246 (with 1 missed cleavage) (B, C).

A

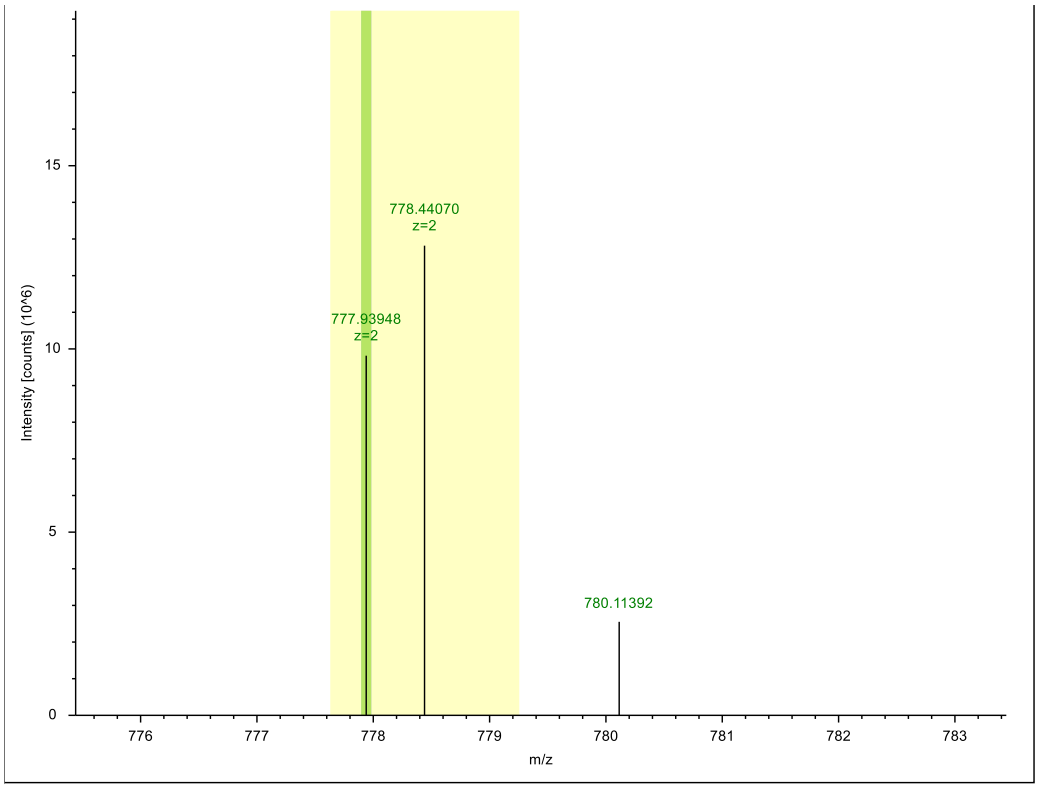

B

Fragment Matches

Value Type: Theo. Mass [Da]

Ion Series | Neutral Losses | Precursor Ions | Internal Fragments

#1	b⁺	b²⁺	Seq.	y⁺	y²⁺	#2
1	116.03422	58.52075	D			13
2	215.10263	108.05496	V	1439.85083	720.42905	12
3	330.12958	165.56843	D	1340.78241	670.89484	11
4	417.16160	209.08444	S	1225.75547	613.38137	10
5	530.24567	265.62647	I	1138.72344	569.86536	9
6	693.30900	347.15814	Y	1025.63938	513.32333	8
7	915.44582	458.22655	K-Hex-5-...	862.57605	431.79166	7
8	1028.52989	514.76858	I	640.43922	320.72325	6
9	1125.58265	563.29496	P	527.35516	264.18122	5
10	1182.60411	591.80570	G	430.30240	215.65484	4
11	1295.68818	648.34773	L	373.28093	187.14410	3
12	1408.77224	704.88976	L	260.19687	130.60207	2
13			K	147.11280	74.06004	1

C

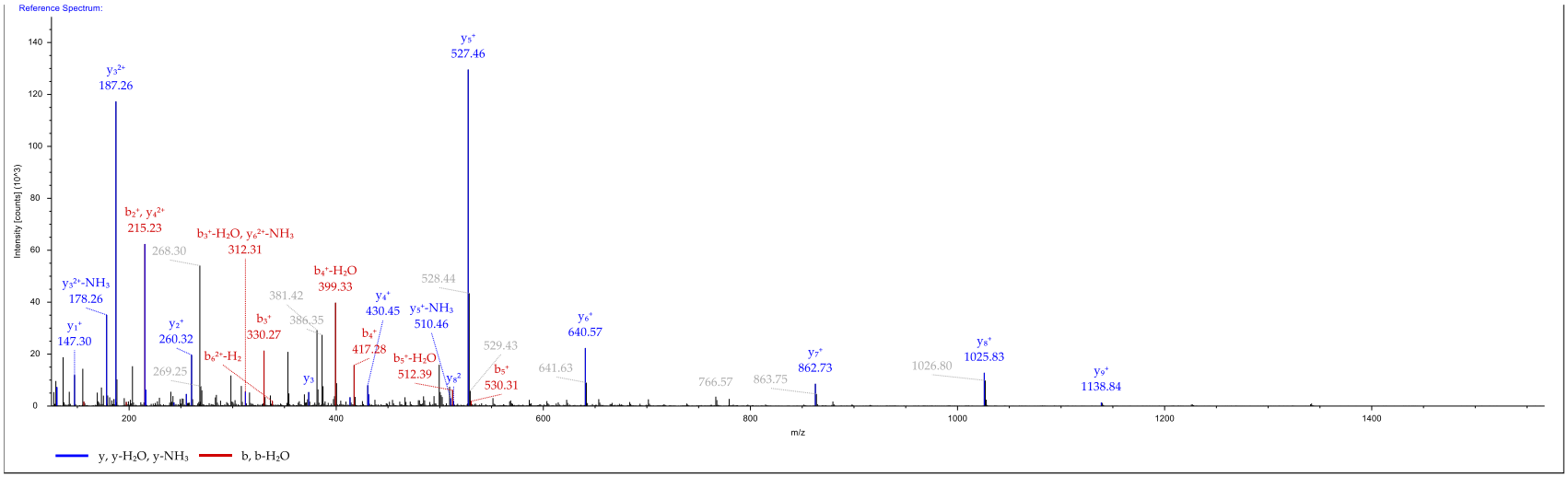

Figure 4B LC-MS/MS analysis showing a 94-Da adduct with Lys 246 from peptide: DVDSIYKIPGLLK in SMHP-treated CTPS. The precursor isotope pattern spectrum (MS1) (A), and MS/MS spectrum for the doubly charged ion of the DV-peptide (*m/z* 777.939 Da; MH^+ = 1554.872 Da) reveal an increase in mass of the b_7^+ ion by 94 Da corresponding to Lys 246 (with 1 missed cleavage) (B, C). Identical DV-peptides were found in the control and SMHP-treated sample and showed a mass increase of 94 Da between the b_7^+ ions arising from the SMHP-modified (915.446 Da) and unmodified peptide (821.404 Da).

A

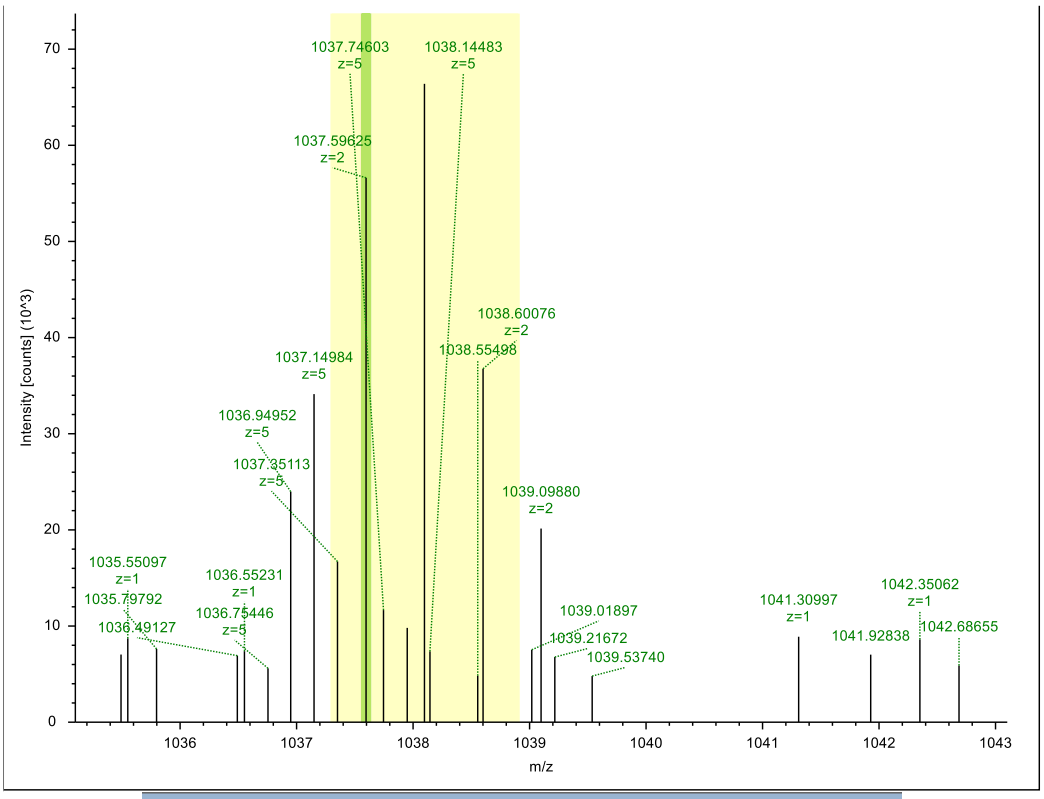

B

Fragment Matches

Value Type: Theo. Mass [Da]

Ion Series | Neutral Losses | Precursor Ions | Internal Fragments

#1	b⁺	b²⁺	Seq.	y⁺	y²⁺	#2
1	58.02874	29.51801	G			20
2	157.09715	79.05222	V	2017.14807	1009.07767	19
3	286.13975	143.57351	E	1918.07966	959.54347	18
4	399.22381	200.11554	I	1789.03707	895.02217	17
5	512.30788	256.65758	L	1675.95300	838.48014	16
6	640.40284	320.70506	K	1562.86894	781.93811	15
7	697.42430	349.21579	G	1434.77398	717.89063	14
8	810.50837	405.75782	L	1377.75251	689.37989	13
9	925.53531	463.27129	D	1264.66845	632.83786	12
10	996.57242	498.78985	A	1149.64150	575.32439	11
11	1109.65649	555.33188	I	1078.60439	539.80583	10
12	1222.74055	611.87391	L	965.52033	483.26380	9
13	1321.80896	661.40812	V	852.43626	426.72177	8
14	1418.86173	709.93450	P	753.36785	377.18756	7
15	1475.88319	738.44523	G	656.31509	328.66118	6
16	1532.90466	766.95597	G	599.29362	300.15045	5
17	1679.97307	840.49017	F	542.27216	271.63972	4
18	1736.99453	869.00090	G	395.20374	198.10551	3
19	1900.05786	950.53257	Y	338.18228	169.59478	2
20			R	175.11895	88.06311	1

C

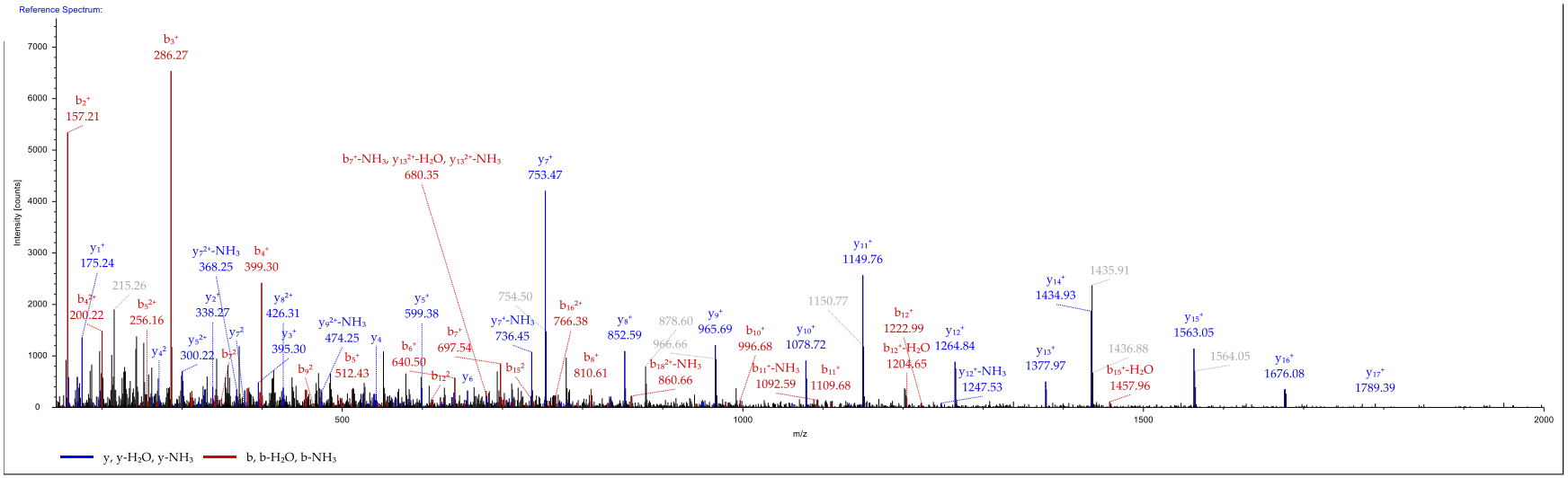

Figure 5B LC-MS/MS analysis showing no adducts with Lys 342 from peptide: GVEILKGLDAILVPGGFGYR in untreated CTPS. The precursor isotope pattern spectrum (MS1) (A), and MS/MS spectrum for the doubly charged ion of the GV-peptide (*m/z* 1037.596 Da; MH^+ = 2074.185 Da) reveal no 94-Da (SMHP modification) adducts with the b_6^+ ion corresponding to Lys 342 (with 1 missed cleavage) (B, C).

A

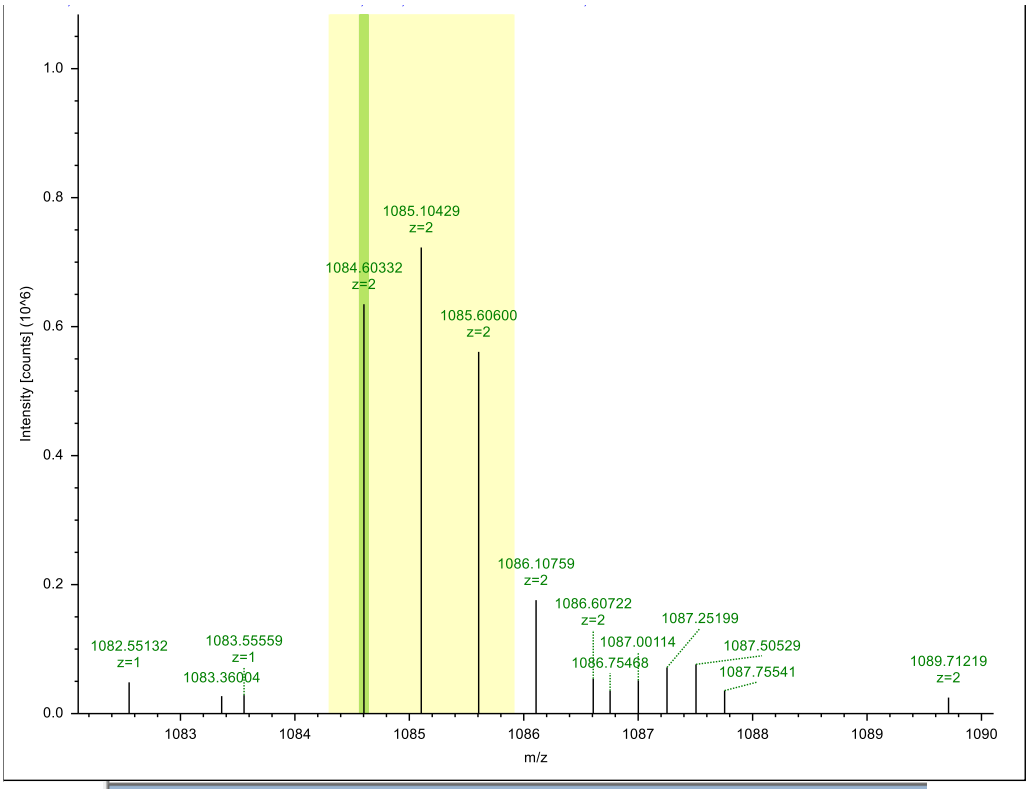

B

Fragment Matches

Value Type: Theo. Mass [Da]

Ion Series | Neutral Losses | Precursor Ions | Internal Fragments

#1	b⁺	b²⁺	Seq.	y⁺	y²⁺	#2
1	58.02874	29.51801	G			20
2	157.09715	79.05222	V	2111.18994	1056.09861	19
3	286.13975	143.57351	E	2012.12152	1006.56440	18
4	399.22381	200.11554	I	1883.07893	942.04310	17
5	512.30788	256.65758	L	1769.99487	885.50107	16
6	734.44470	367.72599	K-Hex-5-...	1656.91080	828.95904	15
7	791.46616	396.23672	G	1434.77398	717.89063	14
8	904.55023	452.77875	L	1377.75251	689.37989	13
9	1019.57717	510.29222	D	1264.66845	632.83786	12
10	1090.61428	545.81078	A	1149.64150	575.32439	11
11	1203.69835	602.35281	I	1078.60439	539.80583	10
12	1316.78241	658.89484	L	965.52033	483.26380	9
13	1415.85083	708.42905	V	852.43626	426.72177	8
14	1512.90359	756.95543	P	753.36785	377.18756	7
15	1569.92505	785.46617	G	656.31509	328.66118	6
16	1626.94652	813.97690	G	599.29362	300.15045	5
17	1774.01493	887.51110	F	542.27216	271.63972	4
18	1831.03640	916.02184	G	395.20374	198.10551	3
19	1994.09972	997.55350	Y	338.18228	169.59478	2
20			R	175.11895	88.06311	1

C

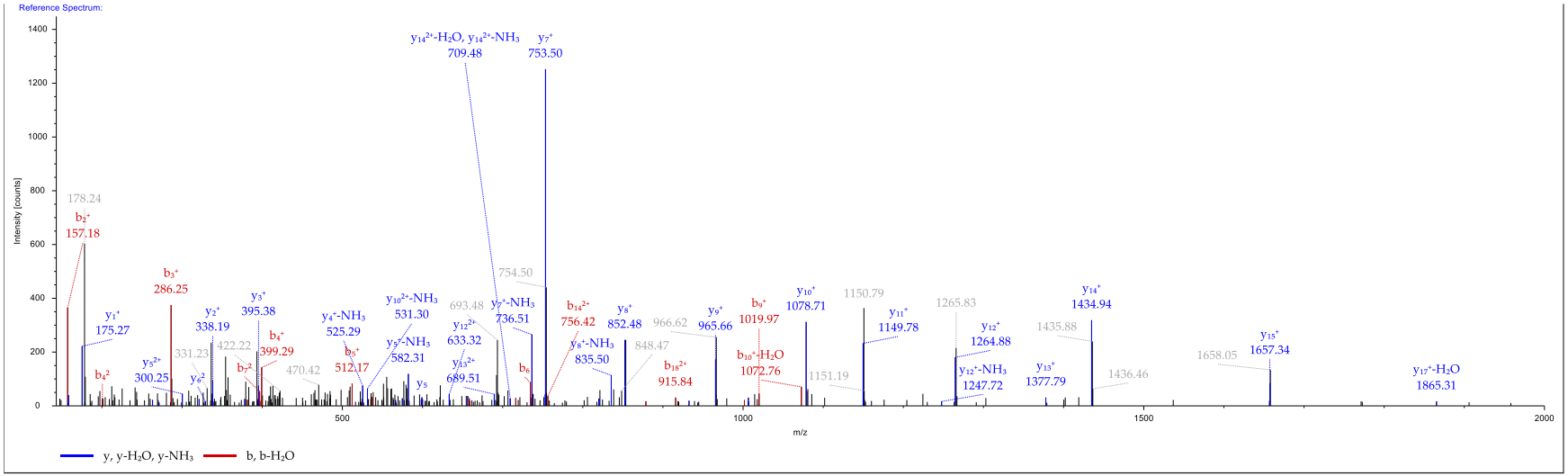

Figure 6B LC-MS/MS analysis showing a 94-Da adduct with Lys 342 from peptide: GVEILKGLDAILVPGGFGYR in SMHP-treated CTPS. The precursor isotope pattern spectrum (MS1) (A), and MS/MS spectrum for the doubly charged ion of the GV-peptide (*m/z* 1084.603 Da; MH^+ = 2168.199 Da) reveal an increase in mass of the b_7^+ ion by 94 Da corresponding to Lys 342 (with 1 missed cleavage) (B, C). Identical GV-peptides were found in the control and SMHP-treated sample and showed a mass increase of 94 Da between the b_7^+ ions arising from the SMHP-modified (734.445 Da) and unmodified peptide (640.403 Da).

A

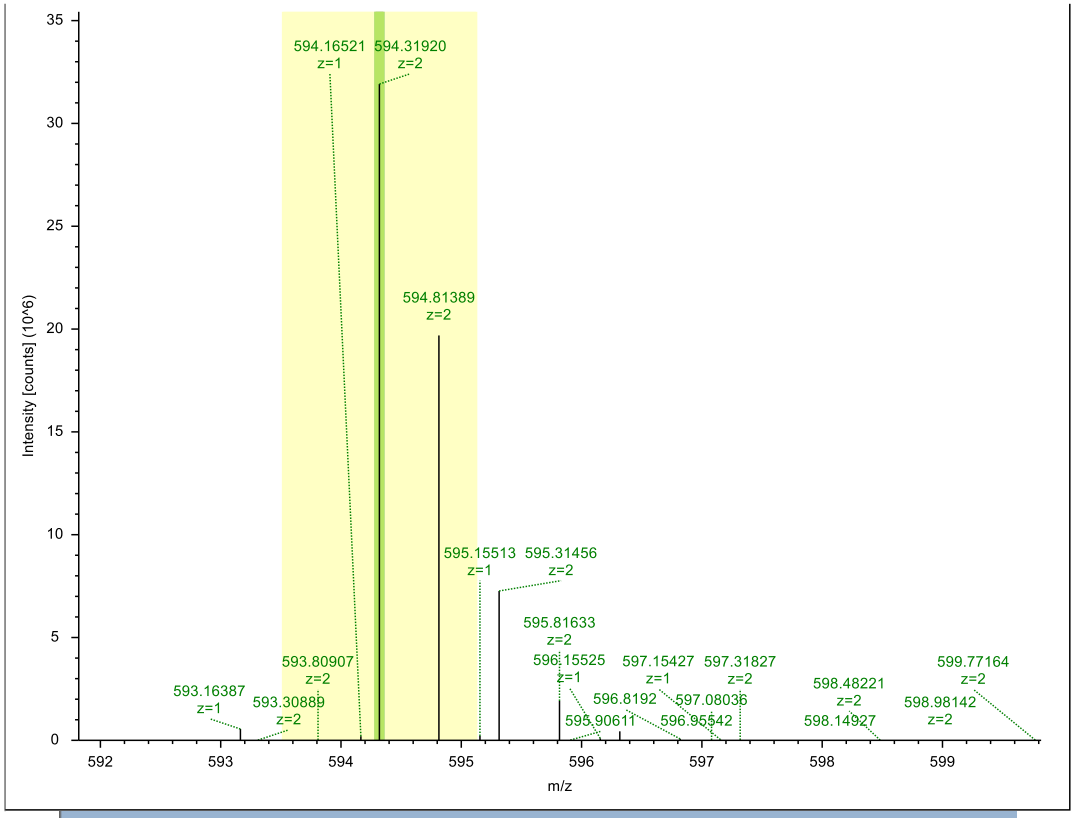

B

Fragment Matches

Value Type: Theo. Mass [Da]

Ion Series | Neutral Losses | Precursor Ions | Internal Fragments

#1	b^+	b^{2+}	Seq.	y^+	y^{2+}	#2
1	116.03422	58.52075	D			11
2	173.05568	87.03148	G	1072.59383	536.80055	10
3	310.11460	155.56094	H	1015.57236	508.28982	9
4	407.16736	204.08732	P	878.51345	439.76036	8
5	520.25142	260.62935	L	781.46069	391.23398	7
6	667.31984	334.16356	F	668.37662	334.69195	6
7	738.35695	369.68211	A	521.30821	261.15774	5
8	795.37841	398.19285	G	450.27110	225.63919	4
9	942.44683	471.72705	F	393.24963	197.12845	3
10	1041.51524	521.26126	V	246.18122	123.59425	2
11			K	147.11280	74.06004	1

C

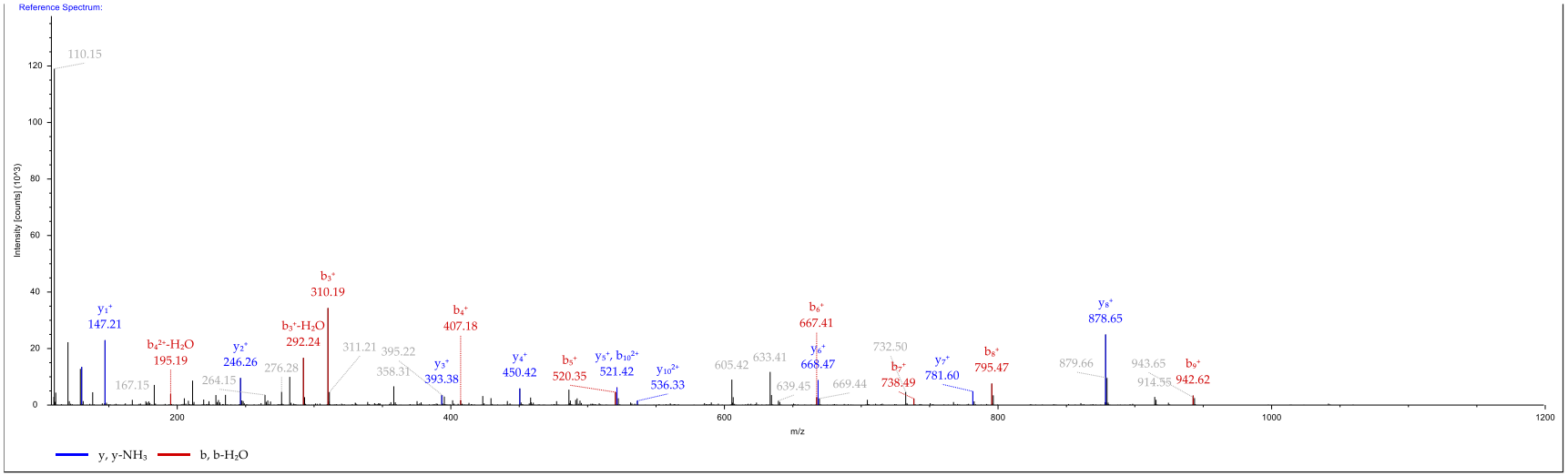

Figure 7B LC-MS/MS analysis showing no adducts with Lys 534 from peptide: DGHPLFAGFVK in untreated CTPS. The precursor isotope pattern spectrum (MS1) (A), and MS/MS spectrum for the doubly charged ion of the DG-peptide (*m*/*z* 594.319 Da; MH^+ = 1187.631 Da) reveal no 94-Da (SMHP modification) adducts with the y_1^+ ion corresponding to Lys 534 (with 0 missed cleavages) (B, C).

A

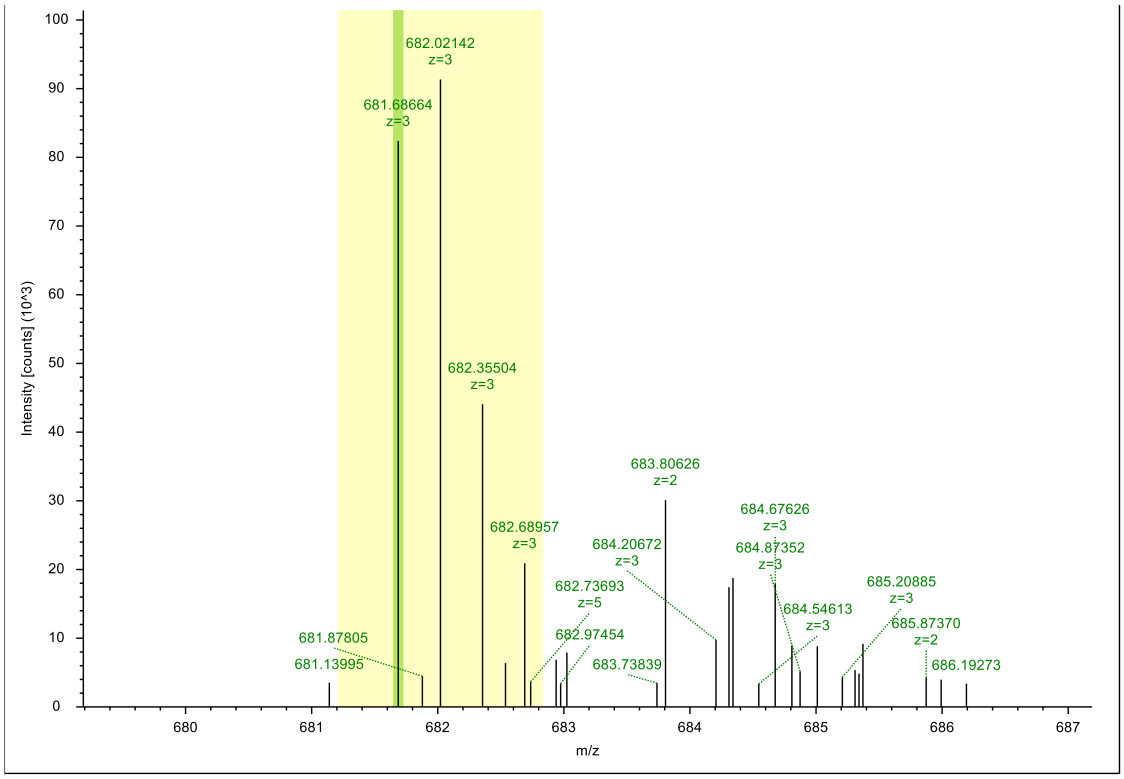

B

Fragment Matches

Value Type: Theo. Mass [Da]

Ion Series | Neutral Losses | Precursor Ions | Internal Fragments

#1	b⁺	b²⁺	b³⁺	Seq.	y⁺	y²⁺	y³⁺	#2
1	116.03422	58.52075	39.34959	D				18
2	173.05568	87.03148	58.35675	G	1928.00649	964.50688	643.34035	17
3	310.11460	155.56094	104.04305	H	1870.98503	935.99615	624.33319	16
4	407.16736	204.08732	136.39397	P	1733.92612	867.46670	578.64689	15
5	520.25142	260.62935	174.08866	L	1636.87335	818.94031	546.29597	14
6	667.31984	334.16356	223.11146	F	1523.78929	762.39828	508.60128	13
7	738.35695	369.68211	246.79050	A	1376.72088	688.86408	459.57848	12
8	795.37841	398.19285	265.79766	G	1305.68376	653.34552	435.89944	11
9	942.44683	471.72705	314.82046	F	1248.66230	624.83479	416.89228	10
10	1041.51524	521.26126	347.84327	V	1101.59388	551.30058	367.86948	9
11	1263.65207	632.32967	421.88887	K-Hex-5-...	1002.52547	501.76637	334.84667	8
12	1334.68918	667.84823	445.56791	A	780.38864	390.69796	260.80107	7
13	1405.72629	703.36679	469.24695	A	709.35153	355.17940	237.12203	6
14	1492.75832	746.88280	498.25763	S	638.31442	319.66085	213.44299	5
15	1621.80092	811.40410	541.27182	E	551.28239	276.14483	184.43231	4
16	1768.86933	884.93830	590.29463	F	422.23980	211.62354	141.41812	3
17	1896.92791	948.96759	632.98082	Q	275.17138	138.08933	92.39531	2
18				K	147.11280	74.06004	49.70912	1

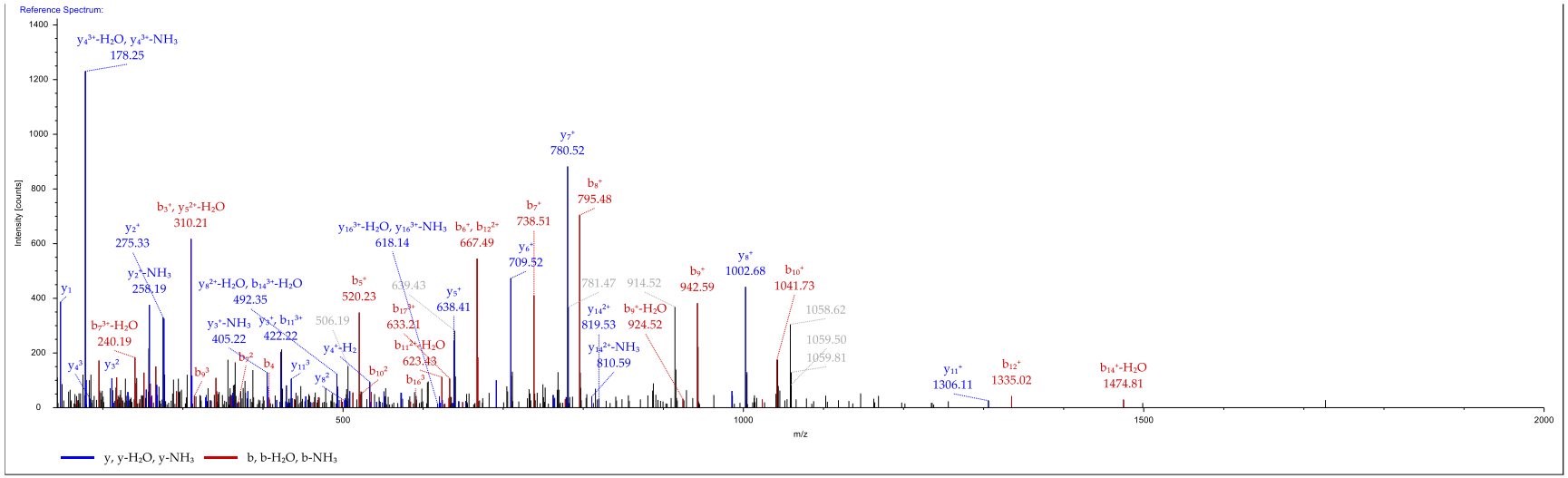

Figure 8B LC-MS/MS analysis showing a 94-Da adduct with Lys 534 from peptide: DGHPLFAGFVKAASEFQK in SMHP-treated CTPS. The precursor isotope pattern spectrum (MS1) (A), and MS/MS spectrum for the triply charged ion of the DG-peptide (*m/z* 681.687 Da; MH^+ = 2043.045 Da) reveal an increase in mass of the b_{11}^+ ion by 94 Da corresponding to Lys 534 (with 1 missed cleavage) (B, C). Identical DG-peptides were not found in the control (0 missed cleavages of DG-peptide) and SMHP-treated sample (1 missed cleavage of DG-peptide), but, as shown, the mass increase of 94 Da from the b_{11}^+ ion identified in the SMHP-treated peptide is absent in the y_1^+ ion of the untreated peptide.

A

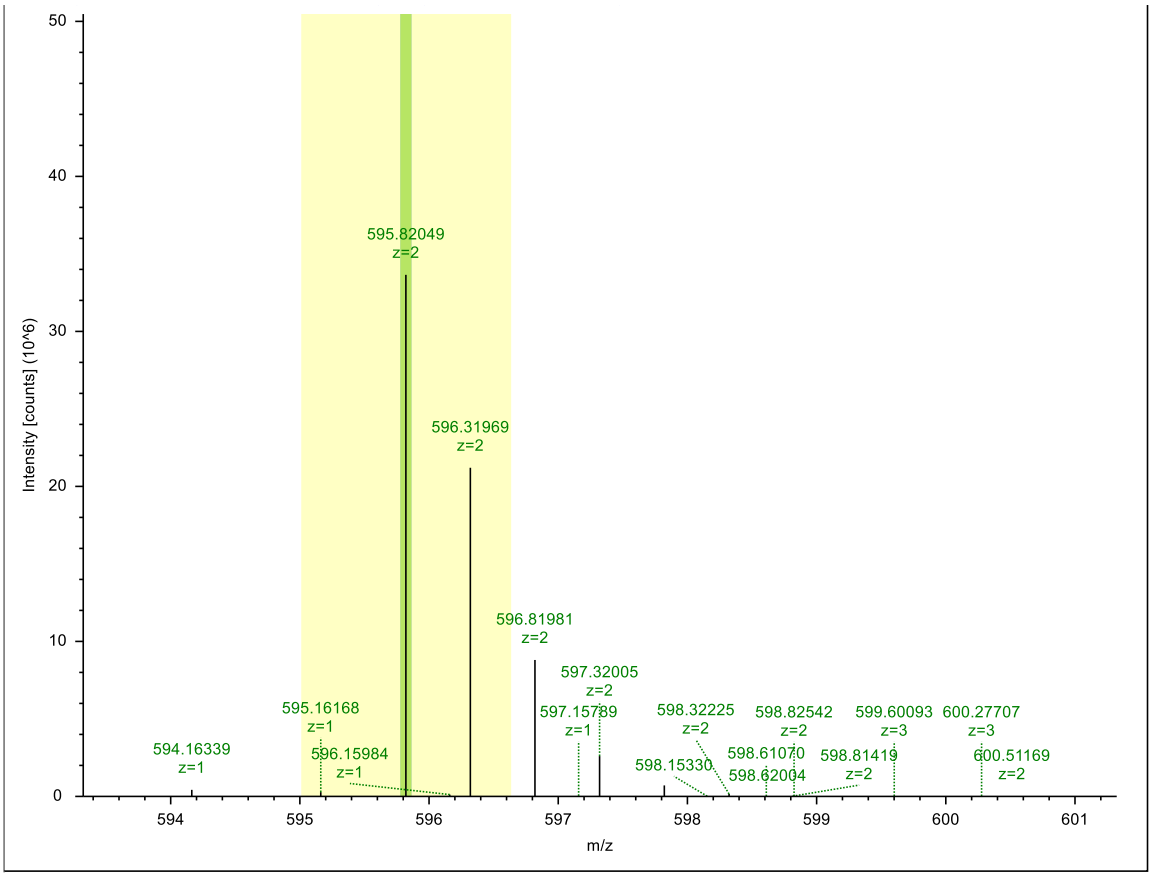

B

Fragment Matches

Value Type: Theo. Mass [Da]

Ion Series | Neutral Losses | Precursor Ions | Internal Fragments

#1	b⁺	b²⁺	Seq.	y⁺	y²⁺	#2
1	114.09134	57.54931	I			10
2	185.12845	93.06787	A	1077.53974	539.27351	9
3	298.21252	149.60990	L	1006.50263	503.75495	8
4	445.28093	223.14410	F	893.41856	447.21292	7
5	605.31158	303.15943	C-Carba...	746.35015	373.67871	6
6	719.35451	360.18089	N	586.31950	293.66339	5
7	818.42292	409.71510	V	472.27657	236.64193	4
8	915.47569	458.24148	P	373.20816	187.10772	3
9	1044.51828	522.76278	E	276.15540	138.58134	2
10			K	147.11280	74.06004	1

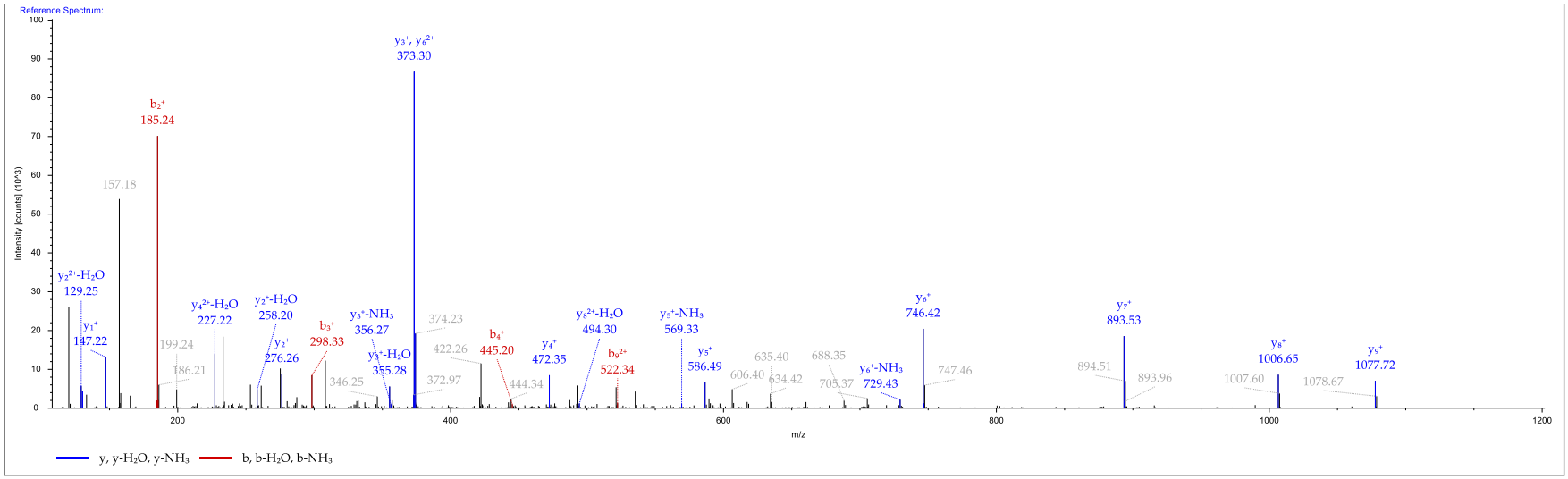

Figure 9B LC-MS/MS analysis showing no adducts with Lys 233 from peptide: IALFCNVPEK in untreated CTPS. The precursor isotope pattern spectrum (MS1) (A), and MS/MS spectrum for the doubly charged ion of the IA-peptide (*m/z* 595.820 Da; MH^+ = 1190.634 Da) reveal no 94-Da (SMHP modification) adducts with the y_1^+ ion corresponding to Lys 233 (with 0 missed cleavages) (B, C). Note: the carbamidomethylation (57 Da) modification on the b_5^+ ion occurs as a result of alkylation with iodoacetamide (IAA) after cysteine reduction with dithiothreitol (DTT).

A

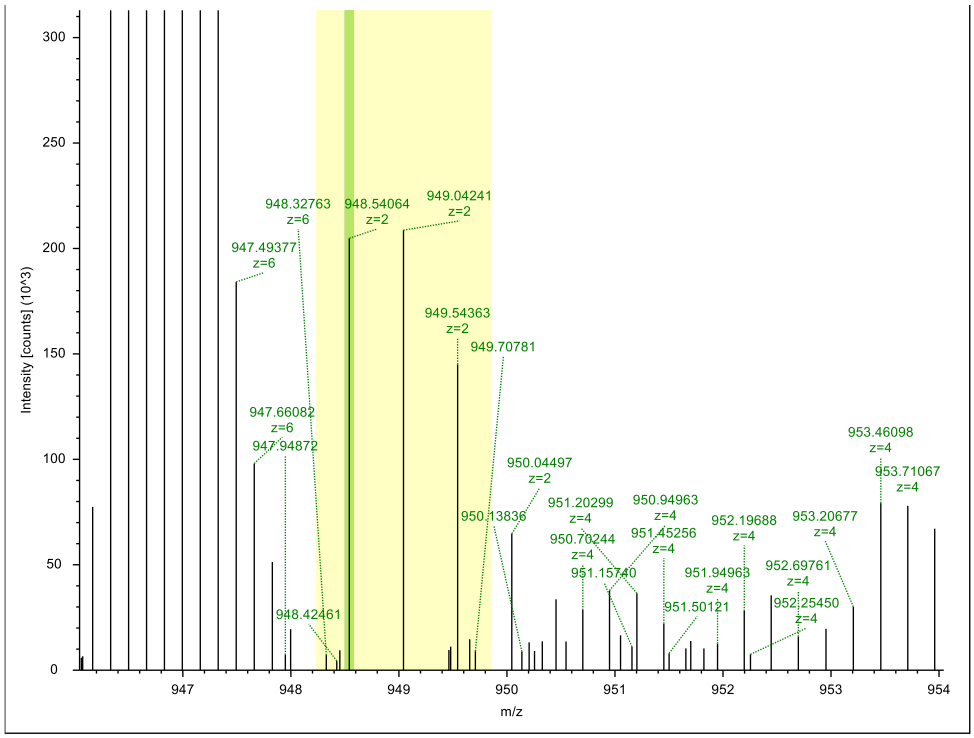

B

Fragment Matches

Value Type: Theo. Mass [Da]

Ion Series | Neutral Losses | Precursor Ions | Internal Fragments

#1	b⁺	b²⁺	Seq.	y⁺	y²⁺	#2
1	114.09134	57.54931	I			16
2	185.12845	93.06787	A	1782.98225	891.99476	15
3	298.21252	149.60990	L	1711.94514	856.47621	14
4	445.28093	223.14410	F	1598.86107	799.93418	13
5	605.31158	303.15943	C-Carba...	1451.79266	726.39997	12
6	719.35451	360.18089	N	1291.76201	646.38464	11
7	818.42292	409.71510	V	1177.71908	589.36318	10
8	915.47569	458.24148	P	1078.65067	539.82897	9
9	1044.51828	522.76278	E	981.59791	491.30259	8
10	1266.65510	633.83119	K-Hex-5-...	852.55531	426.78130	7
11	1337.69222	669.34975	A	630.41849	315.71288	6
12	1436.76063	718.88395	V	559.38137	280.19433	5
13	1549.84470	775.42599	I	460.31296	230.66012	4
14	1636.87672	818.94200	S	347.22890	174.11809	3
15	1749.96079	875.48403	L	260.19687	130.60207	2
16			K	147.11280	74.06004	1

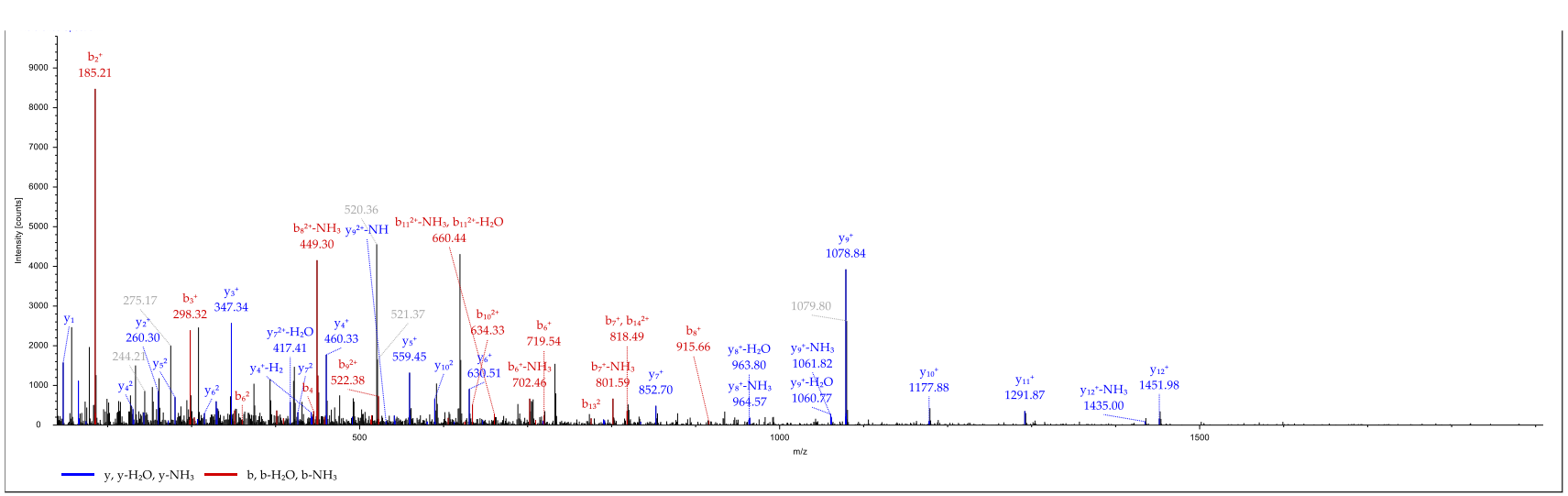

Figure 8B LC-MS/MS analysis showing a 94-Da adduct with Lys 233 from peptide: IALFCNVPEKAVISLK in SMHP-treated CTPS. The precursor isotope pattern spectrum (MS1) (A), and MS/MS spectrum for the doubly charged ion of the IA-peptide (*m/z* 948.541 Da; MH^+ = 1896.074 Da) reveal an increase in mass of the b_{10}^+ ion by 94 Da corresponding to Lys 233 (with 1 missed cleavage) (B, C). Identical IA-peptides were not found in the control (0 missed cleavages of IA-peptide) and SMHP-treated sample (1 missed cleavage of IA-peptide), but, as shown, the mass increase of 94 Da from the b_{10}^+ ion identified in the SMHP-treated peptide is absent in the y_1^+ ion of the untreated peptide. Note: the carbamidomethylation (57 Da) modification on the b_5^+ ion occurs as a result of alkylation with iodoacetamide (IAA) after cysteine reduction with dithiothreitol (DTT).

A

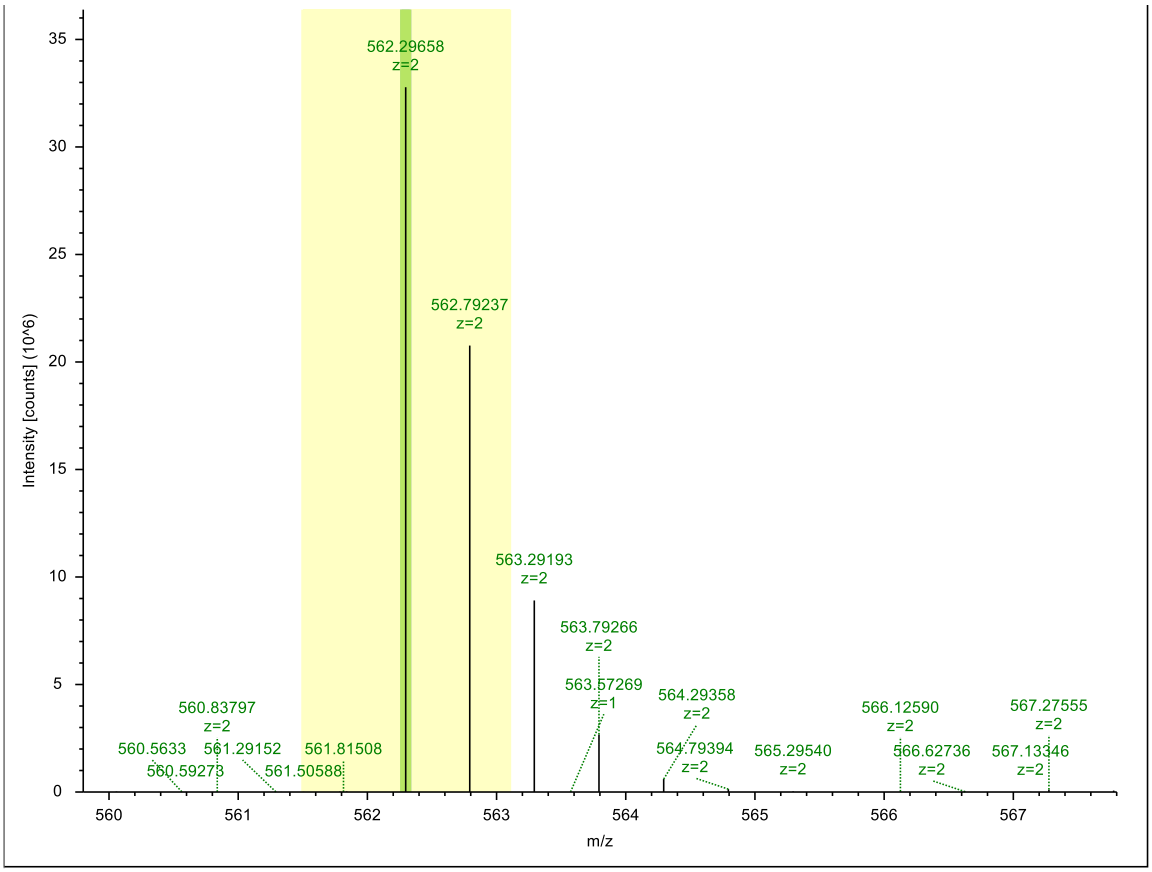

B

Fragment Matches

Value Type: Theo. Mass [Da]

Ion Series | Neutral Losses | Precursor Ions | Internal Fragments

#1	b^+	b^{2+}	Seq.	y^+	y^{2+}	#2
1	164.07061	82.53894	Y			9
2	293.11320	147.06024	E	960.51828	480.76278	8
3	392.18161	196.59444	V	831.47569	416.24148	7
4	506.22454	253.61591	N	732.40727	366.70727	6
5	620.26747	310.63737	N	618.36434	309.68581	5
6	751.30795	376.15761	M	504.32142	252.66435	4
7	864.39202	432.69965	L	373.28093	187.14410	3
8	977.47608	489.24168	L	260.19687	130.60207	2
9			K	147.11280	74.06004	1

C

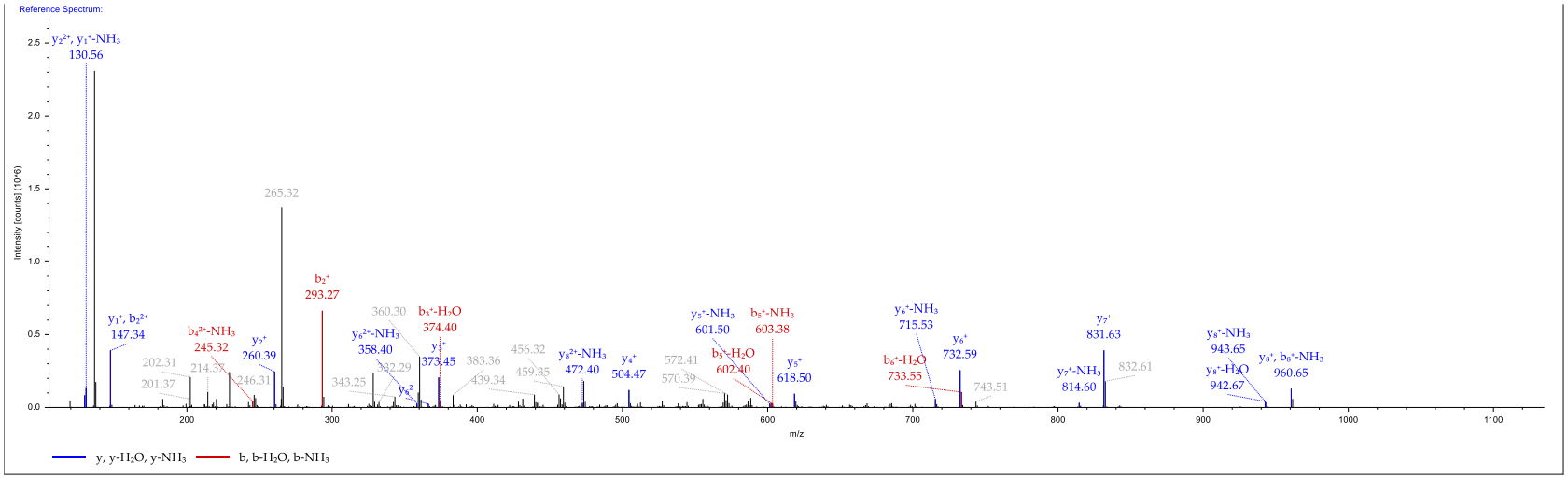

Figure 9B LC-MS/MS analysis showing no adducts with Lys 479 from peptide: YEVNNMLLK in untreated CTPS. The precursor isotope pattern spectrum (MS1) (A), and MS/MS spectrum for the doubly charged ion of the YE-peptide (*m/z* 562.297 Da; MH^+ = 1123.586 Da) reveal no 94-Da (SMHP modification) adducts with the y_1^+ ion corresponding to Lys 479 (with 0 missed cleavages) (B, C).

A

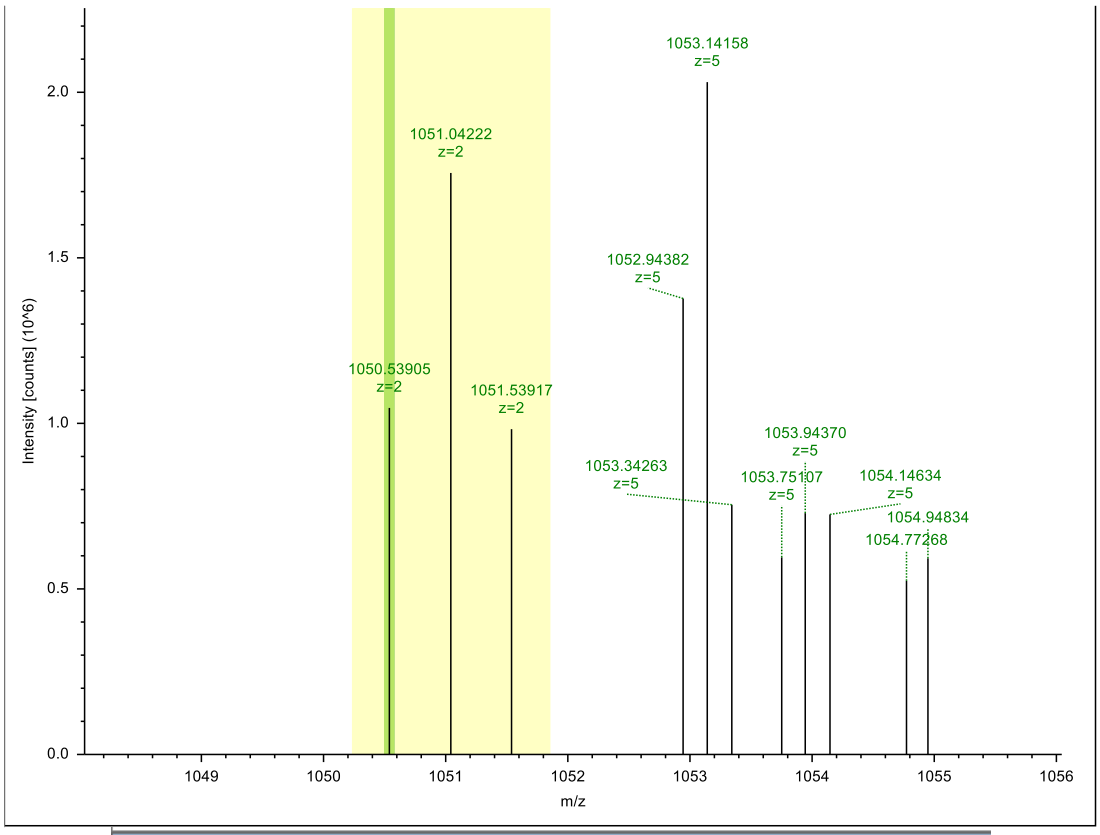

B

Fragment Matches

Value Type: Theo. Mass [Da]

Ion Series | Neutral Losses | Precursor Ions | Internal Fragments

#1	b⁺	b²⁺	Seq.	y⁺	y²⁺	#2
1	164.07061	82.53894	Y			17
2	293.11320	147.06024	E	1937.01607	969.01167	16
3	392.18161	196.59444	V	1807.97348	904.49038	15
4	506.22454	253.61591	N	1708.90506	854.95617	14
5	620.26747	310.63737	N	1594.86214	797.93471	13
6	751.30795	376.15761	M	1480.81921	740.91324	12
7	864.39202	432.69965	L	1349.77872	675.39300	11
8	977.47608	489.24168	L	1236.69466	618.85097	10
9	1199.61290	600.31009	K-Hex-5-...	1123.61060	562.30894	9
10	1327.67148	664.33938	Q	901.47377	451.24052	8
11	1440.75555	720.88141	I	773.41519	387.21124	7
12	1569.79814	785.40271	E	660.33113	330.66920	6
13	1684.82508	842.91618	D	531.28854	266.14791	5
14	1755.86220	878.43474	A	416.26159	208.63444	4
15	1812.88366	906.94547	G	345.22448	173.11588	3
16	1925.96772	963.48750	L	288.20302	144.60515	2
17			R	175.11895	88.06311	1

C

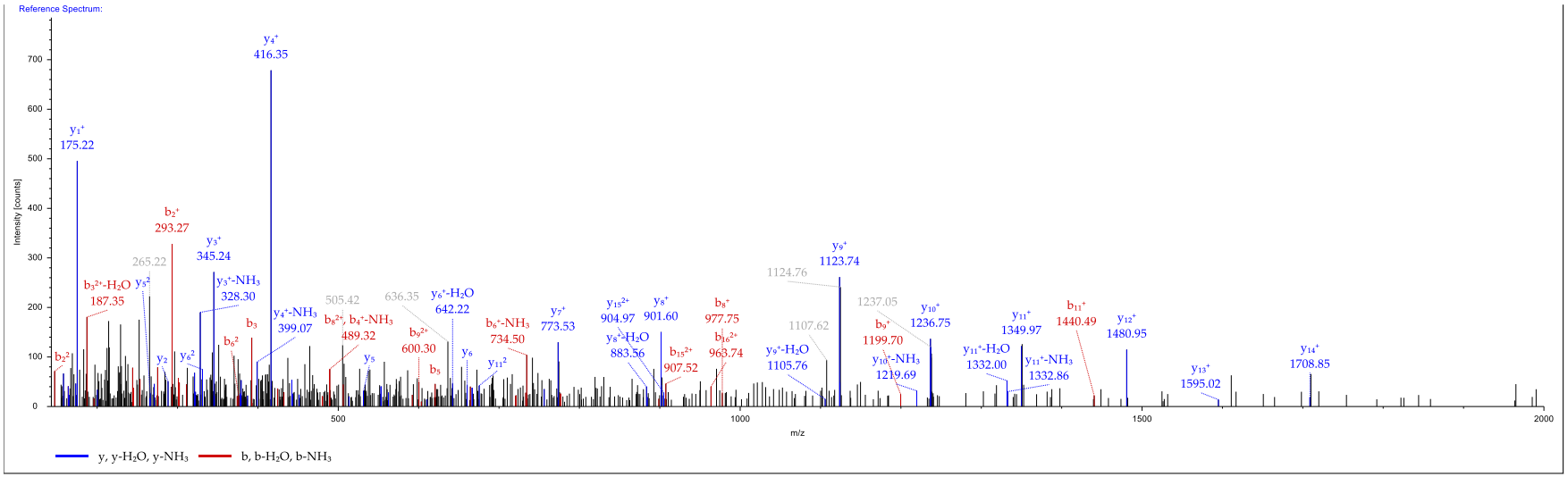

Figure 10B LC-MS/MS analysis showing a 94-Da adduct with Lys 479 from peptide: YEVNNMLLKQIEDAGLR in SMHP-treated CTPS. The precursor isotope pattern spectrum (MS1) (A), and MS/MS spectrum for the doubly charged ion of the IA-peptide (*m/z* 1050.539 Da; MH^+ = 2100.071 Da) reveal an increase in mass of the b_9^+ ion by 94 Da corresponding to Lys 479 (with 1 missed cleavage) (B, C). Identical YE-peptides were not found in the control (0 missed cleavages of YE-peptide) and SMHP-treated sample (1 missed cleavage of YE-peptide), but, as shown, the mass increase of 94 Da from the b_9^+ ion identified in the SMHP-treated peptide is absent in the y_1^+ ion of the untreated peptide.

A

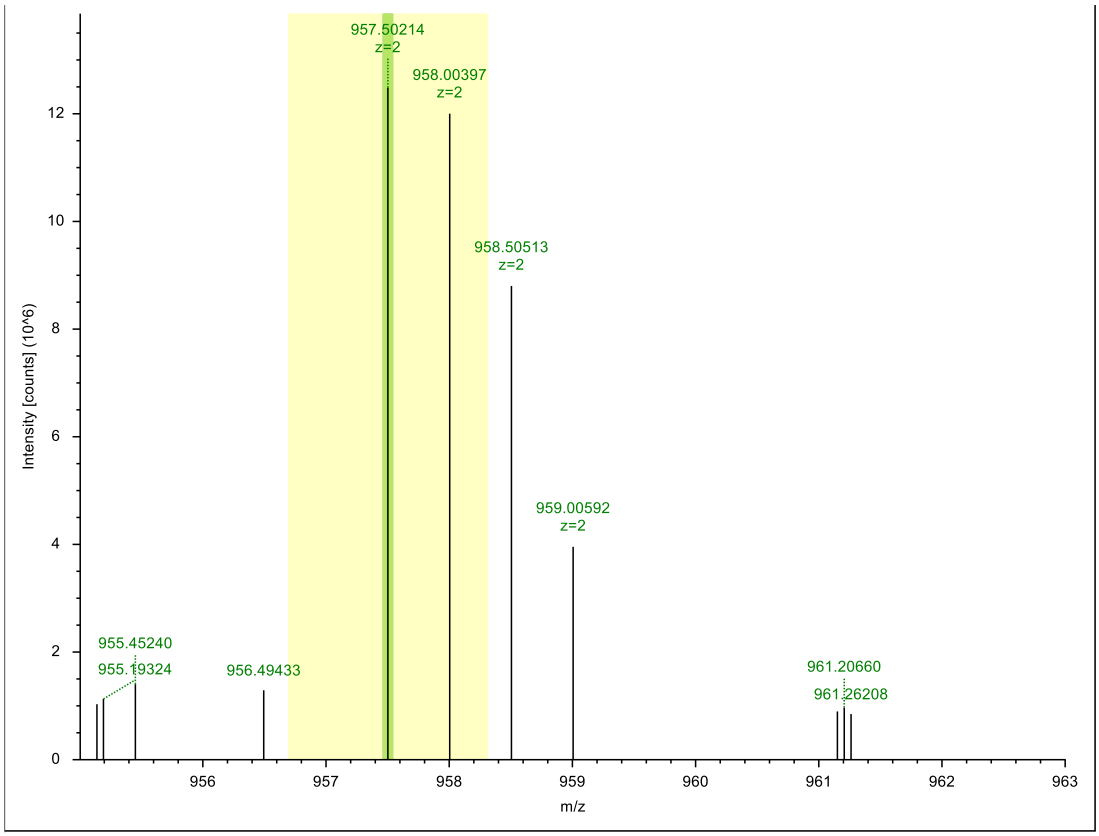

B

Fragment Matches

Value Type: Theo. Mass [Da]

Ion Series | Neutral Losses | Precursor Ions | Internal Fragments

#1	b⁺	b²⁺	Seq.	y⁺	y²⁺	#2
1	114.09134	57.54931	I			16
2	211.14410	106.07569	P	1800.92005	900.96366	15
3	268.16557	134.58642	G	1703.86728	852.43728	14
4	381.24963	191.12845	L	1646.84582	823.92655	13
5	494.33370	247.67049	L	1533.76175	767.38452	12
6	716.47052	358.73890	K-Hex-5-...	1420.67769	710.84248	11
7	803.50255	402.25491	S	1198.54086	599.77407	10
8	931.56113	466.28420	Q	1111.50884	556.25806	9
9	988.58259	494.79493	G	983.45026	492.22877	8
10	1101.66665	551.33697	L	926.42879	463.71804	7
11	1216.69360	608.85044	D	813.34473	407.17600	6
12	1331.72054	666.36391	D	698.31779	349.66253	5
13	1494.78387	747.89557	Y	583.29085	292.14906	4
14	1607.86793	804.43760	I	420.22752	210.61740	3
15	1767.89858	884.45293	C-Carba...	307.14345	154.07536	2
16			K	147.11280	74.06004	1

C

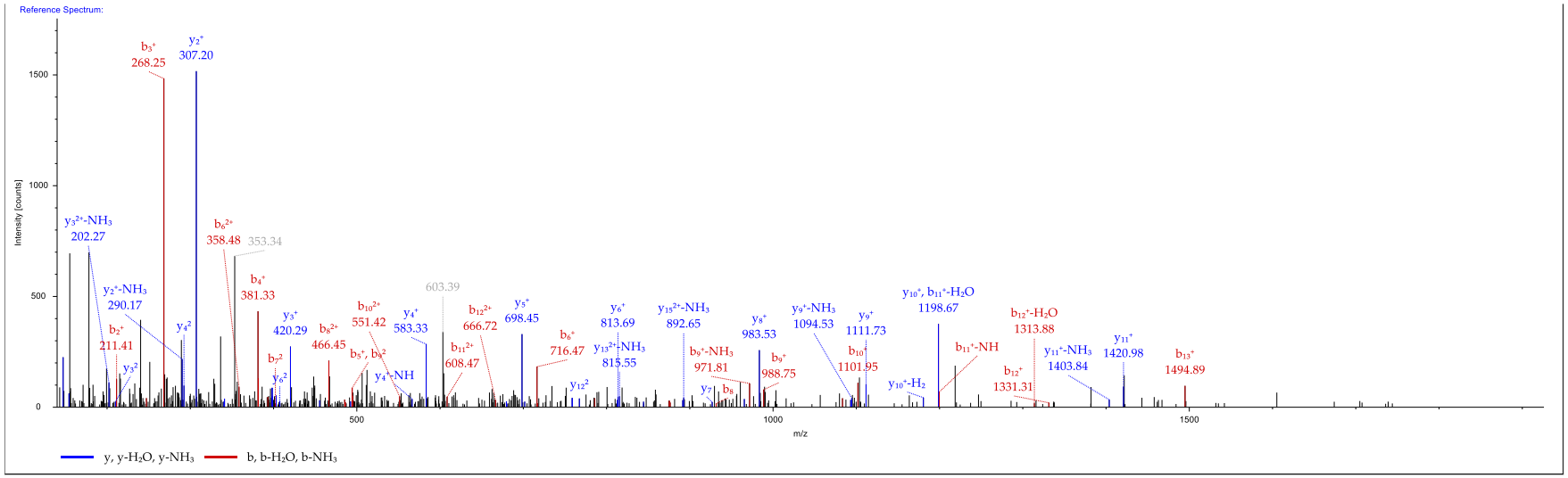

Figure 11B LC-MS/MS analysis showing a 94-Da adduct with Lys 252 from peptide: IPGLLKSQGLDDYICK in SMHP-treated CTPS. The precursor isotope pattern spectrum (MS1) (A), and MS/MS spectrum for the doubly charged ion of the IP-peptide (*m/z* 957.502 Da; MH^+ = 1913.997 Da) reveal an increase in mass of the b_6^+ ion by 94 Da corresponding to Lys 252 (with 1 missed cleavage) (B, C). Identical peptides were not found in the control and SMHP-treated sample, but, as shown, the mass increase of 94 Da from the b_6^+ ion identified in the SMHP-treated peptide is absent in the y_1^+ ion of the untreated peptide: DVDSIYKIPGLLK (Figure 3B). Note: the carbamidomethylation (57 Da) modification on the b_{15}^+ ion occurs as a result of alkylation with iodoacetamide (IAA) after cysteine reduction with dithiothreitol (DTT).

A

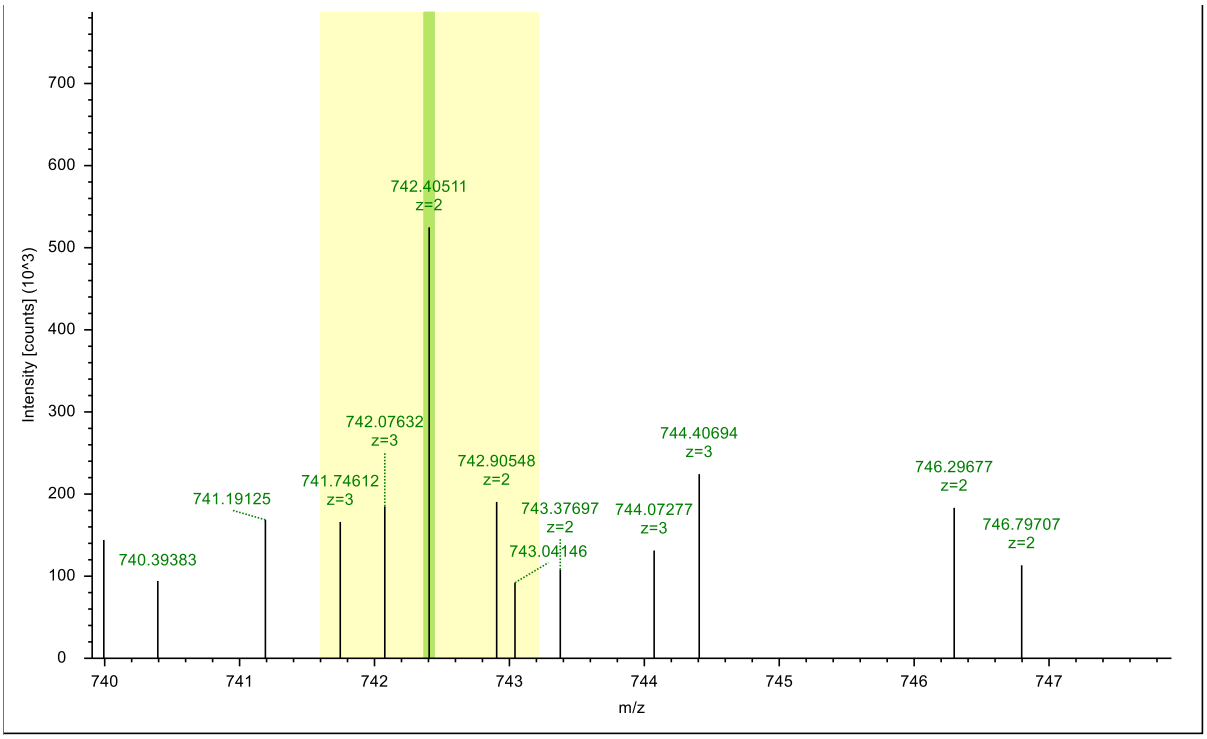

B

Fragment Matches

Value Type: Theo. Mass [Da]

Ion Series | Neutral Losses | Precursor Ions | Internal Fragments

#1	b^+	b^{2+}	Seq.	y^+	y^{2+}	#2
1	72.04439	36.52583	A			12
2	294.18122	147.59425	K-Hex-5-...	1412.76063	706.88395	11
3	407.26528	204.13628	I	1190.62381	595.81554	10
4	478.30239	239.65484	A	1077.53974	539.27351	9
5	591.38646	296.19687	L	1006.50263	503.75495	8
6	738.45487	369.73107	F	893.41856	447.21292	7
7	898.48552	449.74640	C-Carba...	746.35015	373.67871	6
8	1012.52845	506.76786	N	586.31950	293.66339	5
9	1111.59686	556.30207	V	472.27657	236.64193	4
10	1208.64962	604.82845	P	373.20816	187.10772	3
11	1337.69222	669.34975	E	276.15540	138.58134	2
12			K	147.11280	74.06004	1

C

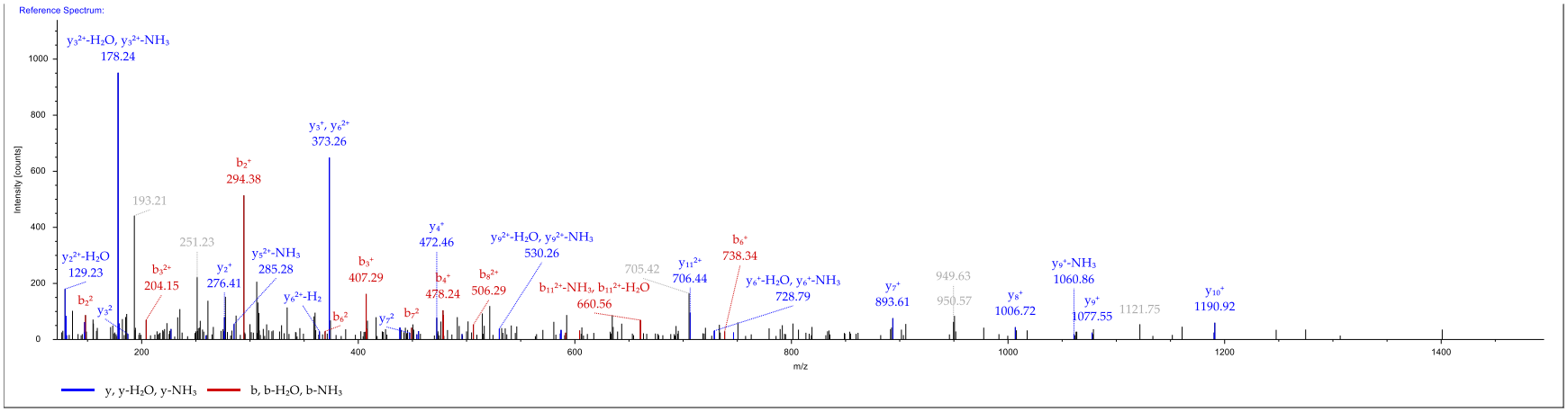

Figure 12B LC-MS/MS analysis showing a 94-Da adduct with Lys 223 from peptide: AKIALFCNVPEK in SMHP-treated CTPS. The precursor isotope pattern spectrum (MS1) (A), and MS/MS spectrum for the doubly charged ion of the AK-peptide (*m/z* 742.405 Da; MH^+ = 1483.803 Da) reveal an increase in mass of the b_2^+ ion by 94 Da corresponding to Lys 223 (with 1 missed cleavage) (B, C). The sequence coverage for untreated CTPS (control) in Figure 1B shows that Lys 223 was not covered, but was covered in the SMHP-treated CTPS (sample) (Figure 2B). Note: the carbamidomethylation (57 Da) modification on the b_7^+ ion occurs as a result of alkylation with iodoacetamide (IAA) after cysteine reduction with dithiothreitol (DTT).

A

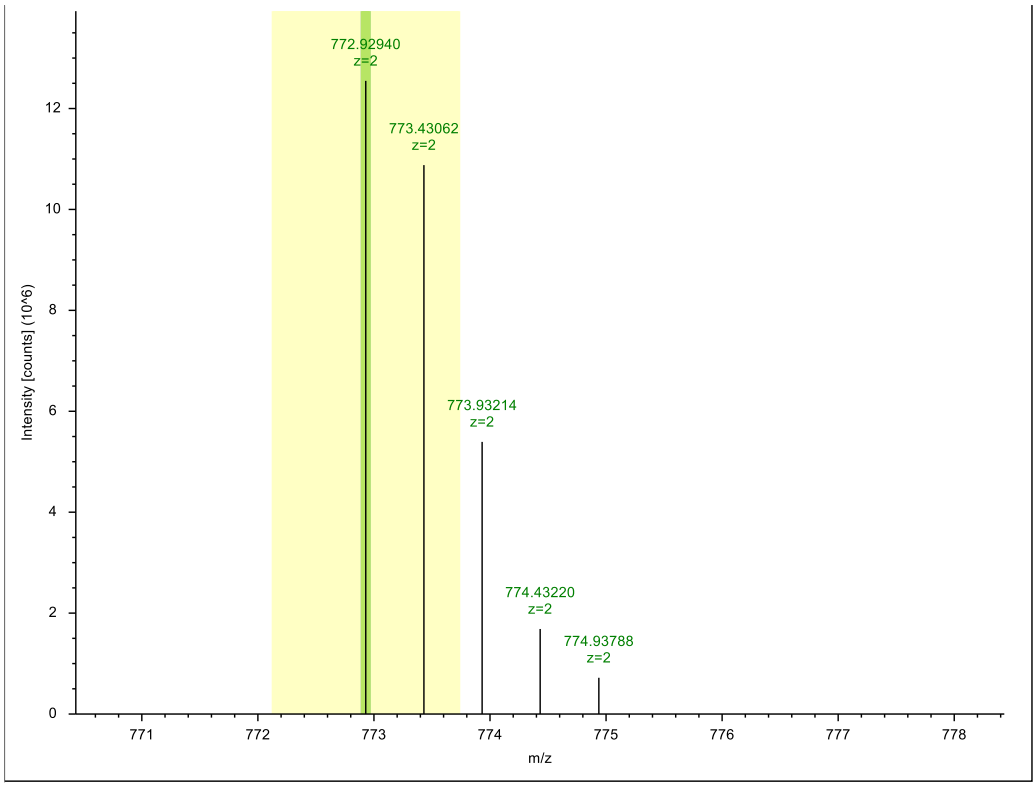

B

Fragment Matches

Value Type: Theo. Mass [Da]

Ion Series | Neutral Losses | Precursor Ions | Internal Fragments

#1	b⁺	b²⁺	Seq.	y⁺	y²⁺	#2
1	72.04439	36.52583	A			13
2	171.11280	86.06004	V	1473.81992	737.41360	12
3	284.19687	142.60207	I	1374.75151	687.87939	11
4	371.22890	186.11809	S	1261.66744	631.33736	10
5	484.31296	242.66012	L	1174.63541	587.82135	9
6	706.44979	353.72853	K-Hex-5-...	1061.55135	531.27931	8
7	821.47673	411.24200	D	839.41452	420.21090	7
8	920.54514	460.77621	V	724.38758	362.69743	6
9	1035.57209	518.28968	D	625.31917	313.16322	5
10	1122.60411	561.80570	S	510.29223	255.64975	4
11	1235.68818	618.34773	I	423.26020	212.13374	3
12	1398.75151	699.87939	Y	310.17613	155.59170	2
13			K	147.11280	74.06004	1

C

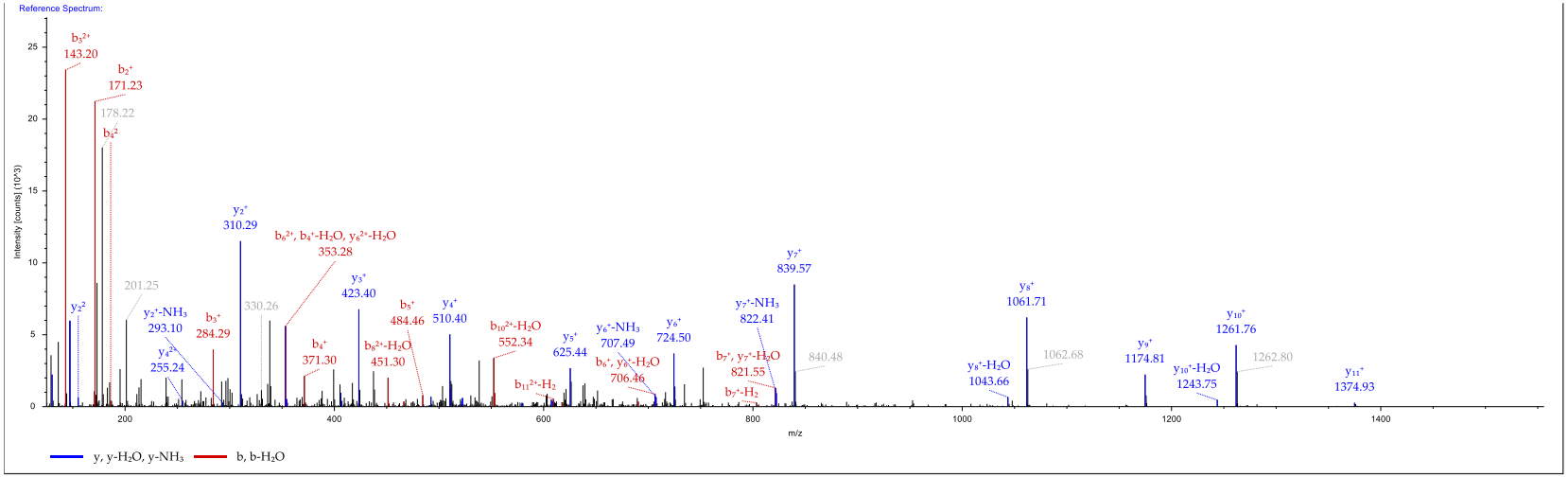

Figure 13B LC-MS/MS analysis showing a 94-Da adduct with Lys 239 from peptide: AVISLKDVDSIYK in SMHP-treated CTPS. The precursor isotope pattern spectrum (MS1) (A), and MS/MS spectrum for the doubly charged ion of the AK-peptide (*m/z* 772.929 Da; MH^+ = 1544.852 Da) reveal an increase in mass of the b_6^+ ion by 94 Da corresponding to Lys 239 (with 1 missed cleavage) (B, C). The sequence coverage for untreated CTPS (control) in Figure 1B shows that Lys 239 was not covered, but was covered in the SMHP-treated CTPS (sample) (Figure 2B).